Indian Institute of Technology Guwahati
Department of Physics

Dynamics of reheating: towards decoding its signatures

A thesis submitted by:
Md Riajul Haque

to

Indian Institute of Technology Guwahati
in partial fulfillment of the requirements
for the award of the degree of
Doctor of Philosophy in Physics

May 2022

Statement

.

The work contained in the thesis entitled "**Dynamics of reheating: towards decoding its signatures**" has been carried out at the Department of Physics, Indian Institute of Technology Guwahati, India by me, under the supervision of Dr. Debaprasad Maity. The material of this thesis is original and has not been submitted elsewhere for any other degree or diploma. Works presented in the thesis are all my own unless referenced to the contrary in the text.

Md Riajul Haque

Md Riajul Haque
PhD student
Department of Physics
Indian Institute of Technology Guwahati
Guwahati, Assam, India-781039
Date: 30/05/22

Disclaimer

.

The bibliography included in this thesis is, by no means, complete; rather contains the ones which are consulted thoroughly by me. I apologize for inadvertently missing out on some of the research papers, review articles, and other scientific documents pertaining to this thesis which also should have been cited. For illustration purposes, some of the figures in this thesis are taken from other sources and properly cited.

Certificate

.

It is certified that the work contained in the thesis entitled "**Dynamics of reheating: towards decoding its signatures**" by Md. Riajul Haque (roll number-176121018), a Ph.D. student of the Department of Physics, IIT Guwahati, was carried out under my supervision. The material of this thesis is original and has not been submitted elsewhere for any other degree or diploma.

Debaprasad Maity
.....
(Signature of the supervisor)

Dr. Debaprasad Maity
Associate Professor,
Indian Institute of Technology Guwahati,
Guwahati-781039, Assam, India
Date: 30/5/22

Acknowledgement

.

First and foremost, I would like to express my sincere gratitude to my Ph.D. advisor, Dr. Debaprasad Maity, for his guidance on research topics, consistent support, patience, and kindness with which he treated me throughout the entire period of my doctoral studies. His enthusiasm and approach to research and life have always pushed me to look at every challenge as a chance to learn and progress as a researcher. Without him, this thesis would certainly not have been completed. I have certainly learned a lot from all the discussions with him. I would consider myself fortunate if I could have imbibed even a little of his passion for physics.
My sincere gratitude also goes to my collaborator Prof. L. Sriramkumar, Tanmoy paul, and Pankaj Saha, for their help in some projects.
I would like to express my gratitude to my doctoral committee members, Dr. Pankaj Kumar Mishra, Prof. Santabrata Das, Dr. Bibhas Ranjan Majhi, and Dr. Sayan Chakrabarti for their encouragement and insightful comments, which helped me to improve my presentation skills and also my understanding of my work.
My sincere gratitude goes to the current and former Heads of the Department of Physics, Prof. A. Perumal and Prof. Subhradip Ghosh, for providing me with all the facilities for my research and all the faculty members of the physics department and the non-teaching staff.
I would like to thank Department of Physics, Indian Institute of Technology Guwahati for the financial support and various helps.
I would like to thank my senior and current Ph.D. group mates Dr. Pankaj Saha, Mousumi Maitra, Rajesh Karmakar, Sourav Pal, Gargi Sen, Banarshree Baishya, Rajesh Mondal, Ayan Chakraborty and Subhasis Maity for all the fruitful discussions we have had.
I would like to convey my heartfelt regards to my seniors Rajesh Da, Subhajit Da, Sayan da, Rakesh Da, and Ambaresh Da, for various help and discussions. I would remember the help and company of my friends Arghyajit, Surojit, Mandira, Samit, Pronoy, Sanket, and Swarup.
I would like to thank my parents and my uncle for all the emotional support and unconditional love. The expansion of universe starts and ends with them.
This thesis is dedicated to the memories of my loving uncle whom I lost recently.
I want to express my gratitude to my close friend Anisa for her support, unconditional love, and immense mental support during this journey.
I am indebted to all the people with whom I have interacted or learned from. Especially to the organizers and teachers of various schools which I attended during the course. Those proved to really invaluable to my understanding of the subject.

Md Riajul Haque
Gauwahati
May 2022

Abstract

The early history of our observable universe and its development are based on two major poles: cosmic inflation and big-bang nucleosynthesis (BBN). The inflation successfully creates the homogeneous, isotropic, and spatially flat universe, and BBN successfully produces all the light elements with correct abundance values. These two phenomena happen at two widely separated energy scales with inflation at around 10^{16} GeV and BBN at around 10 MeV. However, except in some phenomenological studies, not much physics is understood of the stage which occurs between the two, mainly because of the lack of observations. Inflation creates exponentially large empty space contained with only homogeneous inflaton fields. Hence, the natural physical process that could occur is the transfer of inflaton energy into the standard model fields, which can subsequently set the initial condition for BBN. The phase where this energy transfer from inflaton to radiation happens is called reheating. Based on our current theoretical understanding, this phase consists of many non-trivial physical phenomena such as perturbative, non-perturbative quantum particle production, thermalization, etc. In all these physical phenomena during reheating, what assumes that the central stage is the homogeneous oscillating inflaton. How the radiation fields are coupled with the inflaton, how the produced radiation is thermalized, and how long the decay processes last are some of the central questions that are still the active areas of research in reheating. The lack of experimental observations makes this phase essentially unconstrained. However, there are many attempts to constrain the reheating phase through some indirect cosmological observables such as primordial gravitational wave, primordial magnetic field, dark matter abundance, and cosmic microwave background (CMB) anisotropy, and these are the main topics of discussion in our present thesis work. We have two main themes of the present thesis, which are as follows:

Modeling the dynamics of reheating: Suppose the inflaton coupling with the radiation field is sufficiently high. In that case, the initial stage of the reheating phase may become non-perturbative, and the resonant non-thermal growth of particle number dominates the process as compared to the perturbative one due to coherent inflaton oscillations. Motivated by this, in the second chapter, we propose a Two-phase reheating scenario where the dynamics describe the aforementioned initial non-perturbative stage with an effective equation of state followed by the standard perturbative reheating. Some model-independent lattice simulation results are incorporated as the boundary conditions while solving the dynamical equations of the proposed scenario. Due to the initial non-thermal phase, it predicts maximum reheating temperature (T_{re}^{max}), which turned out to be lower than that of the standard perturbative single-phase prediction. However, the initial seed value of the effective equation of state significantly affects the value of that maximum reheating temperature. We further generalize the scenario by including dark matter (DM), which is assumed to be produced from the radiation bath. We studied possible constraints on different inflaton coupling and DM production cross-sections considering CMB anisotropy and DM abundance.

Reheating phase is observationally not very well understood, and hence phenomenological construction of such phase is challenging. In the conventional approach, we introduce arbitrary coupling among the inflaton and daughter fields which could only be constrained through indirect observations. Therefore, any cosmological predictions of such approaches depend on the unknowns and hence are not robust, which could be observationally verified. To obtain universal predictions and gain an insight into the reheating process itself, in the second part of chapter five, we took a model-independent approach by switching off all unknown couplings between the inflaton and daughter sector. Surprisingly, we discovered that universal gravitational interaction is enough to reheat our universe with some definite predictions. We named such a scenario Gravitational reheating (GRe). Our analysis revealed that gravitational reheating is consistent with a very restricted class of inflation

models and narrow reheating temperature and DM mass ranges.

Signatures of reheating on cosmological observable: To decode the signatures of reheating, we have studied the evolution of various fundamental fields while passing through the reheating phases, which are as follows:

- **Through primordial magnetic field:** In the third chapter, we have shown that the reheating phase can play a crucial role in alleviating strong coupling and back-reaction problems in the inflationary magnetogenesis model along with the CMB. Faradays, electromagnetic induction changes the magnetic field dynamics drastically during the reheating phase, and this phenomenon not only converts a large class of magnetogenesis models observationally viable without any theoretical problem but also can uniquely fix the average inflaton equation of state.
- **Through primordial gravitational waves (GWs):** In chapter four, we closely examine the effects of the reheating phase on the spectrum of primordial GWs observed today. We show that the perturbative decay of the inflaton leads to oscillations in the GWs spectrum, which can possibly help us interpret finer aspects of the reheating mechanism if observed. We also examine the effects of a secondary phase of reheating driven possibly by an exotic, non-canonical, scalar field, and interestingly for a suitable value of the Equation of state parameter, the GWs can be of the strength, as suggested by the recent NANOGrav observations.
- **Through Gravitational dark matter:** In the first part of chapter five, we have analyzed a minimal production mechanism of dark matter, where dark matter is assumed to be produced from inflaton and radiation bath through only the gravitational interaction during reheating. Ignoring any other internal parameters except the dark matter mass and spin, a particular inflation model such as α-attractor, with a specific scalar spectral index (n_s), has been shown to uniquely fix the dark matter mass.

List of Publications in reverse chronological order

1. **Md Riajul Haque** and Debaprasad Maity, *Gravitational Reheating*, arXiv:2201.02348.
2. **Md Riajul Haque** and Debaprasad Maity, *Gravitational dark matter: free streaming and phase space distribution*, arXiv:2112.14668.
3. **Md Riajul Haque**, Debaprasad Maity, Tanmoy Paul and L. Sriramkumar, *Decoding the phases of early and late time reheating through imprints on primordial gravitational waves*, *Phys. Rev. D* 104, 063513 (2021), arXiv:2105.09242.
4. **Md Riajul Haque**, Debaprasad Maity and Sourav Pal, *Probing the reheating phase through primordial magnetic field and CMB*, *Phys. Rev. D* 103, 103540 (2021), arXiv:2012.10859.
5. **Md Riajul Haque**, Debaprasad Maity and Pankaj Saha, *Two phase reheating: CMB constraints on inflaton and dark matter phenomenology*, *Phys. Rev. D* 102, 083534 (2020), arXiv:2009.02794 .
6. **Md Riajul Haque** and Debaprasad Maity, *Reheating Constraints on Inflaton, Dark Matter: Swampland Conjecture*, *Phys. Rev. D* 99, 103534 (2019), arXiv:1902.09491. (Not included in this Thesis work)

Talks and Poster presentations at workshops and conferences

1. Presented a poster titled *"Reheating constraints through decaying inflaton"* at **2019 YITP Asian-Pacific Winter School and Workshop on Gravitation and Cosmology**, in Yukawa Institute for Theoretical Physics, Kyoto University, during February 11-15, 2019.

2. Delivered a talk titled *" Probing the reheating phase through primordial magnetic field and CMB"* at the **IIT Guwahati and Tokyo Institute of Technology 2nd joint workshop on topics in Condensed Matter Physics, High Energy Physics, Cosmology and Astrophysics** during December 15-18, 2020.

3. Presented a poster titled *"Two-phase reheating: constraints on inflation and dark matter"* at **31st Meeting of Indian Association of General Relativity and Gravitation**, during December 19-20, 2020.

4. Delivered a talk titled *" Probing the reheating phase through primordial magnetic field and CMB"* at the **AAPPS-DACG Workshop 2021 on Astrophysics, Cosmology and Gravitation**, organized by APCTP during October 4-8, 2021.

5. Delivered a talk, titled *"Decoding the phases of early and late time reheating through imprints on primordial gravitational waves"* at the **27th International Conference of International Academy of Physical Sciences on Advances in Relativity and Cosmology** organized by the Department of Mathematics, Birla Institute of Technology and Science – Pilani during October 26-28, 2021.

Notations and Conventions

.

Throughout this thesis we use natural units $\hbar$=c=k_B=ϵ_0=1. In this unit Reduced Planck mass is given by $M_p = \frac{1}{\sqrt{8\pi G}}$.

Greek indices μ,ν and so on go over the four space-time co-ordinates $x^\mu = [x^0, x^1, x^2, x^3]^T$ with x^0 for the time coordinate.

Minkowski metric is given by $\eta_{\mu\nu} = diag[1, -1, -1, -1]$.

Latin labels i, j, k and so on go over the three spatial co-ordinates.

Spatial vectors are written in boldface.

The Ricci tensor, defined in terms of the Christoffel symbols, is

$$R_{\mu\nu} = \partial_\lambda \Gamma^\lambda_{\mu\nu} - \partial_\nu \Gamma^\lambda_{\mu\lambda} + \Gamma^\lambda_{\lambda\rho}\Gamma^\rho_{\mu\nu} - \Gamma^\rho_{\mu\lambda}\Gamma^\lambda_{\nu\rho}, \tag{1}$$

and the Ricci scalar is $R = g^{\mu\nu}R_{\mu\nu}$.

The spatial Fourier transform of a field $f(\mathbf{x})$ is $f_\mathbf{k} = \int f(\mathbf{x}) e^{-i\mathbf{k}.\mathbf{x}} d^3\mathbf{x}/(2\pi)^3$ and the inverse transform is $f(\mathbf{x}) = \int f_\mathbf{k} e^{i\mathbf{k}.\mathbf{x}} d^3\mathbf{k}$.

Contents

Part I

Standard Cosmology: Inflationary dynamics and initial condition for reheating

Introduction 1

..everything can be created from nothing, And "everything might include a lot more than what we can see. In the context of inflationary cosmology, it is fair to say that the universe is the ultimate free lunch."

Alan Guth in 'THE INFLATIONARY COSMOLOGY'

1.1 Big-Bang cosmology and the need for inflation

The theoretical foundation of the standard model of cosmology began with two striking observations: 1) The further away the two galaxies are larger their receding velocity, which suggests that our universe is expanding in time. 2) Universe is filled with Cosmic Microwave Background (CMB) radiation which is homogeneous and isotropic in nature [1, 2], which suggests that our universe is spatially homogeneous and isotropic. To make our long story short, these two observations paved the solid foundation of standard theoretical big-bang cosmology, which essentially deals with the expanding universe at a very large scale with the two fundamental principles of spatial homogeneity and isotropy. In spite of having great success of standard Big-Bang cosmology in explaining many observational facts, standard big-bang invites fundamental problems and questions as well, which are deeply connected with the initial condition from which our universe is supposed to start its journey. The obvious one is the big-bang singularity which naturally arises due to diverging energy density when we look back at the time. Dealing with this obvious one has been theoretically challenging and intimately connected with understanding the nature of gravity at the quantum level. However, the standard model of cosmology has few non-obvious problems, out of which two are well known as the Horizon and the flatness problem, and all these are studied in the framework of Freedman-Lemaitre-Robertson-Walker (FLRW) cosmology.

1.1.1 FLRW Cosmology

Studying cosmology begins with the following FLRW metric, which obeys spatial homogeneity and isotropy,

$$ds^2 = dt^2 - a(t)^2 \left(\frac{dr^2}{1 - k\, r^2} + r^2 d\theta^2 \, + r^2 \, sin^2\theta \, d\phi^2 \right) \tag{1.1}$$

where a represents the scale factor and t is the cosmic time. k specifies the constant curvature of the spatial three-dimensional space with $k = (1, 0, -1)$ corresponding to closed, flat, and open cosmological universe accordingly. The governing equations are the Einstein equation

$$R_{\mu\nu} - \frac{1}{2} R\, g_{\mu\nu} \; = 8\pi G T_{\mu\nu} \tag{1.2}$$

where the Ricci tensor and the Ricci scalar are defined as

$$R_{\mu\nu} = \partial_\lambda \Gamma^\lambda_{\mu\nu} - \partial_\nu \Gamma^\lambda_{\mu\nu} + \Gamma^\lambda_{\lambda\rho}\Gamma^\rho_{\mu\nu} - \Gamma^\rho_{\mu\lambda}\Gamma^\lambda_{\nu\rho} \quad ; \quad R = g^{\mu\nu} R_{\mu\nu} \, . \tag{1.3}$$

For the standard Big-Bang cosmology, the large-scale universe is expected to be isotropic and homogeneous, and hence the energy-momentum tensor $T^{\mu\nu}$ is naturally assumed as time-dependent with vanishing anisotropic stress part,

$$T^{00} = \rho(t), \, T^{ij} = -a(t)^{-2} \delta^{ij} \, P(t) \, . \tag{1.4}$$

Where ρ and P are symbolized as the total energy density and pressure of the universe, respectively. With these components of the energy-momentum tensor, the Friedman equations 1.2 lead to the following two independent equations for the scale factor and the energy density,

$$H^2 = \left(\frac{\dot{a}}{a} \right)^2 \; = \; \frac{8\pi G}{3} \rho - \frac{k}{a^2} \, , \tag{1.5}$$

$$\frac{\ddot{a}}{a} \; = \; -\frac{4\pi G}{3} \left(\rho + 3P \right) \, . \tag{1.6}$$

Where $H = \dot{a}/a$ is identified as Hubble parameter. Throughout our thesis, we will confine ourselves to the case $k = 0$, which is precisely related to the flatness problem mentioned earlier. Subsequently, the Friedmann equations for $k = 0$ are

$$H^2 = \frac{\rho}{3M_p^2} \quad ; \quad \dot{H} + H^2 = \frac{1}{6M_p^2} \left(\rho + 3P \right) \, . \tag{1.7}$$

The reduced Planck mass M_p is defined as $M_p = \sqrt{1/8\pi G} = 2.4 \times 10^{18}$ GeV. If we consider the universe is filled with a single energy component with the following equation of state $P = \omega\rho$, one obtains the solution,

$$\begin{aligned} a(t) = t^{\frac{2}{3(1+\omega)}} \quad ; \quad \rho = \rho_0^\omega \left(\frac{a}{a_0} \right)^{-3(1+\omega)} \quad & \text{For } \omega \neq -1 \\ a(t) \propto e^{Ht} \quad ; \quad \rho^\Lambda = \Lambda \quad & \text{For } \omega = -1. \end{aligned} \tag{1.8}$$

Where the constant equation of state $\omega = (0, 1/3, -1)$ corresponds to matter, radiation, and cosmological constant dominated universe, respectively. Based on a large number of

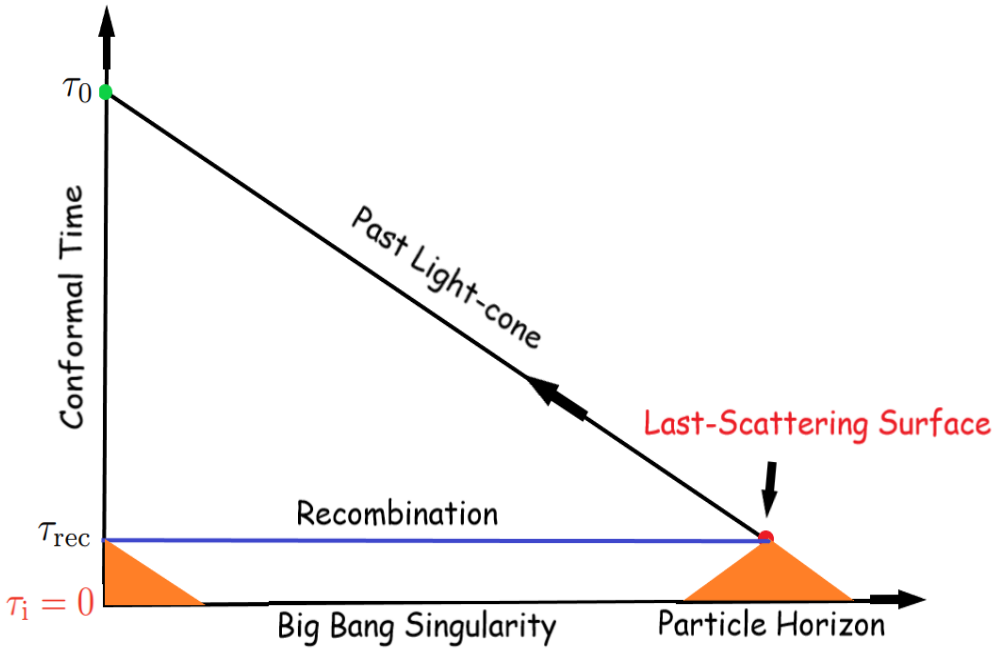

FIGURE 1.1: The conformal diagram in the standard FRW cosmology. The light cones correspond to two opposite points in the observed CMB that did not have any overlapping region before the singularity point. As a result, they were never in causal contact in the conventional Big Bang model.

cosmological observations, currently, we live in a cosmological constant dominated universe. As we go backward in time, the universe becomes matter-dominated and radiation-dominated. If we consider all the energy components together, the Hubble equation assumes the following form,

$$H(z)^2 = \rho_0^r \left(\frac{a}{a_0}\right)^{-4} + \rho_0^m \left(\frac{a}{a_0}\right)^{-3} + \Lambda = \frac{\rho_c^{0\,2}}{3M_p^2}\left(\Omega_0^m(1+z)^3 + \Omega_0^r(1+z)^4 + \Omega_\Lambda\right). \quad (1.9)$$

The new parameters, $\Omega_0^m = \rho_0^m/\rho^0$, $\Omega_0^r = \rho_0^r/\rho^0$, $\Omega_0^\Lambda = \rho_0^\Lambda/\rho^0$, are the density parameter at present $t = t_0, a = a_0$ for matter, radiation, and cosmological constant respectively which are normalized by the critical energy density $3M_p^2H_0^2 = \rho_c^0 = \rho_0^m + \rho_0^r + \Lambda$ measured at present. The scale factor is expressed in terms of redshift parameter: $z = a_0/a(t) - 1$. At present, the value of $z = 0$. The current estimated value of those density parameters are $\Omega_0^m \simeq 0.3$, $\Omega_0^r = 10^{-5}$, and $\Omega_0^\Lambda \simeq 0.7$. One can solve the above equation numerically; however, it is obvious from the above equation and also solutions of Eqs.1.8 that the energy density diverges, which is the well-known Big-Bang singularity. However, in this thesis, we deal with reheating era, which connects the radiation and the early inflation era. In the following section, we will discuss problems that demand the need to introduce an inflationary paradigm in the standard Big-Bang cosmology.

1.1.2 Horizon Problem

This is the problem that naturally arises from the first observation we mentioned in the beginning: 1) Further away two galaxies are, the larger the receding velocity from each other,

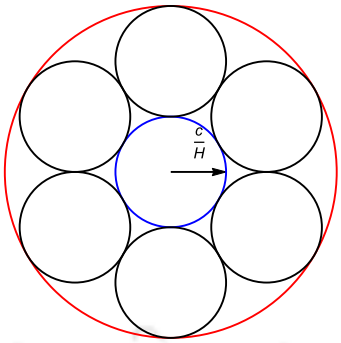

Figure 1.2: Casually disconnected Hubble patches

which can be mathematically expressed in terms of scale factor $a(t)$ as,

$$D(t) \propto a(t) \implies v_{rec} = \frac{dD}{dt} \propto \frac{da}{dt} = \frac{1}{a}\frac{da}{dt}a(t) = HD(t), \tag{1.10}$$

where $(D(t), v_{rec})$ are the distance between any two galaxies and receding velocity, respectively. Where $H = \dot{a}/a$ is the Hubble constant. However, it is not a constant in time, which will be very important for our later purpose. The beginning of the universe in the finite past (around 13 billion years) immediately creates a conceptual problem for the standard big-bang paradigm. The trouble emerges if we assume the distance between any two galaxies, $a(t)$ is larger than a particular value L_H,

$$D(t) \geq L_H = \frac{c}{H(t)} \implies v_{rec} \geq c, \tag{1.11}$$

c is the velocity of light. It signifies that the expanding universe can be divided into multiple causally disconnected patches separated by the Hubble horizon of size $L_H = 1/H$. Two systems living in two causally disconnected patches will evolve independently. Their physical properties are naturally expected to be different. What has been observed experimentally is the extremely homogeneous and isotropic distribution of radiation (CMB) and matter across a large number of Hubble patches. Surprisingly the very foundation of standard big-bang is based on those two assumptions of homogeneity and isotropy. The standard big-bang expansion we have been discussing so far is decelerated in nature. This essentially suggests that the Hubble volume increases with time for the radiation or matter-dominated universe. For example, radiation dominated universe.

$$a(t) \sim t^{1/2} \implies H(t) = \frac{1}{2t} \implies L_H(t) = 2ct. \tag{1.12}$$

Therefore, the region of space we are able to access today say at t_0 within the present Hubble volume, (red circle in Fig-1.2) can be thought of as the collection of $N = L_H(t_0)/L_H(t_{dec}) \sim 10^4$ number of disconnected Hubble patches in the past at time $t_{dec}(< t_0)$. And, the radiation we see today (t_0) because of the causal connection was actually originated or, in cosmological language, decoupled in the past (t_{dec}) from those causal disconnection patches. The point of photon decoupling at a particular time in the past is observed as three dimensional CMB surface (known as the last scattering surface) in the observer's sky from which CMB photons originated. Surprisingly from the distribution of radiation known as Cosmic Microwave Background (CMB), the radiation temperature T_{cmb} which is one of the important physical properties, turns out be

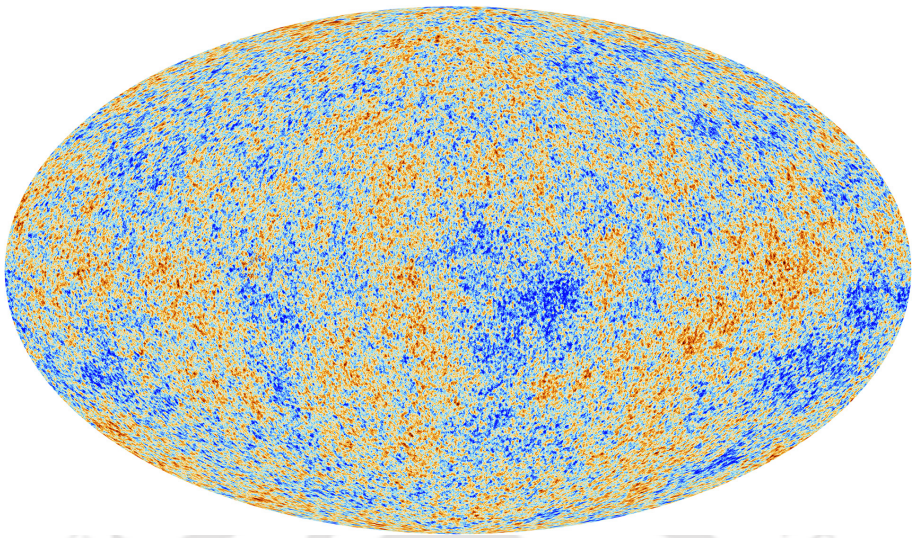

FIGURE 1.3: A sky map of the Cosmic Microwave Background temperature [Image courtesy: ESA website].

extremely homogeneous background temperature $T_{cmb} = 2.7K$ up to a very tiny fluctuation, $\delta T_{cmb}/T_{cmb} = 10^{-5}$. This observation challenges the very successes of the standard big-bang paradigm and its fundamental assumptions, which are appeared to be self-contradicting. Such uniform nature of CMB indicates that in the past, CMB photons must be in causal contact. But the conformal time elapsed between the initial and CMB decoupling time indicates a serious issue: most of the CMB spots have non-overlapping past light cones, and they were never in causal contact (see Fig.1.1 in this context). The natural question appears in mind *that nearly* 10^4 *disconnected patches formed cosmic microwave backgrounds, and they did not get sufficient time to communicate; then why do they have almost the same temperature and densities? This is the so-called Horizon problem.* Before making the above statement more precise, let us introduce the concept of particle horizon.

Augular size of the Particle horizon: To further refine the above statement, we consider the comoving particle horizon, which is defined as the maximum comoving distance traveled by the photon from the beginning of Big-Bang to any arbitrary later time t as

$$\chi_{ph}(t) = \int_0^t \frac{dt'}{a(t')} = \tau(t) - \tau(0)\,. \tag{1.13}$$

Where τ is the conformal time. Such horizon size measures the maximum volume of the space at time t, which is causally connected. In the CMB experiment, measurement is done in terms of angular coordinates. Therefore, at the time of decoupling, let us calculate the angle subtended by the comoving particle horizon, θ_{hor} with respect to the observer at present. θ_{hor} is defined as the ratio between the comoving particle horizon at the time of CMB decoupling χ_{dec} and the comoving angular diameter distance d_A of the CMB surface at $t = t_{dec}$ or equivalently at the redshift parameter $z_{dec} \simeq 3400$.

$$\theta_{hor} = \frac{\chi_{ph}(t_{dec})}{d_A}\,. \tag{1.14}$$

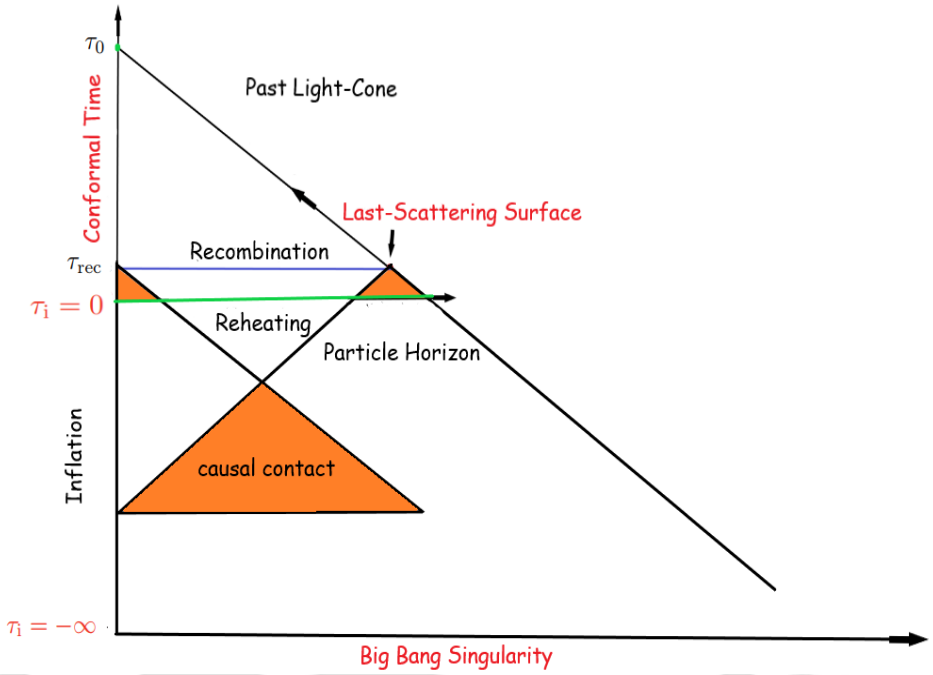

Figure 1.4: The solution to the horizon problem: Conformal diagram for inflationary cosmology. Hubble sphere shrinks during inflation which is otherwise expanded during the standard cosmological evolution (still dark energy takes over the dominating component of the universe). Here the singularity of the standard FRW cosmology is replaced by the reheating surface. Interestingly introducing inflation now, all points in CMB were in causal contact as they have overlapping regions before the singularity.

The comoving angular diameter of an object at the time of decoupling can again be expressed as

$$d_A = \int_0^{z_{dec}} \frac{dz}{H(z)}\,, \tag{1.15}$$

By using the Eq.1.9 one can numerically estimate

$$\chi_{ph}(t_{dec}) = \tau(t_{dec}) - \tau(0)\,,\; d_A = \tau(0) - \tau(z_{dec})\,. \tag{1.16}$$

Plugging the expression, one numerically evaluates the angle $\theta_{hor} \sim 1.16°$. Based on causality, one should not expect to have any correlation when $\theta > 2\theta_{hor} \sim 2.3°$. Therefore, the main conflict with observation is why the correlation in CMB exists even for $\theta \geq 2°$.
Furthermore, on a large scale, the tiny temperature anisotropy measured in the CMB has a nearly scale-invariant power spectrum (for this instance, see Fig.1.3). Such fluctuation in temperature can be explained in terms of tiny fluctuation in the matter density at the epoch of photon decoupling, and later such fluctuations act as a seed for large-scale structure formation. The standard Big-Bang cosmological scenario fails to describe the origin of such fluctuation in the density spectrum as well.

1.1.3 Solution of the Horizon Problem

It is clear from the above discussion that the horizon problem in the standard cosmology arises due to the growing Hubble sphere. A simple solution would be to introduce an additional phase

with a shrinking Hubble radius in the early universe, specifically before the usual standard Big-Bang. If the phase lasts long enough, the horizon problem can be avoided. The decreasing Hubble radius requires a strong energy condition violating phase $1+3\,\omega<0$, which implies

$$\frac{d}{dt}\,(aH)^{-1}<0\,. \tag{1.17}$$

Now, due to the shrinking Hubble radius, the standard Big Bang singularity is pushed toward a negative conformal time

$$\tau_i\propto\frac{2}{1+3\omega}\,a_i^{\frac{1}{2}(1+3\omega)}=-\infty \qquad \text{for}\ \ \omega<-\frac{1}{3}\,. \tag{1.18}$$

Therefore, the integration in Eqn. (1.13) is now controlled by the lower limit. Fig.1.4 shows the new conformal diagram by introducing an additional inflationary era. The widely separated points in CMB now get enough time to intersect before the conventional singularity point $\tau=0$. Thus the uniform structure of CMB is no longer a mystery. Further, now the standard initial singularity point indicates the time of reheating and the time both before and after $\tau=0$ exists. Due to the decreasing comoving Hubble radius, the large-scale re-entering of the present universe is inside the horizon before the end of the inflation (for this instance, see Fig. 3). *The period of inflation successfully solves the horizon problem.*

1.1.4 Solution of the Flatness problem

The flatness problem is closely related to the initial energy value problem of a Newtonian particle moving under gravity. In the context of the standard Big Bang, an important question is how one sets the initial energy of the uniformly distributed matter at the beginning. This can be clearly understood from the Friedmann equation 1.9 when written in terms of normalized energy density parameter $\Omega=\rho/\rho_c$ as

$$\Omega-1=\Omega_k=\frac{k}{a^2H^2}\,, \tag{1.19}$$

where $\rho_c=3M_p^2H^2$ is the critical energy density at any arbitrary time. The initial energy distribution will be determined by the unknown parameter k, which is the curvature of the special section measuring the deviation of Ω from unity. The recent observation of the anisotropy in CMB suggests $|\Omega_k|<0.005$ with the 95% CL at the present epoch. This can immediately be attributed to the near flatness of the special section. The natural solution could be to set $k=0$ without any physical reason, which is precisely the flatness problem of the standard Big-Bang scenario. However, insisting that k be non-zero but small in the present universe invites severe fine-tuning problems. Due to decreasing comoving Hubble radius $(aH)^{-1}$ going backward in time, Ω_k decreases with extreme precision. At the time of BBN, $|\Omega_K^{BBN}-1|<<10^{-17}$, considering $T_{BBN}\sim 1$ MeV and $z_{eq}\sim 10^3$. However, at GUT era with $T_{GUT}\sim 10^{16}$ GeV, it becomes $|\Omega_K^{GUT}-1|<<10^{-55}$. Thus, we must set the initial condition precisely; otherwise, the universe collapses or expands too fast before the large-scale structure can form. This issue in standard cosmology is known as *the flatness problem.*

As we mentioned earlier, the curvature $|1-\Omega|$ is related to the evolution of the comoving Hubble radius $(aH)^{-1}$, and whenever it increases with time, curvature grows. In contrast with the standard evolution, during inflation, $(aH)^{-1}$ decreases, and the universe is moved towards flatness. Hence including inflation, we can precisely set the initial conditions that solve the flatness problem. During inflation, the solution of $\Omega=1$ is an attractor type.

1.1.5 Conditions for inflation

What we observed in our previous discussion is that particularly the decreasing behavior of the comoving Hubble sphere seems to be the defining property of inflation which can simultaneously resolve the horizon and the flatness problem. In this section, we will elaborate on this and further understand the details behavior of the inflationary phase. The decreasing Hubble radius implies accelerated expansion,

$$\frac{d}{dt}(aH)^{-1} = \frac{d}{dt}(\dot{a})^{-1} = -\frac{\ddot{a}}{(\dot{a})^2} < 0 \qquad \Rightarrow \ddot{a} > 0\,. \tag{1.20}$$

For our latter purpose, let us define a new parameter called slow roll parameter ϵ as

$$\frac{d}{dt}(aH)^{-1} = -\frac{1}{a}(1-\epsilon)\,, \qquad \text{where } \epsilon \equiv -\frac{\dot{H}}{H^2} > 0\,. \tag{1.21}$$

The nomenclature of the parameter ϵ can be understood from the perspective of the matter field, which will be responsible for the inflation to occur. The decreasing comoving horizon then corresponds to

$$\epsilon = -\frac{\dot{H}}{H^2} = -\frac{d\,lnH}{dN} < 1 \tag{1.22}$$

where we define another parameter called inflationary e-folding number N, which measures the magnitude of expansion and is defined as

$$N = \int d\,lna = \int H\,dt\,. \tag{1.23}$$

So far, we have discussed and defined the geometric quantities of inflationary spacetime. However, all these properties can be translated into the properties of the energy-momentum tensor, which needs to follow by the matter field. One of the Friedmann equations is

$$\dot{H} + H^2 = -\frac{1}{6M_p^2}(\rho + 3P) = -\frac{H^2}{2}\left(1 + 3\frac{P}{\rho}\right)\,. \tag{1.24}$$

Inserting the above Eqn.(1.24) in the expression of ϵ, one can find

$$\epsilon = \frac{3}{2}\left(1 + \frac{P}{\rho}\right) < 1\,, \tag{1.25}$$

which implies $w = \frac{P}{\rho} < -1/3$. Therefore, the most important conclusion we arrived at from the condition of inflation is that the matter field which can lead to inflaton is required to produce negative pressure in the system.

1.1.6 Duration of inflation

From our discussion so far, it is understood that inflation can successfully resolve the standard cosmological problems. A natural question now is what should be the duration of the inflation to solve the Horizon problem. The straightforward answer is that to solve the Horizon problem,

the comoving Hubble radius at the beginning of the universe $(a_I H_I)^{-1}$ must be greater than the observed universe today

$$(a_I H_I)^{-1} > (a_0 H_0)^{-1} \,. \tag{1.26}$$

After the end of the inflation, taking only the radiation domination still present day, the ratio between the comoving Hubble radius at the end of the inflation and toady be

$$\frac{a_0 H_0}{a_{end} H_{end}} \sim \frac{a_{end}}{a_0} = \frac{T_0}{T_{end}} \sim 10^{-28} \,. \tag{1.27}$$

To estimate the above number, we consider the evolution of the Hubble parameter as $H \propto a^{-2}$ due to radiation domination after inflation. Further, use has been made of the straightforward relation between the scale factor and the radiation temperature T as $a(t) \propto 1/T$. The temperature at the end of the inflation is approximately assumed as $T_{end} \sim 10^{15}$ GeV and the present-day CMB temperature as $T_0 = 10^{-3}$ eV. The Eqn.(1.26) suggests that

$$(a_I H_I)^{-1} > (a_0 H_0)^{-1} \sim 10^{28} \, (a_{end} H_{end})^{-1} \,, \tag{1.28}$$

which implies $\frac{a_{end}}{a_I} > 10^{28}$. Therefore, the crude estimation of the e-folding number during inflation must be $N = ln(\frac{a_{end}}{a_I}) > 64$ or in other words, to solve the Horizon problem successfully, inflation requires roughly 60 e-folds.

1.2 Inflationary dynamics and setting the background for reheating

In this section, we consider the most common model of single-field inflation where a scalar field, the inflaton ϕ, drives the inflation. The value of the field ϕ depends on both position in space ($\vec{x}$) and time. Each field value has an associated potential energy density $V(\phi)$. As the field value changes with time, it also has a kinetic energy density. Consider a scalar field, the inflaton ϕ, minimally coupled to Einstein's gravity with the canonical kinetic term, the action reads

$$S = \int d^4x \sqrt{-g} \left[\frac{M_p^2}{2} R - \frac{1}{2} g^{\mu\nu} \partial_\mu \phi \partial_\nu \phi - V(\phi) \right] + S_{matter} \tag{1.29}$$

where $V(\phi)$ is an arbitrary function and four-dimensional Ricci scalar R derived from the metric $g^{\mu\nu}$. S_{matter}, the matter action term includes the complete information concerning the other components of the matter sector, such as the terms representing the couplings between the inflaton to other sectors, including the Standard Model Lagrangian. At the background label, our universe is isotropic and homogeneous on a large scale. Hence, to solve the inflationary dynamics, one can safely assume all the background fields are only time-dependent. From the Euler-Lagrange equation for the inflaton field, inflaton field follows the following equation,

$$\ddot{\phi} + 3H\dot{\phi} - \frac{\vec{\nabla}\phi}{a^2} + V'(\phi) = 0 \,, \tag{1.30}$$

where $V'(\phi) = \frac{dV(\phi)}{d\phi}$. The energy-momentum tensor of the scalar field can be written as

$$T_{\mu\nu} = \partial_\mu \phi \partial_\nu \phi - g_{\mu\nu} \left(\frac{1}{2} g^{\alpha\beta} \partial_\alpha \phi \partial_\beta \phi - V(\phi) \right) . \tag{1.31}$$

The energy density ρ_ϕ and pressure density P_ϕ can be calculated from the time-time and space-space component of the stress-energy tensor accordingly, as

$$\rho_\phi = T^0{}_0 = \frac{1}{2}\dot{\phi}^2 + V(\phi) + \frac{(\nabla\phi)^2}{2a^2} \tag{1.32}$$

$$P_\phi = \frac{T^i{}_i}{3} = \frac{1}{2}\dot{\phi}^2 - V(\phi) - \frac{(\nabla\phi)^2}{6a^2}\,. \tag{1.33}$$

Homogeneity and isotropy condition infers that the dominating component of the scalar field should be the function of t only, and the inflaton condensate delivers a classical background during the inflation as well as at the initial stage of reheating. Thus the energy density and pressure of the homogeneous scalar field can be simply written as

$$\rho_\phi = \frac{1}{2}\dot{\phi}^2 + V(\phi),\; P_\phi = \frac{1}{2}\dot{\phi}^2 - V(\phi)\,. \tag{1.34}$$

From the above expression, we can immediately realize that in order to have inflation, one needs to satisfy $V(\phi) >> \dot{\phi}^2$ such that $P_\phi \sim -\rho_\phi$ or, in other words, potential energy dominates over the kinetic energy drives the inflation. Upon substitution of the evolution equation of ρ_ϕ (Eqn.1.34) into the Friedmann equation (Eqn.1.7), one can find

$$H^2 = \frac{1}{3M_p^2}\left(\frac{1}{2}\dot{\phi}^2 + V(\phi)\right) \tag{1.35}$$

Now, the Euler-Lagrangian equation for ϕ, which is also known as the Klein Gordon equation, turns out as

$$\ddot{\phi} + 3H\dot{\phi} + V'(\phi) = 0\,, \tag{1.36}$$

where the $V'(\phi)$ term acts as a force, and the expansion of the universe $H\dot{\phi}$ leads to friction.

1.2.1 Slow-roll inflation

We have already derived the equation of motion of the inflaton (Klein-Gordon equation) and have shown how the accelerated expansion is possible. Combining the Klein-Gordan equation Eqn. (1.36) together with the Friedmann equation Eqn. (1.35), we can derive the continuity equation as

$$\dot{H} = -\frac{1}{2}\frac{\dot{\phi}^2}{M_p^2}\,, \tag{1.37}$$

Upon substitution of the above equation into the definition of ϵ (Eqn.(1.22)), one can find

$$\epsilon = \frac{1}{2}\frac{\dot{\phi}^2}{M_p^2 H^2}\,. \tag{1.38}$$

During inflation $\epsilon < 1$, implies that the kinetic term makes a small contribution to the total energy density. This is the necessary condition for inflation, referred to as the slow-roll condition justifying its name we have introduced before.
This is not enough to have met such a slow roll condition, and it further needs to persist long enough period of time so that one obtains sufficient inflationary e-folding number mentioned

before. Hence, dynamics have to be highly damped, and thus we require another slow roll condition associated with the change of ϵ itself,

$$|\eta| = \frac{|\dot{\epsilon}|}{H\epsilon} = \frac{dln\epsilon}{dN} = 2\frac{\ddot{\phi}}{H\dot{\phi}} - 2\frac{\dot{H}}{H^2} = 2(\epsilon - \delta) < 1, \tag{1.39}$$

where δ defined as the dimensionless acceleration per Hubble time $\delta = -\frac{\ddot{\phi}}{H\dot{\phi}}$ and both $\{\epsilon, |\delta|\} << 1$, indicates $\{\epsilon, |\eta|\} << 1$. Therefore to make inflation happen and persists $\{\epsilon, |\delta|\} << 1$, this is the so-called slow roll approximation. The slow-roll condition indicates the following simplification in the Friedmann and Klein-Gordon equation

$$H^2 \simeq \frac{V(\phi)}{3M_p^2}, \, 3H\dot{\phi} \simeq V'(\phi)\,. \tag{1.40}$$

Substituting the above equation Eqn.(1.40) into (1.38), one can find

$$\epsilon = \frac{M_p^2}{2}\left(\frac{V'(\phi)}{V(\phi)}\right)^2 \quad ; \quad \eta \simeq M_p^2\frac{V''(\phi)}{V(\phi)}. \tag{1.41}$$

The total e-folding number of accounting accelerated expansion

$$N = \int_{a_{ini}}^{a_{end}} d\,lna = \int_{t_{ini}}^{t_{end}} H(t)dt\,, \tag{1.42}$$

where a_{ini} and a_{end} are the scale factor associated with beginning of inflation at t_{ini} and end of inflation (set by the condition $\epsilon(t_{end}) = 1$) respectively. In the slow-roll regime, we can write the e-folding number before the inflation end be

$$N = \int_{\phi_{ini}}^{\phi_{end}} \frac{1}{\sqrt{2\epsilon}}\frac{d\phi}{M_p}\,. \tag{1.43}$$

ϕ_I and ϕ_{end} are the field values defined at the boundaries.
In the later part of this chapter, we consider various inflationary models and calculate inflationary quantities. To get an understanding about the motion of the inflaton field, we consider specific form of the potential as $V(\phi) = \frac{1}{2}m^2\phi^2$ (chaotic inflation model [3]). For slow roll, inflaton field assumes the super-Planckian value $\phi > \sqrt{2}M_p \equiv \phi_{end}$. The approximate analytic expression of the slow-roll trajectory and the expansion takes the following expression

$$\dot{\phi} \simeq -\sqrt{\frac{2}{3}}M_p m, \;\; a \simeq a_{ini}\, exp\left[\frac{mt}{\sqrt{6M_p}}\left(\phi_{ini} - \frac{M_p m}{\sqrt{6}}t\right)\right]. \tag{1.44}$$

This is obviously valid within the slow-roll regime but for a broad range of initial values ϕ_{ini} leading to an inflation solution as an attractor.

1.2.2 End of inflation and beginning of reheating

Successful inflation must feature a graceful exit into the deacceleration stage in order to get back to the standard cosmology. In the chaotic inflation model, the graceful exit problem can be avoided naturally. The inflationary phase comes to an end dynamically once the slow

roll condition is violated and the homogeneous inflaton field starts to oscillate around its minimum. Assuming quadratic inflaton potential considered above, one can immediately obtain the approximate oscillatory solution as

$$H \simeq \frac{2}{3t}\left(1+\frac{sin\,(2mt)}{2mt}\right), \tag{1.45}$$

$$\phi \simeq \frac{2\sqrt{2}M_p\,cos(mt)}{\sqrt{3}mt}\left(1+\frac{sin\,(2mt)}{2mt}\right). \tag{1.46}$$

Detailed study of this phase is our main objective of the present thesis. The inflation itself is not the complete story of the early universe. Even though it successfully inflates the universe, the problem arises with connecting the inflationary phase with the standard Big-Bang Nucleosynthesis (BBN), which happens later with a comparatively lower energy scale in the radiation-dominated era. This is where the story becomes even more non-trivial. After the inflation end, the space becomes empty except homogeneous distribution of inflaton fields. Then, our natural mechanism would be to transfer the inflaton energy in order to set the ideal initial condition for the standard big-bang Nucleosynthesis (BBN). Hence, the inflaton has to decay through dynamical processes called reheating, which essentially bridges the two distinct phases of inflation and the standard radiation domination. The oscillating scalar field after the end of inflation behaves like the classical background, which will decay into radiation. Depending upon the inflaton coupling strength with the radiation field, inflaton can decay through both perturbative or non-perturbative channels, and consequently, the duration of reheating can be long or short. Such behaviors are expected to leave their imprints on various cosmological observables, which will be discussed throughout the thesis. In this thesis, we will mainly focus on the perturbative decay of inflaton, and it is called perturbative reheating. Our primary goal of this section would be to introduce the perturbative reheating scenario briefly. During reheating, the Hubble expansion of the universe will be mainly dominated by the oscillating homogeneous scalar field with a generic form of the inflaton potential $V(\phi) \propto |\phi|^{2n}$ near its minimum. Since the expansion time scale is always greater than the oscillation time scale of the inflaton, in the perturbative limit, the expansion can be generically described by an effective inflaton equation of state ω_ϕ averaging over the single oscillation. Multiplication of the Kelin-Gordan equation (Eqn.1.36) by ϕ and averaging over one oscillation, we can find

$$\langle\dot{\phi}^2\rangle \simeq \langle\phi V'(\phi)\rangle\,. \tag{1.47}$$

The energy and pressure density using the above estimation (Eqn.1.47) leads to

$$\rho_\phi \simeq \frac{1}{2}\langle\dot{\phi}^2\rangle + \langle V(\phi)\rangle = (n+1)\,\langle V(\phi)\rangle\,, \tag{1.48}$$

$$P_\phi \simeq \frac{1}{2}\langle\dot{\phi}^2\rangle - \langle V(\phi)\rangle = (n-1)\,\langle V(\phi)\rangle\,, \tag{1.49}$$

which implies the average inflaton equation of state

$$\omega_\phi = \left(\frac{n-1}{n+1}\right). \tag{1.50}$$

For quadratic type potential, $n=1$, the equation of state behaves as non-relativistic matter like $\omega_\phi = 0$. Whereas, for quartic type potential $n=2$, the equation of state behaves as radiation-like $\omega_\phi = 1/3$. When $n \leq 1/2$, $\omega_\phi \leq -1/3$ which implies that the universe inflates as $\ddot{a} > 0$. However, Oscillations about minima always lead to a decelerating universe with $\omega > -1/3$.

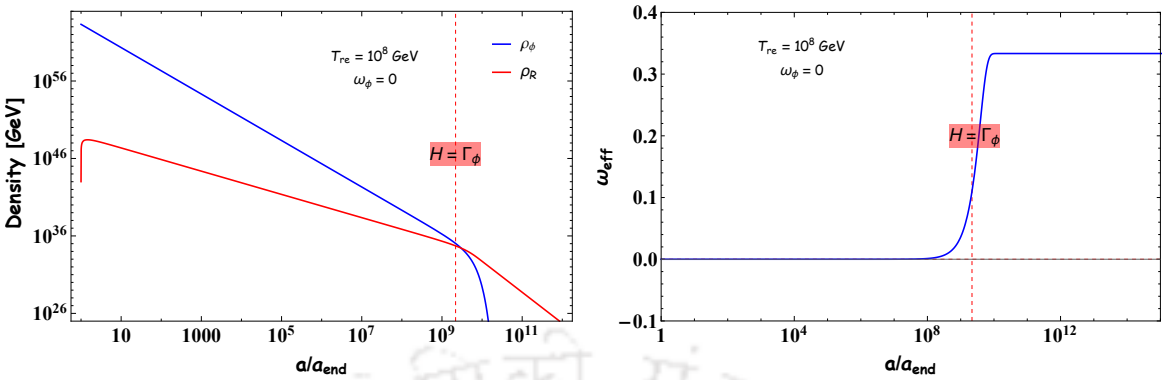

FIGURE 1.5: **Left panel:** The evolution of inflaton and radiation energy densities as a function of normalized scale factor with $T_{re} = 10^8$ GeV and $\omega_\phi = 0$. **Right panel:** Variation of the effective equation of state ω_{eff} as a function of normalized scale factor with same reheating paremeters as left panel.

1.2.3 Perturbative reheating dynamics

In conventional reheating studies, we typically consider the perturbative reheating scenario ([4]). In such a scenario, after the inflation end, the inflaton energy density ρ_ϕ, gradually disintegrates into the radiation energy density ρ_R following the Boltzmann equations. Consequently, the effective EoS parameter during the reheating phase becomes time-dependent (for this instance, see right panel of Fig. 1.5). In our analysis below, for simplicity, we shall consider that the EoS parameter ω_ϕ of the inflaton field during the phase of reheating remains constant.
The primary idea of perturbative reheating can be illustrated with the following phenomenological equations for inflaton decaying into daughter fields containing only the massless radiation particles. [5–8]

$$\dot{\rho}_\phi + 3H(1+w_\phi)\rho_\phi = -\Gamma_\phi(1+w_\phi)\rho_\phi \tag{1.51}$$
$$\dot{\rho}_R + 4H\rho_R = \Gamma_\phi(1+w_\phi)\rho_\phi\,. \tag{1.52}$$

supplemented with the Hubble equation $H^2 = (\rho_\phi + \rho_R)/3M_p^2$. The phenomenological decay width Γ_ϕ is introduced, which will govern the entire process of transferring inflaton energy with density (ρ_ϕ) to radiation energy with density (ρ_R). After the decay process is completed, the daughter/radiation field will thermalize, and the reheating phase is set to end. The end of reheating is typically identified with the condition $\Gamma_\phi = H$ that indicates the point where the decay term starts to dominate over expansion. Hence, the decay process will be completed within a short time scale after this point (for better understanding, see Fig. 1.5). Once the inflaton equation of state is given, considering the evolution of $\rho_\phi + \rho_{rad} = \rho_{eff}$ together, we can define the effective equation of state during reheating as

$$\omega_{eff} = \left\langle \frac{3p_\phi + \rho_R}{3(\rho_\phi + \rho_R)} \right\rangle . \tag{1.53}$$

Hence, ω_{eff} will essentially lie between $(\omega_\phi, 1/3)$ through non-trivial dynamics for decaying inflaton ρ_ϕ and the increasing radiation field ρ_R (see right panel of Fig. 1.5).

During this process, if one assumes the produced radiation to be instantaneously thermalized, the associated radiation temperature T can be obtained from the Stefan-Boltzmann law,

$$\rho_R = \left(\frac{\pi^2}{30}\right) g_{re} T^4 \,. \tag{1.54}$$

Where g_{re} represents the effective degrees of freedom associated with the radiation bath calculated at the end of the reheating. Assuming Γ_ϕ is a constant parameter, and the inflation equation of state $w_\phi = 0$ throughout reheating, the expression for the inflaton energy density turns out to be

$$\rho_\phi(t) = \rho_\phi^{end} \left(\frac{a}{a_{end}}\right)^{-3} e^{\Gamma_\phi (t - t_{end})}, \tag{1.55}$$

where $\rho_\phi^{end} \sim V(\phi_{end})$ represents total inflaton energy density at inflation end. $V(\phi_{end})$, a_{end} are the value of the potential and scale factor at inflation end. The scale factor varies as $a(t) \propto t^{2/3}$ and Hubble parameter $H(t) = 2/3t$ during the reheating phase dominated by the matter equation state. Using those relations, one can estimate the radiation component as

$$\rho_{\rm R}(t) \simeq \frac{3}{5} \rho_\phi^{end} \left(\frac{t}{\tau_\phi}\right) \left[1 - \left(\frac{t_{end}}{t}\right)^{\frac{5}{3}}\right], \tag{1.56}$$

where τ_ϕ is the inflaton decay time identified as $\tau_\phi \equiv \Gamma_\phi^{-1}$. The initial condition for the radiation component set as $\rho_{\rm R} = 0$. The evolution of both inflaton and the radiation energy density as a function of the normalized scale factor is shown in the left panel of Fig. 1.5. From Fig. 1.5, we can see that starting with zero; the radiation component quickly gets to a maximum value just after the inflation ends and then decreases due to the universe's expansion, and the rate of decrease changes when the decay term is comparable with the expansion rate. From the definition of the temperature given in Eq. (1.54), we can determine the maximum possible radiation temperature as

$$T_{\rm max} \sim g_{re}^{-\frac{1}{4}} V(\phi_{end})^{\frac{1}{8}} (M_p \, \Gamma_\phi)^{\frac{1}{4}} \tag{1.57}$$

The inflaton decay will be complete at the instant when $t = 1/\Gamma_\phi$ at $H \sim \Gamma_\phi$. Thus, one can determine the reheating temperature T_{re} from the radiation temperature at the end of reheating as

$$H = \Gamma_\phi \simeq \frac{\rho_R^{\frac{1}{2}}}{\sqrt{3} M_p} \simeq \left(\frac{\pi \sqrt{g_{re}}}{90^{\frac{1}{2}}}\right) \frac{T_{\rm re}^2}{M_p} \,. \tag{1.58}$$

From the above equation, one can express reheating temperature in terms of decay width as

$$T_{re} = \left(\frac{90}{g_{re} \pi^2}\right)^{\frac{1}{4}} \sqrt{\Gamma_\phi M_p} \,. \tag{1.59}$$

Another important reheating parameter is the reheating e-folding number N_{re}, which provides the information about the duration of reheating, expressed as

$$N_{re} = \log\left(\frac{a_{re}}{a_{end}}\right) \tag{1.60}$$

where a_{re} is the scale factor at reheating end. There are some possible values of T_{re}

$$10\,\mathrm{MeV} \lesssim T_{\mathrm{re}} \lesssim V(\phi_{end})^{\frac{1}{4}} \tag{1.61}$$

where the lower bound is from the BBN constraints, and the inflationary energy scale sets the upper bound. Still, now there is no such cosmological observable that can directly constrain the reheating phase. Accordingly, we have to depend on indirect measurements such as CMB, dark matter, primordial gravitational wave, primordial magnetic field, etc., which is one of the main goals of the thesis.

1.2.4 When perturbative reheating is valid?

We have discussed the decay of the inflaton into radiation by an effective phenomenological decay width Γ_ϕ. In this section, our essential plan is to discuss its origin briefly in terms of fundamental interaction and the possible limits on the inflaton decay where perturbative reheating is possible. However, non-perturbative particle production mechanisms can not be ignored during reheating if the coupling is strong enough. Consequently, let us note the parameter space in which the perturbative mechanism of reheating will work well over the non-perturbative one. In the following discussion, we assume a few fundamental interactions and the possible limits:

1.2.4.1 Scalar $\phi\chi^2$ interaction

Let's start our discussion with the case where inflaton decays into pair of scalar particles $\phi \to \chi\chi$ with the interaction term as follows $\mathcal{L} = -g\phi\chi^2$. In this case, we can calculate the vacuum decay width of the inflaton in terms of coupling parameter as [9]

$$\Gamma_{\phi\to\chi\chi} = \frac{g^2}{8\pi m_\phi}\sqrt{1-\left(\frac{2m_\chi}{m_\phi}\right)^2} \simeq \frac{g^2}{8\pi m_\phi}, \tag{1.62}$$

where m_ϕ, m_χ are identified as the mass of the inflaton and produced daughter particle, accordingly, and g represents the coupling constant. The mode function for the produced particle χ_k can follow the Mathieu equation,

$$\ddot{\chi_k} + (A_k - 2q\cos(2z))\chi_k = 0. \tag{1.63}$$

Where, $z = (m_\phi t - 2z - \pi/2)$, $A_k = 4k^2/m_\phi^2$, $q = 4g\Phi/m_\phi^2$. The amplitude of the inflaton field at the start of the oscillation is represented by Φ. The solution to the above Mathieu equation turns out as $\chi_k \propto exp(\mu_k z)$. The resonance is effective as long as

$$q^2 m \gtrsim H \tag{1.64}$$

From the resonance condition, one can estimate the validity of perturbative reheating in terms of the dimensionless coupling constant $\tilde{g} = g/m_\phi$ as * [10]

$$\tilde{g} \leq \frac{V_{end}^{\frac{1}{4}}}{\phi_{end}}\left(\frac{m_\phi}{24M_p}\right)^{\frac{1}{2}}, \tag{1.65}$$

*The initial amplitude Φ can be replaced by ϕ_{end}, the field value at the end of inflation, which essentially denotes a lower bound on the inflaton decay width

which further can be expressed in terms of the decay constant as

$$\Gamma_\phi \leq \frac{V_{end}^{\frac{1}{2}}}{\phi_{end}^2}\left(\frac{m_\phi^2}{192\pi M_p}\right) \implies \Gamma_\phi^{cri}(\text{model}) = \frac{V_{end}^{\frac{1}{2}}}{\phi_{end}^2}\left(\frac{m_\phi^2}{192\pi M_p}\right) \tag{1.66}$$

Thus, if the decay width fulfills the above condition, the reheating dynamics are governed by only the perturbative scenario. Once we fixed the model $\Gamma_\phi^{cri}(\text{model})$ qualitatively separates the non-perturbative and perturbative regions.

1.2.4.2 Scalar $\phi\chi^3$ interaction

In this case, we assume three-body decay of the inflaton and interaction Lagrangian leads

$$\mathcal{L} = -y\phi\chi^3 \quad , \tag{1.67}$$

where the coupling constant is y. For the three-body decays of the inflaton field $\phi \to \chi\chi\chi$ vacuum decay width associated with inflaton can be calculated by Dalitz plot [11] as,

$$\Gamma_{\phi\to\chi\chi\chi} = \frac{y^2 m_\phi}{3!64\,(2\pi)^3} \quad . \tag{1.68}$$

The mode function, χ_k, is determined from the same Mathieu equation. Therefore, the previous analysis for $\phi\chi^2$ interaction can be correlated if we replace $\tilde{g}m_\phi\Phi \to h^2\Phi^2$ and the condition on the perturbative reheating turns out as

$$q \backsim \frac{y^2\Phi^2}{m_\phi^2} \leq 1 \quad . \tag{1.69}$$

The lower bound on the coupling parameter for resonance can be computed under the substitution $\Phi \to \phi_{end}$. The significance of the perturbative reheating is followed by the above equation and can be illustrated in terms of decay rate as,

$$\Gamma_\phi \leq \frac{m_\phi^3}{3!64\,(2\pi)^3\,\phi_{end}^2} \implies \Gamma_\phi^{cri}(\text{model}) = \frac{m_\phi^3}{3!64\,(2\pi)^3\,\phi_{end}^2} \tag{1.70}$$

1.2.5 Inflaton decaying into a pair of fermions

Let us move our discussion to another possibility where the inflaton field decays into massless fermions obeying the following Yukawa interaction

$$\mathcal{L}_{int} = -h\phi\bar{\psi}\psi \quad , \tag{1.71}$$

here, h denotes the dimensionless coupling constant. The vacuum decay width is shown as

$$\Gamma_{\phi\to\bar{\psi}\psi} = \frac{h^2 m_\phi}{8\pi} \quad . \tag{1.72}$$

In this scenario, the validity condition for the perturbative reheating, as shown in [12], can be expressed as [12],

$$q = \frac{h^2\Phi^2}{m_\phi^2} \leq 1 \quad . \tag{1.73}$$

Therefore, concerning the decay rate, the equation (5.3) is written as,

$$\Gamma_\phi \leq \frac{m_\phi^3}{\phi_{end}^2\,(8\pi)} \quad \Longrightarrow \; \Gamma_\phi^{cri}(\text{model}) = \frac{m_\phi^3}{\phi_{end}^2\,(8\pi)} \tag{1.74}$$

In our discussion in chapter-2, we proposed a Two-phase reheating scenario where we can identify a similar critical decay at the transition point of effective non-perturbative dynamics to the perturbative. There we will also examine whether the above conditions for different decay channels are consistent with our analysis or not.

1.2.6 Cosmological perturbations from inflation

During inflation, tiny fluctuations originate from the quantum effects, considered to be the source of the large-scale structure of our observable universe. Until now, we have assumed $\phi(t)$, the inflaton field as the homogeneous field in the FLRW background. Nonetheless, the quantum fluctuations will show inhomogeneities. As long as these inhomogeneities are considered to be small, we can apply the perturbation theory, then the inflaton field reads

$$\phi(\mathbf{x}, t) = \phi(t) + \delta\phi(\mathbf{x}, t). \tag{1.75}$$

Due to these small fluctuations in the field, the inflation will end at different times in the different regions of space. Thus, the different regime will inflate differently, and, as a result, a small inhomogeneous energy density distribution $\delta\rho(\mathbf{x})$ appear. This small density fluctuation can be explained by the observed temperature fluctuations in the Cosmic microwave background.

$$\delta\phi(\mathbf{x}, t) \rightarrow \delta\rho(\mathbf{x}, t) \rightarrow \Delta T(\mathbf{x}) \tag{1.76}$$

In the following subsections, we will investigate the dynamics of these perturbations in the standard inflationary background [13–18]. The inhomogeneities observed in the CMB are extremely small around $\Delta T/T \simeq \mathcal{O}(10^{-5})$, which implies that at the time of CMB decoupling, the universe can be treated as nearly homogeneous and the inhomogeneities are small enough to be estimated with the linear order perturbation theory. Expanding the Einstein equations to the first order, we can analyze the evolution of those perturbations

$$\delta G_{\mu\nu} = 8\pi\, G \delta T_{\mu\nu} \tag{1.77}$$

The above equation indicates that we can consider the perturbation metric and matter field separately. We will discuss the basics of perturbation theory in the following discussion.

1.2.7 Metric perturbation

Energy and matter are the leading sources of curvature in spacetime geometry, and fluctuations in the matter field, as given in Eq. (1.75) will generate fluctuations in the metric. Therefore it is essential to compute the effect of those small fluctuations on the homogeneous background of our universe. This section will first discuss the general form of perturbation and its essential properties. The general form of the metric perturbation can be parameterized as

$$\mathrm{d}s^2 = (1 + 2\Phi)\,\mathrm{d}t^2 - 2a(t)B_i\,\mathrm{d}t\,\mathrm{d}x^i - a^2(\delta_{ij} + h_{ij})\,\mathrm{d}x^i\,\mathrm{d}x^j \tag{1.78}$$

In accord with their behavior under the local spatial rotation group, the 10 degrees of freedom of the perturbation $\delta g_{\mu\nu}(\mathbf{x})$ can be decomposed into the scalar vector and tensor components.

$$\delta g_{\mu\nu} \equiv \Big(\delta g_{00}, \delta g_{0i}, \delta g_{ij}\Big) \tag{1.79}$$

We can write this more explicitly as

- 4 scalar degrees of freedom $\rightarrow \delta g_{00} \equiv \Phi$.
- 4 divergence-less vector degrees of freedom $\rightarrow (\widehat{B}_i, \widehat{E}_i)$. One of which appears as follows,

$$\delta g_{0i} \equiv B_j = \underbrace{\partial_j B}_{scalar} + \underbrace{\widehat{B}_j}_{vector} \quad \text{where} \quad \partial_j \widehat{B}_j = 0.$$

- 2 divergence-less and trace-less tensor degrees of freedom $\rightarrow \delta g_{ij} \equiv h_{ij}$

$$h_{ij} = 2\Psi\delta_{ij} + 2\partial_i\partial_j E + \Big(\partial_i \widehat{E}_j + \partial_j \widehat{E}_i\Big) + 2\widehat{h}_{ij} \quad \text{where} \quad \partial^i \widehat{E}_i = \partial^i \widehat{h}_{ij} = \widehat{h}^i_i = 0.$$

The benefit of such a decomposition is at the linear level. With the help of the linearized Einstein equation, we can examine the evolution of those three classes of perturbations independently. It is easy to represent the scalar-vector-tensor(SVT) decomposition in Fourier space. Henceforth, the Fourier decomposition of fluctuations can be written as

$$X_{\mathbf{k}} = \int \mathrm{d}^3\mathbf{x} X(t,\mathbf{x}) e^{i\mathbf{k}\cdot\mathbf{x}} \quad \text{where,} \quad X \equiv (\delta\phi, \delta g_{\mu\nu}, \cdots) \tag{1.80}$$

Under the consideration of linear perturbation theory, the main outcome is that the vector perturbation only contains a decaying mode [19], which is also predicted from the general coordinate invariance since the gravity sector only holds two propagating degrees of freedom. Accordingly, we will bypass vector mode throughout our analysis. To move our discussion further, let us represent the transformation properties of fluctuation modes with the coordinate transformation $(t \rightarrow t + \alpha,\ x^i \rightarrow x^i + \beta^{,j})$ as

$$\begin{aligned}
\Phi &\rightarrow \Phi - \dot{\alpha}, \\
B &\rightarrow B + \frac{\dot{\beta}}{a} + \frac{1}{a}\alpha, \\
\Psi &\rightarrow \Psi + H\alpha, \\
E &\rightarrow E + \frac{\beta}{a^2}, \\
\widehat{h}_{ij} &\rightarrow \widehat{h}_{ij}.
\end{aligned} \tag{1.81}$$

The transformations convey that all the perturbation variables are not physical or gauge dependent. As an example, $\widehat{h}_{ij}$ is a gauge-invariant perturbation. However, these transformation properties will help us determine the gauge-invariant perturbation variable that we eventually specify as the curvature perturbation observed in the Cosmic microwave background. Before defining those physical perturbations, let us discuss the perturbation of energy-momentum tensor, particularly for inflaton.

1.2.8 Gauge invariant variable and power spectrum for scalar mode

Until now, we discussed different variables of perturbation and their transformation properties. Here, we assume a specific gauge-invariant quantity [19], named comoving curvature perturbation ($\mathcal{R}$) that is defined as

$$\mathcal{R} = \Psi - \frac{H}{\bar{\rho}+\bar{p}}\delta q\,, \tag{1.82}$$

where scalar part of the 3-momentum density is identified as δq that can be written as

$$T^0_i = \delta q_i = \partial_i \delta q + \widehat{\delta q}_i\,. \tag{1.83}$$

One can clearly notice that $\mathcal{R}$ is an invariant quantity under the general coordinate transformation. If we assume the homogeneous inflaton field, the momentum density comes out as $T^0_i = -\dot{\bar{\phi}}\partial_i\delta\phi$. Thus, the co-moving curvature perturbation follows the subsequent form,

$$\mathcal{R} = \Psi + \frac{H}{\dot{\bar{\phi}}}\delta\phi\,. \tag{1.84}$$

In order to proceed further, convenient way to assume a particular gauge

$$\delta\phi = 0, \quad g_{ij} = a^2\Big[(1-2\mathcal{R})\delta_{ij} + h_{ij}\Big], \quad \partial_i h_{ij} = h^i_i = 0\,. \tag{1.85}$$

The applicability of this choice is that, since in this gauge, the inflaton field is unperturbed, and $\mathcal{R}$ acts as a gauge-invariant quantity; all the other scalar perturbation (Φ, B) can be written in term of $\mathcal{R}(t,\mathbf{x})$ (see, for instance, Ref. [16]). Most significantly Ψ measures the three-curvature of the spatial section as $R^{(3)} = (1/3)\nabla^2\Psi$. Therefore in the gauge (1.85), one can write the quadratic action for comoving curvature perturbation $\mathcal{R}$ as

$$S_{(2)} = \frac{1}{2}\int \mathrm{d}^4x a^3 \frac{\dot{\phi}^2}{H^2}\Big[\dot{\mathcal{R}}^2 - \frac{1}{a^2}(\partial_i\mathcal{R})^2\Big]. \tag{1.86}$$

Taking the following *Mukhanov variable*

$$v = z\mathcal{R} \quad \text{with} \quad z^2 = 2a^2\frac{\frac{1}{2}\dot{\phi}^2}{H^2} = 2a^2\epsilon\,, \tag{1.87}$$

the equation of motion for each individual mode turns out to be

$$v_k'' + \Big(k^2 - \frac{z''}{z}\Big)v_k = 0. \tag{1.88}$$

Where "prime" represents derivative with respect to conformal time, the functions z in the overhead equation explicitly depend on the background dynamics; due to that, it is challenging to find a general solution analytically. Therefore, it is usually solved numerically. However, we can find a solution under various limits for inflationary background.

To calculate various correlation functions for this fluctuation, one must quantize this with proper boundary conditions. The steps are similar to the standard free field quantization process. We enable the mode functions $v_{\mathbf{k}}$ to quantum operator as

$$v_{\mathbf{k}} \to \widehat{v}_{\mathbf{k}} = v_{\mathbf{k}}(\eta)\widehat{a}_{\mathbf{k}} + v^*_{-\mathbf{k}}(\eta)\widehat{a}^\dagger_{-\mathbf{k}}\,, \tag{1.89}$$

where the creation and annihilation operators $\widehat{a}^{\dagger}_{-\mathbf{k}}$ and $\widehat{a}_{\mathbf{k}}$ are follow the standard canonical commutation relation.

$$\left[\widehat{a}_{\mathbf{k}}, \widehat{a}^{\dagger}_{-\mathbf{k}}\right] = (2\pi)^3\delta(\mathbf{k}-\mathbf{k}'), \tag{1.90}$$

given that the mode functions are normalized as

$$\left\langle v_k, v_k' \right\rangle \equiv \frac{i}{\hbar}(v_k^* v_k' - v_k^* v_k)\,. \tag{1.91}$$

The above condition delivers us the suitable boundary condition for the solution of Eq. (1.88). The *vacuum* or the ground state identified as

$$\widehat{a}_{\mathbf{k}}\,|0\rangle = 0\,. \tag{1.92}$$

To analyze the solution analytically and find the form of the spectrum, we assume the de Sitter limit $H = \text{const.}(\ \epsilon \to 0)$, which implies

$$\frac{z''}{z} = \frac{a''}{a} = \frac{2}{\eta^2}, \implies z \sim \frac{1}{\eta}\,, \tag{1.93}$$

and the expression for the mode function in (1.88) turns out to be

$$v_k'' + \left(k^2 - \frac{2}{\eta^2}\right)v_k = 0\,. \tag{1.94}$$

The exact solution of the above equation reads

$$v_k = \alpha\frac{e^{-ik\eta}}{\sqrt{2k}}\left(1 - \frac{i}{k\eta}\right) + \beta\frac{e^{ik\eta}}{\sqrt{2k}}\left(1 + \frac{i}{k\eta}\right). \tag{1.95}$$

The free parameters α and β represent the non-uniqueness of the mode functions and can be set uniquely in the subhorizon limit $|k\eta| \gg 1$ using the condition Eq. (1.91). These fixes $\alpha = 1,\ \beta = 0$, indicating the unique Bunch-Davies vacuum and the mode function,

$$v_k = \frac{e^{-ik\eta}}{\sqrt{2k}}\left(1 - \frac{i}{k\eta}\right) \implies v_k \propto \frac{1}{\eta}, \tag{1.96}$$

The last solution is the approximate one and is estimated in the super-horizon limit. At this present stage an essential result one can obtains for the super-horizon modes $|k\eta| \to 0$, $\mathcal{R}_k = z^{-1}v_k \to$ *constant*. Thus, co-moving curvature perturbation freezes out during inflation once they become super-horizon modes. This point will effectively give rise to the physical observables associated with various correlations of $\mathcal{R}_k$. The power spectrum is One such observable representing a two-point correlation function in momentum space. For simplicity assuming de Sitter limit, at the point of horizon crossing $a(t_k)H(t_k) = k$, the two-point correlation function of the curvature perturbation $\mathcal{R}_k = (Hv_k)/(\dot{\phi}a)$ behaves in the following manner

$$\langle \mathcal{R}_{\mathbf{k}}(t)\mathcal{R}_{\mathbf{k}'}(t)\rangle = (2\pi)^3\delta(\mathbf{k}+\mathbf{k}')\frac{H_k^2}{(2k^3)}\frac{H_k^2}{\dot{\phi}_k^2} = (2\pi)^3\delta(\mathbf{k}+\mathbf{k}')\bar{\mathcal{P}}_{\mathcal{R}}(k). \tag{1.97}$$

The dimensionless power spectrum $\mathcal{P}_{\mathcal{R}}(k)$ is generically expressed as

$$\bar{\mathcal{P}}_{\mathcal{R}}(k) = \frac{2\pi^2}{k^3}\mathcal{P}_{\mathcal{R}}(k), \tag{1.98}$$

with,

$$\mathcal{P}_{\mathcal{R}}(k) = \frac{H_k^2}{(2\pi)^2}\frac{H_k^2}{\dot{\phi}_k^2}. \tag{1.99}$$

We have computed the power spectrum under the de-Sitter approximation. if we assume all the quantities are slowly varying, then the scale dependence of the power spectrum is evaluated by spectral index n_s as

$$n_s - 1 = \frac{\mathrm{d}\ln\mathcal{P}_{\mathcal{R}}(k)}{\mathrm{d}\ln k} \simeq -6\epsilon_V + 2\eta_V. \tag{1.100}$$

We will be utilizing the second relation for the spectral index throughout our thesis.

We will explain how we will use this point to convey the CMB temperature with the primordial perturbation in Section 1.3.2. In the subsequent Sub-section, let us briefly discuss the tensor mode.

1.3 Spectrum of GWsgenerated during inflation

We start our discussion with a brief description of the equations governing the tensor perturbations and assuming de-sitter inflation to calculate the spectrum of GWs. Then we introduce the observational quantity of our interest, the dimensionless energy density of GWs.

1.3.1 Generation of GWs during inflation

The tensor perturbation is indicated by h_{ij} that represents the GWs in the FLRW universe. If we consider tensor perturbations, the line element of the spatially flat FLRW universe is given by [20]

$$\dot{s}^2 = a^2(\eta)\left\{-d\eta^2 + [\delta_{ij} + h_{ij}(\eta, \boldsymbol{x})]\ \dot{x}^i\dot{x}^j\right\}. \tag{1.101}$$

As the tensor perturbations are transverse and traceless, they must fulfill the conditions $\partial^i h_{ij} = 0$ and $h^i_i = 0$. We may assume that there is no anisotropic stress are present. In such a scenario, the equation of motion for tensor perturbations h_{ij} can be expressed as

$$h''_{ij} + 2\frac{a'}{a}h'_{ij} - \boldsymbol{\nabla}^2 h_{ij} = 0. \tag{1.102}$$

In the quantization process, the tensor perturbations may be decomposed in terms of the Fourier modes h_k in the following manner [14, 16, 17, 21–27]:

$$\begin{aligned}\hat{h}_{ij}(\eta, \boldsymbol{x}) &= \int \frac{d^3\boldsymbol{k}}{(2\pi)^{3/2}}\,\hat{h}^{\boldsymbol{k}}_{ij}(\eta)\,\mathrm{e}^{i\,\boldsymbol{k}\cdot\boldsymbol{x}} \\ &= \sum_{\lambda=+,\times}\int \frac{d^3\boldsymbol{k}}{(2\pi)^{3/2}}\left[\hat{a}^{\lambda}_{\boldsymbol{k}}\,\varepsilon^{\lambda}_{ij}(\boldsymbol{k})\,h_k(\eta)\,\mathrm{e}^{i\,\boldsymbol{k}\cdot\boldsymbol{x}} + \hat{a}^{\lambda\dagger}_{k}\,\varepsilon^{\lambda *}_{ij}(\boldsymbol{k})\,h^*_k(\eta)\,\mathrm{e}^{-i\,\boldsymbol{k}\cdot\boldsymbol{x}}\right],\end{aligned} \tag{1.103}$$

where $\varepsilon_{ij}^{\lambda}(\boldsymbol{k})$ indicates the polarization tensor, with the index λ representing the polarization $+$ or $\times$ of the GWs. The polarization tensor follows the relations $\delta^{ij}\,\varepsilon_{ij}^{\lambda}(\boldsymbol{k}) = k^{i}\,\varepsilon_{ij}^{\lambda}(\boldsymbol{k}) = 0$, with the normalization condition $\varepsilon^{ij\,\lambda}(\boldsymbol{k})\,\varepsilon_{ij}^{\lambda'*}(\boldsymbol{k}) = 2\,\delta^{\lambda\lambda'}$. The operators $(\hat{a}_{\boldsymbol{k}}^{\lambda}, \hat{a}_{\boldsymbol{k}}^{\lambda\dagger})$ represent the annihilation and creation operators associated with the wave vector $\boldsymbol{k}$. They shall attend the following commutation relations: $[\hat{a}_{\boldsymbol{k}}^{\lambda}, \hat{a}_{\boldsymbol{k}'}^{\lambda'}] = [\hat{a}_{\boldsymbol{k}}^{\lambda\dagger}, \hat{a}_{\boldsymbol{k}'}^{\lambda'\dagger}] = 0$ and $[\hat{a}_{\boldsymbol{k}}^{\lambda}, \hat{a}_{\boldsymbol{k}'}^{\lambda'\dagger}] = \delta^{(3)}(\boldsymbol{k}-\boldsymbol{k}')\,\delta^{\lambda\lambda'}$. Since there are no source of anisotropic stresses, the Fourier mode h_k fulfills the following differential equation

$$h_k'' + 2\,\frac{a'}{a}\,h_k' + k^2\,h_k = 0. \tag{1.104}$$

The tensor power spectrum $\mathcal{P}_{\mathrm{T}}(k)$ can be identified as

$$\langle 0|\hat{h}_{\boldsymbol{k}}^{ij}(\eta)\,\hat{h}_{ij}^{\boldsymbol{k}'}(\eta)|0\rangle = \frac{(2\,\pi)^2}{2\,k^3}\,\mathcal{P}_{\mathrm{T}}(k)\,\delta^{(3)}(\boldsymbol{k}+\boldsymbol{k}'), \tag{1.105}$$

where the vacuum state $|0\rangle$ is described as $\hat{a}_{\boldsymbol{k}}^{\lambda}|0\rangle = 0$ for all $\boldsymbol{k}$ and λ. By using the above decomposition, one can find

$$\mathcal{P}_{\mathrm{T}}(k) = 4\,\frac{k^3}{2\,\pi^2}\,|h_k|^2, \tag{1.106}$$

and the spectrum is calculated on super-Hubble scales during inflation. Inspired by the form of the second-order action which governs the tensor perturbation h_{ij}, the Fourier mode h_k is generally noted in terms of the Mukhanov-Sasaki variable u_k as $h_k = (\sqrt{2}/M_p)\,(u_k/a)$. The Mukhanov-Sasaki variable u_k can satisfy the following equation [14, 16, 17, 21–27]

$$u_k'' + \left(k^2 - \frac{a''}{a}\right)\,u_k = 0. \tag{1.107}$$

We shall focus our discussion on the slow-roll inflation and work with the de Sitter approximation, wherein the scale factor can be expressed as $a(\eta) = (1 - H_I\,\eta)^{-1}$, with H_I indicates the constant Hubble scale during the inflationary era. In such a scenario, $a''/a = 2\,H_I^2/\,(1 - H_I\,\eta)^2$, and to solve Eq. (1.107) we assume Bunch-Davies initial condition. The solution to Eq. (1.107) reads

$$u_k(\eta) = \frac{1}{\sqrt{2\,k}}\,\left[1 + \frac{i\,H_I\,a(\eta)}{k}\right]\,\mathrm{e}^{-i\,k\,\eta}. \tag{1.108}$$

Or, analogously, one can write

$$h_k(\eta) = h_k(a) = \frac{\sqrt{2}}{M_p}\,\frac{i\,H_I}{\sqrt{2\,k^3}}\,\left[1 - \frac{i\,k}{H_I\,a(\eta)}\right]\,\mathrm{e}^{-i\,k/H_I}\,\mathrm{e}^{i\,k/[H_I\,a(\eta)]} \tag{1.109}$$

where the above mentioned de Sitter form sets $a(\eta)$. Let us consider that the end of the inflationary era set at conformal time η_f such that $0 < \eta_f < H_I^{-1}$, and let $a_f = a(\eta_f)$. Upon using the conditions mentioned above, the tensor power spectrum at a_f is given by

$$\mathcal{P}_{\mathrm{T}}(k) = \frac{2\,H_I^2}{\pi^2\,M_p^2}\,\left(1 + \frac{k^2}{k_f^2}\right), \tag{1.110}$$

where the mode that exit the Hubble radius at the end of the inflation is identified as $k_f = a_f\,H_I$. For $k \ll k_f$, the above spectrum transforms to

$$\mathcal{P}_{\mathrm{T}}(k) \simeq \frac{2\,H_I^2}{\pi^2\,M_p^2}\,, \tag{1.111}$$

which is the standard scale-invariant spectrum explained in the scenario of de Sitter inflation [14, 16, 17, 21–27]. In the slow-roll inflationary models, the tensor power spectrum must contain a small spectral tilt that we have ignored in our discussion. Equivalent to the scalar spectral index, the tensor spectral index is identified as

$$n_{\rm T} \equiv \frac{{\rm d}\ln \mathcal{P}_{\rm T}(k)}{{\rm d}\ln k} = -2\epsilon \simeq -2\epsilon_V \,. \tag{1.112}$$

When normalized with respect to that of the scalar fluctuations, tensor fluctuations are known as a scalar to tensor ratio r, which is generally quoted in the context of cosmological observation,

$$r \equiv \frac{\mathcal{P}_{\rm T}(k)}{\mathcal{P}_{\mathcal{R}}(k)} = 16\epsilon \simeq 16\epsilon_V \,. \tag{1.113}$$

1.3.1.1 The dimensionless energy density of GWs

Let us move our discussion toward the main observable quantity of our interest, viz., the dimensionless energy density of the gravitational waves. We are interested in estimating the quantity over the wave number domain, which reenters the Hubble radius during reheating and radiation domination periods.

The energy density of GWs $\rho_{GW}(\eta)$ can be expressed as (see, for example, Refs. [20, 28])

$$\rho_{GW}(\eta) = \frac{M_p^2}{4\,a^2}\left(\frac{1}{2}\,\langle \hat{h}'^2_{ij}\rangle + \frac{1}{2}\,\langle |\boldsymbol{\nabla}\hat{h}_{ij}|^2\rangle\right), \tag{1.114}$$

$\rho_{GW}(k,\eta)$ is defined as the energy density per logarithmic interval and can be expressed as defined through the relation

$$\rho_{GW}(\eta) = \int_0^\infty d\ln k\; \rho_{GW}(k,\eta). \tag{1.115}$$

Utilizing mode decomposition Eqn.(1.103) together with the expressions for $\rho_{GW}(\eta)$, one can obtain $\rho_{GW}(k,\eta)$ as

$$\rho_{GW}(k,\eta) = \frac{M_p^2}{a^2}\,\frac{k^3}{2\,\pi^2}\left(\frac{1}{2}\,|h'_k(\eta)|^2 + \frac{k^2}{2}\,|h_k(\eta)|^2\right). \tag{1.116}$$

The associated dimensionless energy density $\Omega_{GW}(k,\eta)$ expressed as

$$\Omega_{GW}(k,\eta) = \frac{\rho_{GW}(k,\eta)}{\rho_{\rm c}(\eta)} = \frac{\rho_{GW}(k,\eta)}{3\,H^2\,M_p^2}, \tag{1.117}$$

where $\rho_{\rm c} = 3\,H^2\,M_p^2$ is represent the critical density. The dimensionless energy density $\Omega_{GW}(k,\eta)$ calculated *today*, which we symbolized as $\Omega_{GW}(k)$.

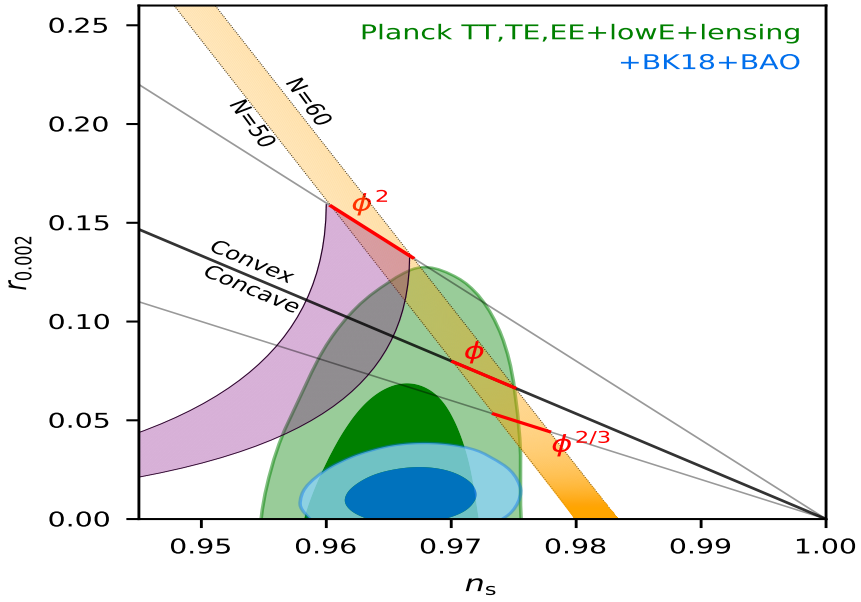

Figure 1.6: Constraints in the r vs. n_s plane for the Planck 2018 analysis. We have also shown BICEP/*Keck* data with Planck 2018 plus BAO data to improve Constraints in the r vs. n_s plane [Image courtesy: BICEP/Keck website].

1.3.2 Observational constraints

So far, we have described the theoretical framework to understand the dynamics of different matter fields and their fluctuations with gravity. However, as highlighted before, our goal is to understand the cosmological observations that can fit with the theoretical prediction. This section will also emphasize how we can relate the inflationary paradigm with the fluctuations in the CMB that we observed today. The properties of those fluctuations can be determined through their evolution. However, we have seen those fluctuations produced during the primordial inflation era. Notably, at $k = aH$ various modes of those fluctuations leave the Hubble horizon. On the other hand, after inflation end, with time, the co-moving Hubble radius $1/aH$ increases and indicates that the outgoing fluctuating modes which leave during inflation will re-enter the horizon at present. That is clearly shown in Fig. 1.6. Accordingly, after horizon re-entry, at all scales, those curvature perturbation modes will eventually evolve into density perturbations on the matter components, which ultimately will be imprinted on CMB. These perturbations oscillate due to gravity and thermodynamic pressure combined once they re-enter the horizon. Since various peaks are present in the temperature correlation functions, these coherent oscillations may be encoded in the CMB. Those peaks due to the different horizon exits/re-entry offer remarkable evidence for the inflationary phase.
The primordial power spectrum for tensor modes, Δ_t and scalar curvature, $\Delta_{\mathcal{R}}$, are parameterized by spectral index and amplitudes of their respective fluctuations as

$$\mathcal{P}_{\mathcal{R}} \equiv A_{\mathcal{R}} \left(\frac{k}{k_*}\right)^{n_s-1}, \quad \mathcal{P}_{\mathrm{T}} \equiv A_{\mathrm{T}} \left(\frac{k}{k_*}\right)^{n_{\mathrm{T}}}; \tag{1.118}$$

Where k_* is the the *pivot* scale set from Planck [29]. From the data of CMB temperature fluctuation, we can find that the amplitude of the curvature fluctuation, which is measured at

the pivot scale of $k_* = 0.05$ Mpc^{-1} be

$$A_{\mathcal{R}} = (2.196 \pm 0.060) \times 10^{-9}. \tag{1.119}$$

The value of the primordial spectral tilt turns out as

$$n_s = 0.9649 \pm 0.0042 \quad \text{at } 68\% \text{ CL} \quad ; \tag{1.120}$$

In addition to that, the possible bound on the tensor to scalar ratio at 95% CL from the Planck 2018 baseline analysis [2] be

$$\frac{\mathcal{P}_{\rm T}}{\mathcal{P}_{\mathcal{R}}} = r_{0.05} < 0.11. \tag{1.121}$$

We can also add BICEP/*Keck* data with Planck 2018 and BAO data to improve the constraint on n_s as well as r. Including BICEP/*keck* data, the restriction on r tightens from $r_{0.05} < 0.11$ to $r_{0.05} < 0.034$.

1.4 Models and inflationary parameters

In this section, we will discuss a few slow-roll inflationary models and calculate the inflationary parameters and predictions that we will be considering throughout our thesis.

1.4.1 Chaotic inflation

Although the chaotic inflation model is not favorable with the cosmological observations, we consider this potential for its simplicity. The form of the chaotic inflation potential is given by, [3]

$$V(\phi) = \frac{1}{2} m^{4-n} \phi^n. \tag{1.122}$$

Where n must be an even integer. If we assume the absolute value of the field, then we can also include the odd integer of n. The mass scale m can be written in terms of CMB observable as

$$m = M_p \left(3\pi^2 r\, A_{\mathcal{R}}\right)^{\frac{1}{4-n}} \left(\frac{1-n_s}{n\,(n+2)}\right)^{\frac{n}{2(4-n)}} . \tag{1.123}$$

$A_s \sim 10^{-9}$ represents the amplitude of the inflaton fluctuation measured from Planck. The effective inflaton mass m_ϕ can be defined by the following relation

$$m_\phi^2 = \partial_\phi^2 V(\phi), \tag{1.124}$$

which is same as m for $n = 2$ and it is constant for $n = 2$. For this model, we can connect CMB parameters (n_s, r) with inflationary parameters such as the inflationary e-folding number, N_k as

$$N_k = \frac{n+2}{2\,(1-n_s)} - \frac{n}{4} \ , \ r = \frac{8n}{n+2}\,(1-n_s) \ . \tag{1.125}$$

Furthermore, we will need the value of the scalar field's energy density ρ_ϕ^{end} at the inflation end to evolve the background beyond inflation. This quantity can be extracted from the condition $\epsilon = 1$. Using this condition, one can express ρ_ϕ^{end} in terms of the potential value at the inflation end $V(\phi_{end})$, as

$$\rho_\phi^{end} \sim \frac{3}{2}V(\phi_{end}) = \frac{3}{4}m^{4-n}\left(\frac{nM_p}{\sqrt{2}}\right)^n , \tag{1.126}$$

Combining these above equations, one can establish the relationship between the CMB observables and reheating parameters through inflation.

1.4.2 Natural inflation

The potential for this model is given by [30, 31]

$$V(\phi) = \Lambda^4\left[1 - \cos\left(\frac{\phi}{f}\right)\right]. \tag{1.127}$$

where Λ indicates the height of the potential, which sets the inflationary energy scale, and f represents the axion decay constant that controls the width of the potential. Λ can be fixed from CMB normalization. Further, by tuning the parameter f, we can suit this model with observation. In the discussion later, we will look at two representative values $f = (10M_p, 50Mp)$, which stand marginally consistent with Planck. The inflationary parameter N_k, the tensor to scalar ratio r, and $V(\phi_{end})$ can be written as

$$N_k = \frac{f^2}{M_p^2}\ln\left(\frac{2f^2(f^2(1-n_s)+M_p^2)}{(2f^2+M_p^2)\,(f^2(1-n_s)-M_p^2)}\right); r = \frac{f^2(1-n_s)-M_p^2}{f^2/4}; V(\phi_{end}) = \frac{2\Lambda^4 M_p^2}{2f^2+M_p^2}, \tag{1.128}$$

where the scale Λ can be extracted using constraints from CMB anisotropies as

$$\Lambda = \left(\frac{3\pi^2 M_p^2 A_{\mathcal{R}}(f^4(1-n_s)^2 - M_p^4)}{2f^2}\right)^{\frac{1}{4}}. \tag{1.129}$$

1.4.3 $\alpha-$attractor model

Here, we assume a class of theoretical models that unifies an extensive number of inflationary scenarios parameterized by α, known as α-attractor (in this context, see Refs. [32, 33]). This class of models has a conformal characteristic that leads to a universal prediction for inflationary observables. The potential of this paradigm is described in the canonical framework as

$$V(\phi) = \Lambda^4\left[1 - e^{-\sqrt{\frac{2}{3\alpha}}\frac{\phi}{M_p}}\right]^{2n}. \tag{1.130}$$

The CMB power spectrum naturally fixes the mass scale Λ, which defines the energy scale of inflation. The shape of the canonically normalized inflaton potential near its minimum is determined by the parameter α. For $n = 1$ and $\alpha = 1$, the above potential turns into the well

known Higgs-Starobinsky model [34, 35]. The quantity N_k and r can be determined by using the slow-roll approximation (see, for instance, Ref.[10])

$$N_k = \frac{3\alpha}{4n}\left[e^{\sqrt{\frac{2}{3\alpha}}\frac{\phi_k}{M_p}} - e^{\sqrt{\frac{2}{3\alpha}}\frac{\phi_{end}}{M_p}} - \sqrt{\frac{2}{3\alpha}}\frac{(\phi_k - \phi_{end})}{M_p}\right] \ , \ r_k = \frac{64n^2}{3\alpha\left(e^{\sqrt{\frac{2}{3\alpha}}\frac{\phi_k}{M_p}} - 1\right)^2} \ . \quad (1.131)$$

Using the condition $\epsilon(\phi_{end}) = 1$, ϕ_{end} and $V(\phi_{end})$ can be written in terms of the parameters α and n as

$$\frac{\phi_{end}}{m_p} \simeq \sqrt{\frac{3\,\alpha}{2}}\, ln\left(\frac{2\,n}{\sqrt{3\,\alpha}} + 1\right), \quad V(\phi_{end}) = \Lambda^4\left(\frac{2n}{2n + \sqrt{3\alpha}}\right)^{2n} \quad (1.132)$$

Using the constraints from the CMB, the parameter Λ can be determined, and it can be expressed in terms of the CMB Observables such as A_s, n_s, and r:

$$\Lambda = M_p\left(\frac{3\pi^2 r A_{\mathcal{R}}}{2}\right)\left[\frac{2n(1+2n) + \sqrt{4n^2 + 6\alpha(1+n)(1-n_s)}}{4n(1+n)}\right]^{\frac{n}{2}} \quad (1.133)$$

Using the current bound of n_s, r from Planck [29], we can give a suitable bound of the parameters Λ, α and n, which are compatible with the Planck data.

1.4.4 Minimal plateau model

The non-polynomial modification of the power-law potential is the minimal plateau inflationary model. The potential associated with minimal plateau inflation is given by [36]

$$V_{min} = \Lambda\frac{m^{4-n}\phi^n}{1 + \left(\frac{\phi}{\phi_*}\right)^n} \ , \quad (1.134)$$

where m and ϕ_* both represent the mass scale. The parameter Λ and m can be fixed from CMB normalization. A wide range of ϕ_* values predicts a lower tensor-to-scar ratio for different values of n consistent with the Planck data [29]. For this model, the inflationary e-folds N_k and r turn out as

$$r = \frac{8M_p^2 n^2}{\phi^2\left(1 + \left(\frac{\phi}{\phi_*}\right)^n\right)^2} \ , \ N_k = \int_{\phi_k}^{\phi_{end}} -\frac{\phi\,(\phi_*^n + \phi^n)}{nM_p^2\phi_*^n}d\phi \ . \quad (1.135)$$

The initial conditions to the subsequent dynamics after inflation is given by $V(\phi_{end})$, which can be written as

$$V(\phi_{end}) = \frac{m^{4-n}\phi_{end}^n}{1 + \left(\frac{\phi_{end}}{\phi_*}\right)^n} \ , \quad (1.136)$$

where

$$m = \left(\frac{3\pi^2 M_p^4 r\, A_{\mathcal{R}}}{2\Lambda\phi_k^n}\left(1 + \left(\frac{\phi_k}{\phi_*}\right)^n\right)\right)^{\frac{1}{4-n}} \ . \quad (1.137)$$

In our analysis, we set $\Lambda = 1$.

This section aims to show how inflation makes the universe homogeneous and isotropic at a large scale which is required from the observational point of view. However, It is not that simple. At the inflation end, the universe is cold and non-thermal. On the other hand, to set the universe for big-bang nucleosynthesis, we need a successful theory that predicts a universe very close to thermal equilibrium at temperatures around 10 MeV. Due to that reason reheating can be an integral part of early universe cosmology. Reheating should incorporate the production of standard model particles and dark matter. In the remaining sections of the Thesis, we deal with our current understanding of reheating after inflation. We should demonstrate that the details of the reheating phase rely on the underlying theory of particle physics beyond the Standard Model as well as how we can understand this phase through imprints on the various cosmological observables.

1.5 Proposal of the thesis

Over the past few decades, our knowledge about the cosmic history of the universe has been improved due to the precise measurements of the temperature anisotropies in the CMB [2, 29]. The observations provide adequate evidence for an early inflationary phase. In the framework of inflation, one can beautifully explain the homogeneous and isotropic universe at a large scale with negligible spatial curvature and the scale-invariant the primordial curvature perturbations (see reviews [16, 26, 34, 37–41]). On the other hand, in the framework of big-bang, the prediction of big-bang nucleosynthesis (BBN) builds on detailed information about nuclear reactions and points toward a hot and dense universe at a late time scale $t_{BBN} \sim 1$ s at equilibrium temperature $T_{BBN} \sim E_{BBN} \sim 1$ MeV, predicts quantities such as light-element abundances [42]. Thus the early evolution of our observable universe arrived at two major poles: cosmic inflation and big-bang nucleosynthesis. High-precision measurements constrain both inflation and nucleosynthesis, and to date, both theories match observations with impressive accuracy.

Despite these successes, we still have an inadequate understanding of connecting these two important eras in cosmic history. Since the typical inflationary energy scale at the end can be as high as 10^{16} GeV, with the duration corresponding to $\Delta t_{inf} \geq 10^{-36}$ s, there is a massive gap in terms of energy (and time) scale between the periods of inflation and BBN, which is poorly understood from both theory and observation. The electroweak symmetry-breaking and QCD phase transitions represent an intermediate stage between inflation and BBN at an energy scale of around 100 GeV but are still unable to cover the entire energy gap.

After inflation, most of the information about potentially complicated dynamics washed out before BBN. As a result, present cosmological experiments are unable to probe the period between inflation and BBN. In spite of this difficulty, we must try to understand the period between inflation and BBN better for both theoretical and observational reasons. On the phenomenological ground, to connect the inflationary cosmology to the BBN, it is necessary to understand how the universe transitioned from the cold, dark, and homogeneous inflaton field dominated universe to the hot, thermalized, radiation-dominated state. The transition era from inflation end to radiation domination is identified as reheating phase when the energy of the inflaton must be transferred to relativistic degrees of freedom as the dominant components collectively called radiation and leaving a hot, thermal, radiation-dominated universe. Most

importantly, this reheating process not only explains the cosmic origin of the radiation and dark matter (DM) component that we observe today but also accounts for the production of the primordial black holes (PBHs), gravitational waves(GWs), as well as the generation of matter-antimatter asymmetry observed in our universe (baryogenesis). The dynamics of reheating are rich and have a potential source of observational signature that can provide clues to how inflation can be connected with known high-energy physics. To get a complete picture, any proposed unified theory of high-energy physics must include a complete understanding of both inflation, reheating, and the later expansion history of the universe.

With the current advances in observational cosmology, the constraints on inflation improving, reheating will be an essential part of research in the coming years. Unlike inflation, the phase of reheating is not constrained by any direct observables. One of the most interesting observational implications of reheating is its effect on the expansion history of the universe between inflation and BBN, which influences the relation between physical scales of the CMB mode that we observe today and that at the time of Horizon exit during the beginning of the inflation. Therefore, the poorly constrained post-inflationary expansion history, especially the reheating phase, influences predictions for cosmological observables of specific inflation models [43–47].

The preliminary study regarding reheating phase focused on perturbative decays of individual inflaton into daughter particles [5, 6, 48]. However, at the end of inflation, the inflaton field oscillated around the minimum of its potential and could involve highly nonperturbative resonances, known as preheating stage [7, 8, 49–54]. This phase is governed by parametric resonance and may be analyzed in a linearized approximation to first order in field fluctuations. Moreover, perturbative decays of the inflaton still play a crucial role at the later stages of the reheating process and help to complete the transfer of energy from the inflaton to the mostly radiation particles.

Investigations in the field of reheating have been focused on two main challenges. 1) Studies the background dynamics of reheating with an understanding of the different stages in the reheating process, from nonlinear fragmentation of the fields soon after inflation to the stage which leads to the thermalization of the universe in a radiation-dominated universe at some reheating temperature and accounting the production of all particles including dark matter, radiation to get perfect state of our present universe. 2) Understanding the reheating phase through various cosmological observables such as the primordial magnetic field, gravitational waves, dark matter, etc. Several efforts have been dedicated to observational signatures of reheating [55–59], as well as their implications for inflationary observables [45, 60–66]. These two areas we are mainly focusing on in this Thesis.

The entire Thesis is divided into six chapters, including the introduction. This Thesis is meant to start with a brief overview of the inflationary paradigm with a general introduction to the field of reheating after inflation and the motivation behind the Thesis (chapter one). In chapter two, we initially provided a brief description of the standard Single-phase reheating scenario, and then we analyzed our proposed Two-phase reheating, where the initial preheating phase is described by effective dynamics followed by the perturbative reheating. Moreover, we also include dark matter production during reheating for completeness. In chapter three, we try to understand the phase of reheating in the light of the large-scale magnetic field we observe today. Chapter four discusses how we can decode the early and late time reheating phases through imprints on primordial gravitational waves. Finally, in chapter five, to shed light on the model-independent observable predictions, we propose a reheating scenario where the inflaton is coupled with all the daughter fields only gravitationally and successfully reheating the universe without introducing any arbitrary interactions among the fields. We provide a

brief conclusion and future directions in chapter six.

Part II

Dynamics of reheating: towards decoding its signatures

Reheating constraints through decaying inflaton : Single-phase to Two-phase reheating *2*

> *"The most important thing accomplished by the ultimate discovery of the 3°K radiation background (Penzias and Wilson, 1965) was to force all of us to take seriously the idea that there was an early universe"*
>
> *Steven Weinberg, in The First Three Minutes: A Modern View of the Origin of the universe*

Unlike inflation models, the reheating phase is poorly constrained due to a lack of direct observations. Furthermore, this phase is generically assumed to erase all its microscopic details due to inherent thermalization, which plays an important role in achieving the thermalized radiation-dominated universe. All these facts do not prevent one from studying such a phase due to its immense importance in terms of new physics phenomena in connection with inflaton decay which can influence various cosmological observables, and this will be our main focus of the present thesis. One can certainly imagine that the modified expansion history of the universe due to reheating prior to the hot Big-Bang nucleosynthesis (BBN) [42, 67–69], will naturally affect the physical size associated with any scale which could be observed in Cosmic microwave background (CMB) [70], and hence gives rise to the possibilities of indirectly constrain the dynamics of reheating. Further, the underlying process of reheating along thermalization while the inflaton is decaying into various daughter fields is widely believed to have connections with various fundamental cosmological issues related to the production of baryon asymmetry in the universe (baryogenesis) [71–77], the origin of dark matter [78] to name a few. Recently, there are interesting studies on how the reheating process can influence the propagation as well as generation of primordial gravitational waves [79–89].

Therefore, the dynamics of reheating are rich and will have important observational signatures. In this chapter, our primary focus will be to discuss the inflaton decaying into various fields, their observables, and constraints. We will discuss the process in the framework of perturbative reheating, which has been widely discussed in the literature [4]. However, most interesting observation of how reheating phase can possibly constrain the inflationary dynamics through CMB was first proposed in [45, 47, 90] (see Fig.2.1 in this context). In those analyses,

the reheating dynamics were modeled by an effective equation of state parameters. Further generalization has been made by considering the full system of Boltzmann equations of inflaton decaying into daughter fields system [91]. Our studies will be fully based on these two scenarios and the subsequent development of a more realistic framework that can be connected with various real cosmological observables. To this end, we would like to advertise the fact that the Boltzmann approach [91] turned out to be more realistic as it can naturally incorporate the dark matter sector, and consequently, the dark matter sector can be linked with the visible sector through CMB observation ([92]). For our purpose, we name the above-discussed perturbative reheating scenario as single-phase reheating.

After the end of inflation, the inflaton oscillates around its minimum, which is known to produce daughter particles through parametric resonance for appropriate coupling. Such a non-perturbative phase is known as preheating. In general preheating has been proved to be inefficient in completely reheating the universe. Hence, it must be followed by perturbative reheating. Combining both these phases in a single framework has not been studied in the literature, and this is precisely the analysis we discuss in the present chapter based on our paper [93]. The present scenario with two combined phases will be called two-phase reheating. After setting the stage of the single-phase reheating along with its constraints, we discuss in detail two-phase reheating. For the sake of simplicity, we described the non-perturbative preheating phase considering an effective equation of state, and while solving Boltzmann equations, we will not perform lattice simulation; rather, all the universal outcomes of the lattice simulation will be imported [94–96], as crucial inputs in our two-phase dynamics. If the inflaton potential is quadratic in nature $V(\phi) \propto \phi^2$ at its minimum, the lattice simulation shows that after the end of preheating, the equation of state (EOS) of the system does not reach that of the radiation. On the other hand if $V(\phi) \propto \phi^n$ with $n \geq 4$, the EOS reaches at the radiation equation of state $\omega \to 1/3$ at the end of preheating [60, 95–97]. Generically, it has been observed in the lattice simulation that after the end of preheating, only 50% of the inflaton's initial energy decays into radiation. All these important results will be considered crucial inputs in our two-phase reheating analysis. For the purpose of the reader, let us briefly describe the main idea behind the two-phase reheating model: Endowed with the above few universal features of lattice results, we will parameterize the initial non-perturbative stage (henceforth, phase I with an effective equation of state (ω_{eff}). This phase is assumed to be continued until the inflaton energy decays into 50% of its initial energy, and the subsequent perturbative stage (henceforth, phase II) follows. While evolving through phase I and connecting to phase II, the total energy conservation sets a stringent restriction the possible values of ω_{eff} during phase I as opposed to the conventional analysis [45, 47, 90]. Furthermore, the perturbative decay in phase II will be restricted by the CMB constraints [91].
The plan of this chapter is as follows: In sec.2.1, we describe the general analysis of single-phase reheating. In sec.1.2.4, we will try to specify the possible limits on perturbative reheating considering some specified form of the interaction between inflation and radiation fields. Finally, in sec.2.2, we analyze our proposed two-phase reheating. Here are the details of this section 2.2. In sub-sec.2.2.1, we illustrate the strategy of our numerical study for Two-phase reheating. After that, in sub-sec.2.2.2, we will try to find out an analytical estimation of the maximum radiation temperature and reheating temperature. Next, in sub-sec.2.2.3, we consider different inflationary models and analyze them in the context of the Two-phase scenario and compare it with conventional reheating dynamics. sub-sec.2.2.4 analyzes the possible constraints on the coupling parameter corresponding to different inflaton-radiation

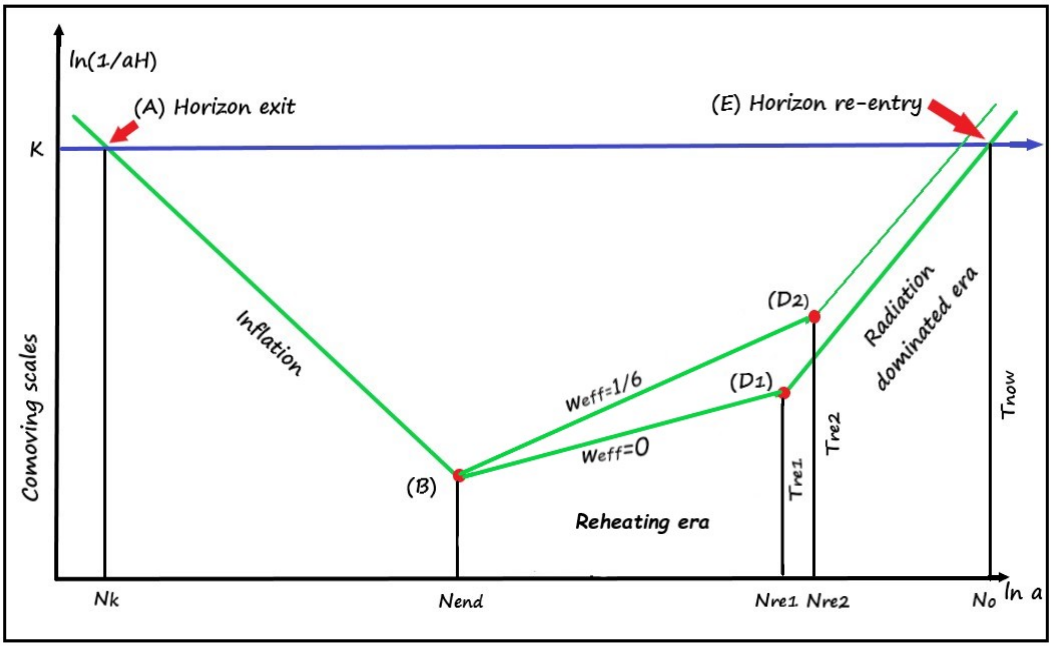

FIGURE 2.1: The evolution of the comoving Hubble scale ($\frac{1}{aH}$) connects the inflationary phase with the CMB. The end of the inflation is denoted by point B. The inflationary phase and radiation-dominated era connect through the reheating phase. The points D_1 and D_2 are the ending point of the reheating era for two different effective equations of state $\omega_{eff} = (0, 1/6)$ respectively. For a particular value of the spectral index (lower values of n_s, towards n_s^{min}), the reheating temperature calculating by considering $\omega_{eff} = 1/6$ is quite lower in comparison with $\omega_{eff} = 0$. That's why for that particular values of n_s, the duration of the reheating era is quite wider for $\omega_{eff} = 1/6$ in connection with $\omega_{eff} = 0$ ($N_{re2} > N_{re1}$).

field interactions. Furthermore, in sub-sec.2.2.5, we include additional dark matter components and discuss the viable restrictions on the dark matter parameter space for the Two-phase reheating scenario.

2.1 Single phase reheating

After inflation, the inflaton oscillates around its minimum, and the reheating phase starts. Depending upon the coupling parameters, nonperturbative reheating may occur. Before we directly jump into constructing the Two-phase reheating model where the initial stage is dominated by nonperturbative reheating, let us first elaborate on widely studied single-phase reheating with two types of scenarios: 1) Reheating phase is described by an effective equation of state (EoS) parameter ω_{eff}. 2) The perturbative reheating scenario where the inflaton decays into radiation with a constant decay width Γ_ϕ.

2.1.1 Reheating constraints analysis for dynamics described by an averaged EoS parameter

For this scenario, we follow the effective fluid description of reheating dynamics proposed in [45, 47, 90], where inflaton energy is assumed to be converted into radiation instantaneously at the end of reheating. The dynamics is parametrized by a thermalization temperature T_{re},

e-folds N_{re} counted from the end of the inflation, and an effective EoS ω_{eff}.
If one assumes a constant effective EoS during reheating, the total energy density at the end of the reheating ρ_{re} can easily be related to the energy density at the end of the inflation ρ_ϕ^{end} as

$$\frac{\rho_\phi^{end}}{\rho_{re}} = \left(\frac{a_{end}}{a_{re}}\right)^{-3(1+\omega_{eff})} , \tag{2.1}$$

where a_{end} represents the scale factor at the end of inflation, and a_{re} refers to the end of reheating. Writing this above equation in terms of e-folds

$$N_{re} = ln\left(\frac{a_{re}}{a_{end}}\right) = \frac{1}{3\,(1+\omega_{eff})}\, ln\left(\frac{\rho_\phi^{end}}{\rho_{re}}\right) = \frac{1}{3\,(1+\omega_{eff})}\, ln\left(\frac{3}{2}\,\frac{V(\phi_{end})}{\rho_{re}}\right) . \tag{2.2}$$

The reheating temperature can be related to the energy density at the end of the reheating as

$$\rho_{re} = \frac{\pi^2}{30}\, g_{re}\, T_{re}^4 , \tag{2.3}$$

where g_{re} represents effective degrees of freedom associated with radiation.
The main goal of this reheating constraint analysis is to understand the relations among early universe inflation dynamics, intermediate reheating dynamics, and late time dynamics. A particular cosmological scale k going out of the horizon during inflation will reenter the horizon during late time cosmological evolution. This fact will provide an important relation among different phases just mentioned as follows:

$$\ln\left(\frac{a_k H_k}{a_0 H_0}\right) = -N_k - N_{re} + \ln\left(\frac{a_{re} H_k}{a_0 H_0}\right), \tag{2.4}$$

where, a particular scale k satisfies the relation $k = a_0 H_0 = a_k H_k$. (a_0, H_0), are the cosmological scale factor and Hubble constant at the present time, respectively. Furthermore, making the standard assumption that the entropy is conserved during the evolution from the end of reheating to the current phase, one can estimate the reheating temperature in terms of the present CMB temperature in the following manner

$$g_{s,re} T_{re}^3 = \left(\frac{a_0}{a_{re}}\right)^3 \left(2T_0^3 + 6\frac{7}{8} T_{\nu 0}^3\right) , \tag{2.5}$$

where $g_{s,re}$ represents the effective number of degrees of freedom for entropy at reheating. ($T_0, T_{\nu 0} = (4/11)^{1/3} T_0$), temperature of the CMB photon and neutrino background at the present day respectively. Upon substitution of Eqn.(2.4) into (2.5), one can arrive at the following well known relation

$$T_{re} = \left(\frac{43}{11 g_{re}}\right)^{\frac{1}{3}} \left(\frac{a_0 T_0}{k}\right) H_k e^{-N_k} e^{-N_{re}} = \mathcal{G}_k e^{-N_{re}} , \tag{2.6}$$

where $\mathcal{G}_k = \left(\frac{43}{11 g_{re}}\right)^{\frac{1}{3}} \left(\frac{a_0 T_0}{k}\right) H_k e^{-N_k}$. Equating Eqns.(2.6), (2.3), and (2.2) e-folding number N_{re} turns out as

$$N_{re} = \frac{4}{(1-3\omega_{eff})} \left[-\frac{1}{4} ln\left(\frac{45}{\pi^2 g_{re}}\right) - \frac{1}{3} ln\left(\frac{11 g_{s,re}}{43}\right) - ln\left(\frac{k}{a_0 T_0}\right) - ln\left(\frac{V_{end}^{1/4}}{H_k}\right) - N_k \right] . \tag{2.7}$$

In our subsequent study, we identify the cosmological scale k as the pivot scale set by Planck, $k/a_0 = 0.05\ Mpc^{-1}$ and $g_{re} = g_{s,re} \sim 100$. Before defining any inflationary model, using these values, one can obtain a simplified expression for N_{re}

$$N_{re} = \frac{4}{1-3\,\omega_{eff}} \left[61.6 - ln\left(\frac{V_{end}^{1/4}}{H_k}\right) - N_k \right] . \tag{2.8}$$

2.1.2 Reheating constraints analysis for perturbatively decaying inflaton

As a second possibility, we shall consider the perturbative reheating scenario. In such a case, after inflation, the inflaton energy density, say, ρ_ϕ, gradually decays into the radiation energy density, say, ρ_R, with the decay process being governed by the Boltzmann equations. As a result, the effective EoS parameter during the reheating phase becomes time-dependent. In our analysis below, for simplicity, we shall assume that the EoS parameter ω_ϕ of the scalar field during the reheating phase remains constant. Such an assumption is valid as far as the oscillation time scale of the inflaton is much smaller than the Hubble time scale. This turns out to be generally true when the field is oscillating immediately after the end of inflation, and we should point out that such a behavior has also been seen in lattice simulations [94, 95, 98]. Hence, for a wide class of inflationary potentials that behave as $V(\phi) \propto \phi^{2n}$ near the minimum, the time-averaged EoS parameter of the inflaton can be expressed as $\omega_\phi = (n-1)/(n+1)$ [99]. We should emphasize that this scenario is different from the one considered in the previous section wherein the explicit decay of the inflaton field was not taken into account. Specifically, in the earlier case, the energy density of the inflaton was supposed to be converted instantaneously into the energy density of radiation at a given time, leading to the end of the phase of reheating. Let us explain the methodology of our analysis that helps us identify the regime of its validity, which will further motivate the reader to consider a physically more acceptable Two-phase reheating process. While discussing this, we will see one of the important results: the existence of a maximum reheating temperature. Subsequently, the generalization to the Two-phase reheating will show how the maximum reheating temperature reduces depending upon the initial condition. Let us start with the following Einstein equation for the cosmological scale factor and conservation of energy:

$$\begin{aligned} \ddot{n}_{re} &= -2\dot{n}_{re}^2 + \frac{1-3\omega_\phi}{6M_p^2}\rho_\phi \\ \dot{\rho}_\phi &+ 3\dot{n}_{re}(\rho_\phi + p_\phi) + \dot{\rho}_R + 4\dot{n}_{re}\rho_R = 0, \end{aligned} \tag{2.9}$$

Where "ρ_ϕ" and "ρ_R" are the energy densities of two different components: inflaton and radiation, respectively. At any instant of time during reheating, we parametrize the duration of reheating by e-folding number $n_{re}(t) = \ln(a/a_i)$, where "a" is the cosmological scale factor. The time derivative of n_{re} is the Hubble expansion parameter $\dot{n}_{re} = H$ during reheating. The fundamental difference between our present analysis followed from [91] and that in [45] is the consideration of Eq.2.9, where we consider the multiple dynamical components. Furthermore, the effective equation of state defined in the introduction, ω_{eff} is time-dependent and interpolates between two values $(\omega_\phi, 1/3)$. However, in [45], the authors have taken it to be constant during their analysis. Therefore, we employ realistic decay dynamics in the reheating constraint analysis and provide a new framework to go beyond, which is our main purpose of the present section. Keeping the above points in mind, let us express the total

energy density as,

$$\rho_R + \rho_\phi \quad = \quad e^{-4n_{re}} \left(\rho_\phi^i + (1 - 3\omega_\phi) \int_{t_i}^{t} \rho_\phi e^{4n_{re}} dn_{re} \right). \tag{2.10}$$

which is followed by the conservation eq.2.9. The index "i" stands for the initial stage of reheating, which also marks the end of inflation. At the beginning of reheating we set $\rho_R(t_i) = 0$. For solving the above set of equations, the boundary condition is set by the inflaton energy density as $\dot{n}_{re}(t_i) = H(t_i) = \sqrt{\rho_\phi^i / 3M_p^2}$. The physical quantity of our interest is the ratio of the radiation energy density and the inflaton energy density. From eq.2.10, one gets

$$\frac{\rho_R^f}{\rho_\phi^i} = e^{-4N_{re}} - \frac{\rho_\phi^f}{\rho_\phi^i} + (1 - 3\omega_\phi) e^{-4N_{re}} \int_i^f \frac{\rho_\phi}{\rho_\phi^i} e^{4n_r} dn_{re} \, . \tag{2.11}$$

Where "f" corresponds to the final value of radiation density. We define the total e-folding number during reheating as $N_{re} = n_{re}(t_f)$.
The usual approach is to define the EoS of the total energy density during reheating and study its evolution. However, here we consider only the radiation part with inflaton during reheating and try to understand the evolution of its temperature T_{rad} as a function of scalar spectral index and finally connect the temperature with CMB one on a large scale [91]. The reheating temperature T_{re} is identified with radiation temperature T_{rad} at thermal equilibrium between the decaying inflaton and the radiation. From the entropy conservation of thermal radiation, the relation among $T_{rad} = T_{re}$ at equilibrium can be expressed as given in Eqn.2.6. In our subsequent study, we compare our result with the corresponding estimated scalar spectral index $n_s = 0.9682 \pm 0.0062$ [100, 101].

Following the discussion in the introduction for the perturbative reheating and considering the inflaton decay width to be Γ_ϕ, once obtains the maximum radiation temperature as,

$$T_{rad}^{max} \simeq \left(\frac{39^2 M_p^2 (\dot{n}_{re}^i)^2}{\pi^2 g_{re}} \right)^{\frac{1}{8}} \sqrt{T_{re}}. \tag{2.12}$$

Where, the standard definition of reheating temperature $T_{re} = 0.45 \, (200/g_{re})^{1/4} \sqrt{\Gamma_\phi M_p}$ has been used. From the above equation, if one identifies a special point where two temperature meets, $T_{rad}^{max} = T_{re}$, one gets an approximate analytical expression for the maximum possible reheating temperature for a given decay width. Our numerical analysis also shows the maximum reheating temperature at the aforementioned special point,

$$T_{re}^{max} \simeq \left(\frac{39^2 \rho_\phi^i}{3\pi^2 g_{re}} \right)^{\frac{1}{4}}. \tag{2.13}$$

Interestingly, the maximum reheating temperature T_{re}^{max} can be computed exactly for a special case when $w_\phi = 1/3$. The corresponding result is as follows,

$$T_{rad}^{max}|_{\omega_\phi = \frac{1}{3}} \quad \simeq \quad \left(\frac{30 \rho_\phi^i}{\pi^2 g_{re}} \frac{\Gamma_\phi}{4\dot{n}_i + \Gamma_\phi} \right)^{\frac{1}{4}} \tag{2.14}$$

$$T_{re}^{max}|_{\omega_\phi=\frac{1}{3}} \quad = \quad \lim_{\Gamma_\phi \gg 4\dot{n}_i} T_{rad}^{max}|_{\omega_\phi=\frac{1}{3}} = \left(\frac{30\rho_\phi^i}{\pi^2 g_{re}}\right)^{\frac{1}{4}} .$$

This expression is exactly the same as previously discussed. For this special value of $\omega_\phi = 1/3$, we also have exact expression for all the reheating parameters (T_{re}, N_{re}) as follows,

$$T_{re} = \mathcal{G}_k \left(1 - \sqrt{\frac{4\rho_\phi^i}{3M_p^2\Gamma_\phi^2}} \ln\left[1 - \frac{\pi^2 g_{re}\mathcal{G}_k^4}{3^2.5V(\phi_{end})}\right]\right)^{-\frac{1}{2}} . \tag{2.15}$$

$$N_{re} = \frac{1}{2}\ln\left[1 - \sqrt{\frac{4\rho_\phi^i}{3M_p^2\Gamma_\phi^2}} \ln\left[1 - \frac{\pi^2 g_{re}\mathcal{G}_k^4}{3^2.5V(\phi_{end})}\right]\right] \tag{2.16}$$

At this point, let us again emphasize the fact that as long as we are in the perturbative regime, the relation among the scalar spectral index n_s and the reheating temperature T_{re} can be understood from our detailed analysis above.

2.1.2.1 Procedure for numerical analysis and boundary condition

Let us describe the strategy of our numerical study. We can identify the inflation model-dependent input parameters as $N_k, H_k, V(\phi_{end})$ as function of spectral index n_s for a particular CMB scale k. Considering simple canonical inflation potential, the CMB observables can be related to the slow-roll parameters and value of H_k (Hubble parameter at the point of horizon exit of CMB mode) as

$$n_s = 1 - 6\epsilon_k(\phi_k) + 2\eta_k(\phi_k)\ ,\ r = 16\epsilon_k(\phi_k)\ \ , H_k = \frac{\pi M_p\sqrt{r_k A_s}}{\sqrt{2}}\ \ , \tag{2.17}$$

where we have used the slow roll approximation and $A_s = H^4/(4\pi^2\dot{\phi}^2)$. From the slow-roll approximation, we also obtain

$$H_k^2 \simeq \frac{1}{3M_p^2}V(\phi_k)\,, \tag{2.18}$$

where ϕ_k is the value of the scalar field ϕ at the Hubble crossing of mode k. Likewise, another inflation model-dependent input parameter, N_k denotes the e-fold at which the wave number k leaves the Hubble radius when counted from the end of inflation

$$N_k = \log\left(\frac{a_{end}}{a_k}\right) = \int_{\phi_{end}}^{\phi_k}\frac{3}{2}\frac{V(\phi)}{V'(\phi)}d\phi = \int_{\phi_k}^{\phi_{end}}\frac{|d\phi|}{\sqrt{2\epsilon_v}M_p}\ \ , \tag{2.19}$$

where, the field value at the end of inflation ϕ_{end} for a particular scale k, is computed from the condition of the end of inflation,

$$\epsilon(\phi_{end}) = \frac{1}{2M_p^2}\left(\frac{V'(\phi_{end})}{V(\phi_{end})}\right)^2 = 1, \tag{2.20}$$

where a_k and a_{end} are the scale factors at the horizon crossing of mode k and at the end of inflation, respectively. The above equations (2.17), (2.18), and (2.19) establishes the relation

between the observable quantities (n_s, A_s, r) and the parameter in the potential at the leading order in ϵ_k and η_k. As the initial conditions for subsequent reheating dynamics are set by the end of the inflation, the reheating parameters N_{re}, T_{rad} will implicitly depend upon the scalar spectral index n_s for a given scale; therefore, one can establish the connection between CMB anisotropy and reheat through inflation.
During this perturbative reheating dynamics various components of the total energy density satisfy the following standard Boltzmann equations [4, 91],

$$\dot{\rho}_\phi + 3H(1+\omega_\phi)\rho_\phi + \Gamma_\phi \rho_\phi (1+\omega_\phi) = 0 \ , \tag{2.21}$$

$$\dot{\rho}_R + 4H\rho_R - \Gamma_\phi \rho_\phi (1+\omega_\phi) = 0 \ . \tag{2.22}$$

To solve these equations numerically, we need to identify the initial conditions for the individual field components that can be written as

$$\rho_\phi(A=1) = \frac{3}{2}V(\phi_{end}) \, ; \, \rho_R(A=1) = 0 \, , \tag{2.23}$$

where the rescaled scale factor is defined as $A = a/a_{end}$. Once we numerically solve the reheating dynamics, we can define reheating temperature T_{re} from the radiation temperature T_{rad} when the condition $H(t) = \Gamma_\phi$ is satisfied,

$$H(A_{re})^2 = \left(\frac{\dot{A}_{re}}{A_{re}}\right)^2 = \frac{\rho_\phi(\Gamma_\phi, A_{re}, n_s^k) + \rho_R(\Gamma_\phi, A_{re}, n_s^k))}{3M_p^2} = \Gamma_\phi^2 \ , \tag{2.24}$$

where A_{re} is the normalized scale factor at the end of the reheating. Accordingly, the reheating temperature in terms of radiation temperature (T_{rad}) is expressed as,

$$T_{re} = T_{rad}^{end} = \left(\frac{30}{\pi^2 g_*(T)}\right)^{1/4} \rho_R(\Gamma_\phi, A_{re}, n_s^k)^{1/4} \ . \tag{2.25}$$

Now connecting equations (2.24), (2.25), and (2.6), we can establish one to one correspondence between T_{re} and Γ_ϕ.

Unifying dark sector: Earlier, we discussed the reheating process, where inflaton decays only into radiation. In the present discussion, we add additional dark matter components and discuss the impact on dark matter phenomenology. The assumption is that inflaton decays into radiation and then radiation to dark matter. The methodology of the analysis will be the same as before, except the new additional dynamical equations for dark matter. The subsequent perturbative phase will now be governed by two more parameters related to the dark matter component. Apart from the inflaton equation of state ω_ϕ and the inflaton decay constant Γ_ϕ, we have a thermal average of dark matter annihilation cross-section $\langle\sigma v\rangle$, and the dark matter mass M_X. The corresponding dimensionless comoving energy densities' dynamics will be governed by the Boltzmann equation [91].

$$\Phi' = -c_1 \frac{A^{1/2}\Phi}{\sqrt{\frac{\Phi}{A^{3\omega_\phi}} + \frac{R}{A} + \frac{X\langle E_X\rangle}{m_\phi}}} \ , \tag{2.26}$$

$$R' = c_1 \frac{A^{\frac{3(1-2\omega_\phi)}{2}}\Phi}{\sqrt{\frac{\Phi}{A^{3\omega_\phi}} + \frac{R}{A} + \frac{X\langle E_X\rangle}{m_\phi}}} + c_2 \frac{A^{-3/2}\langle\sigma v\rangle 2\langle E_X\rangle M_p}{\sqrt{\frac{\Phi}{A^{3\omega_\phi}} + \frac{R}{A} + \frac{X\langle E_X\rangle}{m_\phi}}} \left(X^2 - X_{eq}^2\right) \ , \tag{2.27}$$

$$X' = -c_2 \frac{A^{-5/2}\langle\sigma v\rangle M_p m_\phi}{\sqrt{\frac{\Phi}{A^{3\omega_\phi}} + \frac{R}{A} + \frac{X\langle E_X\rangle}{m_\phi}}} \left(X^2 - X_{eq}^2\right) . \tag{2.28}$$

where, for numerical purposes, the dimensionless variables are defined as

$$\Phi \equiv \frac{\rho_\phi a^3}{m_\phi} \; ; \; R \equiv \rho_R a^4 \; ; \; X \equiv n_X a^3 \quad . \tag{2.29}$$

Here prime $'$ represents the derivative with respect to A. The average energy of the dark matter particle is expressed as $\langle E_X\rangle = \frac{\rho_X}{n_X} \simeq \sqrt{M_X^2 + 9T^2}$ [4]. The equilibrium number density of the dark matter particle can be described in terms of the modified Bessel function of the second kind [4]

$$n_X^{eq} = \frac{gT^3}{2\pi^2}\left(\frac{M_X}{T}\right)^2 K_2\left(\frac{M_X}{T}\right) \; , \tag{2.30}$$

and the constants c_1 and c_2 are delineate as,

$$c_1 = \frac{\sqrt{\frac{3}{8\pi}} M_p \Gamma_\phi}{m_\phi^2} \; , \; c_2 = \sqrt{\frac{3}{8\pi}} \quad . \tag{2.31}$$

Where g represents internal degrees of freedom associated with dark matter particles. The initial conditions to solve the Boltzmann equations are set at the end of inflation to be,

$$\Phi(1) = \frac{3}{2}\frac{V(\phi_{end})}{m_\phi^4} \; ; \; R(1) = X(1) = 0 \quad . \tag{2.32}$$

Now including the dark matter component, the condition for ending of the reheating dynamics is set by the following equation,

$$H^2 = \frac{\rho_\phi(\Gamma_\phi, N_{re}, n_s) + \rho_R(\Gamma_\phi, N_{re}, n_s)) + \rho_X(\Gamma_\phi, N_{re}, n_s)}{3M_p^2} = \Gamma_\phi^2 \quad . \tag{2.33}$$

supplemented with the observational constraint namely the relation between reheating temperature follows from the above equation and present CMB temperature $T_0 = 2.7K \simeq 2.35 \times 10^{-13}\ GeV$ though the relation Eq.(2.6). the additional observational constraint is the observed value of the dark matter abundance defined as Ω_X [2, 102]

$$\Omega_X h^2 = \langle E_X\rangle \frac{X(T_F)\ T_F\ A_F}{R(T_F)\ T_0\ m_\phi} \Omega_R h^2 \ = 0.1199 \pm 0.0022, \tag{2.34}$$

which is expressed in terms of radiation abundance Ω_R ($\Omega_R h^2 = 4.3 \times 10^{-5}$). T_F is the temperature at the very late time when both comoving dark-matter and radiation energy components become constant. While solving the Boltzmann equations, the above-mentioned conditions will constrain the dark matter parameter $\langle\sigma v\rangle$ (thermal average of the cross-section times velocity) for a fixed value of the dark matter mass, M_X, and the inflaton decay constant in terms reheating temperature.

Another important motivation for this chapter would be to incorporate the non-perturbative aspects of reheating into our formalism, which we discussed in our subsequent section. Before going into this in detail, let us point out the regime of validity of perturbative reheating, which we already discussed in section-1.2.4 for different coupling. In our subsequent analysis, we also want to examine whether the critical condition on the decay channel, which indicates the transition from non-perturbative to perturbative dynamics, is consistent with our analysis or not for the different inflationary models.

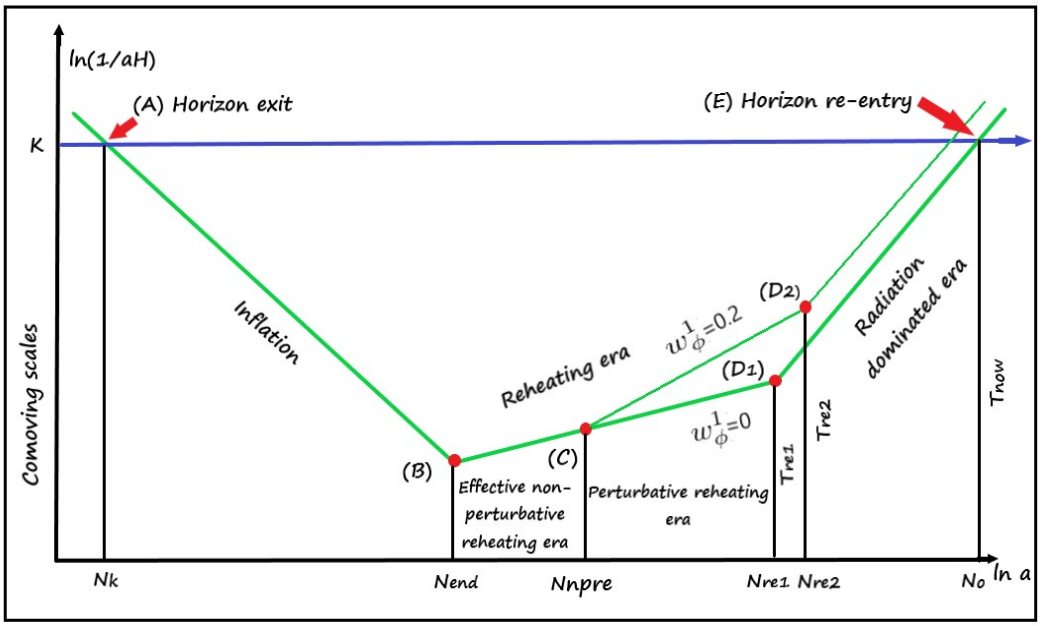

FIGURE 2.2: The evolution of the comoving Hubble scale ($\frac{1}{aH}$) connects the inflationary phase with the CMB. The end of the inflation is denoted by point B. The inflationary phase and radiation-dominated era connect through the reheating phase, which contains two different regions, the effective non-perturbative reheating era, and the perturbative reheating era. C denotes the ending point of the non-perturbative reheating era. The points D_1 and D_2 are the ending point of the perturbative reheating era for two different inflaton equations of state during perturbative reheating $\omega^1_\phi = (0, 0.2)$ respectively. For the perturbative reheating era with the inflaton equation of state $\omega^1_\phi = (0, 0.2)$, the e-folding number, basically, the duration of the perturbative process are different. For a particular value of the spectral index (lower values of n_s, towards n_s^{min}), the decay width calculating by considering $\omega^1_\phi = 0.2$ is quite lower in comparison with $\omega^1_\phi = 0$. That's why for that particular values of n_s, the duration of the perturbative era is quite wider for $\omega^1_\phi = 0.2$ in connection with $\omega^1_\phi = 0$ ($N_{re2} > N_{re1}$).

2.2 Two-phase reheating: Regime of effective nonperturbative and perturbative reheating

Preheating is the standard and well-studied mechanism to consider the non-perturbative effect during reheating. This stage is essentially the combination of a highly non-linear process of parametric resonance and subsequent thermalization. The well-known fact is that the non-perturbative preheating mechanism does not completely decay inflaton into the radiation field. Therefore, subsequent perturbative decay will be necessary to complete the reheating process. To the best of our knowledge, the reference [91] has considered this issue for the first time and studied perturbative reheating, followed by preheating considering a specific model of chaotic type inflation. However, generically the preheating mechanism is model-dependent. Hence, combining the end of preheating and subsequent model-independent perturbative reheating is somewhat irreconcilable. Therefore, our objective in the following sections would be to reconcile these two phases.

Instead of dwelling on explicit non-perturbative computation during the preheating stage, we will adopt an effective model-independent approach following the reference [45]. The basic idea is to assume the dynamics of preheating to be solely governed by an effective equation of

state ω_{eff} supplemented with the total energy conservation law in terms of its constituents. As already emphasized in the introduction, the information about the non-perturbative dynamic will be encoded, considering its universal features in our effective dynamics.

As pointed out already, during the non-perturbative dynamics, inflaton decay is not complete, and typically it is around 50% of its total comoving energy, which is being transferred into the daughter fields. Furthermore, in inflation models with quadratic potential near the minimum, the non-perturbative reheating does not lead to the equation of state, $\omega = \frac{1}{3}$, which is expected at the endpoint of reheating [95, 98]. Our essential idea would be to correctly utilize those results as the endpoint conditions of our proposed effective dynamics in place of preheating. After the end of this, the usual Boltzmann perturbative reheating process will follow. The second phase completes the reheating process by leading to the correct state equation with relativistic degrees of freedom as the dominant components collectively called radiation. Fig.2.2 illustrates our methodology of calculation. Throughout this section, we call this a two-phase reheating process.

phase-I: (*Effective non-perturbative phase*) During the early stage of reheating, the phase will be described by total energy density $\rho_T = \rho_R + \rho_\phi$ and the constant effective equation state w_{eff}. Hence the evolution will be described by,

$$\rho_T = \rho_{Te}\left(\frac{a_{end}}{a}\right)^{3(1+\omega_{eff})} , \tag{2.35}$$

where ρ_{Te} is the total energy density at the end of the inflation. a_{end} is the scale factor at the end of the inflation. In this section, we will build up our formalism by considering two matter components with ρ_ϕ, ρ_R as the inflaton energy density and radiation energy density, respectively, at any instant of time. In the subsequent section, we will add dark matter as a third component as an extension. Nonetheless, from the total energy expression, one can write down the following equation follows from Eq.(2.35),

$$\dot{\rho_\phi} + \dot{\rho_R} + 3H(1+\omega_{eff})(\rho_\phi + \rho_R) = 0 \ . \tag{2.36}$$

To reduce the number of unknown parameters, to this end we will also utilize total energy conservation relation considering individual equation of state of the inflaton (ω_ϕ) and the radiation field ($\omega_R = 1/3$) described as

$$\dot{\rho_\phi} + 3H(1+\omega_\phi)\rho_\phi + \dot{\rho_R} + 4H\rho_R = 0 \ . \tag{2.37}$$

Given the aforementioned constraint relation, one obtains the possible restricted value of the effective equation of state, ω_{eff}. To find those restrictions we combine above two EQs.(2.36) and (2.37), and obtain the following consistency relation,

$$\frac{\rho_R}{\rho_\phi + \rho_R} = \frac{3\,(\omega_\phi - \omega_{eff})}{3\,\omega_\phi - 1} \ . \tag{2.38}$$

Right at the end of inflation or the beginning of the preheating phase, the energy density of the radiation part will naturally be close to zero $\rho_R \simeq 0$. As time evolves, ρ_R increases due to decaying inflaton. This initial condition automatically restricts the possible values of ω_{eff} to be very close to that of the inflaton equation of state ω_ϕ. *, Of course, more appropriate approach would be to assume the inflaton equation of state evolving from the value very close to ω_ϕ to the value required in the next phase.* We will comment on this issue

at the appropriate place during our discussion. However, from the usual numerical lattice simulation, the inflaton dominates the preheating phase's significant duration. Hence, the equation of state will naturally be close to that of the inflaton field. Thus, our effective dynamics approach towards preheating truly captures all these necessary properties of the non-perturbative dynamics. As ω_{eff} turned out to be no longer a free parameter and constrained by the above consistency relation (2.38), our following analysis will be based on this important result. Throughout our study we consider models for which the inflaton equation of state during phase-I $\omega_\phi = 0$, and consequently following Eq.2.38 we choose two values of effective equation of state $\omega_{eff} = (10^{-6}, 10^{-3})$. This choice will automatically fixes the initial radiation densities during phase-I as $\rho_R/(\rho_\phi + \rho_R) = (3 \times 10^{-6}, 3 \times 10^{-3})$. We will see the maximum reheating temperature crucially depends upon these initial conditions.

Phase-II: (*Perturbative phase*) Once the preheating dynamics end the usual Boltzmann perturbative reheating follows. During this period various components of the total energy density satisfy the following standard Boltzmann equations [4],

$$\dot{\rho}_\phi + 3H(1+\omega_\phi^1)\rho_\phi + \Gamma_\phi \rho_\phi (1+\omega_\phi^1) = 0 \ , \tag{2.39}$$

$$\dot{\rho}_R + 4H\rho_R - \Gamma_\phi \rho_\phi (1+\omega_\phi^1) = 0 \ , \tag{2.40}$$

where the inflaton field ϕ decays into radiation with the decay rate Γ_ϕ. ω_ϕ^1 represents inflaton equation of state during perturbative reheating. Important to note that inflaton equation of state during phase-I, ω_ϕ is taken to be different than that of phase-II, ω_ϕ. *This is where we will again consider lattice simulation results as another important input.*

Now that we have identified the full reheating phase in terms of two distinct stages, we will numerically solve all those equations self consistently. With the appropriate dimensionless rescaled variables for the inflaton and radiation energy densities,

$$\Phi = \frac{\rho_\phi a^{3(1+\omega_\phi)}}{m_\phi^{(1-3\omega_\phi)}} \ ; \ R = \rho_R a^4 \quad , \tag{2.41}$$

governing equations for the effective dynamical preheating phase turn into the following form,

$$\left.\begin{aligned} \tfrac{\Phi'}{A^{3\omega_\phi}} + \tfrac{R'}{A} &= 0 \ , \\ \tfrac{\Phi'}{A^{2+3\omega_\phi}} + \tfrac{R}{A^4}[3(1+\omega_{eff}) - 4] + \tfrac{R'}{A^3} + \tfrac{3\,\Phi\,(\omega_{eff}-\omega_\phi)}{A^{3(1+\omega_\phi)}} &= 0 \end{aligned}\right\} , \quad \text{Phase I} \tag{2.42}$$

and the associated governing equations for the subsequent perturbative phase will reduce into

$$\left.\begin{aligned} \Phi^{'} + C_1(1+\omega_\phi^1)\tfrac{A^{1/2}\Phi}{X} &= 0 \ , \\ R^{'} - C_1(1+\omega_\phi^1)\tfrac{A^{\frac{3(1-2\omega_\phi^1)}{2}}\Phi}{X} &= 0 \end{aligned}\right\} . \quad \text{Phase-II} \tag{2.43}$$

The rescaled scale factor is defined as $A = \frac{a}{a_{end}}$. "Prime"($'$) represents derivative with respect to A. The constant C_1 and redefined variables are,

$$X = \sqrt{\frac{\Phi}{A^{3\,\omega_\phi^1}} + \frac{R}{A}} \ ; \ C_1 = \frac{\sqrt{3} M_p \Gamma_\phi}{m_\phi^2} \ . \tag{2.44}$$

m_ϕ is the mass of the inflaton. In the next section, we will describe the methodology for solving the above set of equations numerically.

2.2.1 Procedure for numerical analysis and boundary conditions

In section (2.1.2.1), we already identify inflationary model-dependent input parameters as a function of scalar spectral index n_s for a given scale. Moreover, as the initial conditions for the reheating phase followed by the inflationary dynamics, the reheating parameters N_{re} and T_{re} will implicitly depend upon the scalar spectral index n_s. Therefore, one can show the connection between CMB anisotropy and the reheating through inflation.

Phase-I initial condition: The initial conditions for phase-I of the reheating dynamics (effective non-perturbative era) are set by the end of inflation at $A = 1$ and the equation (2.38). Those are as follows,

$$\Phi(A=1) = \frac{3}{2}\frac{V(\phi_{end})}{m_\phi^4} \quad ; \quad R(A=1) = \frac{3\,(\omega_{eff} - \omega_\phi)}{1 - 3\,\omega_{eff}}\;\Phi(A=1)\;. \tag{2.45}$$

Subsequent perturbative dynamics will now crucially depend on the endpoint of the first phase of reheating, namely the phase-I. On this issue, we rely on the actual non-perturbative lattice simulation results [94, 95, 98] considering a specific model of reheating where the inflaton field is assumed to couple with the reheating field. This system has been studied quite extensively [103, 104] in the literature by using the publicly available numerical package LATTICEEASY[105] and its parallelized version CLUSTEREASY[106]. The non-perturbative analysis for different inflationary models has been proved to yield some universal results, which will be our important input for the numerical analysis. Extensive works on non-perturbative reheating analysis yield an important fact that only the 50% of the total comoving inflaton energy density is getting transferred into the daughter field. Additionally, the inflaton equation of state tends to achieve a steady-state value depending upon the power-law form of the inflaton potential near its minimum. For example, if one assumes the inflaton potential to be of power-law from $V(\phi) \sim \phi^n$, for chaotic type model namely $n = 2$, the non-perturbative phase ends with a steady value of the equation of state ~ 0.2. However, for other values of $n \geq 4$, the equation of state approaches $\omega = \frac{1}{3}$ at the endpoint of the non-perturbative reheating. These are the crucial quantitative results from the non-perturbative preheating dynamics we will be utilizing in our analysis for the phase-II dynamics.

Phase-II initial condition: After the phase-I dynamics, the pertubative dynamics will automatically follow. However, an important point would be to identify the appropriate boundary conditions. The starting moment of phase-II will be set by the normalized scale factor $A_{npre} = a_{npre}/a_{end}$ which is the ratio between the scale factor at the end of the effective non-perturbative epoch namely phase-I a_{npre}, and the end of the inflation. The initial conditions for the dimensionless comoving densities are

$$\Phi = \Phi(A_{npre}) \quad ; \quad \frac{R(A_{npre})}{R(A_{npre}) + \Phi(A_{npre})} \simeq \frac{1}{2}. \tag{2.46}$$

It is important to realize that the initial condition is determined by 50% decay of the total comoving energy density ρ_T. Further, we have numerically checked that our results do not seem to depend both qualitatively as well as quantitatively much on the amount of decay within $40\% - 60\%$ of the total energy at the end of phase-I. For the analysis, we further assume the inflaton equation of state $\omega_\phi^1 \simeq 0.2$ irrespective of the models under consideration. *This approximate value is again another important input from the Lattice simulation.* For comparison, we also consider the cases where either phase-I or phase-II evolution completely governs the reheating dynamics.

Determining the reheating parameters: Once we solve the reheating dynamics numerically, we can define reheating temperature T_{re} when the condition (2.24) is satisfied. Accordingly, the reheating temperature in terms of radiation energy density is expressed in Eqn. (2.25). Furthermore, Now the e-folding number during reheating N_{re} consists of two contributions carried out in two distinct phases as

$$N_{re} = \log\left(\frac{a_{re}}{a_{end}}\right) = \log\left(\frac{a_{re}}{a_{npre}}\frac{a_{npre}}{a_{end}}\right) = N_{pre} + N_{npre} \ , \tag{2.47}$$

$$N_{pre} = \log\left(\frac{a_{re}}{a_{npre}}\right) \ ; \ N_{npre} = \log\left(\frac{a_{npre}}{a_{end}}\right) \ , \tag{2.48}$$

where N_{pre} and N_{npre} are the e-folding number during perturbative and effective nonperturbative region respectively. Combining equations (2.6) and (2.47), we obtain the most important modification of Eq.(2.6) relating the reheating and inflationary parameters,

$$T_{re} = \left(\frac{43}{11g_{re}}\right)^{1/3}\left(\frac{a_0T_0}{k}\right)H_k e^{-N_k}e^{-N_{npre}}e^{-N_{pre}} \ . \tag{2.49}$$

Now connecting equations (2.24), (2.25) and (2.49), we can establish one to one correspondence between T_{re} and Γ_ϕ.

As described before, we will consider three possible cases and compare the results

Case-I	$N_{npre} \neq 0$, $N_{pre} \neq 0$	Phase-I + Phase-II	
Case-II	$N_{npre} \neq 0$; $N_{pre} = 0$	Kamionkawski et al [45] (See section (2.1.1))	(2.50)
Case-III	$N_{npre} = 0$; $N_{pre} \neq 0$	Phase-II (Discussed in the previous section(2.1.2))	

To this end, let us specifically mention case II, when perturbative dynamics cease to exist. This particular procedure proposed in [45], has been studied quite extensively in the literature [91]. In this particular phase, dynamics is solely governed by the effective equation of state ω_{eff}. The explicit decay of inflaton does not appear in the computation. However, information about the decay constant Γ_ϕ is extracted from the equilibrium condition $\Gamma_\phi = H$, where the reheating temperature (T_{re}) is defined as $T_{re} = 0.2\left(\frac{200}{g_{re}}\right)^{1/4}(\Gamma_\phi M_p)^{1/2}$. However, not to ignore an important difference between the phase-I described before and the approach devised in [45] or case-II for the present study is the additional conservation equation (2.38). This essentially differentiates the regime of applicability of these two approaches. Phase-I dynamics is assumed to be applicable in the early non-perturbative regime. Whereas, since condition (2.38) does not exist, the original Kamionkowski et al. [45] approach is effectively applicable throughout the full period of reheating without any microscopic details. Further, the value of ω_{eff} is no longer constrained to be very closed to the inflaton equation of state during phase-I. This relation helps us to compare the results for various scenarios we consider. **To avoid symbol confusion whenever we study case-II, we use the symbol ω^K_{eff} instead ω_{eff} which we reserve for two-phase reheating dynamics.**

2.2.2 Maximum radiation temperature and reheating temperature: The analytic study

Before moving on to a particular model, let us analytically estimate the maximum reheating temperature and its dependence upon the initial condition following the same line as before. Considering the standard definition of radiation temperature $T_{rad} = \left(\frac{30}{\pi^2 g_{re}}\rho_R\right)^{1/4}$, and computing the radiation energy density during phase II following the Eqs.(2.39), (2.40), (2.36) and (2.37) the approximate radiation temperature assumes the following form (see appendix 6.2 for details calculation)

$$T_{rad} = \left(\frac{\rho_\phi^{in}\Gamma_\phi(1+\omega_\phi^1)}{\beta x^4 H_{in}}\left[\frac{2}{5-c}\left(x^{\frac{5-c}{2}}-1\right)+\frac{\rho_R^{in}}{\rho_\phi^{in}}\left(\frac{1-x^{\frac{c+3}{2}}}{c+3}+\frac{H_{in}}{\Gamma_\phi(1+\omega_\phi^1)}\right)\right]\right)^{1/4} , \quad (2.51)$$

where x, β, c and H_{in} express as

$$x = \frac{a}{a_{npre}} \ , \ \beta = \frac{\pi^2 g_{re}}{30} \ , \ c = 3\,\omega_\phi^1 \ , \ H_{in} = \frac{\sqrt{\rho_\phi^{in}}}{\sqrt{3}M_P} \quad . \quad (2.52)$$

In the above expression ρ_ϕ^{in}, ρ_R^{in} represent inflaton and radiation energy density respectively at the end of phase-I or the beginning of phase-II

$$\rho_\phi^{in} = \rho_\phi(a = a_{npre}) \ , \ \rho_R^{in} = \rho_R(a = a_{npre}) \quad . \quad (2.53)$$

The maximum radiation temperature defined at the point $x_{max} = a_{max}/a_{npre}$, where $\frac{dT_{rad}}{dx} = 0$, which gives us the maximum radiation temperature for Two-phase reheating expressed in terms of dimensionless comoving densities,

$$T_{rad}^{max} \simeq D^{1/4}\left[1+\frac{(3+c)R(A_{npre})}{8\Phi(A_{npre})A_{npre}^{1-c}}\left(\frac{1-x_{max,p}^{\frac{c+3}{2}}}{c+3}+\frac{\sqrt{\Phi(A_{npre})A_{npre}^{-3(1+\omega_\phi^1)}m_\phi^4}}{\sqrt{3}M_p\Gamma_\phi(1+\omega_\phi^1)}\right)\right] \quad (2.54)$$

$$D = \left(\frac{2\Gamma_\phi\sqrt{3M_p^2\Phi(A_{npre})A_{npre}^{-3(1+\omega_\phi^1)}m_\phi^4}}{(3+c)\,\beta x_{max,p}^4}\right)^{1/4} \ , \ x_{max,p} = \left(\frac{8}{3+c}\right)^{\frac{2}{5-c}} \quad . \quad (2.55)$$

One particularly notices the correction term in the maximum radiation temperature due to initial comoving radiation density $R(A_{npre})$ at the beginning of phase II. It boils down to well know expression $T_{re}^{max} = D^{1/4}$ in the $R(A_{npre}) = 0$ limit. In this above expression, we ignored the contribution of dark matter. However, generically during the reheating period, dark matter is not the dominant component, therefore, the numerical value of the reheating temperature will not be affected. The analytic expression for the dimensionless comoving density during phase II related to the density at the end of inflation will be

$$\Phi(A_{npre}) = (1-3\omega_{eff})\,\Phi(A=1)A_{npre}^{-3\omega_{eff}} \quad . \quad (2.56)$$

Where A_{npre} is the normalized scale factor at the end of the effective dynamics (phase I)

$$A_{npre} = \frac{1-3\omega_{eff}}{3\omega_{eff}} \quad . \tag{2.57}$$

One of our important results from the above expression for the maximum reheating temperature is the highest radiation temperature, which is defined at $T_{rad}^{max} = T_{re}^{max}$ corresponding to a given n_s^{max}. As we change the value of $\omega_{eff} = (10^{-3} \to 10^{-6})$, the maximum reheating temperature changes as $T_{re}^{max} = (10^{13} \to 10^{10})$ GeV. Once we set $R(A_{npre}) = 0$, the maximum reheating temperature becomes $T_{re}^{max} \sim 10^{15}$ GeV as expected (see Eqs.(2.13). Proceeding further, we can also obtain the approximation expression for the reheating temperature itself. Utilizing the expression of the Hubble constant at the equilibrium point ($H_{re} = \Gamma_\phi$), and subsequent entropy conservation, one arrives at the following expression

$$T_{re}^4 \simeq \frac{x_{re}^4 \rho_\phi^{in}}{\beta}\left[\frac{G^4\beta}{\rho_\phi^{in}} + \frac{5-c}{2\,(c+3)}\frac{\rho_R^{in}}{\rho_\phi^{in}}\left(\frac{G^4\beta}{\rho_\phi^{in}} - \frac{\rho_R^{in}}{\rho_\phi^{in}}\right)x_{re}^{c-1}\right] \quad . \tag{2.58}$$

Where, $x_{re} = a_{re}/a_{npre}$ can be recognize as

$$x_{re} = \left(\frac{\alpha}{\eta}\right)^{\frac{1}{c-1}} \quad , \tag{2.59}$$

Here

$$\alpha = \frac{G^4\beta}{\rho_\phi^{in}}\,;\, \eta = \frac{5-c}{2}\left(\frac{G^4\beta}{\rho_\phi^{in}} - \frac{\rho_R^{in}}{\rho_\phi^{in}}\right)\left[\frac{\rho_R^{in}}{(c+3)\,\rho_\phi^{in}} + \frac{5-c}{2}\frac{3M_p^2H_{in}^2}{\rho_\phi^{in}\left(1+\omega_\phi^1\right)^2}\left(\frac{G^4\beta}{\rho_\phi^{in}} - \frac{\rho_R^{in}}{\rho_\phi^{in}}\right)\right]. \tag{2.60}$$

For the detailed derivation of all the aforementioned equations for the reheating temperature, see Appendix 6.2. Now we will consider a class of inflationary models of inflation and analyze our proposed Two-phase reheating scenario.

2.2.3 Inflation models and numerical results

Based on our methodology discussed above, we will now consider a class of inflationary models for which the inflaton potentials assume to be quadratic form. We will also point out the regime of validity of the effective non-perturbative and perturbative era for the different inflationary models. After the inflation, the inflaton field generically oscillates around the minimum of its potential $V(\phi)$. Reheating field coupled with the oscillating inflaton is generically prone to non-perturbative particle production. Our objective is to replace these non-perturbative dynamics with an effective dynamical equation, which is solely governed by the effective equation of state, ω_{eff} supplemented with the additional constraint relation Eqn.(2.38). We have already observed that during phase-I, ω_{eff} is close to that of the inflaton equation of state, ω_ϕ. Near the minimum of the potential if the form is taken to be power law as $\propto \phi^n$, over multiple oscillations, the average inflaton equation of state is expressed as [99]

$$\omega_\phi = \frac{P_\phi}{\rho_\phi} \approx \frac{\langle \phi V'(\phi) - 2V(\phi)\rangle}{\langle \phi V'(\phi) + 2V(\phi)\rangle} = \frac{n-2}{n+2} \quad . \tag{2.61}$$

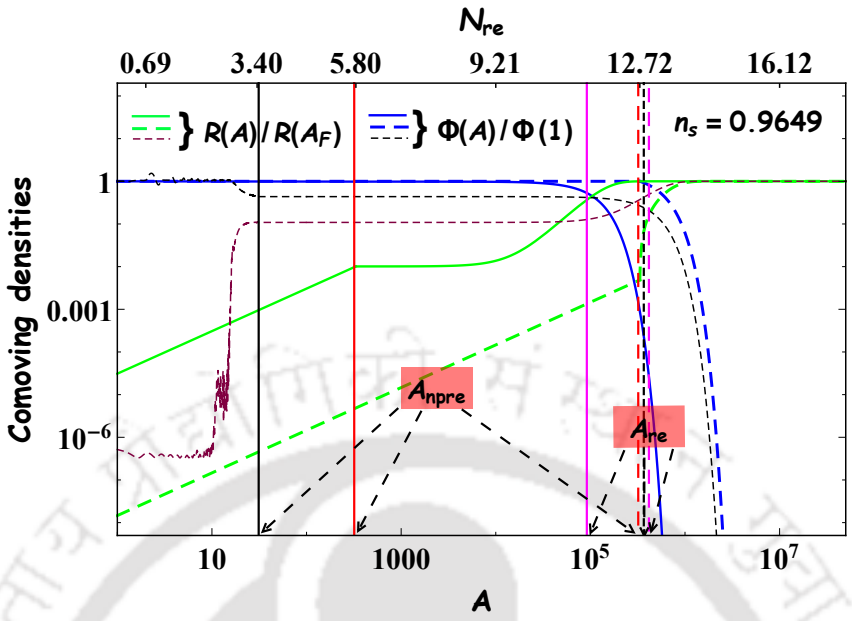

FIGURE 2.3: We plot the evolution of the different energy components (inflaton and radiation) with the normalized scale factor for chaotic inflation model with $n = 2$. The blue and green curve indicates the variation of comoving densities, the inflaton, and radiation density, respectively, for our proposed two-phase dynamics (case-I). The red and pink line represents the normalized scale factor at the ending of phase I and II accordingly. Furthermore, the solid and dashed curves correspond to the two different values of the effective equation of state $\omega_{eff} = (10^{-3}, 10^{-6})$. Whereas, the result for considering standard non-perturbative lattice simulation, during phase I, is shown by the dashed black and brown line.

For $n = 2$ model, ω_ϕ assumes dust like equation of state ($\omega_\phi = 0$). Throughout the subsequent study, we consider those inflationary models which have quadratic potential near their minimum. Therefore, during phase-I of reheating, we set $\omega_\phi = 0$. To this end, let us emphasize again that during phase-II, when the reheating dynamics enter into the perturbative phase, we assume the inflaton equation of state $\omega_\phi^1 \simeq 0.2$, which is one of the important lattice simulation results mentioned earlier. Further, we analyze phase-I dynamics considering two specific choices of the effective equation of state $\omega_{eff} = (\omega_\phi + 10^{-3}, \omega_\phi + 10^{-6})$ which are closed to ω_ϕ.

2.2.3.1 Plots and important model-independent observations :

Before we go into a detailed discussion on various inflationary models, let us first illustrate different plots and important model-independent observations. For each model we have drawn two different plots: one in (Γ_ϕ *vs* N) space where it shows the variation of reheating e-folding number N depending upon the inflaton decay constant. As noted earlier, we have considered different scenarios. For our proposed Two-phase reheating scenario (case-I), we have studied two possible values of the phase-I effective equation of state, $\omega_{eff} = 10^{-3}$ corresponding to solid green and solid black curves, and $\omega_{eff} = 10^{-6}$ corresponding to dotted green and dotted black curves. For all cases, $\omega_\phi = 0$. One of the most important outcomes of our analysis is the emergence of a critical inflaton decay constant $\Gamma_\phi = \Gamma_\phi^{cri}$ denoted by red dots associated with each particular ω_{eff}. This indicates the fact that for $\Gamma_\phi > \Gamma_\phi^{cri}$, the reheating period will be dominated by phase-I, effective non-perturbative dynamics, otherwise, it is perturbative dominated. The critical value of inflaton decay constant increases with the decreasing ω_{eff}.

This can be understood from several interconnecting physical effects. First of all most important Eq.(2.38),

$$R(A=1) = \frac{(\omega_{eff} - \omega_\phi)}{1 - 3\omega_{eff}}\, \Phi(A=1), \tag{2.62}$$

which not only fixes the approximate value of ω_{eff} but also sets the initial condition for phase-I dynamics. Further, the larger the value of ω_{eff}, the higher will be initial radiation density $R(A=1)$ which automatically leads to a smaller value of phase-I e-folding number N_{npre}. Therefore, a particular Γ_ϕ will naturally lead to larger N_{pre}, as associated with each Γ_ϕ there exits a reheating temperature which follows from $T_{re} \propto e^{-N_{re}} = e^{-(N_{pre}+N_{npre})}$. On the other hand critical Γ_ϕ^{cri} is a point where $N_{pre} = N_{npre}$ in N *vs* Γ_ϕ space. From these two conditions, one can argue that transition from perturbative to non-perturbative reheating phase would occur for a larger critical value Γ_ϕ^{cri} for larger ω_{eff} value. Given a reheating model with specific inflaton-daughter field interaction, we have also discussed the existence of critical inflation decay constant $\Gamma_\phi^{cri}(model)$ which were shown by vertical red lines in the plots. From the theoretical values of the critical inflaton decay constant, (Γ_ϕ *vs* N_k) plots indicate that the value of ω_{eff} must lie within $(10^{-3}, 10^{-6})$ irrespective of the inflationary models considered. At this point let us understand the physical meaning of non-vanishing initial radiation density $\rho_R(A=1) \simeq (10^{-3}, 10^{-6})\rho_\phi^{in}$ considering $\omega_{eff} = (10^{-3}, 10^{-6})$. We replace the full non-perturbative dynamics with effective dynamics, which naturally does not capture the complete picture. Typically non-perturbative phase contains three distinct phases: parametric resonance phase, thermalization phase, and steady-state phase. And this is the initial parametric resonance phase, where explosive particle production can naturally give rise to the required initial radiation density $\rho_R(A=1) \simeq 10^{-6} \sim 10^{-3}$ in the unit of total density ρ_ϕ almost instantly.

To see whether our proposed phase I dynamics is justified or not, we compare our result with actual non-perturbative results. In order to do that, we use non-perturbative lattice simulation during the preheating, considering a specific inflaton-reheating field interaction $\frac{1}{2}g^2\phi^2\chi^2$. In all the lattice simulation results, the initial radiation density typically assumes $\rho_R(A=1) \simeq 10^{-4}$ in units of initial inflaton energy density, which essentially lies within what we have considered. Once the preheating phase reaches the steady-state condition, we again solve perturbative dynamics and found that the reheating ends at around the same value of A_{re} (shown by the dashed black line), where our two-phase reheating ends for $\omega_{eff} = 10^{-3}$ (solid pink line) and for $\omega_{eff} = 10^{-6}$ (dashed pink line) accordingly. Therefore, our effective Two-phase reheating approach seems to capture the essential properties of non-perturbative lattice results, except for the non-perturbative e-folding number, which will be taken up in the future.

Nevertheless, for comparison, in the same plot, we also have drawn the total reheating e-folding number for the other two cases: dotted pink lines for case II and solid blue lines for case III mentioned before. It turns out that the total number of reheating e-folding numbers for case-II, case-III, and the case-I, $N_{re} = (N_{npre} + N_{pre})$ are almost the same for all different values of the equation of state.

In an another class of plots in (n_s *vs* T_{re}) space, we describe the variation of reheating temperature T_{re} with respect to the scalar spectral index n_s. From these plots, we can read that the Two-phase reheating process (case-I) is crucially dependent upon the value of ω_{eff}. Furthermore, case-I results are qualitatively similar to that of the case-II for $\omega_{eff}^K = 0.212$. On the other hand, perturbative reheating (case-III) results are qualitatively similar to that

of the case-II for $\omega^K_{eff} = 0$. For the usual perturbative reheating scenario (case-III) the semi-analytic approach discussed before reveals the existence of maximum possible reheating temperature $\sim 10^{15}$ GeV. Our numerical computation also indicates the same thorough solid blue lines. Further, case-II scenario also has the same prediction of model-independent maximum reheating temperature T^{max}_{re} irrespective of the value of its effective equation of state $\omega^K_{eff} = (0, 0.212)$ shown through solid pink lines and dotted pink lines respectively. For conventional reheating dynamics (case-II & case-III), the maximum reheating temperature directly corresponds to instantaneous reheating with the total e-folding number $N_{re} \to 0$. This can also be straightforwardly connected with the maximum possible scalar spectral index n^{max}_s. The proposed two-stage reheating dynamics (case-I) instead predicts very different results in this regard. First of all, instantaneous reheating ceases to exit in this scenario because of its underlying assumptions. As $N_{pre} \to 0$, $N_{re} \to N_{npre}$, which automatically leads to different values of $(T^{max}_{re}, n^{max}_s)$ followed from the condition $N_{re} = N_{npre}$, which naturally assumes model independent values such as $N_{npre} \sim 6$ for $\omega_{eff} = 10^{-3}$, and $N_{npre} \sim 12$ for $\omega_{eff} = 10^{-6}$. The smaller the effective equation of state during phase-I, larger will be its duration N_{npre} and consequently T^{max}_{re} will be reduced. As expected from our earlier analytical calculation the important results are the values of maximum reheating temperature $T^{max}_{re} \sim (10^{13}, 10^{10})$ GeV for $\omega_{eff} = (10^{-3}, 10^{-6})$ respectively. The physical origin of these two different limiting temperatures is clear from the fact that the increase of T_{re} is directly connected with the increase of Γ_ϕ. Hence with the increasing temperature reheating dynamics undergoes a transition from perturbative to non-perturbative regime at particular critical temperature T^{cri}_{re} associated with Γ^{cri}_ϕ, leading to a distinct value of N_{npre} which is different for different ω_{eff} value. This leads to different T^{max}_{re}. Therefore, an important conclusion we can arrive at is that given the approximate estimates of model specific critical decay width $\Gamma^{cri}_\phi(model)$, the maximum reheating temperature T^{max}_{re} should be within $(10^{10} - 10^{13})$ GeV, irrespective of the dynamics of the second phase-II and inflationary model under consideration. However, we must note that the associated maximum values of the n^{max}_s are model-dependent, which will be discussed for each model.

2.2.3.2 Chaotic inflation

For a brief description of this model, see section (1.4.1). Here, for the purpose of our study, we only consider $n = 2$ mainly because $\omega_\phi = 0$. The details of the initial conditions and the relation between reheating temperature (T_{re}) and inflationary index (n^k_s), we follow the methodology explained in the section (2.2.1).

Observations: Important results for chaotic inflation are depicted in Fig.(2.4). As stated at length, the initial effective equation of state ω_{eff} plays a crucial role in driving the whole reheating dynamics. For our purpose we took two sample values $(10^{-3}, 10^{-6})$. According to these two values, the critical values of the inflaton decay constants are found to be $\Gamma^{cri}_\phi = (2.46 \times 10^3, 2.73 \times 10^{-7})$ GeV. Similarly, we can address critical values (transition from perturbative to non-perturbative reheating) in terms of reheating temperature. For this model, the critical values of the reheating temperature set to be $T^{cri}_{re} \simeq (2.7 \times 10^{10}, 3 \times 10^5)$ GeV with for the equation of state $\omega_{eff} = (10^{-3}, 10^{-6})$. This entails the fact that If $\Gamma_\phi > \Gamma^{cri}_\phi$ $(T_{re} > T^{cri}_{re})$, the reheating phase will be dominated by non-perturbative process.

For concreteness, let us bring specific reheating models into consideration. We have discussed three different interaction models with associated non-perturbative constraints equations (1.70), (1.66) and (1.74). Associated with those we have theoretical values of the critical inflaton decay

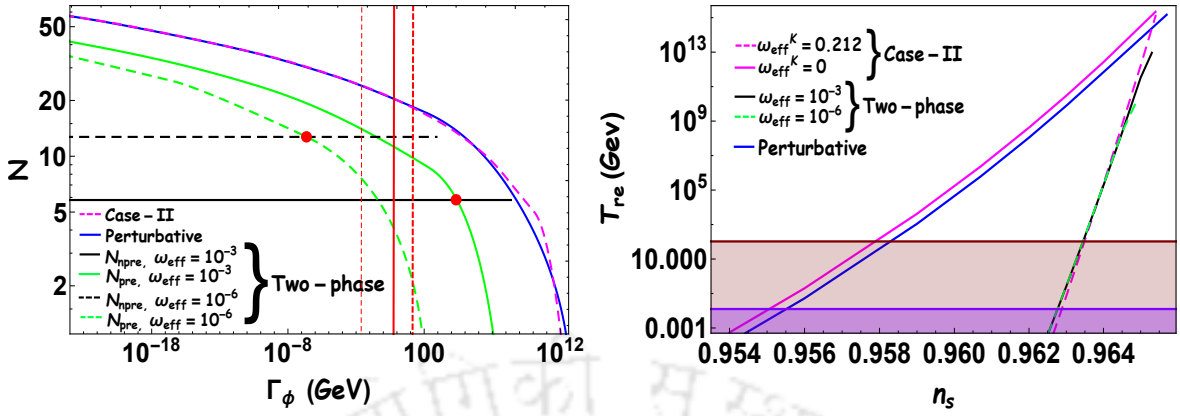

FIGURE 2.4: We plot on the left side, the variation of the e-folding number as a function of inflation decay width (Γ_ϕ) and on the right side, variation of reheating temperature (T_{re}) as a function of n_s for chaotic inflation model with $n = 2$. The plot on the left side, variation of N_{npre} (e-folding number during first phase of reheating), N_{pre} (e-folding number during perturbative reheating) are shown by black, and green lines (solid and dashed) for two different values of $\omega_{eff} = (10^{-3}, 10^{-6})$. The intersection points of N_{npre} and N_{pre} for different values of ω_{eff} are shown by red circle. The blue and dashed pink lines indicate the variation of the e-folding number during reheating for purely perturbative, and the analysis is given by Kaminkowski et al. 2014 [45] with $\omega^K_{eff} = 0$ respectively. The thick dashed, thin dashed, and solid red line corresponds to the three different values of the decay constant at the transition point of non-perturbative to the perturbative era from the theoretical point of view provided by equations (1.74), (1.66) and (1.70). All plots are drawn within 2σ range of n_s [29]. The light brown region is below the electroweak scale $T_{ew} \backsim 100$ GeV and the violet region below 10^{-2} GeV would ruin the predictions of big bang nucleosynthesis (BBN).

.

constants $\Gamma^{cri}_\phi(model) = (0.003, 0.5, 11.8)$ GeV respectively. The first two values correspond to inflaton decaying into the scalar particle, and the third one corresponds to decaying into a pair of fermionic particles. Interestingly, comparing those numerical and theoretical values of Γ^{cri}_ϕ, one can observe that the initial effective equation of state ω_{eff} during phase-I must lie within $(10^{-3}, 10^{-6})$. This essentially suggests that all the three models of inflaton interaction will lead to initial radiation density within the value $(10^{-3}, 10^{-6})$ instantaneously, which we can immediately read off from Fig.(2.3).

In all the reheating scenarios discussed and proposed so far, a model-independent maximum reheating temperature exists. However, the associated maximum value of the spectral index n_s^{max} turned out to be model dependent. In the conventional perturbative reheating discussed before, and also the constraints from reheating (case-II) scenario, $N_{re} \to 0$ provides the condition for n_s^{max}. For Two-phase reheating scenario (case-I) the phase-I effective dynamics is inevitable, which leads to different condition $N_{re} \approx N_{npre}$ for the maximum possible n_s^{max} compatible with CMB observation. Furthermore, for each model one can define minimum spectral index n_s^{min} which can be associated with minimum possible reheating temperature set by BBN constraints [67]-[69], which is $T_{re}^{min} = 10^{-2}$ GeV. Taking into account both the possibilities, for case-I we obtain the possible bound on the spectral index $0.9628 \leq n_s \leq 0.9653$ and $0.9628 \leq n_s \leq 0.9649$ for $\omega_{eff} = (10^{-3}, 10^{-6})$ respectively. For case-II [45], the bound is $0.955 \leq n_s \leq 0.9654$, $0.9629 \leq n_s \leq 0.9654$ for $\omega^K_{eff} = (0, 0.212)$ respectively. Additionally, for purely perturbative dynamics case-III, one obtains $0.9555 \leq n_s \leq 0.9657$. Important to remind at this point, all these bounds are consistent with CMB within 2σ error of n_s. From the maximum n_s^{max}, the maximum value of the inflationary e-folding number (N_k^{max}) can be obtained. For example for case-I scenario we have $N_k^{max} \simeq (57, 56)$ with effective equation of state $\omega_{eff} = (10^{-3}, 10^{-6})$ respectively. Whereas, for case-II, $N_k^{max} \simeq 57$ and for case-III,

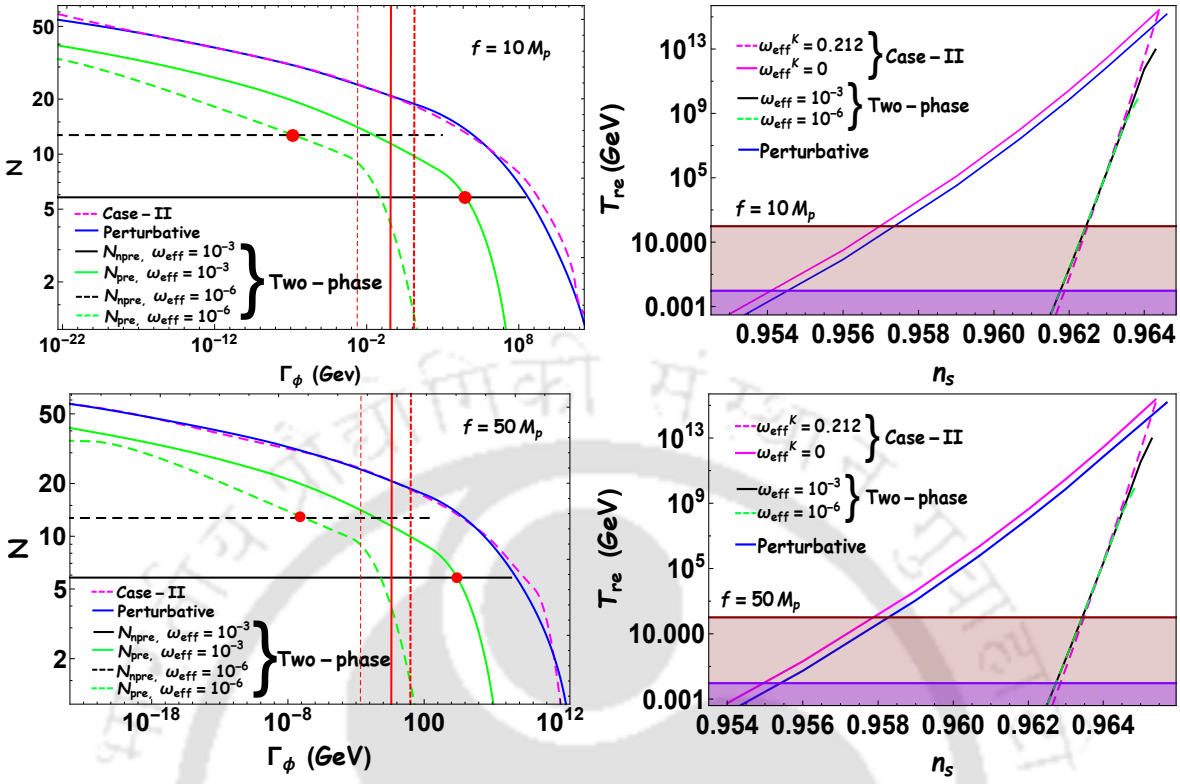

FIGURE 2.5: All plots are the same as in the previous Fig.2.4. The main difference is that here we have plotted for the natural inflation model for $f = (10, 50)M_p$.

.

$N_k^{max} \simeq 58$.

The variation of the reheating temperature as a function of the spectral index for the different reheating mechanisms is shown in Fig.(2.4). The behavior of reheating temperature with respect to n_s appears to be model-independent.

2.2.3.3 Axion inflation

The details of this model and the initial conditions to solve the differential equations for the effective non-perturbative and perturbative era are provided in secs (1.4.2) and (2.2.1). Here, to be consistent with CMB data, we consider two sample super-Planckian values of the axion decay constant, $f = (10, 50)M_p$.

Observations: The main results of the axion inflationary model are depicted in Fig. (2.5). As has been mentioned earlier we have considered two sample values of the axion decay constant $f = (10, 50)M_p$. For a fixed value of axion decay constant, $f = 10M_p$, the critical values of inflaton decay constant assume $\Gamma_\phi^{cri} \simeq (3.7 \times 10^4, 1.1 \times 10^{-7})$ GeV, and that of the reheating temperatures are $T_{re}^{cri} \simeq (4 \times 10^{10}, 1.8 \times 10^5)$ GeV. Similarly for $f = 50M_p$, $\Gamma_\phi^{cri} \simeq (2.7 \times 10^4, 1.1 \times 10^{-7})$ GeV and $T_{re}^{cri} \simeq (9 \times 10^{10}, 1.9 \times 10^5)$ GeV. For both the cases the effective equation of states are taken to be $\omega_{eff} = (10^{-3}, 10^{-6})$. One the other hand the theoretical value of the critical inflaton decay constants for three different interacting reheating models are calculated to be, $\Gamma_\phi^{cri}(model) = (2.8 \times 10^{-3}, 0.45, 10.8)$ GeV for $f = 10M_p$, and

Table 2.1: Reheating models and their associated bound on inflationary parameters (Axion inflation)

$f = 10M_p$

Inflationary parameter	Case-I (Two-phase)		Case-II		Case-III (Perturbative)
	$\omega_{eff} = 10^{-3}$	$\omega_{eff} = 10^{-6}$	$\omega^K_{eff} = 0$	$\omega^K_{eff} = 0.212$	$\omega_\phi = 0$
n_s^{min}	0.9618	0.9618	0.9541	0.9619	0.9545
n_s^{max}	0.9643	0.9639	0.9644	0.9644	0.9646
N_k^{max}	57.06	56.39	57.23	57.23	57.58

$f = 50M_p$

Inflationary parameter	Case-I (Two-phase)		Case-II		Case-III (Perturbative)
	$\omega_{eff} = 10^{-3}$	$\omega_{eff} = 10^{-6}$	$\omega^K_{eff} = 0$	$\omega^K_{eff} = 0.212$	$\omega_\phi = 0$
n_s^{min}	0.96275	0.96275	0.9549	0.9629	0.9554
n_s^{max}	0.9653	0.9649	0.9654	0.9654	0.9657
N_k^{max}	57.14	56.48	57.31	57.31	57.81

$\Gamma_\phi^{cri}(model) = (3.2 \times 10^{-3}, 0.51, 12.3)$ GeV for $f = 50M_p$. Those values of decay constants are determined from equations (1.70), (1.66) and (1.74) accordingly. Let us point out again that the first two values correspond to inflaton decaying into the scalar particle, and the third one corresponds to decaying into a pair of fermionic particles. Here again, from the left panel of Fig.2.5, one concludes that if the universe undergoes Two-phase reheating, considering the specific interaction during reheating the initial ω_{eff} during phase-I must lie within $(10^{-3}, 10^{-6})$. The lower limit of n_s has been set by the minimum possible reheating temperature due to the big-bang nucleosynthesis (BBN) constraint. With increasing spectral index from its minimum value n_s^{min} along with decay width, the perturbative e-folding number N_{pre} depreciates towards zero and the total e-folding number, N_{re} approaches towards N_{npre} which is identified as the point of T_{re}^{max} and n_s^{max}. Following the discussion of chaotic inflation model, in the Table (2.1), we provide possible limiting value the inflationary parameters $(n_s^{min}, n_s^{max}, N_k^{max})$ parameters for three different reheating scenarios. These limiting values, in turn, will restrict the possible values of reheating parameters. Therefore, the more we decrease the error of the inflationary parameter, the more precisely we will be able to fix the reheating parameters.

2.2.3.4 $\alpha-$attractor model

We have already discussed how this kind of inflationary model can be related to CMB observables in sec-1.4.3. Moreover, all the initial conditions for phase-I and II will be the same as before (for this instance, see section (2.2.1)). For our purpose, we have taken two values of α(1,100)

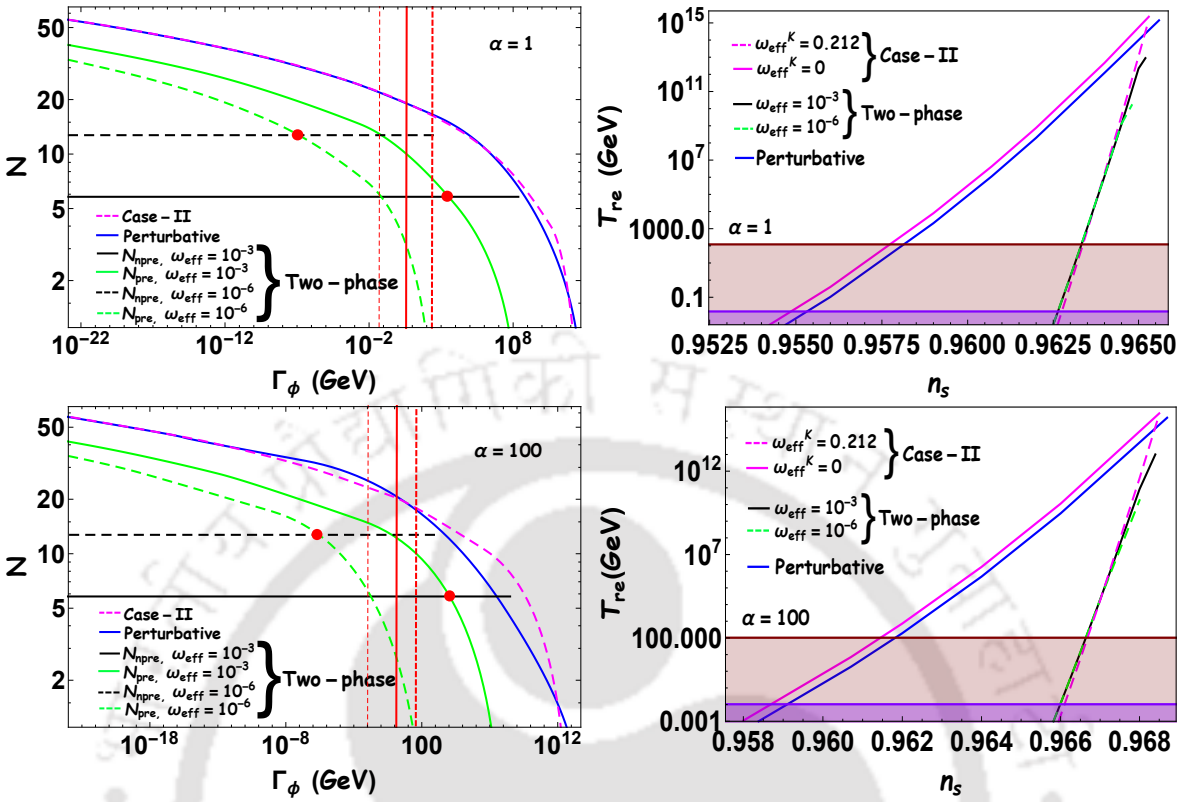

FIGURE 2.6: All plots are same as in the previous Fig.(2.4). The main difference is that here we have plotted for α-attractor model for $\alpha = (1, 100)$ with $n = 1$. However, the plot for $\alpha = 1$ and $n = 1$ is for Higgs-Starbinsky model.

.

with $n = 1$ and compared their outcomes.

Observaions: With two sample values of $\alpha = (1, 100)$, the model dependent critical values of the inflaton decay constant assume $\Gamma_\phi^{cri}(model) = (0.069, 5.03, 260.3)$ GeV and $(0.01, 1.6, 42.2)$ GeV for three different kinds of the decay processes. Whereas our numerical analysis predicts the critical decay constant to be $\Gamma_\phi^{cri} = (3.44 \times 10^3, 1.37 \times 10^{-7})$ GeV for $\alpha = 1$ and $\Gamma_\phi^{cri} = (1.27 \times 10^4, 3.90 \times 10^{-6})$ GeV for $\alpha = 100$ with $\omega_{eff} = (10^{-3}, 10^{-6})$ respectively. Within these values, all the model-dependent critical decay constants must lie (see Fig. (2.6)). In addition to that, the reheating temperature connected with the critical value of the inflaton decay constant turns out to be $T_{re}^{cri} \simeq (2.3 \times 10^5, 3.5 \times 10^{10})$ GeV for $\alpha = 1$ and for $\alpha = 100$, $T_{re}^{cri} \simeq (1.2 \times 10^6, 7.2 \times 10^{10})$ GeV with $\omega_{eff} = (10^{-6}, 10^{-3})$ accordingly. Similar to the other inflation model discussed above, in Table-(2.2), the possible constraints on the inflationary parameters can be obtained.

2.2.3.5 Minimal plateau model

In the minimal plateau model scenario, the details of this potential and the inflation model-dependent input parameters, which are essential to determine the initial conditions for the subsequent reheating dynamics, are mentioned in section(1.4.4). Here for numerical purposes, we have chosen $\phi_* = (0.001, 0.1)M_p$ with $n = 2$. As we mentioned earlier, our main intention

Table 2.2: Reheating models and their associated bound on inflationary parameters (α-attractor model)

Higgs-Starobinsky model ($\alpha = 1$)

Inflationary parameter	Case-I (Two-phase)		Case-II		Case-III (Perturbative)
	$\omega_{eff} = 10^{-3}$	$\omega_{eff} = 10^{-6}$	$\omega^K_{eff} = 0$	$\omega^K_{eff} = 0.212$	$\omega_\phi = 0$
n_s^{min}	0.9626	0.9626	0.9548	0.9628	0.9552
n_s^{max}	0.9652	0.9648	0.9653	0.9653	0.9656
N_k^{max}	55.36	54.72	55.52	55.52	56.02

$\alpha = 100$

Inflationary parameter	Case-I (Two-phase)		Case-II		Case-III (Perturbative)
	$\omega_{eff} = 10^{-3}$	$\omega_{eff} = 10^{-6}$	$\omega^K_{eff} = 0$	$\omega^K_{eff} = 0.212$	$\omega_\phi = 0$
n_s^{min}	0.966	0.966	0.9587	0.9661	0.959
n_s^{max}	0.9684	0.968	0.9685	0.9685	0.9657
N_k^{max}	56.73	56.03	56.91	56.91	57.27

is to see the modification in reheating parameters (T_{re}, N_{re}) in comparison with the usual single-phase analysis

Observations: The important results of the minimal plateau inflationary model are depicted in Fig.(2.7). In this model the value of $\Gamma_\phi^{cri}(model)$ for three different decay process assume $\Gamma_\phi^{theo} = (0.7,\ 34.2, 2749.2)$ GeV for $\phi_* = 0.01$, and $(15.3, 231.7, 5.8 \times 10^4)$ GeV for $\phi_* = 0.001 M_p$. As usual those values are obtained from Eqs.(1.70, 1.66, 1.74) with $\phi_* = (0.01,\ 0.001) M_p$ accordingly. On the other hand our numerical analysis estimates the value of $\Gamma_\phi^{cri} = (2.3\times10^3,\ 4.8\times10^{-7})$ GeV for $\phi_* = 0.01 M_p$, and $\Gamma_\phi^{cri} = (394.7,\ 2.7\times10^{-8})$ GeV for $\phi_* = 0.001 M_p$. As discussed for other inflationary scenarios, for each model parameter value of ϕ_* two bracketed values of Γ_ϕ^{cri} are calculated for $\omega_{eff} = (10^{-3}, 10^{-6})$ respectively. The reheating temperature linked with the decay width Γ_ϕ^{cri}, can be found to be $T_{re}^{cri} \simeq (2.80\times10^5,\ 2.25\times10^{10})$ GeV considering $\phi_* = 0.01 M_p$, and for $\phi_* = 0.001 M_p$, $T_{re}^{cri} \simeq (5.80\times10^4,\ 8.76\times10^9)$ GeV with $\omega_{eff} = (10^{-6},\ 10^{-3})$ accordingly. Interestingly, for this minimal inflation scenario a specific choice of $\phi_* = 0.01 M_p$, $\omega_{eff} = 10^{-3}$, Γ_ϕ^{cri} approximately matches with that of $\Gamma_\phi^{cri}(model)$ for a specific reheating scenario when inflaton decaying into a pair of fermionic particles with the interaction $\phi\bar{\psi}\psi$. Similarly for $\phi_* = 0.001 M_p$, $\omega_{eff} = 10^{-3}$, we found $\Gamma_\phi^{cri} \simeq \Gamma_\phi^{cri}(model)$ when reheating dynamics is governed by the inflaton decaying into pair of scalar particles with the interaction $\phi\chi^2$. Associated with the reheating temperature, the bound on the inflationary parameters is given in Table-(2.3).

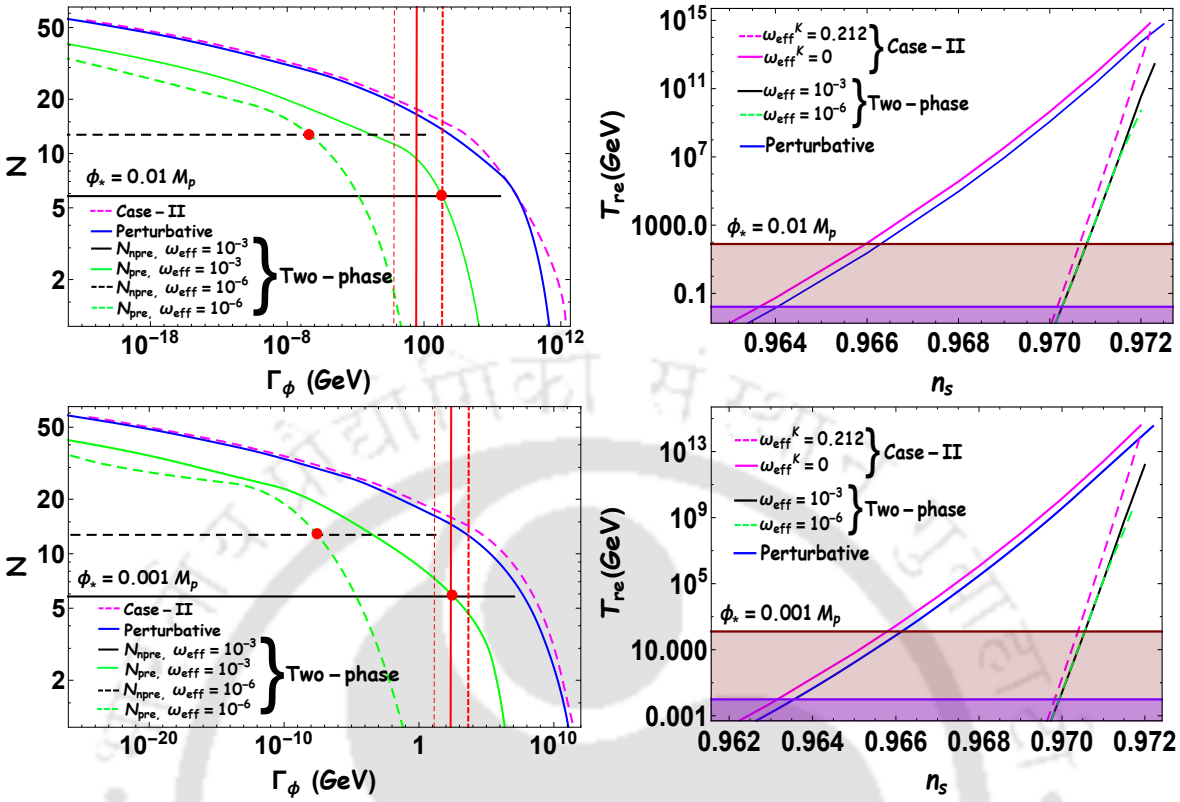

FIGURE 2.7: All plots are the same as in the previous Fig.2.4. The main difference is that here we have plotted for the minimal inflation model with $\phi_* = (0.01, 0.001)M_p, n = 2$.

2.2.4 Constraining the inflaton coupling parameters

So far, we have discussed mainly understanding the reheating parameters and their constraints from reheating. In this section we qualitatively translate those results into constraints on coupling parameters ($\tilde{g} = g/m_\phi, y, h$) corresponding to specific inflaton-scalar interactions $\tilde{g}m_\phi\phi\chi^2, y\phi\chi^3$, and inflaton-fermion interaction $h\phi\bar{\psi}\psi$ respectively. So far, our analysis was independent of the specific inflaton interaction model. Therefore, the inflaton decay width was a free parameter with one-to-one correspondence with the reheating temperature. Constraining reheating models is very challenging from the perspective of its observational limitations. Therefore, indirect constraints on the inflaton coupling parameters through reheating dynamics would be significant from the model building point of view. Reheating temperature estimates the allowed ranges of dimensionless coupling parameters via the inflaton decay constant Γ_ϕ. This section for illustration only considers two observationally viable inflationary models: Higgs-Starobinsky and minimal plateau models with $n = 2$, which are consistent with the current observational bound on $r < 0.064$ [29].

Bounds on couplings: The constraints on different coupling constants are shown in figure 2.8. Plots show how the dimensionless coupling parameter $\tilde{g}$, h, and y are intimately linked with CMB anisotropy via the inflationary observables such as (n_s, r_k) for different types of reheating dynamics. The mapping $T_{re} \to \Gamma_\phi \to (\tilde{g}, y, h)$ are directly followed from Eqs.(1.62, 1.68, 1.72, 2.25). From these equations, we obtain the constraints on the coupling parameters

Table 2.3: Reheating models and their associated bound on inflationary parameters (Minimal plateau model)

$\phi_* = 0.01M_p$

Inflationary parameter	Case-I (Two-phase)		Case-II		Case-III (Perturbative)
	$\omega_{eff} = 10^{-3}$	$\omega_{eff} = 10^{-6}$	$\omega^K_{eff} = 0$	$\omega^K_{eff} = 0.212$	$\omega_\phi = 0$
n_s^{min}	0.9703	0.9703	0.9637	0.9702	0.9640
n_s^{max}	0.9723	0.972	0.9722	0.9722	0.9725
N_k^{max}	54.16	53.58	53.96	53.96	54.55

$\phi_* = 0.001M_p$

Inflationary parameter	Case-I (Two-phase)		Case-II		Case-III (Perturbative)
	$\omega_{eff} = 10^{-3}$	$\omega_{eff} = 10^{-6}$	$\omega^K_{eff} = 0$	$\omega^K_{eff} = 0.212$	$\omega_\phi = 0$
n_s^{min}	0.9700	0.9700	0.9632	0.9698	0.9636
n_s^{max}	0.9720	0.9717	0.9719	0.9719	0.9722
N_k^{max}	53.57	53.00	53.38	53.38	53.96

with respect to the inflationary parameters. Any realistic reheating scenario should include all possible inflaton coupling based on underlying symmetry. Therefore, the assumption that a specific inflaton coupling's contribution is the dominant one throughout the entire reheating period may not be relevant. Hence, a more pragmatic approach would be to construct particle physics motivated models, which we left for our future study. However, as a toy model analysis, the present study may guide us in building scenarios that include all the standard model fields. Nevertheless, based on our reheating discussions so far, we compare the constraints for all the cases. To this end let us point out that in terms of a mathematical expression, the decay width Γ_ϕ associated with the coupling parameters $\tilde{g}$ and h is the same. Therefore, for each model under consideration we have two different figures in the $(\tilde{g}/h, n_s)$ and (y, n_s) space. Given the observation from CMB temperature anisotropy, the coupling parameters for the Higgs-inflation model, which are assumed to be responsible for entire reheating process, are found to be constrained within $1.31 \times 10^{-17} \leq (\tilde{g}, h) \leq 0.01$ (solid black curve) and $1.38 \times 10^{-17} \leq (\tilde{g}, h) \leq 2.55 \times 10^{-5}$ (dotted green curve) for two different values of effective equation state $\omega_{eff} = (10^{-3}, 10^{-6})$ respectively. Whereas for the same values of the effective equation of state the coupling constant y for three body interaction $(y\phi\chi^3)$ lies within $8.07 \times 10^{-16} \leq y \leq 0.85$ (solid black curve), and $8.47 \times 10^{-16} \leq y \leq 1.50 \times 10^{-3}$ (dotted greed curve). Important but straightforward to note that the largest values of the coupling constant $\tilde{g}_{max}/h_{max} = (0.01, 2.55 \times 10^{-5})$, and $y_{max} = (0.85, 1.50 \times 10^{-3})$ correspond to maximum reheating temperature $T_{re}^{max} = (10^{10}, 10^{13})$ GeV respectively. Reemphasizing the fact that two

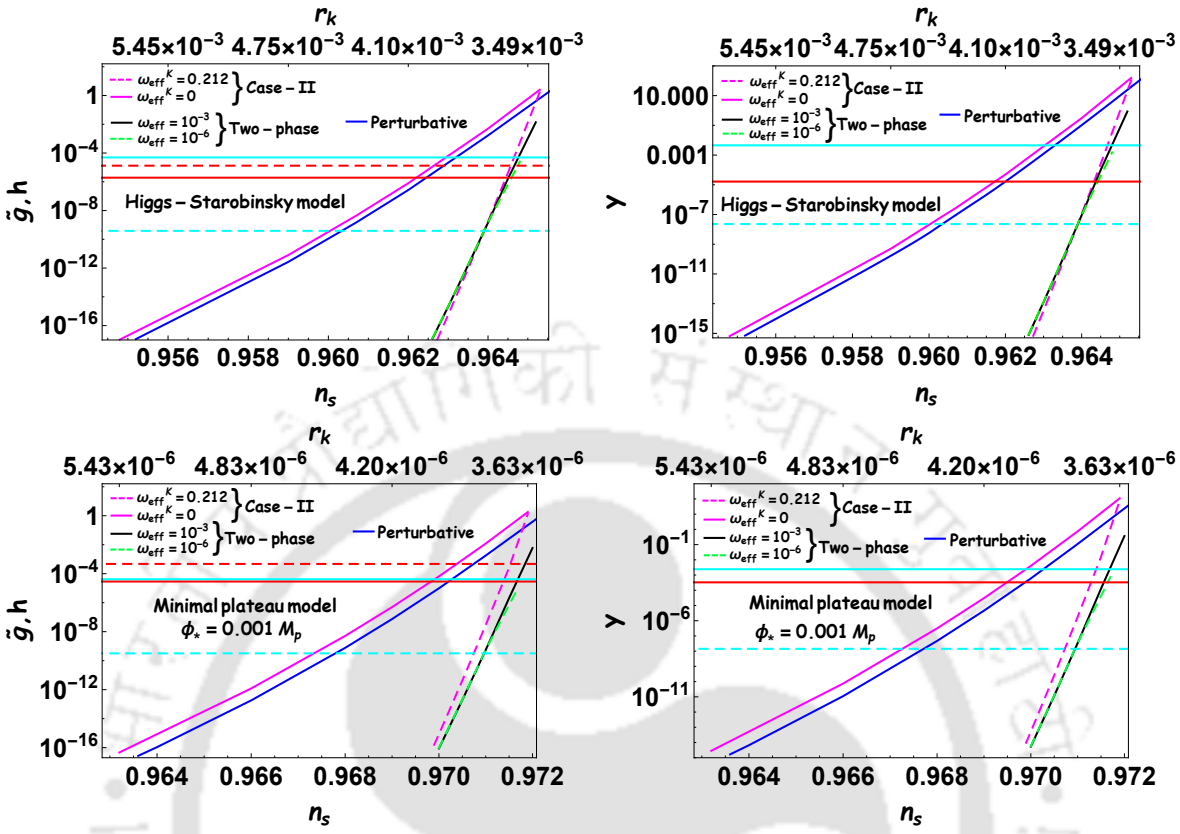

FIGURE 2.8: We have plotted the spectral index dependence of the dimensionless coupling constant $\tilde{g} = \frac{g}{m_\phi}$ with $g\phi\chi^2$ interaction, y with three bodies $y\phi\chi^3$ interaction and Yukawa coupling with $y\phi\psi\bar{\psi}$ interaction. The upper two plots are for the Higgs-Starobinsky inflation model, and the lower two plots are for the minimal plateau inflation model with $\phi_* = 0.001 M_p$, $n = 2$. The solid and dashed pink line corresponds to the usual reheating dynamics given by Kaminkowski et al. [45] for $\omega_{eff}^K = (0,\ 0.212)$ respectively. The solid blue line indicates the results of the perturbative analysis. The results for our developed two-phase reheating mechanism are represented by the solid black line and dashed green line for $\omega_{eff} = (10^{-3},\ 10^{-6})$ accordingly. In the first and third plots, the solid and dashed red line implies the transition point from parametric resonance to perturbative dynamics for two different kinds of interaction, $g\phi\chi^2$ and $y\phi\psi\bar{\psi}$, measured from theoretical constraints provided by the equation (1.65) and (1.73). Similarly, in the second and fourth plot, the solid red line corresponds to the three bodies $y\phi\chi^3$ interaction. Additionally, the solid and dashed sky blue line indicates the coupling constant at the intersection points of the e-folding numbers, N_{npre} and N_{pre}, above which value the effective dynamics start dominating over perturbative dynamics for $\omega_{eff} = (10^{-3},\ 10^{-6})$ respectively. All the plots are drawn within the minimum and maximum values of the spectral index. The minimum values of the spectral index (n_s^{min}) corresponds to $T_{re} \approx 10^{-2}$ GeV and for maximum values of spectral index (n_s^{max}), $N_{re} \approx N_{npre}$ in our analysis and $N_{re} \to 0$ in conventional reheating dynamics.

different limiting values of coupling constants are realizable only in the high-temperature limit for two different ω_{eff}. All the above estimates are for the two-phase reheating process (case-I). For the other two scenarios, the bounds on the coupling constant can be read from Table-(2.4). The interesting interplay between the inflationary theory parameters and the emergent reheating parameters governed by the CMB anisotropy gives important constraints on the theory itself. Apart from having the maximum possible values of the coupling constants, compatible with CMB observations, there exists a critical value of the same born out of Γ_ϕ^{cri}, which entails whether the reheating is perturbative or non-perturbative phase dominated. For minimal plateau model, we found ($\tilde{g}_{cri} \approx 3.46 \times 10^{-5}$) for $\omega_{eff} = 10^{-3}$, which closely matches with the associated perturbative constraints $\tilde{g}_{cri}(model) \approx 2.38 \times 10^{-5}$. For the Higgs-Starobinsky

Table 2.4: Reheating models and their associated bound on coupling parameters

Higgs-Starobinsky model

Coupling parameter	Case-I (Two-phase)		Case-II		Case-III (Perturbative)
	$\omega_{eff} = 10^{-3}$	$\omega_{eff} = 10^{-6}$	$\omega^K_{eff} = 0$	$\omega^K_{eff} = 0.212$	$\omega_\phi = 0$
$\tilde{g}_{min}, h_{min}$	1.31×10^{-17}	1.38×10^{-17}	1.06×10^{-17}	1.13×10^{-17}	1.15×10^{-17}
$\tilde{g}_{max}, h_{max}$	0.01	2.55×10^{-5}	2.52	1.71	2.48
y_{min}	8.07×10^{-16}	8.47×10^{-16}	6.51×10^{-16}	6.98×10^{-16}	7.10×10^{-16}
y_{max}	0.85	1.50×10^{-3}	155.10	105.31	152.76

Minimal plateau model ($\phi_* = 0.001 M_p$)

Coupling parameter	Case-I (Two-phase)		Case-II		Case-III (Perturbative)
	$\omega_{eff} = 10^{-3}$	$\omega_{eff} = 10^{-6}$	$\omega^K_{eff} = 0$	$\omega^K_{eff} = 0.212$	$\omega_\phi = 0$
$\tilde{g}_{min}, h_{min}$	8.74×10^{-17}	9.27×10^{-17}	4.62×10^{-17}	1.58×10^{-16}	2.70×10^{-17}
$\tilde{g}_{max}, h_{max}$	5.90×10^{-3}	1.19×10^{-5}	1.79	1.30	1.12
y_{min}	5.38×10^{-15}	5.71×10^{-15}	2.84×10^{-15}	9.73×10^{-15}	1.66×10^{-15}
y_{max}	0.36	7.37×10^{-4}	110.26	80.31	68.93

inflation model, $h_{cri} \simeq 5.3 \times 10^{-5}$ for $\omega_{eff} = 10^{-3}$ and the associated perturbative constraints for Yukawa interaction is $h_{cri}(model) \simeq 1.33 \times 10^{-5}$. Therefore, we can infer from this observation that our two-phase reheating scenario essentially captures the necessary features of the non-perturbative phase.

So far, we have discussed the reheating dynamics considering inflaton and radiation as the two dynamical components. However, as we all know, dark matter is another important constituent of our present universe. One of this component's important properties is that its coupling with the standard model fields must be very weak. Apart from this, not much is known about its other fundamental properties, such as charge, mass, and coupling. Experimental searches of this particle are going on across the globe without much success till now. The searches include both directly as well as indirectly observing the properties of this object and, finally, jointly constraining the parameter region. We will study the dark matter phenomenology-based CMB parameter space following our previous work [92]. We essentially generalize our Two-phase reheating formalism and include dark matter as the third dynamical matter component.

2.2.5 Unifying the dark sector

In the previous section, we discussed the Two-phase reheating process, where inflaton decays only into radiation. In the present discussion, we add additional dark matter components and discuss the impact on dark matter phenomenology. The assumption is that inflaton decays into radiation and then radiation to dark matter. The methodology of the analysis will be the same as before, except for the new additional dynamical equations for dark matter.

Phase-I:(*Effective non-perturbative phase*) The dynamics is governed by

$$\rho_t = \rho_\phi + \rho_R + \rho_X = \rho_{end}\left(\frac{a_{end}}{a}\right)^{3(1+\omega_{eff})} , \tag{2.63}$$

where the new component ρ_X is the energy density of the dark matter particle with mass M_X and energy of the dark matter is expressed as $\langle E_X\rangle = \sqrt{M_X^2 + 9T^2}$ [4]. T is the temperature. The above equation can be written in differential form as,

$$\dot{\rho_\phi} + \dot{\rho_R} + \dot{\rho_X} + 3H(1+\omega_{eff})(\rho_\phi + \rho_R + \rho_X) = 0 . \tag{2.64}$$

Besides the above equation, we consider an additional conservation equation characterizing the dynamics of every individual energy component during this phase as,

$$\dot{\rho_\phi} + 3H(1+\omega_\phi)\rho_\phi + \dot{\rho_R} + 4H\rho_R + \dot{\rho_X} + 3H\rho_X = 0 . \tag{2.65}$$

To solve the above equations (2.65) and (2.64), we need one more condition. We define the ratio of the dark matter and the radiation energy density as $\gamma = \frac{\rho_X}{\rho_R}$. After combining the above two equations one finds,

$$\frac{\rho_R}{\rho_\phi + \rho_R + \rho_X} = \frac{\rho_R}{\rho_\phi + \rho_R + \gamma\rho_R} = \frac{3\,(\omega_\phi - \omega_{eff})}{3\,\omega_\phi\,(1+\gamma) - 1} . \tag{2.66}$$

At the initial stage of the reheating, radiation energy density must be very small $\rho_R \simeq 0$. Hence, as discussed extensively for the two-component reheating, here also ω_{eff} must assume the value very close to the inflaton equation of state ω_ϕ, at least near the beginning. In terms of dimensionless variable, this phase can be written as

$$\frac{\Phi'}{A^{3\omega_\phi}} + \frac{R'}{A} + \frac{\langle E_X\rangle X'}{m_\phi} = 0 , \tag{2.67}$$

$$\frac{\Phi'}{A^{2+3\omega_\phi}} + \frac{R}{A^4}[3(1+\omega_{eff}) - 4] + \frac{3\langle E_X\rangle X}{m_\phi A^3}\omega_{eff} + \frac{R'}{A^3} + \frac{3\Phi(\omega_{eff} - \omega_\phi)}{A^{3(1+\omega_\phi)}} + \frac{X'\langle E_X\rangle}{m_\phi A^2} = 0 , \tag{2.68}$$

here the dimensionless dark matter density $X = \frac{\rho_X}{\langle E_X\rangle}a^3$.

Phase-II (*perturbative phase*)The subsequent perturbative phase will now be governed by two more parameters related to the dark matter component followed by the Eqns. (2.26), (2.27), and (2.28), the only difference is that the inflaton equation of state is replaced by ω_ϕ^1.

Initial conditions: The general form of the initial conditions during the first phase of reheating (phase-I) are,

$$\Phi(1) = \frac{3}{2}\frac{V(\phi_{end})}{m_\phi^4} , \; R(1) = \frac{3\,(\omega_{eff} - \omega_\phi)}{1 - 3\,\omega_{eff}\,(1+\gamma)}\Phi(1) , \; X(1) = \frac{\gamma\, m_\phi}{\langle E_X\rangle}R(1) . \tag{2.69}$$

The initial values of the energy densities for the phase II will be set at the normalized scale factor A_{npre} as

$$\Phi = \Phi(A_{npre}); \frac{R(A_{npre})}{R(A_{npre}) + \Phi(A_{npre}) + X(A_{npre})} \simeq \frac{1}{2}; X(A_{npre}) = \frac{\gamma\ m_\phi}{\langle E_X \rangle} R(A_{npre}). \quad (2.70)$$

As described in detail in section 2.2.1, radiation energy density is again assumed to be 50% of the total comoving energy density right after the completion of phase-I. Therefore, the dark matter number density will automatically be fixed for a given γ value. All the required equation of states for two different phases are assumed to take the same approximate values $\omega_\phi^1 \simeq 0.2$ and $\omega_\phi \simeq 0$. The methodology of solving the dynamics will be the same as before except for some additional constraints in the dark sector after the end of reheating, which is already described in section (2.1.2.1).

The detailed analysis only on phase-II has already been done in [91] including the dark matter phenomenology. Nevertheless, we only consider dark matter production via a freeze-in mechanism. This mechanism indicates that the dark matter will never reach equilibrium with the thermal bath. This kind of dark matter is known as FIMP (feebly interacting dark matter) [107–117]. We can illustrate the production of dark matter via the Freeze-in mechanism through the heavy mediator during reheating is sensitive to the early history of the universe before the UV dominated era [118–127].

Physical constraints: Further constraints on the dark matter parameter space will be inherited if one considers various theoretical limits on the scattering cross-section. The cross-section can not be arbitrarily large. Perturbative unitarity usually limits the cross-section $\langle \sigma v \rangle$ in term of mass, $\langle \sigma v \rangle_{max} = \frac{8\pi}{M_X^2}$ [128], which are shown by pink solid lines in Figs.(2.9, 2.10). On the other hand, we will also have another bound on the cross-sections coming from the fact that during reheating dark matter production peaks around the temperature of $T_* = \frac{M_X}{4}$ [4]. This provides a natural condition on the dark matter number density $n_X(T) < n_X^{eq}(T_*)$ as for $T < T_*$ the dark matter production would be frozen, and it must be diluted subsequently due to the expansion of the universe. Aforementioned condition on the dark matter number density sets an upper bound on the cross-section $\langle \sigma v \rangle \approx \langle \sigma v \rangle_{T=T_*}$ [4] [129]

$$\langle \sigma v \rangle_* \leq 7 \times 10^{-14} \left(\frac{2}{g}\right) \left(\frac{g_*(T_*)}{10}\right) \left(\frac{10}{g_*(T_{re})}\right)^{\frac{1}{2}} \left(\frac{M_X}{10GeV}\right) \left(\frac{100MeV}{T_{re}}\right)^2 GeV^{-2} \quad . \quad (2.71)$$

We call it as reheating bound in the plot. This condition is depicted by black solid lines and black dotted lines for perturbative and two-phase reheating scenarios respectively in Figs.(2.9, 2.10). We have shown both of these bounds in the subsequent plots for different inflation models once we fixed the dark matter mass. *Interesting observation that can be made from this theoretical constraint is that given a dark matter mass, the perturbative unitarity bound and the dynamical condition Eq.2.71 modify the possible range of allowed n_s values obtained from the previous analysis. This can directly shed light on the inflationary model building. Conversely, one can state that for a given inflationary model, CMB can shed light on the possible nature of the dark matter candidate via reheating phase.*

Nevertheless, unifying the dark sector into a single reheating framework is the primary motivation of this section. The basic philosophy is to look into further constraints on the dark-matter parameter space in a more realistic framework of Two-phase reheating dynamics and compare it with that of the usual perturbative reheating analysis [91]. An important outcome is the constraints due to CMB temperature anisotropy. Particularly, constraints imparted on the

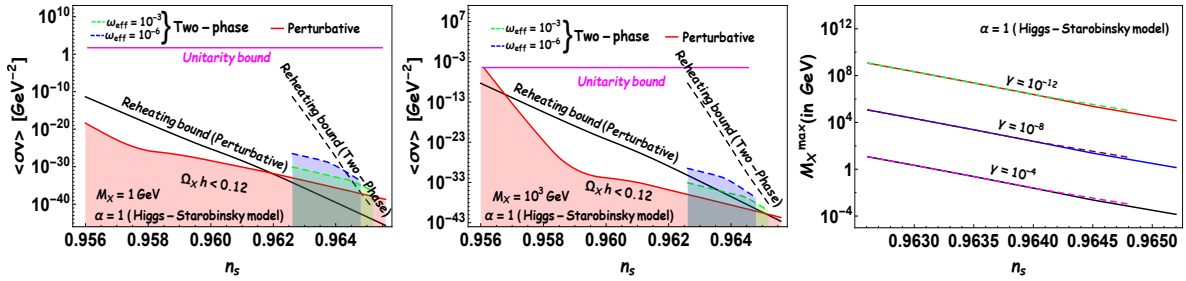

FIGURE 2.9: In the first two plots, we have plotted the contour of $\Omega_X h^2 = 0.12$ in the $n_s - \langle \sigma v \rangle$ plane with a fixed value of dark matter mass within the minimum and maximum values reheating temperature for the Higgs-Satrobinsky model. In the case of Two-stage reheating, we have chosen a fixed value of $\gamma = 10^{-11}$ (ratio of the dark-matter energy density to the radiation density) during the first stage of reheating. The allowed parameter space is shown by the shaded region below the contour line. The pink horizontal line corresponds to the unitarity bound. The solid and dashed black line corresponds to the reheating bound for two different reheating processes. On the right-hand side, we have plotted the maximum permitted values of dark matter mass as a function of the spectral index for three different values of γ. Here the solid and dashed lines are for $\omega_{eff} = (10^{-3}, 10^{-6})$ respectively.

.

dark matter and inflationary parameter space ($\langle \sigma v \rangle - n_s$) by the CMB anisotropy could enable us to constrain the viable inflationary models through dark matter observable. Conversely, given a viable inflationary model, CMB can potentially shed light on the possible properties of dark matter. Keeping this in mind, we study dark matter phenomenology considering two observationally viable inflationary models: Higgs-Starobinsky and minimal plateau models, which are consistent with the current observational bound on $r < 0.064$ [29].

2.2.5.1 Higgs-Starobinsky model and dark matter phenomenology

We have already discussed about the model in the introduction section (1.4), and the constraints on the reheating parameters (N_{re}, T_{re}) in terms of spectral index (n_s) determined in section (2.2.1). The inclusion of dark matter does not affect much on those parameters. Therefore, the main constraints will be on the thermally averaged cross-section times velocity $(\langle \sigma v \rangle)$ and the dark matter mass M_X. The first two plots of Fig.2.9 depict the variation of annihilation cross-section as a function of the spectral index for two different values of dark-matter mass $M_X = (1, 10^3)$ GeV. The range of n_s is taken to be within (n_s^{min}, n_s^{max}) depending upon the model of reheating. For comparison, we include the perturbative reheating scenario [91] as well. Since the viable range of scalar spectral index n_s is reduced for the Two-phase reheating than that of the perturbative case, consequently the allowed range of $\langle \sigma v \rangle$ is shrunk as shown by green dotted and blue dotted lines. Due to larger allowed range of n_s ($n_s^{min} \simeq 0.956, n_s^{max} \simeq 0.9655$), the perturbative reheating [91] widens the allowed range of dark matter annihilation cross-section as $2.25 \times 10^{-39} \leq \langle \sigma v \rangle \leq 4.2 \times 10^{-19}$ for $M_X = 1\ GeV$ and $2.3 \times 10^{-42} \leq \langle \sigma v \rangle \leq 2.51 \times 10^{-5}$ for $M_X = 10^3$ GeV. Whereas for Two-phase reheating scenario, for both values of dark matter mass, we can observe the narrower range of $(n_s^{min} \simeq 0.9626, n_s^{max} \simeq 0.9652)$ for $\omega_{eff} = 10^{-3}$ and $(n_s^{min} \simeq 0.9626, n_s^{max} \simeq 0.9648)$ for $\omega_{eff} = 10^{-6}$. These ranges of n_s are well within the 1σ range of spectral index, $n_s = 0.9649 \pm 0.0042$ (68 % CL, Planck TT,TE,EE+lowE+lensing) from Planck [29]. Detailed constraints on the annihilation cross-section for Higgs inflation model are provided in Table-(2.5). Therefore, one can observe the significant differences on the allowed range of dark matter annihilation cross-section for two different reheating scenarios (perturbative and Two-phase). It is important to note that the dark matter parameter space is

Table 2.5: Model parameters and associated constraints on the dark matter parameters for different reheating dynamics:Higgs-Starobinsky model

$M_X = 1$ GeV

				Constraints due to **reheating bound**		
	Case-I (Two-phase)		Perturbative	Case-I (Two-phase)		Perturbative
	$\omega_{eff} = 10^{-3}$	$\omega_{eff} = 10^{-6}$	$\omega_\phi = 0$	$\omega_{eff} = 10^{-3}$	$\omega_{eff} = 10^{-6}$	$\omega_\phi = 0$
n_s^{min}	0.9626	0.9626	0.9560	0.9626	0.9626	0.9560
n_s^{max}	0.9652	0.9648	0.9655	0.9645	0.9643	0.9619
$\langle\sigma v\rangle_{min}$	3.2×10^{-37}	1.7×10^{-34}	2.2×10^{-39}	1.6×10^{-34}	7.7×10^{-32}	1.7×10^{-32}
$\langle\sigma v\rangle_{max}$	8.1×10^{-31}	3.1×10^{-27}	4.2×10^{-19}	8.1×10^{-31}	3.1×10^{-27}	4.2×10^{-19}

$M_X = 10^3$ GeV

				Constraints due to **reheating bound**		
	Case-I (Two-phase)		Perturbative	Case-I (Two-phase)		Perturbative
	$\omega_{eff} = 10^{-3}$	$\omega_{eff} = 10^{-6}$	$\omega_\phi = 0$	$\omega_{eff} = 10^{-3}$	$\omega_{eff} = 10^{-6}$	$\omega_\phi = 0$
n_s^{min}	0.9626	0.9626	0.9561	0.9626	0.9626	0.9568
n_s^{max}	0.9652	0.9648	0.9655	0.9652	0.9648	0.9650
$\langle\sigma v\rangle_{min}$	9.5×10^{-41}	1.6×10^{-37}	2.3×10^{-42}	9.5×10^{-41}	1.6×10^{-37}	2.0×10^{-41}
$\langle\sigma v\rangle_{max}$	8.1×10^{-34}	3.1×10^{-30}	2.5×10^{-5}	8.1×10^{-34}	3.1×10^{-30}	8.5×10^{-12}

constrained by the CMB anisotropy through the inflationary models, or alternatively one can state, *how various dark matter experimental observations can have the potential to constrain the inflationary model through our unified reheating analysis.*

The inclusion of dark matter dynamics and the associated theoretical constraints discussed in the previous section has put further limits on the range of n_s compatible with the dark matter observation. For example, the perturbative reheating scenario modifies the highest possible value of the spectral index n_s^{max} as $\rightarrow 0.9619$, and for Two-phase reheating dynamics n_s^{max} shifts as $(0.9652, 0.9648) \rightarrow (0.9645, 0.9643)$ with $\omega_{eff} = (10^{-3}, 10^{-6})$ accordingly for $M_X = 1$ GeV. This modified maximum n_s condition leads to the minimum values of the dark matter cross-section $\langle\sigma v\rangle_{min} \approx 1.66 \times 10^{-32}$ GeV^{-2} for perturbative case and $\langle\sigma v\rangle_{min} \approx (1.65 \times 10^{-34}, 7.75 \times 10^{-32})$ GeV^{-2} for Two-phase reheating case with two different values of $\omega_{eff} = (10^{-3}, 10^{-6})$. Instead of $M_X = 10^3$ GeV , the unitary bound put stringent constraints on n_s^{min}, only for perturbative process. Further, dynamics during reheating

(reheating bound) bounds the cross-section within $1.98 \times 10^{-41} \leq \langle\sigma v\rangle \leq 8.5 \times 10^{-12}$ for perturbative scenario. However, for $M_X = 10^3$ GeV, there is no effect of theoretical constraints on the bound of dark matter annihilation cross-section obtained from the Two-phase reheating analysis.

From the first two plots of Fig.(2.9), we read the variation of the cross-section for two different effective equations of state ω_{eff}. As we decrease the value of the ω_{eff} from $10^{-3} \rightarrow 10^{-6}$, the e-folding number N_{npre}, which is nearly independent of inflationary parameter changes from $5.8 \rightarrow 12.2$. Another interesting consequence of the Phase-I dynamics is the maximum possible value of dark matter mass M_X^{max}. To understand the underlying reason behind the origin of M_X^{max}, we have computed analytic expressions considering relativistic dark matter. The dark matter number density at the point of freeze-out n_X^f (see appendix 6.2) is expressed as

$$n_X^f x_f^3 = n_X^{in} + \langle\sigma v\rangle f(x_f) \quad , \tag{2.72}$$

where expressions of various symbols are given in the appendix. $x_f = A_f/A_{npre}$ and A_f is the normalized scale factor when both comoving dark matter and radiation components become constant. By using the above expression, we can obtain dark matter abundance as

$$\begin{aligned} \Omega_X h^2 &\simeq \frac{\langle E_X\rangle_f x_f^{-3}}{\rho_R(x_f)} \frac{T(x_f)}{T_{now}} \left(n_X^{in} + \langle\sigma v\rangle f(x_f)\right) \Omega_R h^2 \\ &= \frac{\sqrt{M_X^2 + 9T(x_f)^2} x_f^{-3}}{\rho_R(x_f)} \frac{T(x_f)}{T_{now}} \left(n_X^{in} + \langle\sigma v\rangle f(x_f)\right) \Omega_R h^2 \quad . \end{aligned} \tag{2.73}$$

The above expression indicates that the dark matter abundance increases with increasing dark matter mass. Moreover, at a particular value of the dark matter mass, the dark matter component's initial number density (n_X^{in}) will also play in the final value of the observed dark matter abundance, $\Omega_X h^2 = 0.12$. It can be observed from the equation (2.73), if $M_X > M_X^{max}$, then $\Omega_X h^2$ always ≥ 0.12. Therefore the maximum possible dark matter mass can be obtained from the above equation considering $\Omega_X h^2 = 0.12$ as

$$M_X^{max} = T(x_f)\sqrt{\left(0.12\frac{\beta}{n_X^{in}}\frac{T_{now}T(x_f)^2}{\Omega_R h^2 x_f^{-3}}\right)^2 - 9} \quad . \tag{2.74}$$

, which is dependent on the initial dark matter number density for the phase-II evolution,

$$n_X^{in} = \frac{\gamma\, m_\phi}{\langle E_X\rangle} \frac{3\left(\omega_{eff} - \omega_\phi\right)}{1 - 3\,\omega_{eff}\,(1+\gamma)} \Phi(A_{npre}) A_{npre}^{-3} m_\phi^3 \quad . \tag{2.75}$$

For a given γ, the initial value of X is clearly set by the value of ω_{eff}. Therefore, for a given value of phase-I dynamics parameters ω_{eff} and γ, a particular value of the dark matter mass exits above which present value of the dark matter abundance, $\Omega_X h^2 \approx 0.12$ can not be achieved irrespective of the cross-section values. Eqs.(2.74) and (2.75) illustrate the behavior of M_X^{max}, inversely proportional to γ as for a fixed value of the spectral index (n_s). From the third plot of Fig.(2.9), we can also observe the same. Likewise for $n_s = 0.9635$, $M_X^{max} = (2.38 \times 10^7, 2.38 \times 10^3, 0.238)$ GeV with $\gamma = (10^{-12}, 10^{-8}, 10^{-4})$ accordingly once we fixed $\omega_{eff} = 10^{-3}$. Furthermore, from the third plot of Fig.(2.9), one can observe that M_X^{max} is nearly independent of the choice of ω_{eff} except for a small deviation as one approach toward n_s^{max}. The straightforward answer could be that M_X^{max} is proportional to the freeze-out radiation temperature $T(x_f)$, which remains invariant with the choice of ω_{eff} value.

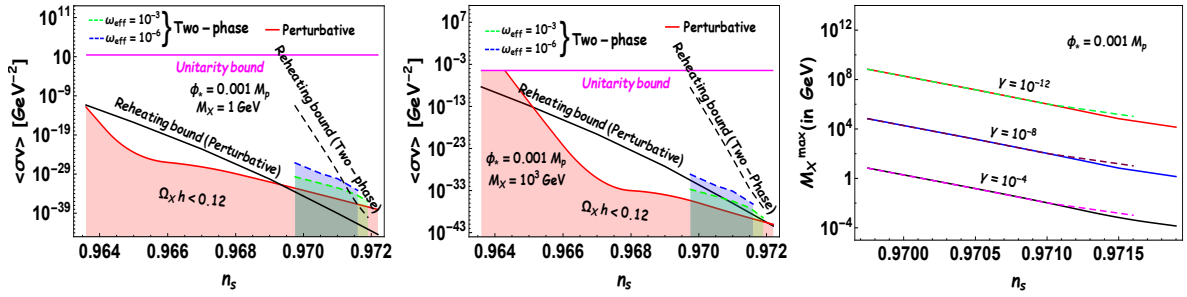

FIGURE 2.10: All plots are the same as in the previous Fig.2.9. The main difference is that here we have plotted for minimal plateau inflation model with $\phi_* = 0.001 M_p$, $n = 2$.

2.2.5.2 Minimal plateau inflation model

The details of this model are discussed in section 1.4. As was already the case for Higgs's inflation, for the minimal inflation model also, the reheating parameters such as (T_{re}, N_{re}) will not be modified much because of dark matter dynamics. The reason is that the contribution of dark matter in the background evolution during the reheating phase is insignificant. Throughout this analysis, we consider $\phi_* = 0.001 M_p$, which satisfies the CMB observation. Another motivation is that as one increases the ϕ^* value, the models assume simple power law. Details constraints on the dark matter parameter space can be read off from Fig.2.10. Furthermore, the numerical values are provided in the table-2.6. From the figure we observed a similar behavior of dark matter annihilation cross-section as a function of the spectral index for two different values of $\omega_{eff} = (10^{-3}, 10^{-6})$ with dark matter mass $M_X = (1, 10^3)$ GeV. For minimal model we again identify the maximum allowed values of dark matter mass M_X^{max} followed by the equations (2.74) and (2.75). Furthermore, for a given value of n_s, the M_X^{max} turns out to be linearly varying with γ . Like, for $n_s = 0.9705$, $M_X^{max} \simeq (1.5 \times 10^7, 1.5 \times 10^3, 0.15)$ GeV with $\gamma = (10^{-12}, 10^{-8}, 10^{-4})$.

2.3 Summary and discussion:

After inflation, reheating has been studied extensively in the literature, either through a perturbative or non-perturbative approach. However, it is believed that both approaches independently should not capture the complete picture of the complicated dynamics. We, for the first time, study this phase to the best of our knowledge, taking into account both approaches together motivated by our previous work [95]. However, instead of considering explicit non-perturbative decay of the inflaton field through parametric resonance, we model the initial phase by effective dynamics governed by the standard conservation laws and parametrized by a constant effective equation of state (ω_{eff}). The combined form of conservation laws and the initial condition of the reheating dynamics put constraints on the effective equation of state during the effective non-perturbative process calling it as phase-I. However, during perturbative analysis due to explicit decay of the inflaton field into radiation, we obtain the non-trivial time-dependent effective equation of state. At this stage, let us remind the reader that in all the PLANCK analysis [29] on constraining the inflationary models w_{eff} is assumed to be a constant free parameter during reheating, which follows from the proposal described in [45]. What we argue is that those assumptions should not be correct. After inflation, every inflationary model

Table 2.6: Model parameters and associated constraints on the dark matter parameters for different reheating dynamics: Minimal plateau model

$\phi_* = 0.001 M_p, M_X = 1$ GeV

				Constraints from **reheating bound**		
	Case-I (Two-phase)		Perturbative	Case-I (Two-phase)		Perturbative
	$\omega_{eff} = 10^{-3}$	$\omega_{eff} = 10^{-6}$	$\omega_\phi = 0$	$\omega_{eff} = 10^{-3}$	$\omega_{eff} = 10^{-6}$	$\omega_\phi = 0$
n_s^{min}	0.96975	0.96975	0.9636	0.96975	0.96975	0.9636
n_s^{max}	0.9719	0.9716	0.9722	0.97136	0.9712	0.9692
$\langle\sigma v\rangle_{min}$	1.3×10^{-36}	6.8×10^{-34}	8.6×10^{-39}	3.8×10^{-34}	7.3×10^{-32}	2.9×10^{-32}
$\langle\sigma v\rangle_{max}$	1.9×10^{-30}	7.3×10^{-27}	1.4×10^{-12}	1.9×10^{-30}	7.3×10^{-27}	1.4×10^{-12}

$\phi_* = 0.001 M_p, M_X = 10^3$ GeV

				Constraints from **reheating bound**		
	Case-I (Two-phase)		Perturbative	Case-I (Two-phase)		Perturbative
	$\omega_{eff} = 10^{-3}$	$\omega_{eff} = 10^{-6}$	$\omega_\phi = 0$	$\omega_{eff} = 10^{-3}$	$\omega_{eff} = 10^{-6}$	$\omega_\phi = 0$
n_s^{min}	0.96975	0.96975	0.9643	0.96975	0.96975	0.9651
n_s^{max}	0.9719	0.9716	0.9722	0.9719	0.9716	0.9720
$\langle\sigma v\rangle_{min}$	3.8×10^{-40}	6.30×10^{-37}	9.1×10^{-42}	3.8×10^{-40}	6.3×10^{-37}	1.8×10^{-41}
$\langle\sigma v\rangle_{max}$	1.9×10^{-33}	7.3×10^{-30}	2.5×10^{-5}	1.9×10^{-33}	7.3×10^{-30}	7.4×10^{-14}

has its own characteristic oscillatory period, which contributes to the equation of state during reheating. Therefore, considering w_{eff} as a free parameter loses some of the fundamental characteristic properties of the inflaton potential itself. Furthermore, if reheating occurs for a longer period of time, the time-dependent w_{eff} during the perturbative process should also be very important to get precise constraints on any inflationary model. This is where our analysis not only can play an important role in better understanding the inflationary models but also opens up the possibility of understanding the micro-physics of the reheating process through CMB physics. As we can clearly see how the CMB power spectrum constrains the value of inflation-radiation coupling parametrized by Γ_ϕ through reheating temperature T_{re}. The usual connection between Γ_ϕ and T_{re} will not be correct anymore once we consider the decaying inflaton as it is a well-known fact that during the reheating process, even at the end of reheating time, $\Gamma_\phi = H$, inflaton does not decay into radiation completely. Therefore, one

Table 2.7: Different inflationary models and associated values of Γ_{ϕ}^{cri} (T_{re}^{cri}), measured in units of GeV (ϕ_* and f in units of M_p)

	α-attractor		Axion		Minimal plateau	
	$\alpha = 1$	$\alpha = 100$	$f = 10$	$f = 50$	$\phi_* = 0.01$	$\phi_* = 10^{-3}$
$T_{re}^{cri}\left(\omega_{eff} = 10^{-3}\right)$	3.5×10^{10}	7.2×10^{10}	4.0×10^{10}	9.0×10^{10}	2.2×10^{10}	8.8×10^{9}
$T_{re}^{cri}\left(\omega_{eff} = 10^{-6}\right)$	2.3×10^{5}	1.2×10^{6}	1.8×10^{5}	1.9×10^{5}	2.8×10^{5}	5.8×10^{4}
$\Gamma_{\phi}^{cri}\left(\omega_{eff} = 10^{-3}\right)$	960.0	1.3×10^{4}	3.7×10^{4}	2.7×10^{4}	2.3×10^{3}	394.7
$\Gamma_{\phi}^{cri}\left(\omega_{eff} = 10^{-6}\right)$	1.4×10^{-7}	3.9×10^{-6}	1.1×10^{-7}	1.1×10^{-7}	4.8×10^{-7}	$2.7*10^{-8}$
$\Gamma_{\phi\to\chi\chi}^{cri}\,(model)$	0.07	0.01	2.8×10^{-3}	3.2×10^{-3}	0.70	15.30
$\Gamma_{\phi\to\chi\chi}^{cri}\,(model)$	5.03	1.60	0.45	0.51	34.20	231.70
$\Gamma_{\phi\to\bar{\psi}\psi}^{cri}\,(model)$	260.30	42.20	10.80	12.30	2.7×10^{3}	5.8×10^{4}

certainly needs to take into account this fact while calculating T_{re} and its connection with the scalar power spectrum n_s in the analysis. However, all the previous theoretical as well as in PLANCK analysis, complete decay of inflaton is assumed while relating the cosmological scales exiting and re-entering the horizon at two different time scales. Therefore, based on the Two-phase reheating scenario, our prediction of reheating temperature corresponding to the inflationary power spectrum is more accurate than the previous analysis.

At first, we analyzed the viable constraints on the decay width as well as reheating parameters (N_{re}, T_{re}) considering the decay of the inflaton field in the perturbative Boltzmann framework. Perturbative dynamics have been shown to give rise to a maximum reheating temperature $T_{re}^{max} \simeq 10^{15}$ naturally, which essentially corresponds to almost instantaneous reheating. As long as the decay width is in the perturbative regime, the result from the only perturbative process is trustworthy. However, because of the straightforward relation between T_{re}, and Γ_{ϕ}, a high reheating temperature limit can correspond to non-perturbative phenomena. This fact motivates us to include non-perturbative aspects of reheating through effective dynamics. In our present scenario, the universe passes through two distinct phases during reheating. Combining the inflation and subsequent standard big-bang evolution with the intermediate Two-phase reheating, our approach predicts the critical value of the inflaton decay constant Γ_{ϕ}^{cri} depending upon the phase-I equation of state ω_{eff}.

The critical point naturally defined at $N_{npre} = N_{pre}$. Therefore, if $\Gamma_{\phi} < \Gamma_{\phi}^{cri}$, the reheating phase will be dominated by perturbative one and vice versa. We also compare our numerical results of Γ_{ϕ}^{cri} with the critical decay width obtained from the theoretical consideration for different type of inflaton-reheating field interactions $g\phi\chi^2$, $y\phi\chi^3$, $h\phi\psi\bar{\psi}$. It turns out that all the theoretical values of $\Gamma_{cri}(model)$ correspond to an effective phase-I equation of state ω_{eff} within $10^{-3} \sim 10^{-6}$. Our actual lattice simulation results also appeared to be compatible with this conclusion (see Fig.2.3). A summary table-2.7 for Γ_{ϕ}^{cri} is given for three observationally viable model. The inclusion of the initial non-perturbative phase naturally

changes the maximum reheating temperature value because of its perturbative definition. T_{re}^{max} is no longer defined at the point of instantaneous reheating $N_{re} \simeq 0$, rather is defined at $N_{re} \approx N_{npre}$, which is equivalent in saying the phase-II e-folding number $N_{pre} \simeq 0$. At the end of phase-I, approximately 50% of the total comoving energy density remains in the form of the inflaton, which naturally leads to different T_{re}^{max} defined in the perturbative phase-II dynamics. This phase further sets the final equation of the state of the system to 1/3. All these results have been shown to be crucially dependent upon the phase-I effective equation of state ω_{eff}. As one changes the value of ω_{eff} from $10^{-3} \rightarrow 10^{-6}$, the phase-I e-folding number N_{npre} changes from $6 \rightarrow 12$. The maximum reheating temperature T_{re}^{max} accordingly changes from $(10^{13} \rightarrow 10^{10})$ GeV. Therefore, the conclusion that can be emphasized is that the value of reheating temperature may encode the information about the non-perturbative phase. Furthermore, all the inflationary models which are compatible with the observed CMB anisotropy predict the same maximum reheating temperature (T_{re}^{max}) for a given ω_{eff}. This is reminiscent of the maximum reheating temperature T_{re}^{max} obtained for purely perturbative reheating dynamics irrespective of the inflation model. Keeping this point in mind, we have performed a comparative analysis of different existing reheating formalisms such as conventional reheating dynamics (case II) and purely perturbative analysis (case III) with our proposed Two-phase (case-I). For both cases II and III, the model-independent maximum value of the reheating temperature turns out to be $T_{re}^{max} \simeq 10^{15}$ GeV, which is reduced to $10^{13} \sim 10^{10}$ GeV when considering Two-phase reheating for $\omega_{eff} = 10^{-3} \sim 10^{-6}$. Further, the Two-phase reheating scenario constraints the inflation model within a very narrow range of allowed scalar spectral index compatible with CMB anisotropy.

Further generalization has been analyzed by including the dark matter component as one of the decay products of the inflaton. Depending upon the mass dark matter annihilation cross-section versus scalar spectral index parameter space has been shown to be reduced because of Two-phase reheating as compared to that of standard reheating dynamics, which can be observed from Fig.2.9 and 2.10. Details of the allowed parameter space for various models can be obtained from the tables 2.5 and 2.6. Because of the non-trivial initial condition for Two-phase dynamics, there exists a maximum possible mass M_X^{max} above which dark matter turned out to be overproduced no matter how small the annihilation cross-section is assumed. In the summary table 2.8, we provide numerical values of maximum possible dark matter mass allowed for different viable models under consideration. As just stated, the value of M_X^{max} is directly connected to γ ($\gamma = \frac{\rho_X}{\rho_R}$), which is defined during phase I. Once we fixed the spectral index for a particular inflation model and these values of M_X^{max} are nearly independent of the choice of ω_{eff}.

Nonetheless, one important point we should understand is that the existing reheating scenarios, either perturbative or non-perturbative, are not the complete description of this phase. A unified description that connects both non-perturbative and perturbative dynamics is more appropriate. In our present study, we, for the first time, try to construct such a unified description. As a first attempt toward this goal, we describe non-perturbative preheating dynamics by effective dynamics. Our present formalism is particularly suited for the class of inflation models with quadratic potential near its minimum. For inflaton potential with a power greater than two, lattice results generically predict the equation of state $\frac{1}{3}$ after the end of non-perturbative dynamics [95]. So for those models, our Two-phase reheating is not applicable. We will be considering this case in our future work. Instead of considering an effective non-perturbative approach, actual non-perturbative dynamics integrated with a perturbative one would be more appropriate. Recently an interesting approach has been proposed to describe

Table 2.8: Models and their associated values of M_X^{max}, measured in units of GeV

Higgs-Starobinsky model

	$\gamma = 10^{-12}$		$\gamma = 10^{-8}$		$\gamma = 10^{-4}$	
	$\omega_{eff}\,(10^{-3})$	$\omega_{eff}\,(10^{-6})$	$\omega_{eff}\,(10^{-3})$	$\omega_{eff}\,(10^{-6})$	$\omega_{eff}\,(10^{-3})$	$\omega_{eff}\,(10^{-6})$
$M_X^{max}(min)$	1.4×10^4	1.1×10^5	1.4	10.6	1.4×10^{-4}	1.1×10^{-3}
$M_X^{max}(max)$	11.7×10^8	11.6×10^8	11.7×10^4	11.6×10^4	11.7	11.6

Minimal plateau model ($\phi_* = 0.001 M_p$)

	$\gamma = 10^{-12}$		$\gamma = 10^{-8}$		$\gamma = 10^{-4}$	
	$\omega_{eff}\,(10^{-3})$	$\omega_{eff}\,(10^{-6})$	$\omega_{eff}\,(10^{-3})$	$\omega_{eff}\,(10^{-6})$	$\omega_{eff}\,(10^{-3})$	$\omega_{eff}\,(10^{-6})$
$M_X^{max}(min)$	1.4×10^4	1.0×10^5	1.4	10.4	1.4×10^{-4}	1.0×10^{-3}
$M_X^{max}(max)$	6.8×10^8	6.7×10^8	6.8×10^4	6.7×10^4	6.8	6.7

preheating phenomena in the Boltzmann framework [130]. In our present Two-phase reheating dynamics, the aforementioned non-perturbative Boltzmann framework could be natural to integrate with the perturbative Boltzmann equations. Another important fact we have not considered is the temperature dependency of the effective numbers of relativistic degrees of freedom (g_*). Constant effective degrees of freedom is reasonably good approximation for a wide range of temperature [131, 132] till the QCD hadronic transition happens at around 10^2 MeV scale, around which the vale of effective degrees of freedom changes as $g_* = 100 \to 10$ [133, 134]. So our eventual plane in the future is to calculate dark matter and the reheating parameter space accurately by acknowledging the precise evolution of those degrees of freedom in the thermal bath [135–137].

Understanding the phase of reheating through primordial magnetic field and CMB *3*

"God runs electromagnetics on Monday, Wednesday, and Friday by the wave theory, and the devil runs it by quantum theory on Tuesday, Thursday, and Saturday."

Lawrence Bragg

In the previous chapter, we proposed two-phase reheating, where the initial preheating phase is described by effective dynamics followed by perturbative reheating. We discussed in detail the constraints on the inflaton and dark matter parameter space considering CMB and present DM abundance. In this chapter, we will consider yet another interesting observable associated with the primordial magnetic field. The primordial magnetic field, together with CMB, will be shown to provide further constraints on the dynamics of reheating and inflation models. We will specifically focus on how the present-day Large-scale magnetic field (LSMF) combined with the CMB anisotropy can probe the reheating phase of the universe. For LSMF we consider simple model of primordial magnetogeneis [138–141]. Primordial magnetogenesis models have been studied quite extensively in the literature [142–148]. The well known mechanisms is to explicit break the conformal invariance in the electromagnetic sector. It is well known that due to conformal invariance free electromagnetic theory does not experience the conformally flat cosmological universe in four dimensions. Hence, to overcome such a problem one usually invokes extra scalar degrees of freedom which directly couples with the electromagnetic field. Such a theory has been shown to generate a non-zero vacuum expectation value of the electromagnetic field from a quantum vacuum without any source term. However, the dynamical nature of the conformal breaking coupling invites new problems which are known as strong coupling and back-reaction problems [149, 150]. For the sake of completeness, we will discuss those problems in detail as we go along. Our main goal of this chapter would be to show how some of such problems can be alleviated by considering the dynamics of reheating [141]. This in turn along with the observation of large-scale magnetic fields in the present universe provides new constraints on the reheating dynamics. Taking into account both the CMB anisotropic constraints on the inflationary power spectrum and the present value of the

large-scale magnetic field, our analysis reveals an important connection among the reheating parameters (T_{re}, w_{re}), magnetogensis models and inflationary scalar spectral index (n_s).

The universe is observationally shown to be magnetized over a wide range of scales. Zeeman splitting, synchrotron emission, and Faraday rotation are some of the fundamental physical mechanisms by which the existence of a magnetic field can be probed. Various astrophysical and cosmological observations of those quantities tell us that our universe is magnetized over scales starting from our earth, the sun, stars, galaxies, galaxy clusters, and the intergalactic medium (IGM) in voids. In the galaxies and galaxy clusters of a few to hundred-kilo parsecs (kpc) scale, the magnetic fields have been observed to be of order a few micro Gauss [151–153]. The γ-ray observations of GRB 190114C, the observed long-term GeV-TeV light curve of the BLAZAR MRK 421 and BLAZAR MRK 501 suggest that even the intergalactic medium (IGM) in voids can host a weak $\sim 10^{-16} - 10^{-20}$ Gauss magnetic field, with the coherence length as large as Mpc scales [154–162]. Furthermore, future space-based $\gamma-$ray observatories such as MAST with improved sensitivity will be able to probe the strength of the extra-galactic magnetic field(EGMF) even below $B < 10^{-18}$ G using the pair echo method [163]. Additionally, Jedamzik et al. [164] derive an upper limit on the PMFs, which is ~ 47 pG for scale-invariant PMFs, using MHD computation. Therefore, all these efforts and observations hint at the importance of understanding large-scale magnetic fields in the theoretical framework. In this context, our main focus of this chapter would be to understand the evolution of large-scale magnetic fields. We will not concentrate on the magnetogenesis scenario, which has already been studied quite extensively in the literature [139, 142–144, 146]. As the mechanism of inflationary magnetogensis is essentially the same, we will specifically consider the well-known Ratra model [138] for our study. Once the electromagnetic field is generated during inflation, the subsequent evolution occurs through the time-evolving plasma. The magnetic field at the cosmological scale can evolve and survive even today while passing through the plasma state[165, 166] of our universe before the structure formation. Therefore, the time-evolving plasma proves to be an ideal environment to have sustainable evolution and growth of the magnetic field. Usual magnetic hydrodynamic evolution in the time-evolving plasma requires a tiny seed initial magnetic field. In the cosmological context, the well-known mechanism for such a seed field is primordial inflationary magnetogenesis. Inflation provides us with a unique mechanism for producing coherent magnetic fields for a wide range of scales. Mpc scale magnetic field can survive until today as a cosmological relic whose magnitude could be $\sim 10^{-9} - 10^{-20}$ G. On the other hand, at small scales, this tiny inflationary magnetic field can play as a seed field which will be further enhanced by the well-known *Galactic dynamo* mechanism[152, 167–170]. A similar mechanism can also be obtained from the Electroweak Phase Transition (EWPT) [171–174].

We consider a standard scenario of inflationary magnetogenesis where the kinetic term of the electromagnetic field is conformally coupled with a scalar field. Background inflation dynamics naturally produce a large-scale electromagnetic field that subsequently evolves through the reheating phase. Instead of going into the details of the magnetogenesis mechanism, we concentrate on dynamics during reheating considering various inflationary models. In our analysis, we assume the negligible Schwinger effect on magnetogenesis. This chapter is arranged as follows: in section 3.1, we discuss the I^2FF model of inflationary magnetogenesis and show how Faraday's induction effect impacts the present-day magnetic field strength. Moreover, we also discuss in detail the methodology of probing the reheating phase through the present-day large-scale magnetic field combined with CMB anisotropy. In section 3.2, we derive an approximate analytical expression that relates the magnetic power spectrum in the present

universe with reheating parameters. In section 3.3, we finally show how our analysis constrains the reheating and magnetogenesis model considering a few observationally viable inflationary scenarios.

3.1 Inflationary magnetogenesis: General discussion

During inflation, the large-scale magnetic field is generated out of the quantum vacuum and then subsequently evolves through various phases of our universe. Therefore, the evolving magnetic field must encode valuable information about the reheating. Considering the present value of the large-scale magnetic field, we can place constraints not only on the parameters of the reheating phase but also on the magnetogenesis model itself. Contrary to the convention, the crucial point of our present analysis is the assumption of conductivity being negligible until the end of reheating. The reason being the universe turns into the plasma state nearly at the end of reheating. From a large number of studies [45, 47, 90, 91], it is observed that almost the entire period of reheating is primarily dominated by inflaton. In the context of the inflationary magnetogenesis scenario, this particular assumption has recently been proposed to be important [141] during reheating. Conventionally after the end of inflation, the magnetic field on the super-horizon scales is assumed to be redshifted with respect to the scale factor a as $B^2 \propto 1/a^4$ provided inflaton energy density transfers into plasma instantaneously, and the universe becomes a good conductor instantly right after the end of inflation. Hence, the electric field ceases to exist. However, in the reference, [141] it has been shown that if the conductivity remains small, redshifts of magnetic energy density become slower, $B^2 \propto 1/a^6H^2$, due to electromagnetic Faraday induction. Here H is the Hubble parameter. This helps one to obtain the required value of the present-day large-scale magnetic field considering a large class inflationary model, which we describe below.

3.1.1 Quantizing the Ratra model: Electromagnetic power spectrum

The simplest magnetogenesis scenario we will be considering here is known as Ratra model [138] with the interaction Lagrangian $I(\phi)^2FF$. In this interacting Lagrangian, the conformal symmetry is explicitly broken by the scalar field coupling function $I(\phi)$. During inflation, the model generally predicts a strong primordial electric field than the magnetic field, and that can backreact to invalidate the mechanism itself. We discuss the model in detail and show how the reheating phase can cure this backreaction problem. In the frame of a comoving observer having four-velocity u^μ $(u^i = 0, u_\mu u^\mu = -1)$, the magnetic and electric fields are defined as

$$E_\mu = u^\nu F_{\mu\nu} \ , \ B_\mu = \frac{1}{2}\epsilon_{\mu\nu\rho\sigma}u^\sigma F^{\nu\rho}. \tag{3.1}$$

Where, $F_{\mu\nu} = \partial_\mu A_\nu - \partial_\nu A_\mu$ is the electromagnetic field tensor and $\epsilon_{\mu\nu\rho\sigma}$ is a totally antisymmetric tensor. The background is the well-known FLRW metric with the time-dependent scale factor $a(\tau)$ expressed in conformal coordinate,

$$ds^2 = a(\tau)^2\left(-d\tau^2 + d\mathbf{x}^2\right) \quad . \tag{3.2}$$

As already described before, the gauge field action is taken to be,

$$S = -\frac{1}{4}\int d^4x\sqrt{-g}I(\tau)^2F_{\mu\nu}F^{\mu\nu} \quad , \tag{3.3}$$

At this point, let us point out that one can consider other inflationary magnetogeneis models with axion-electromagnetic field coupling [175–177], higher curvature coupling [178, 179] and apply our methodology presented here to not only constraint the reheating phase but also make the models under consideration viable.

In the inflationary magnetogenesis scenario, the essential idea is to quantize the electromagnetic field in the classical inflationary background. Here $I(\tau)^2 \equiv I(\phi(\tau))$, therefore, is the time-dependent coupling arising from some classical background scalar field. To maintain generality, we do not specify any background dynamics of the scalar field. Through this coupling, the electromagnetic field experiences the spatially flat expanding FLRW background. To quantize the field components, A_μ are expressed in terms of irreducible scalar and vector components as follows,

$$A_\mu = (A_0, \partial_i S + v_i) \quad \text{with} \quad \partial_i V_i = 0 \quad . \tag{3.4}$$

In the standard canonical quantization procedure, one writes V_i in terms of the annihilation (a_k) and the creation operator $(a_k^\dagger)$ as

$$V_i(\tau, x) = \sum_{p=1,2} \int \frac{d^3k}{(2\pi)^3} \epsilon_i^{(p)}(\mathbf{k}) \left\{ e^{i\mathbf{k}.\mathbf{x}} a_k^{(p)} u_k^{(p)}(\tau) + e^{-i\mathbf{k}.\mathbf{x}} a_k^{\dagger(p)} u_k^{*(p)}(\tau) \right\} \quad , \tag{3.5}$$

here the $\epsilon_i^{(p)}(k)$ is the polarization vector corresponding to the two polarization direction $p = 1, 2$, which satisfy the following relations, $\epsilon_i^{(p)}(\mathbf{k}) k_i = 0$, $\epsilon_i^{(p)}(\mathbf{k}) \epsilon_i^{(q)}(\mathbf{k}) = \delta_{pq}$. The creation and annihilation operators in Eq.(3.5) namely $a_k^{(p)}$ and $a_k^{\dagger(p)}$ are time-independent. They satisfy the commutation relation

$$[a_k^{(p)}, a_h^{(q)}] = [a_k^{\dagger(p)}, a_h^{\dagger(q)}] = 0 \ , \ [a_k^{(p)}, a_h^{\dagger(q)}] = (2\pi)^3 \delta^{pq} \delta^{(3)}(\mathbf{k\text{-}h}) \quad . \tag{3.6}$$

All the dynamics of the field will be encoded into the mode function which satisfies the following equation of motion,

$$u_k^{(p)\prime\prime} + 2\frac{I'}{I} + k^2 u_k^{(p)\prime} = 0. \tag{3.7}$$

Where the prime denotes derivative with respect to the proper time τ. Conventionally the electromagnetic power spectrum is expressed in terms of those mode functions as follows,

$$P_E(k) = \frac{k^3}{2\pi^2 a^4} \sum_{p=1,2} |u_k^{(p)\prime}|^2 \ ; \ P_B(k) = \frac{k^5}{2\pi^2 a^4} \sum_{p=1,2} |u_k^{(p)}|^2. \tag{3.8}$$

However, an elegant way to express the above power spectrum is in terms Bogliubov coefficient which has direct physical interpretation in terms of quantum particle production. This Hamiltonian is written in terms of time-independent creation and annihilation operator as follows,

$$H = \frac{I^2(\tau)}{2} \sum_{p=1,2} \left(k|u_k^{(p)}|^2 + \frac{1}{k}|u_k^{\prime(p)}|^2 \right) \left(a_k^{(p)\dagger} a_k^{(p)} + a_{-k}^{(p)} a_{-k}^{(p)\dagger} \right) + \left(k(u_k^{(p)})^2 + \frac{1}{k}(u_k^{\prime(p)})^2 \right) a_k^{(p)} a_{-k}^{(p)}$$
$$+ \left(k(u_k^{(p)*})^2 + \frac{1}{k}(u_k^{*\prime(p)})^2 \right) a_{-k}^{(p)\dagger} a_k^{(p)\dagger} + \frac{1}{2} \left(a_k^{(p)\dagger} a_k^{(p)} - a_{-k}^{(p)} a_{-k}^{(p)\dagger} \right).$$

This is not diagonal. Therefore, to diagonalize, we employ the Bogoliubov transformation. In this transformation, new set of time-dependent creation and annihilation operators $(b_k^{(p)}(\tau), b_k^{(p)\dagger}(\tau))$ are defined in term of old ones. And the new basis of the Hilbert space so constructed diagonalizes the above Hamiltonian,

$$b_k^{(p)}(\tau) = \alpha_k^{(p)}(\tau)a_k^{(p)} + \beta_k^{(p)*}a_{-k}^{(p)\dagger} \ , \ b_k^{(p)\dagger}(\tau) = \alpha_k^{(p)*}(\tau)a_k^{(p)\dagger} + \beta_k^{(p)}(\tau)a_{-k}^{(p)}. \tag{3.9}$$

Where $\alpha_k^{(p)}$ and $\beta_k^{(p)}$ are the Bogoliubov coefficients defined as

$$\alpha_k^{(p)}(\tau) = I\left(\sqrt{\frac{k}{2}}u_k^{(p)} + \frac{i}{\sqrt{2k}}u_k^{\prime(p)}\right) \tag{3.10}$$

$$\beta_k^{(p)}(\tau) = I\left(\sqrt{\frac{k}{2}}u_k^{(p)} - \frac{i}{\sqrt{2k}}u_k^{\prime(p)}\right). \tag{3.11}$$

The Bogoliubov coefficients follow the following normalization condition

$$|\alpha_k^{(p)}|^2 - |\beta_k^{(p)}|^2 = 1 \tag{3.12}$$

With all these ingredients one represents the power spectrum in terms of Bogoliubov coefficients, $\alpha_k^{(p)}$ and $\beta_k^{(p)}$ as follows,

$$\mathcal{P}_E(k) = \frac{k^4}{4\pi^2 a^4 I^2}\sum_{p=1,2}|\alpha_k^{(p)} - \beta_k^{(p)}|^2 \ ; \ \mathcal{P}_B(k) = \frac{k^4}{4\pi^2 a^4 I^2}\sum_{p=1,2}|\alpha_k^{(p)} + \beta_k^{(p)}|^2 \tag{3.13}$$

Considering the super-horizon limit, the above expressions for the electromagnetic power spectrum can be further simplified by extracting the amplitude and phase of those coefficients. By using the normalization condition Eq (3.12) one can write,

$$|\alpha_k^{(p)} \pm \beta_k^{(p)}|^2 = 1 + 2|\beta_k^{(p)}|^2 \pm |\beta_k^{(p)}|\sqrt{1 + |\beta_k^{(p)}|^2}\cos\{arg(\alpha_k^{(p)}\beta_k^{*(p)})\} \tag{3.14}$$

Where, the phase factor is expressed as $arg(\alpha_k^{(p)}\beta_k^{*(p)}) \equiv \pi + \theta_k^{(p)}$. In the following discussion, we consider a specific model of the electromagnetic coupling function.

3.1.1.1 Magnetogenesis: Modelling the coupling function

In order to study further, we consider the following widely considered power law form of the coupling function [138]

$$I(\tau) = \begin{cases} \left(\frac{a_{end}}{a}\right)^n & a \leq a_{end} \\ 1 & a \geq a_{end}, \end{cases} \tag{3.15}$$

where a_{end} is the scale factor at the end of inflation. At this stage, let us point out that, in all the previous analyses, n has been considered to be an integer. For generality, we assume n to be arbitrary. In the end, we want to constrain its value through observation. Furthermore, after the end of inflation, the function form of $I(\phi)$ will be chosen in such a way that the usual conformal electrodynamics is restored.

Our first interest is to understand how the large-scale magnetic field is assumed to be produced during the initial stage of inflation. In order to do that, we assume the Hubble parameter to be constant throughout our analysis. This also helps us to give a clear picture in terms of analytic solutions. The perfect de-Sitter background with Hubble parameter H_{inf}, one obtains the solution for the mode function as,

$$u_k = \frac{1}{2I}\left(\frac{\pi}{aH_{inf}}\right)^{\frac{1}{2}} H^{(1)}_{-n+\frac{1}{2}}\left(\frac{k}{aH_{inf}}\right), \tag{3.16}$$

which leads to the Bunch-Davies vacuum state at the sub-Horizon scale. $H^{(1)}_{-n+\frac{1}{2}}\left(\frac{k}{aH_{inf}}\right)$ is the Hankel function of the first kind. The Hankel functions are defined in terms of the Bessel function of the first and second (Neumann) kinds.

$$H_\nu\left(\frac{k}{aH_{inf}}\right) = J_\nu\left(\frac{k}{aH_{inf}}\right) + iY_\nu\left(\frac{k}{aH_{inf}}\right) \tag{3.17}$$

Here $\nu = -n \pm \frac{1}{2}$. Defining a new variable $z = k/aH_{inf}$, the time dependent Bogoliubov coefficient are expressed as,

$$\alpha_k = \left(\frac{\pi z}{8}\right)^{\frac{1}{2}}\left\{H^{(1)}_{-n+\frac{1}{2}}(z) - iH^{(1)}_{-n-\frac{1}{2}}(z)\right\} \;;\; \beta_k = \left(\frac{\pi z}{8}\right)^{\frac{1}{2}}\left\{H^{(1)}_{-n+\frac{1}{2}}(z) + iH^{(1)}_{-n-\frac{1}{2}}(z)\right\} \tag{3.18}$$

As we have already described before, our focus is to understand the reheating constraints on inflationary and magnetogenesis models considering the CMB anisotropy and LSMF field, which are naturally classified as large-scale observables. Our discussion will be mainly in the super-horizon limit. Therefore, within this limit following conditions will be satisfied

$$\frac{1}{|\beta^{(p)}_k|^2} \ll \theta^{(p)}_k \ll 1. \tag{3.19}$$

This essentially suggests that any mode starting from the Bunch-Davis vacuum at the sub-horizon scale transforms into a highly squeezed state, parametrized by $|\beta^{(p)}_k|^2 \gg 1$, after its horizon exit during inflation. Using this condition, one gets the following simplified form of the electromagnetic power spectrum,

$$\mathcal{P}_E(k) \simeq \frac{k^4}{4\pi^2 a^4 I^2}\sum_{p=1,2} 4|\beta^{(p)}_k|^2 \;;\; \mathcal{P}_B(k) \simeq \frac{k^4}{4\pi^2 a^4 I^2}\sum_{p=1,2}|\beta^{(p)}_k|^2\left(\theta^{(p)}_k\right)^2 \tag{3.20}$$

For the arbitrary value of n, the final expression for the spectrum assumes the following forms,

$$\begin{aligned}\mathcal{P}_E(k) \simeq{}& \frac{4k^4}{2\pi^2 a^4 I^2}\left(\frac{\pi z}{8}\right)\left\{H^{*(1)}_{-n+\frac{1}{2}}(z)H^{(1)}_{-n+\frac{1}{2}}(z) + iH^{*(1)}_{-n+\frac{1}{2}}(z)H^{(1)}_{-n-\frac{1}{2}}(z)\right\}\\ &-\frac{4k^4}{2\pi^2 a^4 I^2}\left(\frac{\pi z}{8}\right)\left\{iH^{*(1)}_{-n-\frac{1}{2}}(z)H^{(1)}_{-n+\frac{1}{2}}(z) - H^{(1)}_{-n-\frac{1}{2}}(z)H^{*(1)}_{-n-\frac{1}{2}}(z)\right\}\end{aligned} \tag{3.21}$$

$$\mathcal{P}_B(k) \simeq \frac{k^4}{2\pi^2 a^4 I^2}\left(\frac{\pi z}{8}\right)\left\{H^{*(1)}_{-n+\frac{1}{2}}(z)H^{(1)}_{-n+\frac{1}{2}}(z) + iH^{*(1)}_{-n+\frac{1}{2}}(z)H^{(1)}_{-n-\frac{1}{2}}(z)\right\}$$

$$-\frac{k^4}{2\pi^2 a^4 I^2}\left(\frac{\pi z}{8}\right)\left\{iH^{*(1)}_{-n-\frac{1}{2}}(z)H^{(1)}_{-n+\frac{1}{2}}(z)-H^{(1)}_{-n-\frac{1}{2}}(z)H^{*(1)}_{-n-\frac{1}{2}}(z)\right\}$$
$$\left\{arg\left[\frac{\pi z}{8}\left(H^{(1)}_{-n+\frac{1}{2}}(z)-iH^{(1)}_{-n-\frac{1}{2}}(z)\right)\left(H^{*(1)}_{-n+\frac{1}{2}}(z)-iH^{*(1)}_{-n-\frac{1}{2}}(z)\right)\right]-\pi\right\}^2 \tag{3.22}$$

In our final numerical analysis, we will be considering this expression. To this end, it is important to remind the reader, that the widely studied case with a positive integer value of n leads to the following simplified form of the electromagnetic power spectra at the superhorizon scale ($k \ll aH_{inf}$) as [141]

$$\mathcal{P}_E(k) \simeq \frac{8\Gamma(n+\frac{1}{2})^2 H^4_{inf}}{I^2\pi^3}\left(\frac{k}{2aH_{inf}}\right)^{-2(n-2)} \quad ; \quad \mathcal{P}_B(k) \simeq \frac{8\Gamma(n-\frac{1}{2})^2 H^4_{inf}}{I^2\pi^3}\left(\frac{k}{2aH_{inf}}\right)^{-2(n-3)} \tag{3.23}$$

With this expression, subsequent magnetic field evolution has been widely studied, considering the magnetic energy density decreasing as $|B|^2 \sim 1/a^4$.

3.1.1.2 After inflation dynamics: reheating

In order to associate the observed current magnetic field with the magnetic field produced during inflation, it is essential to study the subsequent evolution. Most of the studies so far considered the fact that when I^2 becomes constant at the end of the inflation, the co-moving photon density $|\beta_k^{(p)}|^2$ is conserved. Consequently, the magnetic power redshifts as $\mathcal{P}_B(k) \propto a^{-4}$ until today. Before embarking on our proposal, let us briefly discuss the widely studied case for the sake of completeness. Thus, at the end of the inflation, the phase parameter (θ_k^{end}) and the photon density ($|\beta_k^{end}|^2$) are identified as

$$\theta_k^{end} = \{Arg\left[\alpha_k\left(z_{end}\right)\beta_k^*(z_{end})\right]-\pi\} \quad , \tag{3.24}$$

$$|\beta_k^{end}|^2 = \left(\frac{\pi z_{end}}{8}\right)\left\{H^{*(1)}_{-n+\frac{1}{2}}(z_{end})H^{(1)}_{-n+\frac{1}{2}}(z_{end})+iH^{*(1)}_{-n+\frac{1}{2}}(z_{end})H^{(1)}_{-n-\frac{1}{2}}(z_{end})\right\}$$
$$-\left(\frac{\pi z_{end}}{8}\right)\left\{iH^{*(1)}_{-n-\frac{1}{2}}(z_{end})H^{(1)}_{-n+\frac{1}{2}}(z_{end})-H^{(1)}_{-n-\frac{1}{2}}(z_{end})H^{*(1)}_{-n-\frac{1}{2}}(z_{end})\right\} \quad . \tag{3.25}$$

Here we define $z_{end} \equiv k/a_{end}H_{inf}$. For any arbitrary values of n, the magnetic power spectrum is

$$\mathcal{P}_B^{end}(k) \simeq \frac{k^4}{2\pi^2 a^4_{end}}\left(\theta_k^{end}\right)^2|\beta_k^{end}|^2 \quad . \tag{3.26}$$

For positive integer n, the expression above Eqn.(3.26) boils down to

$$\mathcal{P}_B^{end}(k) \simeq \frac{8\Gamma(n-\frac{1}{2})^2}{\pi^3}H^4_{Inf}\left(\frac{k}{2a_{end}H_{Inf}}\right)^{-2(n-3)} \quad , \tag{3.27}$$

at the super-horizon scale $k \ll aH_{inf}$. Considering nontrivial dynamics, the magnetic power spectrum at the present universe can be correlated with the magnetic power at the end of the inflation through the following standard equation

$$\mathcal{P}_{B0}(k) \simeq \mathcal{P}_B^{end}(k)\left(\frac{a_{end}}{a_0}\right)^4 \quad . \tag{3.28}$$

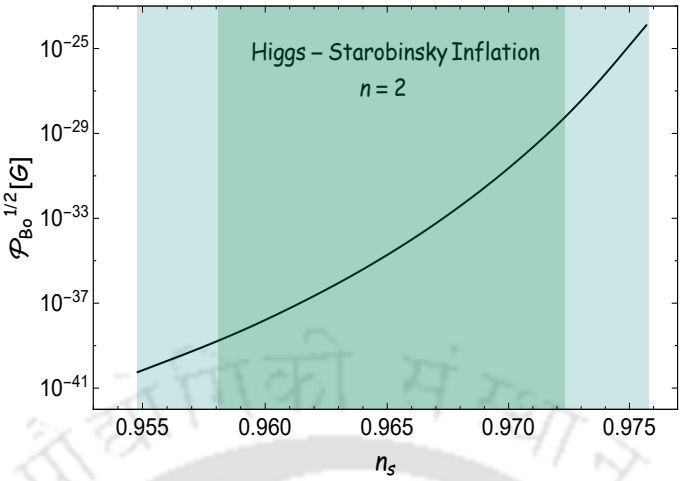

FIGURE 3.1: We plot the variation of the present magnetic field's strength as a function of the spectral index within 2σ range of n_s from Planck [29] for the Higgs-Starobinsky inflationary model. It is clear that the required magnetic field strength $(10^{-9} \sim 10^{-22})$ G is difficult to achieve within the conventional framework unless one introduces a slow decreasing rate of magnetic energy density in some early state of the universe evolution.

Where a_{end}/a_0 can be expressed in terms of inflationary e-folding number (N_k) as

$$\frac{a_{end}}{a_0} = \frac{a_{end}}{a_k}\frac{k'}{a_0 H_{Inf}} = \left(\frac{k'}{a_0}\right)\frac{e^{N_k}}{H_{Inf}} \quad . \tag{3.29}$$

Here $k'/a_0 = 0.05 M_{pc}^{-1}$ is taken as pivot scale set by Planck observation. By combining equations (3.27), (3.28), and (3.29), the expression for the magnetic power considering integer values of n, follow the equation

$$\mathcal{P}_{B0} \simeq \frac{\Gamma(n-\frac{1}{2})^2}{2^{3-2n}\pi^3}\left(\frac{k}{a_0}\right)^{6-2n}\left(\frac{k'}{a_0}\right)^{2n-2} e^{2(n-1)N_k} \quad . \tag{3.30}$$

It has already been observed and also shown in Fig.(3.1) the well-known fact that magnetic strength of order $10^{-9} - 10^{-22}$ Gauss on 1 Mpc scales [139, 156, 180, 181] can not be obtained by the above magnetic power spectrum for high-scale inflation model such as Higgs-Starobinsky inflation. Several models have been constructed to avoid this problem without much success related to the theoretical issues which we discuss in the next section. From here itself, we will advocate the importance of considering the effect of reheating more seriously than the model building. In the recent paper [141], authors have shown that considering negligible electrical conductivity during reheating, Faraday's law of electromagnetic induction plays an interesting role in modifying the magnetic field evolution. Therefore, we want to see how this induction effect can safely generate the presently observed magnetic field for different high-scale inflationary models. Consideration of CMB anisotropy into the analysis further reveals an intricate interconnection among various apparently disconnected cosmological parameters such as $(n_s, P_{B0}, T_{re}, w_{re})$. Consequently, our analysis opens up an interesting new possibility of probing the reheating dynamics and simultaneously constraining the inflationary and magnetogenesis model parameters through the evolution of the primordial magnetic field,

which has not been considered before.
After the end of inflation, the assumption of the gauge kinetic function $I(\phi)$ being unity renders the post-inflationary evolution of the electromagnetic field as standard Maxwellian. Therefore, further production of gauge field from the quantum vacuum ceases to exist. The electromagnetic field produced during inflation will cross the horizon and turn into the classical one, which will evolve during this phase. In the Fourier space, the mode function solution of the free Maxwell equation is,

$$u_k^{(p)} = \frac{1}{\sqrt{2k}}\{\alpha_k^{(p)}(z_{end})e^{-ik(\tau-\tau_{end})} + \beta_k^{(p)}(z_{end})e^{-ik(\tau-\tau_{end})}\} \ , \tag{3.31}$$

here τ_{end} represents the end of inflationary era. For the arbitrary value of n, the phase factor is calculated to be

$$\theta_k^{(p)} = \left\{Arg\left[\alpha_k^{(p)}\left(z_{end}\right)\beta_k^{(p)*}(z_{end})\right] - \pi\right\} - 2k\left(\tau - \tau_{end}\right) \ . \tag{3.32}$$

Where the elapsed conformal time is obtained as

$$\tau - \tau_{end} = \int_{a_{end}}^{a} \frac{da}{a^2 H} \ . \tag{3.33}$$

Since there is no further production of gauge field, the photon number density $|\beta_k|^2$ becomes independent of time and follows the same equation (3.25) as before. However, as emphasized already, the Faraday induction will come into play during this phase. To see this, let us first express the magnetic power spectra at the end of reheating parametrized by the scale factor (a_{re}) as

$$\mathcal{P}_{B_{re}}(k) \simeq \frac{k^4}{2\pi^2 a_{re}^4}(\theta_k^{re})^2|\beta_k^{end}|^2 \ , \tag{3.34}$$

where θ_k^{re} is the phase parameter at the end of the reheating era, which is defined as,

$$\theta_k^{re} = \{Arg\left[\alpha_k\left(z_{end}\right)\beta_k^*(z_{end})\right] - \pi\} - 2k\int_{a_{end}}^{a_{re}} \frac{da}{a^2 H} \ . \tag{3.35}$$

A notable term of the above expression is the second one which leads to the non-conventional dynamics of the magnetic field. Assuming the constant equation of state during reheating dynamics the special term boils down to the following simple form,

$$2k(\tau - \tau_{end}) \to \frac{4k}{3\omega + 1}\left(\frac{1}{aH} - \frac{1}{a_{end}H_{inf}}\right) . \tag{3.36}$$

The phase term contributes to the dynamics of the magnetic power spectrum in two different ways. The conventional one will be associated with the redshift factor $\propto a^{-4}$ emerging from the first term in the right-hand side of the Eq.(3.32). The important one is associated with the redshift factor $\propto a^{-6}H^{-2}$ emerged out from k/aH term. As the expansion of the universe is decelerating after inflation, the leading contribution to the evolution of the magnetic power would be controlled by the latter one Eq.(3.32). However, the electric field energy dilutes following the conventional form

$$\mathcal{P}_E(k) \simeq \frac{2k^4}{\pi^2 a^4}|\beta_k^{end}|^2 \ . \tag{3.37}$$

For large scale ($k \ll aH$), the above expression boils down to,

$$\mathcal{P}_E(k) \simeq \frac{8\Gamma(n+\frac{1}{2})^2}{\pi^3} H_{inf}^4 \left(\frac{k}{2a_{end}H_{inf}}\right)^{-2(n-2)} \left(\frac{a_{end}}{a}\right)^4 \quad , \tag{3.38}$$

for integer values of n. After the end of reheating, inflaton energy is converted into conducting plasma containing all the standard model particles. Due to large electrical conductivity, the primordial electric field decays to zero, and comoving large-scale magnetic energy density freezes to a constant value until today. Therefore, the final general expression of our interest is the present-day magnetic field strength given as

$$\mathcal{P}_{B_0}(k) = \mathcal{P}_{B_{re}}(k) \left(\frac{a_{re}}{a_0}\right)^4 \simeq \frac{k^4}{2\pi^2} (\theta_k^{re})^2 |\beta_k^{end}|^2 \frac{1}{a_0^4} \quad . \tag{3.39}$$

If we take the integer value of n, at the super horizon scale, the above expression will transform into [141]

$$\mathcal{P}_{B0}(k) \simeq \frac{8\Gamma(n-\frac{1}{2})^2}{\pi^3} H_{inf}^4 \left(\frac{k}{2a_{end}H_{inf}}\right)^{-2(n-3)} \left(\frac{a_{end}}{a_0}\right)^4 \left\{1 + (2n-1)\int_{a_{end}}^{a_{re}} \frac{da}{a} \frac{a_{end}H_{inf}}{aH}\right\}^2 , \tag{3.40}$$

where a_0 is the scale factor at the present time. In the next section, we will briefly discuss standard theoretical issues related to the magnetogenesis model.

3.1.2 Discussion on strong coupling and backreaction problem

In order to generate the large-scale magnetic field of required strength, conventional magnetogenesis models encounter either the strong coupling or backreaction problem. In order to alleviate these issues, several attempts [140, 149, 182–195] have been made either by advocating different forms of the gauge coupling function or taking non-trivial dynamics of the coupling fields during reheating. In the context of the simplest magnetogenesis model proposed in [138], the gauge kinetic function $I(\tau)$ can essentially be interpreted as time-dependent effective electromagnetic coupling. By considering field-theoretic argument and experimental observations [149, 150] it is generically argued that the model either suffers from the strong coupling problem or backreaction problem.

In our previous discussion, we have chosen the effective electromagnetic coupling function as a monomial function of the scale factor,

$$I = \left(\frac{a_{end}}{a}\right)^n = e^{N_k n} \quad , \tag{3.41}$$

where $N_k = \ln(a/a_{end})$ associated with a particular scale k is identified as the e-folding number during inflation. It is clear from the above expression that once the value of n is chosen to be negative, the gauge kinetic function increases during inflation. Now the behavior of $I(\tau)$ is so chosen that it boils down to unity after inflation. Therefore, during inflation, its magnitude must be less than unity. This is where the origin of the strong coupling problem in the electromagnetic sector lies. Under the field redefinition $A_\mu \to \sqrt{I}A_\mu$, the effective electromagnetic coupling α_{eff}, defined through the fermion-gauge field interaction $\mathcal{L}_{int} = eA_\mu J^\mu$ modified as

$$\alpha_{eff} = \frac{e^2}{4\pi I} = \frac{\alpha}{I}. \tag{3.42}$$

e is the charge of the fermionic field contributing to the electric current. α is the standard electromagnetic coupling. Nonetheless, as one goes early in the inflationary phase, the effective electromagnetic coupling necessarily becomes very large, which turns the theory non-perturbative. The perturbative computation of magnetogenesis discussed in our previous section will no longer be valid. Keeping this problem aside, if we still follow the analysis as before, large effective electromagnetic coupling α_{eff}, will naturally suppress the gauge field production. This may lead to the magnetic field according to the observed value without any backreaction problem.

On the other hand, if one considers positive values of $n \geq 0$, the whole reasoning expressed just now will be reversed. The gauge kinetic function $I(\tau)$ will be larger than unity, and hence the perturbative magnetogenesis analysis will be perfectly valid for this case. However, a considerable reduction of the effective electromagnetic coupling $\alpha_{eff} \propto 1/I(\tau)$, specifically during the early inflationary stage of our interest, significantly enhances the production of electromagnetic energy. In such a scenario, the quantum production of electromagnetic energy may take over the background energy density. This is precisely the backreaction problem, which jeopardizes the very idea of quantum production from a fixed inflationary background. To avoid the backreaction problem, the energy density of the gauge field must be smaller than the total background energy density $\rho_{tot} = 3M_p^2 H_{Inf}^2$. For subsequent calculation, let us define the useful parameter which quantifies the amount of background energy density during inflation against the gauge field energy density ρ_A as,

$$\frac{\rho_A}{\rho_{tot}} \leq \zeta \quad . \tag{3.43}$$

Where ζ is associated with the amplitude of the curvature perturbation measured from CMB anisotropy. The CMB observation constrain the amplitude of the curvature perturbation as $\zeta = 4.58 \times 10^{-5}$ [29]. The total gauge field energy density at a given scale factor a_T during inflation can be calculated by using equations (3.13) and (3.18) as

$$\begin{aligned}
\rho_A(a_T) &= \rho_E(a_T) + \rho_B(a_T) = \frac{I(a_T)^2}{2} \int_{k_{IR}}^{k_T} \frac{dk}{k} \left\{\mathcal{P}_E(k, a_T) + \mathcal{P}_B(k, a_T)\right\} \\
&= \frac{I(a_T)^2}{2} \int_{k_{IR}}^{k_T} \frac{dk}{4\pi k H_{inf}} \left(\frac{k}{a_T}\right)^5 \left\{ \left| H^{(1)}_{-n-\frac{1}{2}} \left(\frac{k}{a_T H_{inf}}\right) \right|^2 + \left| H^{(1)}_{-n+\frac{1}{2}} \left(\frac{k}{a_T H_{inf}}\right) \right|^2 \right\}.
\end{aligned}$$

In the above expression, the k-integration ranges from k_{IR} to k_T. Associated with our observable universe, the IR cutoff k_{IR} corresponds to the highest mode that exits the horizon at the beginning of the inflation or approximately the CMB scale, and $k_T \sim a_T H_{inf}$ denotes the mode that crosses the horizon at any arbitrary scale $a = a_T$. In order to avoid backreaction, the energy density across the scales emerging during inflation ($a_k \leq a_T \leq a_{end}$), should satisfies the condition (3.43). So we can set a limit on index $0 < n < n_{max}$ of the gauge coupling function above which the Eq.(3.43) will be violated. Thus within the aforementioned range of n, we can take care of strong coupling and backreaction problems simultaneously.
For example, the scale-invariant electric power spectrum which corresponds to $n = 2$, the total gauge field energy density at the end of the inflation is

$$\rho_A = \rho_E + \rho_B \sim \frac{9}{4} \frac{H_{Inf}^4}{\pi^2} N_k + \frac{H_{Inf}^4}{8\pi^2} \left(1 - e^{-2N_k}\right) \quad . \tag{3.44}$$

The ratio between the gauge field and the total background energy density is always less than the amplitude of the curvature perturbation ($\rho_A/\rho_{tot} \sim 10^{-10}$) for all allowed values of

the spectral index. For the scale-invariant electric power spectra model, therefore, the back reaction, as well as the strong coupling problem, can be avoided. However, during the entire inflation period, such models generically produce a magnetic field of insufficient strength and we will see how the reheating phase helps to enhance the magnitude of the magnetic field to a desirable strength.

Another interesting case is when the generated magnetic field is scale-invariant, which corresponds to $n = 3$. However, immediate problem arises in the electric field power spectrum $\mathcal{P}_E(k) \propto \left(\frac{k}{aH_{Inf}}\right)^{-2} \to \infty$ (see equation 3.23), which increases rapidly in the large scale limit $\frac{k}{aH_{Inf}} \to 0$. Hence electrical energy density exceeds the background inflaton energy density much before the end of the inflation. However, it can be cured by changing the coupling function as follows,

$$I(\tau) = \begin{cases} \left(\frac{a_{br}}{a}\right)^n & a \leq a_{br} \\ 1 & a \geq a_{br}, \end{cases} \tag{3.45}$$

where a_{br} is the scale factor defined at a particular point during inflation when

$$\frac{\rho_E(a_{br}) + \rho_B(a_{br})}{3M_p^2 H_{Inf}^2} = \zeta \quad . \tag{3.46}$$

Therefore, the primary assumption is that the standard maxwell theory is recovered at a point a_{br} not after the end of inflation. In such a scenario, one can naturally solve the backreaction problem for the $n = 3$ magnetogenesis model. However, from the detailed analysis, we found it difficult to obtain the magnetic field within the observable limit. The magnetic field strength turns out to be within $(10^{-45} - 10^{-50})$ G, which is very small compared with the observational limit. We will discuss this possible scenario in our future work. In our subsequent discussion, we will mainly concentrate on the model with the scale-invariant electric power spectrum during inflation.

3.1.3 Reheating dynamics: Connecting Reheating and Primordial magnetic field via CMB

By now, it has become clear that the primary importance of the reheating phase is to enhance the strength of the large-scale magnetic field to the required order. We understood the fact that Faraday's law of electromagnetic induction plays a crucial role in this regard. Therefore, to obtain the correct order of the current magnetic field, understanding the reheating dynamics as well as the evolution of the magnetic field during this period will be of utmost importance. To do that, we will consider two possible reheating models and compare the result.

Case-I: Dynamics described by an effective EoS parameter : For this, we follow the effective one fluid description of reheating dynamics proposed in [45], where inflaton energy is assumed to be converted into radiation instantaneously at the end of reheating (see, for instance, section (2.1.1) for details).

Reheating parameters and primordial magnetic field : Since electrical conductivity during the entire period of reheating is assumed to be negligible, the electric field continues to exist in the post-inflationary era until the universe becomes a perfect conductor. This is the non-zero electric field during reheating, whose dynamics will significantly change the dynamics

of the magnetic field and produce a strong magnetic field today.
For this present reheating model, the phase parameter at the end of the reheating θ_k^{re} in equation (3.35) can be defined as,

$$\theta_k^{re} = \{Arg\left[\alpha_k\left(z_{end}\right)\beta_k^*(z_{end})\right] - \pi\} - \frac{4}{3\ \omega_{eff}+1}\left(\frac{k}{a_{re}H_{re}} - \frac{k}{a_{end}H_{Inf}}\right)\ , \tag{3.47}$$

where H_{re} is the Hubble rate at the endpoint of reheating. Using the evolution of effective density $\rho \propto a^{-3(1+\omega_{eff})}$, one can extract the information about the Hubble parameter at the end of reheating (H_{re}) as

$$H_{re} = H_{inf}A_{re}^{-\frac{3}{2}(1+\omega_{eff})}\ , \tag{3.48}$$

with the normalized scale factor $A_{re} = a_{re}/a_{end} = e^{N_{re}}$. For integer values of n, the earlier expression of the phase parameter turns out as

$$\theta_k^{re} \simeq \frac{2}{2n-1}\frac{k}{a_{end}H_{inf}}\left\{1 + \frac{4n-2}{3\omega_{eff}+1}\left(\frac{a_{end}H_{inf}}{a_{re}H_{re}} - 1\right)\right\}\ . \tag{3.49}$$

Furthermore, utilizing equations (3.49) and (3.34), one can obtain the magnetic power spectrum during the reheating epoch as,

$$\mathcal{P}_{B_{re}}(k) \simeq \frac{8\Gamma(n-\frac{1}{2})^2}{\pi^3 H_{Inf}^{-4}}\left(\frac{k}{2a_{end}H_{inf}}\right)^{-2(n-3)}\left(\frac{a_{end}}{a}\right)^4\left\{1 + \left(\frac{4n-2}{3\omega_{eff}+1}\right)\left(\frac{a_{end}H_{inf}}{aH} - 1\right)\right\}^2\ . \tag{3.50}$$

After reheating, the conductivity of the universe becomes sufficiently large. As a consequence, the electric field dies out very fast, and the magnetic field redshifts as $\mathcal{P}_B \propto a^{-4}$ till today. Since the comoving magnetic power spectrum is conserved after reheating, the present-day magnetic field obeys the following relation [141]

$$\mathcal{P}_{B_0}(k) \simeq \frac{8\Gamma(n-\frac{1}{2})^2}{\pi^3 H_{Inf}^{-4}}\left(\frac{k}{2a_{end}H_{Inf}}\right)^{-2(n-3)}\left(\frac{a_{end}}{a_0}\right)^4\left\{1 + \left(\frac{4n-2}{3\omega_{eff}+1}\right)\left(\frac{a_{end}H_{inf}}{a_{re}H_{re}} - 1\right)\right\}^2\ , \tag{3.51}$$

where the ratio between the scale factor a_0 and a_{re}, considering entropy conservation can be expressed as

$$\frac{a_0}{a_{re}} = \left(\frac{11g_{s,re}}{43}\right)^{\frac{1}{3}}\frac{T_{re}}{T_0}\ . \tag{3.52}$$

From the preceding expression, we observe that the magnetic field's present strength explicitly depends on the reheating and inflationary parameters. Therefore, this opens up a new possibility for probing the early phases of the universe, particularly the reheating phase, through the large-scale magnetic field. For a specific value of the spectral index, the $\mathcal{P}_{B_0}$ has a one-to-one correspondence with the effective equation of state of reheating ω_{eff} and reheating temperature T_{re}. Therefore, an important conclusion we arrived at is that *the effective equation of state is no longer a free parameter; rather, it can be fixed by the present value of* $\mathcal{P}_{B_0}$ *via CMB.*

Case-II: Perturbative reheating dynamics: In the earlier case, we have not taken into account explicit decay of the inflaton field, and additionally, the effective equation of state was assumed to be constant. In this case, we consider a perturbative reheating scenario following the methodology discussed in [91] (see, for instance, section (2.1.2) for details).

Connecting reheating and primordial magnetic field : In order to connect the reheating and primordial magnetic field through the CMB, it is necessary to understand the cosmological evolution of the electromagnetic field during the post-inflationary epoch, especially during reheating, which modifies the present strength of the magnetic power spectrum. As we consider the perturbative decay of the inflaton field during reheating, the phase parameter (3.35) now explicitly depends on the evolution of the two energy components, ρ_ϕ and ρ_R with time

$$\theta_k^{re} = \{Arg\left[\alpha_k\left(z_{end}\right)\beta_k^*(z_{end})\right] - \pi\} - 2k\int_{a_{end}}^{a_{re}} \frac{\sqrt{3}M_p}{\sqrt{\rho_\phi(a)+\rho_R(a)}}\frac{da}{a^2}\ . \tag{3.53}$$

Furthermore, for integer values of coupling parameters at the super horizon scale, one can find [141]

$$\theta_k^{re} \simeq \frac{2}{2n-1}\frac{k}{a_{end}H_{Inf}}\left\{1+(2n-1)\int_{a_{end}}^{a_{re}}\frac{\sqrt{3}M_p}{\sqrt{\rho_\phi(a)+\rho_R(a)}}\frac{a_{end}H_{inf}}{a}\frac{da}{a}\right\}\ , \tag{3.54}$$

where the time-dependent density components will be followed from Eqns.(2.21) and (2.22). Thus, after combining equations (3.40), (3.52), and (3.54), one can obtain the magnetic power spectrum in the present universe as

$$\mathcal{P}_{B0}(k) \simeq \frac{\Gamma(n-\frac{1}{2})^2}{\pi^3}\frac{2^{2n-3}\ (2.6\times10^{39})}{(6.4\times10^{-39})^{2n-6}}\left(\frac{k}{a_0}M_{pc}\right)^{-2(n-3)}\left(\frac{11g_{s,re}}{43}\right)^{\frac{2-2n}{3}}\left(\frac{T_{re}}{T_0}\right)^{2-2n}$$
$$\left(\frac{H_{inf}}{GeV}\ \frac{1}{A_{re}}\right)^{2(n-1)}\left\{1+(2n-1)\int_1^{A_{re}}\frac{\sqrt{3}M_pH_{Inf}}{\sqrt{\rho_\phi(a)+\rho_R(a)}}\frac{dA}{A^2}\right\}^2 G^2\ . \tag{3.55}$$

In the preceding expression, we can clearly see the appearance of the reheating parameters, which are the function of inflationary observables. Therefore, we will be able to put bounds on the reheating as well as inflationary model parameters. As we emphasized before, from the measurement of the CMB anisotropy, our goal of this chapter would be to constraints the reheating dynamics through inflationary parameters considering the present strength of the magnetic field $\mathcal{P}_{B_0}^{1/2}$.

3.2 Magnetic power spectrum in the present universe in terms of reheating parameters: an analytic study

Before employing the numerical analysis, in this section, we present an approximate calculation for the present value of the magnetic power spectrum and estimate its value in terms of reheating parameters (T_{re}, N_{re}). Following our previous work [93], the radiation temperature

assumes the following form considering Case-II reheating scenario,

$$T_{rad} \simeq \left\{ \frac{2\Gamma_\phi(1+\omega_\phi)}{5-3\omega_\phi} \frac{3M_p^2 H_{Inf}}{\beta A^4} \left(A^{\frac{5-3\omega_\phi}{2}} - 1 \right) \right\}^{\frac{1}{4}} , \tag{3.56}$$

where $\beta = \pi^2 g_{re}/30$. Further, utilizing the above expression of the radiation temperature, we can calculate the approximate expression of the reheating temperature. Subsequently, at the point of A_{re} the condition $H(A_{re}) = \Gamma_\phi$ is satisfied, and one can define the reheating temperature as

$$T_{re} \simeq \left(\frac{2\Gamma_\phi(1+\omega_\phi)}{5-3\omega_\phi} \frac{3M_p^2 H_{inf}}{\beta A_{re}^{\frac{3+3\omega_\phi}{2}}} \right)^{\frac{1}{4}} . \tag{3.57}$$

Here the decay width Γ_ϕ and the normalized scale factor at the end of reheating (A_{re}) can be approximated as,

$$\Gamma_\phi \simeq \frac{(5-3\omega_\phi)\beta G^4 A_{re}^{\frac{3\omega_\phi-5}{2}}}{6M_p^2 H_{Inf}}, A_{re} \simeq \left(\frac{(5-3\omega_\phi)^2 \beta G^4}{12(1+\omega_\phi)^2 M_p^2 H_{Inf}^2} \right)^{\frac{1}{1-3\omega_\phi}} , \tag{3.58}$$

where, $G = \left(\frac{43}{11 g_{s,re}}\right)^{\frac{1}{3}} \left(\frac{a_0 T_0}{k'}\right) H_k e^{-N_k}$. From the Eqn.(3.34) it is obvious that during reheating phase, the electromagnetic power spectrum is crucially dependent upon the evolution of the phase θ_k, which gives rise to the induced magnetic field. Importantly after the reheating phase ends large-scale magnetic field freezes inside the plasma. Therefore, the hierarchy between the inflationary and reheating energy scale sets the strength of the magnetic field today after the inflation. This naturally leads to interesting constraints on the reheating parameters $(T_{re}, N_{re}, w_{eff})$ through the current value of the large-scale magnetic field. Inflaton energy density dominates during the initial period of the reheating phase, which enables one to obtain an approximate solution of the inflaton energy density as

$$\rho_\phi(A) = \rho_\phi^{end} A^{-3(1+\omega_\phi)} e^{-\Gamma_\phi(t-t_i)} \simeq \rho_\phi^{end} A^{-3(1+\omega_\phi)} . \tag{3.59}$$

This helps us to obtain the approximate Hubble parameter as

$$H(A) = \sqrt{\frac{\rho_\phi(A)+\rho_R(A)}{3M_p^2}} \simeq \frac{H_{Inf}}{A^{\frac{3(1+\omega_\phi)}{2}}} \sqrt{e^{-\Gamma_\phi(t-t_i)} + \frac{A^{\frac{3(1+\omega_\phi)}{2}}}{\eta}} \simeq \frac{H_{Inf}}{A^{\frac{3(1+\omega_\phi)}{2}}} \sqrt{1 + \frac{A^{\frac{3(1+\omega_\phi)}{2}}}{\eta}} , \tag{3.60}$$

where $\eta = \frac{(5-3\omega_\phi)H_{inf}}{2\Gamma_\phi(1+\omega_\phi)}$. With all the above approximate expressions, one can arrive the following expression of the present magnetic power spectrum

$$\mathcal{P}_{B0}(k) \simeq \frac{\Gamma(n-\frac{1}{2})^2}{\pi^3} \frac{2^{2n-3}\ (2.6\times10^{39})}{(6.4\times10^{-39})^{2n-6}} \left(\frac{k}{a_0} Mpc\right)^{-2(n-3)} \left(\frac{11 g_{s,re}}{43}\right)^{\frac{d}{3}} \left(\frac{T_{re}}{T_0}\right)^d \left(\frac{H_{inf}}{GeV}\frac{1}{A_{re}}\right)^{-d}$$
$$\left\{ 1 + (2n-1)\left[\frac{2}{3\omega_\phi+1}\left(\eta^{\frac{3\omega_\phi+1}{3(1+\omega_\phi)}} - 1 \right) + \frac{4}{3\omega_\phi-1}\eta^{1/2}\left(A_{re}^{\frac{3\omega_\phi-1}{4}} - \eta^{\frac{3\omega_\phi-1}{6(1+\omega_\phi)}} \right) \right] \right\}^2 G^2 . \tag{3.61}$$

where $d = 2-2n$. Interestingly, our analytical expression of the magnetic power spectrum roughly matches the numerical values.

3.3 Inflation models and numerical results

The main aim of our study is to see how the present value of the large-scale magnetic field, together with CMB anisotropy, can be used to probe the reheating dynamics and put combined constraints on the reheating and inflationary parameters space. We consider different inflationary models and study how the present limits on the magnetic field strength constrain the effective reheating equation of state ω_{eff} in terms of the inflationary scalar spectral index n_s. Further, the allowed range of the current magnetic field can be shown to impose an upper limit on the values of the spectral index n_s^{max} and effective equation of state ω_{eff}^{max}, which in turn provides a bound on the maximum possible reheating temperature T_{re}^{max}. Moreover, to connect reheating parameters such as (T_{re}, ω_{eff}) with the present magnetic field power spectrum $\mathcal{P}_{B_0}^{1/2}$, we take into account the gauge kinetic function with power $n = 2$. We also studied interesting constraints on the maximum possible value of the magnetogenesis model parameter $n = n_{max}$ and associated maximum reheating temperature T_{re}^{max} for the different inflationary models.

3.3.1 Geneal discussion on our results

In the conventional study, the magnetic energy density is assumed to be diluted adiabatically with the universe's expansion as $1/a^4$ starting from the end of inflation. This framework never gives rise to enough present-day magnetic field strength for high reheating temperatures. In comparison, the high reheating temperature is generically expected in the effective field theory framework. It is in this parlance dynamics of the magnetic field during reheating should be important to understand. The most important point of our study is the constraints set on the effective reheating equation of state ω_{eff}. With a particular present-day value of P_{B_0}, the CMB anisotropic constraint and entropy conservation law automatically fix the reheating equation of state uniquely. Interestingly, this would place a severe restriction on the inflaton potential, which we will study in detail in our subsequent work. We mainly concentrate on the scale-invariant electric power spectra ($n = 2$) and their evolution for two possible reheating scenarios discussed before. One corresponds to the instantaneous conversion of inflaton energy to radiation at the end of the reheating. The second one is perturbative reheating, where inflaton energy density is transferred into radiation gradually with finite inflaton decay width.

Case-I, dynamics described by an effective EoS parameter : Even though we consider the scale-invariant electric field, it is important to remember that it will survive only until the end of reheating. This will condition the magnitude of the large-scale magnetic field in the present-day universe. This intertwined nature of the reheating, inflationary parameters and the large-scale magnetic field is depicted in Fig.(3.2). From the first panel of Fig.(3.2), we can clearly predict a unique value of ω_{eff} associated with a specific choice of the present magnetic field strength once one fixes the scalar spectral index n_s. Additionally, for a given ω_{eff}, the reheating temperature is also determined uniquely. *Therefore, taking into account CMB constraints, the reheating phase, conditioned by the negligible electrical conductivity, can be uniquely probed by the evolution of the primordial magnetic field .*
In order to have quantitative understanding of our analysis, in the Tables-(3.1), (3.3) and (3.6), important reheating parameters such as ω_{eff} and T_{re} for different sample values of the current magnetic field are given for a particular values of the spectral index $n_s^{central} = 0.9649$. For any specific choice of the current magnetic field strength within the observational limit, there exists a maximum allowed value of the spectral index n_s^{max} and associated ω_{eff}^{max}, which further leads

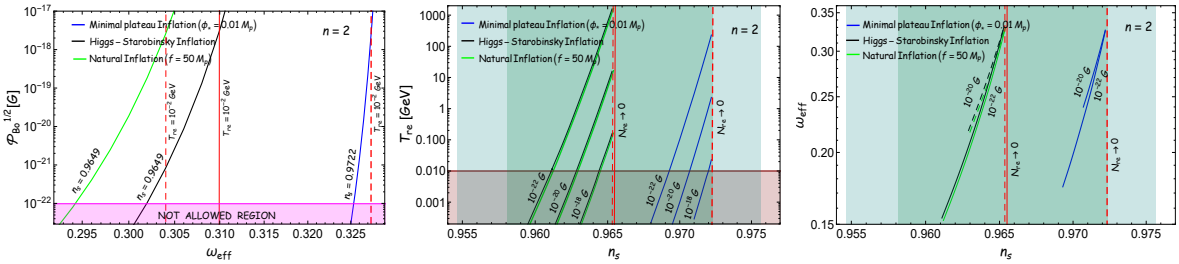

FIGURE 3.2: We plot the magnetic field variation on the upper left side as a function of the effective equation of state for a fixed value of the spectral index. The light pink region indicates the not allowed region as the strength of the magnetic field in that region is less than 10^{-22} G (observed value of the magnetic field on scales $\approx 1Mpc$ must be $B^0_{cosmic} > 10^{-22}$ G [139]). The allowed value of the present magnetic field range from 10^{-22} G to the point where the reheating temperature reaches 10^{-2} GeV (comes from BBN constraints), marked as a solid and dashed red line. In the middle, we have plotted the variation of reheating temperature as a function of the spectral index for three different values of the current magnetic field $\mathcal{P}^{1/2}_{B_0} = (10^{-18}, 10^{-20}, 10^{-22})$ G. The light brown region indicates the reheating temperature (T_{re}) below 10^{-2} GeV, which would ruin the predictions of big bang nucleosynthesis (BBN). In the last plot, we have shown the variation of the effective equation of state as a function of the spectral index (n_s) with two different values of $\mathcal{P}^{1/2}_{B_0} = (10^{-20}, 10^{-22})$ G, within the minimum and maximum values of reheating temperature. The deep and light green band indicates 1σ and 2σ range of n_s from Planck [29]. Here we have plotted the results for three different inflationary models (Natural inflation, Higgs-Starobinsky inflation, minimal plateau model) for the k-independent electric power spectrum ($n = 2$).

to the maximum permissible value of the reheating temperature shown in the Tables (3.2), (3.4), (3.7). We consider three distinct values of $\mathcal{P}^{1/2}_{B_0} = (10^{-18}, 10^{-20}, 10^{-22})$ G throughout the discussion. Most importantly, results for the case of instantaneous reheating scenario are the constraints on the effective reheating equation of state $0.15 < \omega_{eff} < 0.33$ for quadratic inflaton potential near its minimum. Furthermore, the minimum limiting value of magnetic field ($P^{1/2}_{B_0} < 10^{-22}$) G, set an associated maximum reheating temperature around ~ 1 TeV. Therefore, magnetogenesis models with scale-invariant electric fields appear to be compatible with only the low-scale inflationary model.

Perturbative reheating model (case-II) : The present-day magnetic field and the reheating temperature are intimately connected through the inflaton equation of state, which can be guessed from the previous analysis. However, perturbative reheating is observed to be better suited for understanding the nature of both the inflaton and magnetogenesis models. An important characteristic outcome in considering the perturbative reheating scenario is that the evolution of the large-scale magnetic field permits us to understand the nature of the inflaton field and its observational viability through the constraints on the inflaton equation of state. For example, as long as the scale-invariant power spectra model is concerned, $\omega_\phi = 0$ can not produce the required strength of the magnetic field, which indicates the fact that an inflaton field with quadratic potential near its minimum is not compatible with the observation. However, assuming a higher inflaton equation of state $\omega_\phi = (p-2)/(p+2) > \frac{1}{3}$ the observable magnetic field strength can be successfully generated within the perturbative reheating framework shown in the last two plots of the figs.(3.3). Further, considering the magnetic field strength within the observational limit, the maximum and minimum allowed values of the spectral index n_s, the inflaton equation of state ω_ϕ and the associated reheating temperature are provided in the Tables (3.5), (3.8) for different inflationary models.

With this general discussion, in the following sections, we consider various inflationary models and discuss their quantitative predictions in detail.

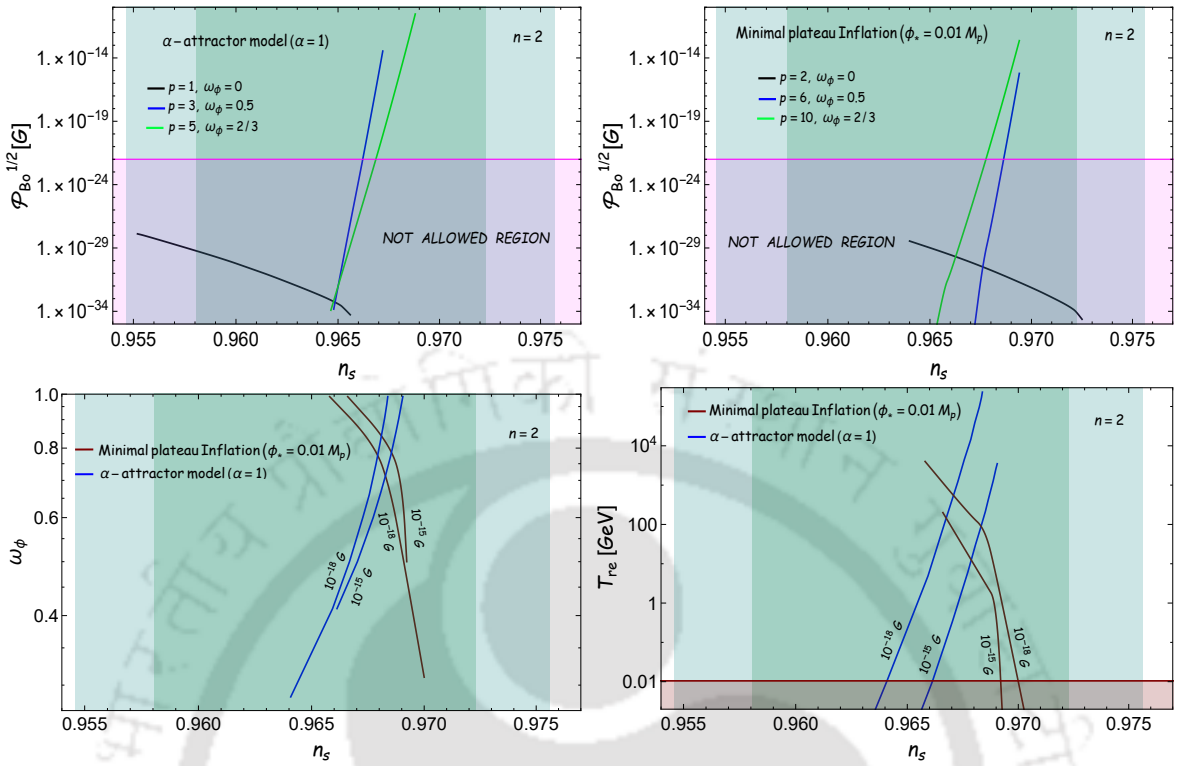

FIGURE 3.3: In the first two plots, we have shown the variation of the present-day magnetic field as a function of the spectral index within the minimum and maximum values of the reheating temperature for different inflationary models, considering the perturbative dynamics of reheating with inflaton equation of state ($\omega_\phi = (0, \frac{1}{2}, \frac{2}{3})$). The light pink region indicates the not allowed region as the strength of the magnetic field in that region is less than 10^{-22} G (observed value of the magnetic field on scales $\approx 1Mpc$ must be $B^0_{cosmic} > 10^{-22}$ G [139]). We plot on the lower left side the variation of the inflaton equation of state ω_ϕ as a function of the spectral index for two different values of the magnetic field $\mathcal{P}^{1/2}_{B_0} = (10^{-15}, 10^{-18})$ G. On the lower right side, we have plotted the variation of reheating temperature as a function of the spectral index with the same fixed values of the $\mathcal{P}^{1/2}_{B_0}$. The light brown region indicates the reheating temperature (T_{re}) below 10^{-2} GeV, which would ruin the predictions of big bang nucleosynthesis (BBN).

3.3.2 Natural inflation

We already mentioned the details of this model in sec.1.4. As we have the connection relation (Eqs. 3.51, 3.55) between the reheating parameters and the parameters of magnetogenesis model, in the following, we discuss their implications and various constraints for the inflationary magnetogenesis model with $n = 2$ for two aforementioned reheating scenarios.

In the first panel of the Fig.(3.2), for PLANCK central value of $n_s = 0.9649$, the reheating equation of state ω_{eff} has to be bounded within a very small window $(0.294, 0.304)$ which is close to the radiation equation of state. The upper bound is associated with the BBN limit of $T_{re} \sim 10^{-2}$ GeV. From the third panel of Fig.(3.2), one observes that with the decreasing magnetic field, the maximum allowed reheating temperature is increasing, which

Table 3.1: Probing reheating phase (fixing effective equation of state and reheating temperature)

Natural inflation model ($f = 50M_p$)

Parameters	Current value of the magnetic field ($\mathcal{P}_{B_0}^{1/2}$) measured in unit of Gauss			
	n_s	Scale invariant electric field ($n = 2$)		
		10^{-18} G	10^{-20} G	10^{-22} G
ω_{eff}	0.9649	0.303	0.299	0.294
T_{re} (GeV)		0.033	3.36	339.30

Table 3.2: Constraining reheating and inflationary parameters through inflationary magnetogenesis

Natural inflation model ($f = 50M_p$)

Parameters	Current value of the magnetic field ($\mathcal{P}_{B_0}^{1/2}$) measured in unit of Gauss		
	Scale invariant electric field ($n = 2$)		
	10^{-18} G	10^{-20} G	10^{-22} G
n_s^{min}	0.9645	0.9630	0.9612
n_s^{max}	0.9654	0.9654	0.9654
ω_{eff}^{min}	0.2842	0.2171	0.1523
ω_{eff}^{max}	0.3307	0.3303	0.3298
T_{re}^{min}(GeV)	10^{-2}	10^{-2}	10^{-2}
T_{re}^{max}(GeV)	0.16	16.42	1.6×10^3

seems intuitively obvious as reheating e-folding is accordingly decreasing. All the above results are for the case-I reheating scenario.

For the perturbative reheating (case-II) model with $\omega_\phi = 0$, the large-scale magnetic field's maximum strength is $\sim 10^{-28}$ G, which is much smaller compared to the observational limit. Hence we can conclude that *the natural inflation model is not compatible with the large-scale magnetic field observation within the perturbative reheating framework. This is attributed to the fact that axion potential is quadratic in nature near its minimum.*

3.3.3 $\alpha-$attractor model

The details of this model is already given in sec.(1.4). We consider $\alpha-$attractor model with $\alpha = 1$ for two different reheating scenarios described before. Detail prediction and model

Table 3.3: Probing reheating phase (fixing effective equation of state and reheating temperature)

Higgs-Starobinsky inflation model

Parameters	Current value of the magnetic field ($\mathcal{P}_{B_0}^{1/2}$) measured in unit of Gauss			
	n_s	Scale invariant electric field ($n = 2$)		
		10^{-18} G	10^{-20} G	10^{-22} G
ω_{eff}	0.9649	0.3093	0.3061	0.3019
T_{re} (GeV)		0.044	4.45	447.62

Table 3.4: Constraining reheating and inflationary parameters through inflationary magnetogenesis

Higgs-Starobinsky inflation model

Parameters	Current value of the magnetic field ($\mathcal{P}_{B_0}^{1/2}$) measured in unit of Gauss		
	Scale invariant electric field ($n = 2$)		
	10^{-18} G	10^{-20} G	10^{-22} G
n_s^{min}	0.9644	0.9629	0.9611
n_s^{max}	0.9653	0.9653	0.9653
ω_{eff}^{min}	0.2852	0.2185	0.1538
ω_{eff}^{max}	0.3314	0.3311	0.3307
T_{re}^{min}(GeV)	10^{-2}	10^{-2}	10^{-2}
T_{re}^{max}(GeV)	0.16	15.7	1.6×10^3

constraints can be read from Figs.(3.2), (3.3) and Tables (3.3), (3.4), (3.8). Taking a particular central value of the scalar spectral, $n_s = 0.9649$, the effective equation of state is constrained within a very narrow range $(0.302, 0.310)$. As has been mentioned and also seen for the axion model, a large-scale magnetic field appeared to be consistent with low reheating temperature with maximum value ~ 1 TeV for $\mathcal{P}_{B_0}^{1/2} \sim 10^{-22}$ G.

For the perturbative case, $\omega_\phi = 0$ turned out to be observationally unsuitable. However, for the model with $p = (3, 5)$ where the inflaton equation states assume $\omega_\phi = (0.5, \frac{2}{3})$ accordingly, are observed to be potentially consistent with observation. Most importantly the perturbative reheating supports higher value of reheating temperature $T_{re}^{max} \sim (2.4 \times 10^4, 2.1 \times 10^6)$ GeV for magnetic field strength $\mathcal{P}_{B_0}^{\frac{1}{2}} \sim 10^{-22}G$, with $\omega_\phi = (0.5, \frac{2}{3})$ respectively. Quantitative values of all the reheating parameters and inflationary parameters $(n_s, \omega_\phi, T_{re})$ corresponding to different sample values of $\mathcal{P}_{B_0}^{1/2}$ are provided in Table-(3.5). This can provide us clear picture of the

Table 3.5: Constraining reheating and inflationary parameters through inflationary magnetogenesis: Perturbative reheating dynamics (Here for $\alpha-$attractor model $\alpha = 1$ and for minimal model $\phi_* = 0.01\ M_p$)

Parameters	Current value of the magnetic field ($\mathcal{P}_{B_0}^{1/2}$) measured in unit of Gauss			
	Scale invariant electric field ($n = 2$)			
	10^{-15} G		10^{-18} G	
	$\alpha-$ attractor	minimal	$\alpha-$attractor ($\alpha = 1$)	minimal
n_s^{min}	0.966125	0.969224	0.964075	0.96580
n_s^{max}	0.96905	0.9666	0.96838	0.9700
ω_ϕ^{min}	0.412	0.500	0.286	0.3100
ω_ϕ^{max}	0.99	0.99	0.99	0.99
T_{re}^{min}(GeV)	10^{-2}	10^{-2}	10^{-2}	10^{-2}
T_{re}^{max}(GeV)	3.5×10^3	200.1	2.32×10^5	4.0×10^3

Table 3.6: Probing reheating phase (fixing effective equation of state and reheating temperature)

Minimal plateau model ($\phi_* = 0.01 M_p$)

Parameters	Current value of the magnetic field ($\mathcal{P}_{B_0}^{1/2}$) measured in unit of Gauss			
	n_s	Scale invariant electric field ($n = 2$)		
		10^{-18} G	10^{-20} G	10^{-22} G
ω_{eff}	0.9722	0.32725	0.3264	0.3253
T_{re} (GeV)		0.023	2.28	228.6

viability of the $\alpha-$attractor model in the context of inflationary magnetogenesis scenarios.

3.3.4 Minimal plateau model

In this section, we will introduce a special class of the inflationary model, the minimal plateau models proposed in [36]. For details of this model see sec.(1.4). For the numerical purpose, we choose $\phi_* = 0.01 M_p$.

Details constraints on the reheating parameter space can be read from Figures (3.2), (3.3) and Tables (3.5), (3.6),(3.7) and (3.8). Let us point out that for the minimal-inflation model, the constraints on the reheating parameters in terms of scalar spectral index and large-scale magnetic field qualitatively differ from that of the $\alpha-$attractor model shown in Fig.(3.3).

Table 3.7: Constraining reheating and inflationary parameters through inflationary magnetogenesis

Minimal plateau model ($\phi_* = 0.01M_p$)

Parameters	Current value of the magnetic field ($\mathcal{P}_{B_0}^{1/2}$) measured in unit of Gauss		
	Scale invariant electric field ($n = 2$)		
	10^{-18} G	10^{-20} G	10^{-22} G
n_s^{min}	0.972	0.9707	0.9693
n_s^{max}	0.9722	0.9722	0.9722
ω_{eff}^{min}	0.3144	0.239	0.1743
ω_{eff}^{max}	0.32725	0.3264	0.3253
T_{re}^{min}(GeV)	10^{-2}	10^{-2}	10^{-2}
T_{re}^{max}(GeV)	0.023	2.3	228.6

Table 3.8: Different inflationary models and their associated bounds on reheating temperature (T_{re}) and present magnetic field ($\mathcal{P}_{B0}^{\frac{1}{2}}$), measured in units of Gauss (Perturbative reheating dynamics)

Parameters	α-attractor model ($\alpha = 1$)		Minimal model ($\phi_* = 0.01M_p$)	
	$\omega_\phi = 0.5$	$\omega_\phi = 2/3$	$\omega_\phi = 0.5$	$\omega_\phi = 2/3$
$\mathcal{P}_{B0}^{\frac{1}{2}}$ (minimum)	10^{-22}	10^{-22}	10^{-22}	10^{-22}
$\mathcal{P}_{B0}^{\frac{1}{2}}$ (maximum)	3.4×10^{-14}	2.9×10^{-11}	6.0×10^{-16}	2.3×10^{-13}
n_s^{min}	0.9662	0.9669	0.9687	0.9678
n_s^{max}	0.9672	0.9688	0.9694	0.9694
T_{re}^{min} (GeV)	10^{-2}	10^{-2}	10^{-2}	10^{-2}
T_{re}^{max} (GeV)	2.4×10^4	2.1×10^6	1.7×10^3	2.3×10^4

This difference can be attributed to the qualitatively different nature of the potential near its minima and the initial condition at the beginning of reheating. The numerical values and their constraints of reheating parameters (ω_{eff}, T_{re}) for different sample values of $\mathcal{P}_{B_0}^{1/2}$ can be read from the Table-(3.7) for reheating dynamics described by an effective EoS, and Table-(3.8), third panel of Fig.(3.3) for perturbative reheating case.

Table 3.9: Different inflationary models and their associated bounds on reheating temperature (T_{re}) and present magnetic field ($\mathcal{P}_{B0}^{\frac{1}{2}}$) (measured in units of Gauss), considering maximum allowed value of the coupling parameter n_{max} (here for Axion model, we consider $f = 50\ M_p$ and for Minimal model $\phi_* = 0.01\ M_p$)

Parameters	Axion		Higgs-Starobinsky		Minimal
	$n_s^{max}(0.9654)$	$n_s^{central}$	$n_s^{max}(0.9653)$	$n_s^{central}$	$n_s^{max}(0.9722)$
n_{max}	2.136	2.138	2.142	2.144	2.179
$\mathcal{P}_{B0}^{\frac{1}{2}}$ (minimum)	10^{-22}	10^{-22}	10^{-22}	10^{-22}	10^{-22}
$\mathcal{P}_{B0}^{\frac{1}{2}}$ (maximum)	2.6×10^{-13}	5.5×10^{-14}	4.2×10^{-14}	1.3×10^{-14}	2.3×10^{-14}
T_{re}^{min} (GeV)	10^{-2}	10^{-2}	10^{-2}	10^{-2}	10^{-2}
T_{re}^{max} (GeV)	2.3×10^7	5.8×10^6	4.9×10^6	1.4×10^6	2×10^6
ω_{eff}^{min}	0.3281	0.2762	0.3297	0.2904	0.3218
ω_{eff}^{max}	0.3309	0.3042	0.3315	0.3120	0.3274

3.3.5 Constraining magnetogenesis model: maximum possible value of n and corresponding reheating temperature T_{re}

The scaling properties of the large-scale magnetic field as a function of momentum are not particularly well understood from the observation point of view. Throughout this chapter, though, we have emphasized two special cases of interest related to scale-invariant electric field ($n = 2$) and scale-invariant magnetic field ($n = 3$). Any other value of n, which is not special, could have observational relevance in the near future. Keeping this motivation in mind, in this section, we study the possible range of n values, which can give rise to the observable strength of the magnetic field. As has already been described before, the direct constraint on the value of n will come from the strong coupling and the backreaction problem leading to the fact that n should lie within $0 \leq n \leq n_{max}$, where n_{max} can be determined from Eqns. (3.43) and (3.44). Our primary goal in this section is to pinpoint the value of n_{max} for different models under consideration. From Fig.(3.4), we can clearly see that the permissible range of n_{max} for various inflationary models should lie approximately within $(2.15 - 2.3)$. As has been observed before, conventional magnetogenesis scenarios are generically viable for low-scale inflationary models or, in other words, low reheating temperature regimes. This turned to be untrue for higher $n \sim n_{max}$. In order to calculate reheating temperature associated with the maximum possible value of the n, we consider two sample value of the spectral index $n_s = (n_s^{central} = 0.9649, n_s^{max})$. Irrespective of the inflationary models under consideration, reheating temperature can be observed as high as $\sim 10^7$ GeV without any backreaction problem. In Table (5.2), we have provided the limiting values of the $(\omega_{eff}, T_{re}, \mathcal{P}_{B_0}^{1/2})$ for two different values of the scalar spectral index n_s.

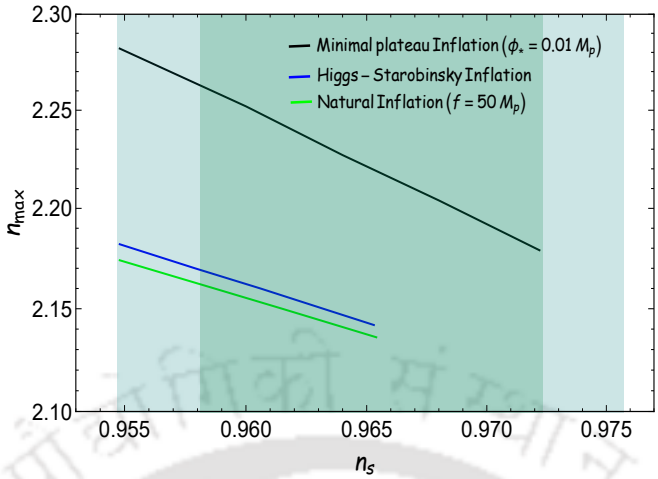

FIGURE 3.4: We plot the variation of maximum value of n (n_{max}) as a function of spectral index within 2σ range, n_s from Planck [29] for different inflationary model. In this plot the maximum values of the spectral index correspond to the instantaneous reheating condition $N_{re} \to 0$.

3.4 Summary and discussion:

Among all the well-known magnetogenesis scenarios, inflationary magnetogenesis is a well-motivated and simple mechanism to explain the large-scale magnetic field of our universe. In this chapter, we specifically focus on the effect of reheating phase on the evolution of the inflationary magnetic field. In this regard, Faraday's effect of magnetic induction plays an important role. The primary assumption behind this mechanism to act during reheating is the negligible electrical conductivity. As a result, the strong electric field can survive during this phase and is dynamically converted into a magnetic field. Hence the resulting primordial magnetic field energy density does not evolve as radiation energy density ($1/a^4$) during this phase; instead, it evolves as $\propto 1/H^2a^6$ till the end of the reheating phase. After the end of the reheating electric field dies out fast due to the large electric conductivity and comoving magnetic energy density freezes out until today. Considering this physical effect, the present-day amplitude of the magnetic field originated during inflation becomes observationally viable with a specific set of reheating parameters. Our motivation for this work is to figure out these constraints on the reheating parameters, which directly shape the inflation and magnetogenesis models.

We have derived explicit connection among the inflationary (n_s), reheating (ω_{eff}, T_{re}), and magnetogenesis (n) model parameters assuming two different reheating scenarios. The large-scale magnetic field gives stringent constraints on both the reheating parameters depending upon the models under consideration. Considering both backreaction and strong coupling problems into account, the maximum allowed value of n would be $n_{max} \sim 2.3$ for all the models, such as natural inflation, Higgs-Starobinsky, and the minimal plateau model. The associated maximum allowed value of n, the reheating temperature has been shown to lie within a wide range of $(10^{-2}, 10^{7})$ GeV.

We also have some definite predictions once we fix the model and the large-scale magnetic field. For reheating scenario with a constant equation of state ω_{eff}, once we fixed the scalar

spectral index, a unique value of ω_{eff} is predicted to be associated with the specific choice of the present-day magnetic field. This unique ω_{eff}, further predicts a specific value of reheating temperature T_{re}. The quantitative values of those parameters for $n = 2$ magnetogenesis model are provided in the Tables (3.1), (3.3) and (3.6). As reheating and inflationary parameters are connected, the present-day strength of the magnetic field also provides possible limits on the inflationary scalar spectral index. This extra bound from inflationary magnetogenesis essentially narrows down the possible value of n_s within the 1σ range of $n_s = 0.9649 \pm 0.0042$ (68% CL, Planck TT,TE,EE+lowE+lensing) from Planck [29] (shown in Tables (3.2), (3.4), and (3.7) for different inflationary models). Model-independent constraint on the effective equation of state is obtained as $(0.15 < \omega_{eff} < \frac{1}{3})$. One of the main drawbacks of describing the reheating dynamics by a constant ω_{eff} is that it does not enable us to decode the nature of the inflation potential near its minimum. This drawback motivated us to consider the reheating in the perturbative framework where inflation equation of state is described by $\omega_\phi \equiv (p-2)/(p+2)$ with inflaton potential $V(\phi) \sim \phi^p$ near its minimum.

For the perturbative reheating scenario, the inflation equation of state $\omega_\phi \gtrsim 0.28$ is found to be observationally viable for $\mathcal{P}_{B0}^{1/2} \gtrsim 10^{-18}$ G. Increasing the lower limit of the observable magnetic field will further increase the lower limit of ω_ϕ. We think it is extremely interesting in the context of inflation model building. This observation provides a strong constraint on the possible form of the inflaton potential near its minimum with $p \gtrsim 3.6$ considering the aforesaid observable limit of the present-day magnetic field strength. Furthermore, if one considers the higher equation of state, the high-scale inflation model with reheating temperature as high as 10^7 GeV is possible. The main outcomes of the perturbative analysis for the different inflationary models are shown in Table-(3.5) and (3.8). In this chapter, we develop the methodology to probe the reheating phase, combining both the present value of the large-scale magnetic field and CMB anisotropy. For that, we considered the simplest magnetogenesis scenario, the so-called Ratra's model. Different magnetogenesis models can be studied straightforwardly following the formalism developed in this chapter to probe reheating phase. This has already been applied in the recent papers [196, 197]. The only differences that may arise are in the allowed reheating and inflationary parameters space. However, to distinguish those models, we need more physical observables such as primordial gravitational wave [198], dark matter, etc. Our eventual plan in the future is to obtain some universal constraints on the reheating and inflationary parameters taking into account various cosmological observables just mentioned.

Decoding the phases of early and late time reheating through imprints on primordial gravitational waves spectrum 4

"When gravitational waves reach the earth, the waves stretch and squeeze space. This is a tiny stretch and squeeze. Far too small to detect with ordinary human senses."

Kip Thorne

Attempts to understand the reheating phase in the literature can be broadly classified into two categories: (i) Studying the background dynamics during reheating which reveals the connection among the inflationary scalar spectral index n_s, reheating temperature, and the reheating equation of state [45, 47, 90, 91]. (ii) Looking for the direct observable imprints of reheating on various cosmological observable with regard to the primordial magnetic field, gravitational waves, dark matter, etc. The last two chapters were devoted to understanding the dynamics of reheating and constraints, taking into account CMB anisotropy, dark matter abundance, and the strength of large-scale magnetic fields in the present universe. In this chapter, we study the evolution of inflationary stochastic gravitational waves, which can potentially encode the dynamical information of reheating in a certain frequency range associated with the reheating phase. In this chapter, our eventual plan would be to decode the phases of early and late time reheating through imprints on primordial gravitational waves.

The inflationary scenario offers the most attractive mechanism for the generation of the primordial perturbations (for the original discussions, see Refs. [199–202]; for reviews, see, for example, Refs. [14, 16, 17, 21–27]). The existence of primordial gravitational waves (GWs) is one of the profound predictions of inflationary dynamics (for the initial discussions, see, for example, Refs. [203, 204]; for recent reviews on the generation of primary and secondary GWs, see, for instance, Refs. [205, 206]). If the primordial GWs or their imprints are detected, it will not only prove the quantum origin of the perturbations, it can also, in principle, provide us with insights into the fundamental nature of gravitation. The primordial GWs provide a unique window to probe the dynamics of our universe during its very early stages, which seems difficult to observe by any other known means. However, the extremely weak nature of the gravitational force makes the detection of GWs rather challenging. Decades of effort towards detecting GWs

have finally achieved success only in the last few years with the observations of GWs from merging binary black holes and neutron stars by LIGO [207–218]. These observations have led to a surge of experimental proposals across the globe to observe GWs over a wide range of frequencies. The proposed GW observatories include advanced LIGO (10–10^3 Hz) [219], ET (1–10^4 Hz) [220, 221], BBO (10^{-3}–10 Hz) [222–224], DECIGO (10^{-3}–1 Hz) [225–228], eLISA (10^{-5}–1 Hz) [229–231], and SKA (10^{-9}–10^{-6} Hz) [232].

Apart from various astrophysical mechanisms that can generate GWs, as we mentioned, inflation provides an exclusive mechanism to produce GWs of quantum mechanical origin (for discussions on the generation of primary and secondary GWs, see, for instance, Refs. [233–246] and references therein). The tensor perturbations generated from the quantum vacuum are amplified during inflation, which subsequently evolves through the various phases of the universe until they reach the GW detectors today. Therefore, the spectrum of primordial GWs today is a convolution of their origin as well as dynamics. On the one hand, they contain the signatures of the mechanism that generates them, viz. the specific model that drives inflation as well as the initial conditions from which the perturbations emerge. On the other, they also carry the imprints of the dynamics of the subsequent cosmological phases as the GWs propagate through them. As is well known, immediately after inflation, the universe is expected to be reheated through the decay of the inflaton into radiation, which eventually leads to the epoch of radiation domination. In this chapter, we shall examine the evolution of primordial GWs with special emphasis on the effects due to the epoch of reheating. Specifically, our aim is to decode the mechanism of reheating from the the spectrum of GWs today.

Over the years, major cosmological observations have considerably improved the theoretical understanding of the various epochs of our universe [29, 247, 248]. However, due to the lack of direct observational signatures, the phase of reheating remains poorly understood. The effects of reheating on the dynamics of GWs have already been examined in the standard cosmological scenario (see, for instance, Refs. [28, 249–255]) as well as in certain non-standard scenarios (see, for example, Refs. [86, 88, 256–264]). Moreover, the imprints of specific microscopic physical effects on the spectrum of GWs — such as decoupling neutrinos [265, 266] or the variation in the number of relativistic degrees of freedom in the early universe [267–269] — have also been explored. In this chapter, we shall study the effects of reheating on the spectrum of primordial GWs over a wide range of scales and illustrate the manner in which the spectrum captures specific aspects of the different phases. We shall consider two of the simplest reheating mechanisms. We shall first consider a scenario wherein the reheating phase is described by an averaged equation of state (EoS) parameter, with reheating ending instantaneously [45, 47, 90]. We shall then consider a scenario wherein there is a gradual change in the EoS parameter from its initial value during the phase of coherent oscillations to its eventual value during radiation domination achieved through the perturbative decay of the inflaton [4, 91, 93, 270, 271]. We shall explicitly illustrate the effects of the reheating dynamics on the spectrum of GWs. It seems worthwhile to highlight here that the following aspects of the reheating dynamics can, in principle, be decoded from the spectrum of primordial GWs: (i) the shape of the inflaton potential near its minimum which is responsible for the end of inflation and the dynamics during reheating, (ii) the decay width of the inflaton, which governs the entire process of reheating and therefore determines the reheating temperature, and (iii) the thermalization time scale over which the EoS parameter during the period of coherent oscillations of the inflaton say, w_ϕ, is modified to the EoS parameter corresponding to radiation. Further, it is expected that determining the inflaton decay width and the thermalization time scale would permit us not only to arrive at the form of the coupling between the inflaton and radiation, but also help

us understand the nature of the coupling amongst all the relativistic degrees of freedom. We shall briefly discuss these possibilities in this chapter, and we shall return to examine the issue in greater detail in a future effort.

Finally, we shall also consider the implications of our analysis on the recent observations involving the pulsar-timing data by the North American Nanohertz Observatory for Gravitational Waves (NANOGrav), which has been attributed to stochastic GWs [272, 273]. A variety of mechanisms can possibly occur in the early universe have been explored in the literature to explain this interesting observation [246, 246, 274–287]. We find that introducing a secondary phase of reheating — apart from the original, inflaton driven, primary reheating phase — can account for the NANOGrav observations. We introduce an exotic, non-canonical scalar field to drive such a phase and show that a suitable EoS for the non-canonical field can lead to primordial GWs of strength as observed by NANOGrav.

This chapter is structured as follows. In sec. 4.1, we shall briefly sketch the arguments leading to the standard scale-invariant spectrum of GWs generated in de Sitter inflation. We shall also discuss the typical inflationary model that we shall have in mind when we later discuss the effects due to reheating. Moreover, we shall introduce the dimensionless density parameter Ω_{GW} characterizing the spectrum of GWs. In sec. 4.2, we shall discuss the evolution of the tensor perturbations during the epoch of reheating. We shall first consider the scenario wherein the epoch of reheating is described by an averaged EoS parameter associated with the inflaton. Such a description allows us to arrive at analytic solutions for the tensor perturbations during the epoch. We shall also consider the scenario of perturbative reheating wherein we take into account the continuous decay of the inflaton into radiation. As it proves to be involved in constructing analytical solutions for the background as well as the tensor perturbations in such a case, we shall resort to numerics. In sec. 4.3, we shall briefly discuss the evolution of the tensor perturbations during the epoch of radiation domination and arrive at the spectrum of GWs today by comparing the behavior of the the energy density of GWs in the sub-Hubble domain with that of radiation. In secs. 4.4 and 4.5, we shall evaluate the the dimensionless energy density of GWs today that arise in the two types of reheating scenarios mentioned above. We shall focus on the spectrum of primordial GWs over wave numbers (or, equivalently, frequencies) that correspond to small scales which reenter the Hubble radius either during the epochs of reheating or radiation domination. In sec. 4.6, we shall numerically evaluate the inflationary tensor power spectrum and discuss the behavior of the the spectrum of GWs today close to the scale that leaves the Hubble radius at the end of inflation. In sec. 4.7, we shall outline the manner in which we should be able to decode various information concerning the epochs of inflation and reheating from the observations of the anisotropies in the cosmic microwave background (CMB) and the spectrum of GWs today. In sec. 4.8, we shall evaluate the spectrum of GWs in a scenario involving late time production of entropy and discuss the implications for the recent observations by NANOGrav. Lastly, in sec. 4.9, we shall conclude with a summary of the main results.

Before we proceed further, a few clarifications concerning the conventions and notations that we shall adopt are in order. We shall work with natural units such that $\hbar = c = 1$, and set the reduced Planck mass to be $M_p = (8\,\pi\,G)^{-1/2}$. We shall adopt the signature of the metric to be $(-,+,+,+)$. Note that Latin indices shall represent the spatial coordinates, except for k, which shall be reserved for denoting the wavenumber of the tensor perturbations, i.e. GWs. We shall assume the background to be the spatially flat Friedmann-Lemaître-Robertson-Walker (FLRW) line element described by the scale factor a and the Hubble parameter H. Also, an overprime shall denote differentiation with respect to the conformal time η. We should mention

that the frequency, say, f, is related to the wave number k of the tensor perturbations through the relation

$$f = \frac{k}{2\,\pi} = 1.55 \times 10^{-15} \left(\frac{k}{1\,\mathrm{M_{pc}}^{-1}}\right) \mathrm{Hz} \tag{4.1}$$

and, as convenient, we shall refer to the spectrum of GWs either in terms of wave numbers or frequencies.

4.1 Spectrum and energy density of GWs generated during inflation

In this section, we shall briefly recall the main equations governing the tensor perturbations (see detailed discussions in the introduction sec-1.3). The tensor power spectrum is expressed as

$$\mathcal{P}_{_{\mathrm{T}}}(k) = \frac{2\,H_I^2}{\pi^2\,M_p^2}\left(1 + \frac{k^2}{k_f^2}\right), \tag{4.2}$$

where $k_f = a_f\,H_I$ is the mode that leaves the Hubble radius at the end of inflation. For $k \ll k_f$, the above spectrum reduces to

$$\mathcal{P}_{_{\mathrm{T}}}(k) \simeq \frac{2\,H_I^2}{\pi^2\,M_p^2}\,, \tag{4.3}$$

which is the well-known scale-invariant spectrum often discussed in the context of de Sitter inflation [14, 16, 17, 21–27]. Actually, in slow roll inflation, the tensor power spectrum will contain a small spectral tilt, which we shall choose to ignore in our discussion. We should emphasize the point that the above scale invariant spectrum is valid only for $k \ll k_f$ since the de Sitter form for the scale factor would not hold true close to the end of inflation. Therefore, in our discussion below, we shall mostly restrict ourselves to wave numbers such that $k < 10^{-2}\,k_f$. In sec. 4.6, we shall evaluate tensor power spectrum numerically in the inflationary model of interest to arrive at the present day spectrum of GWs near k_f.

In order to illustrate the results later, we shall focus on a specific inflationary model that permits slow roll inflation. We shall consider the so-called α-attractor mode. For details of this model see sec.(1.4). We should mention that, hereafter, we shall set the potential parameter α to be unity. The dimensionless energy density of the gravitational waves $\Omega_{GW}(k,\eta)$ is calculated as

$$\Omega_{GW}(k,\eta) = \frac{\rho_{GW}(k,\eta)}{\rho_{\mathrm{c}}(\eta)} = \frac{\rho_{GW}(k,\eta)}{3\,H^2\,M_p^2}, \tag{4.4}$$

where $\rho_{\mathrm{c}} = 3\,H^2\,M_p^2$ is the critical density at time η.

The observable quantity of interest is the dimensionless energy density $\Omega_{GW}(k,\eta)$ evaluated *today*, which we shall denote as $\Omega_{GW}(k)$. We shall often refer to $\Omega_{GW}(k)$ or, equivalently, $\Omega_{GW}(f)$ [recall that f is the frequency associated with the wave number k, cf. Eq. (4.1)], as the spectrum of GWs today. In the following sections, we shall evolve the tensor perturbations through the epochs of reheating and radiation domination. As we shall see, at late times during radiation domination, once all the wave numbers of interest are well inside the Hubble radius, the energy density of GWs behaves in a manner similar to that of the the energy density of radiation. We shall utilize this behavior to arrive at the spectrum of GWs today.

4.2 Evolution of GWs during reheating

In order to follow the evolution of the tensor perturbations post inflation, it proves to be convenient to write (in this context, see, for instance, Ref. [28])

$$h_k(\eta) = h_k^{\rm P}\, \chi_k(\eta), \tag{4.5}$$

where $h_k^{\rm P}$ denotes the primordial value evaluated at the end of inflation, and is given by [cf. Eq. (1.109)]

$$h_k^{\rm P} = h_k(a_f) = \frac{\sqrt{2}}{M_p}\, \frac{i\, H_I}{\sqrt{2\, k^3}} \left(1 - \frac{i\, k}{k_f}\right) {\rm e}^{-i\, k/H_I}\, {\rm e}^{i\, k/k_f}. \tag{4.6}$$

The quantity χ_k is often referred to as the tensor transfer function, which obeys the same equation of motion as h_k, viz. Eq. (1.104).Clearly, the strength of the primordial GWs observed today will not only depend on the amplitude of the tensor perturbations generated during inflation, but also on their evolution during the subsequent epochs. In this section, we shall discuss the evolution of the transfer function χ_k during the epoch of reheating. As we mentioned earlier, we shall consider two types of scenarios for reheating. We shall first consider the case wherein the period of reheating is described by the constant EoS parameter, say, w_ϕ, often associated with the coherent oscillations of the scalar field around the minimum of the inflationary potential. We shall assume that the transition to radiation domination occurs instantaneously after a certain duration of time. In such a case, as we shall see, the transfer function χ_k can arrive at analytically. We shall then consider the scenario of perturbative reheating wherein there is a gradual transfer of energy from the inflaton to radiation. It seems difficult to treat such a situation analytically and, hence, we shall examine the problem numerically. To follow the evolution of GWs in the post-inflationary regime, we shall choose to work with rescaled scale factor as the independent variable rather than the conformal time coordinate. If we define $A = a/a_f$, where $a_f = a(\eta_f)$ is the scale factor at the end of inflation, then we find that the equation governing the transfer function χ_k is given by

$$\frac{d^2\chi_k}{dA^2} + \left(\frac{4}{A} + \frac{1}{H}\,\frac{dH}{dA}\right) \frac{d\chi_k}{dA} + \frac{(k/k_f)^2}{(H/H_I)^2\, A^4}\, \chi_k = 0, \tag{4.7}$$

where, recall that, $k_f = a_f\, H_I$ denotes the wave number that leaves the Hubble radius at the end of inflation. Our aim now is to solve the above equation for the transfer function during the epoch of reheating. As is evident from the equation, the evolution of GWs is dictated by the behavior of the Hubble parameter. Therefore, if we can first determine the behavior of the Hubble parameter during reheating, we can solve the above equation to understand the evolution of transfer function χ_k during the epoch. We shall also require the initial conditions for the transfer function χ_k and its derivative $d\chi_k/dA$ at the end of inflation, i.e. when $a = a_f$ or, equivalently, when $A = 1$. Since we have introduced the transfer function through the relation (4.5), clearly,

$$\chi_k^{\rm I}(A = 1) = 1. \tag{4.8}$$

Also, on using the solution (1.109) and the expression (4.6) for $h_k^{\rm P}$, we find that

$$\frac{d\chi_k^{\rm I}(A = 1)}{dA} = -\frac{(k/k_f)^2}{1 - i\,(k/k_f)} \simeq 0, \tag{4.9}$$

where the final equality is applicable when $k \ll k_f$. We shall make use of these initial conditions to determine the transfer function during the epoch of reheating. In the following two subsections, we shall discuss the solutions in the two scenarios involving the instantaneous and gradual transfer of energy from the inflaton to radiation.

4.2.1 Reheating described by an averaged EoS parameter

Let us first consider the scenario wherein the epoch of reheating is dominated by the dynamics of the scalar field as it oscillates at the bottom of an inflationary potential, such as the α-attractor model (1.130) we had introduced earlier. In such a case, the evolution of the scalar field can be described by an averaged EoS parameter, say, w_ϕ [45, 47, 90]. The conservation of energy implies that the energy density of the inflaton behaves as $\rho_\phi \propto a^{-3\,(1+w_\phi)}$, which, in turn, implies that the Hubble parameter behaves as $H^2 = H_I^2\, A^{-3\,(1+w_\phi)}$. Note that, $H = H_I$ when $A = 1$, as required. As a result, during such a phase, equation (4.7) governing the tensor transfer function reduces to the form

$$\frac{d^2\chi_k}{dA^2} + (5 - 3\,w_\phi)\,\frac{1}{2\,A}\,\frac{d\chi_k}{dA} + \frac{(k/k_f)^2}{A^{1-3\,w_\phi}}\,\chi_k = 0. \tag{4.10}$$

The general solution to this differential equation can be expressed as

$$\chi_k^{\rm RH}(A) = A^{-\nu}\,\left[C_k\,J_{-\nu/\gamma}\left(\frac{k}{\gamma\,k_f}\,A^\gamma\right) + D_k\,J_{\nu/\gamma}\left(\frac{k}{\gamma\,k_f}\,A^\gamma\right)\right], \tag{4.11}$$

where $J_\alpha(z)$ denote Bessel functions of order α, while the quantities ν and γ are given by

$$\nu = \frac{3}{4}\,(1 - w_\phi), \quad \gamma = \frac{1}{2}\,(1 + 3\,w_\phi)\,. \tag{4.12}$$

The coefficients C_k and D_k can be arrived at by using the conditions (4.8) and (4.9) for the transfer function χ_k and its derivative $d\chi_k/dA$ at end of inflation, i.e. when $A = 1$. We find that the coefficients C_k and D_k can be expressed as follows:

$$C_k = \frac{\pi\,k}{2\,\gamma\,k_f}\,\left[\frac{1}{1 - i\,(k/k_f)}\right]\,\left[\frac{k}{k_f}\,J_{\nu/\gamma}\left(\frac{k}{\gamma\,k_f}\right) - \left(1 - \frac{i\,k}{k_f}\right)\,J_{(\nu/\gamma)+1}\left(\frac{k}{\gamma\,k_f}\right)\right]\,\csc\left(\frac{\pi\,\nu}{\gamma}\right), \tag{4.13}$$

$$D_k = -\frac{\pi\,k}{2\,\gamma\,k_f}\,\left[\frac{1}{1 - i\,(k/k_f)}\right]\,\left[\frac{k}{k_f}\,J_{-\nu/\gamma}\left(\frac{k}{\gamma\,k_f}\right) + \left(1 - \frac{i\,k}{k_f}\right)\,J_{-(\nu/\gamma)-1}\left(\frac{k}{\gamma\,k_f}\right)\right]\,\csc\left(\frac{\pi\,\nu}{\gamma}\right). \tag{4.14}$$

We shall later make use of these coefficients and the solution (4.11) to eventually arrive at the spectrum of GWs today. It is useful to note here that the quantity $d\chi_k^{\rm RH}/dA$ is given by

$$\frac{d\chi_k^{\rm RH}}{dA} = \frac{k}{k_f}\,A^{-1+\gamma-\nu}\,\left[C_k\,J_{-(\nu/\gamma)-1}\left(\frac{k}{\gamma\,k_f}\,A^\gamma\right) - D_k\,J_{(\nu/\gamma)+1}\left(\frac{k}{\gamma\,k_f}\,A^\gamma\right)\right]. \tag{4.15}$$

We should mention here that the duration of the reheating phase is characterized by the number of e-folds N_{re} and the reheating temperature T_{re} can be expressed in terms of the equation of state parameter w_ϕ and the inflationary parameters as follows (in this context, see, for example, Refs. [45, 47]):

$$N_{re} = \frac{4}{(3\,w_\phi - 1)}\,\left[N_* + \frac{1}{4}\,ln\left(\frac{30}{\pi^2\,g_{\rm r,re}}\right) + \frac{1}{3}ln\left(\frac{11\,g_{s,\rm re}}{43}\right) + ln\left(\frac{k_*}{a_0\,T_0}\right) + ln\left(\frac{\rho_{\rm f}^{1/4}}{H_I}\right)\right], \tag{4.16}$$

$$T_{re} = \left(\frac{43}{11\, g_{s,\mathrm{re}}}\right)^{1/3} \left(\frac{a_0\, H_I}{k_*}\right) \mathrm{e}^{-(N_* + N_{re})}\, T_0, \tag{4.17}$$

where $T_0 = 2.725\,\mathrm{K}$ is the present temperature of the CMB and H_0 denotes the current value of the Hubble parameter. Moreover, note that k_*/a_0 represents the CMB pivot scale, with a_0 denoting the scale factor today. We shall assume that $k_*/a_0 \simeq 0.05\,\mathrm{Mpc}^{-1}$. We should also point out that N_* denotes the number of e-folds prior to the end of inflation when the pivot scale k_* leaves the Hubble radius.

4.2.2 The case of perturbative reheating

In such a case, after inflation, the inflaton energy density, say, ρ_ϕ, gradually decays into the radiation energy density, say, ρ_R, with a constant decay width Γ_ϕ. As a result, the effective EoS parameter during the reheating phase becomes time-dependent. For a wide class of inflationary potentials that behave as $V(\phi) \propto \phi^{2\,n}$ near the minimum, the time-averaged EoS parameter of the inflaton can be expressed as $w_\phi = (n-1)/(n+1)$ [99]. We should emphasize that this scenario is different from the one considered in the previous section wherein the explicit decay of the inflaton field was not taken into account. Specifically, in the earlier case, the energy density of the inflaton was supposed to be converted instantaneously into the energy density of radiation at a given time, leading to the end of the phase of reheating. In due course, we shall demonstrate the manner in which the detailed mechanism of reheating leaves specific imprints on the spectrum of primordial GWs observed today.

The evolution of the energy densities ρ_ϕ and ρ_R can be followed by the coupled Boltzmann Eqns. (2.21) and (2.22). For further details of this perturbative reheating model, like the initial conditions, methodology of numerical analysis, how reheating ends, etc., see section (2.1.2.1).

With the solutions to the coupled background equations (2.21) and (2.22) at hand, we shall proceed to solve the differential equation (4.7) for the transfer function χ_k during reheating. To illustrate the nature of the solutions, we have plotted the behavior of the Hubble parameter H and the transfer function χ_k in Fig. 4.1 during the period of perturbative reheating. We have chosen specific values for the EoS parameter w_ϕ, the reheating temperature T_{re}, and wave number k in plotting the figures. We have considered a wave number so that the mode reenters the Hubble radius during the period of reheating. As one would have expected, while the amplitude of the transfer function is a constant on super-Hubble scales, it decreases as the mode reenters the Hubble radius and begins to oscillate once inside.

4.3 Evolution during radiation domination and the spectrum of GWs today

The Hubble parameter during the radiation dominated epoch evolves as

$$H^2 = H_{re}^2\, \frac{A_{\mathrm{re}}^4}{A^4} \tag{4.18}$$

with H_{re} and A_{re} denoting the Hubble parameter and the rescaled scale factor at the end of reheating, respectively. During radiation domination, the transfer function is governed by the equation

$$\frac{d^2\chi_k}{dA^2} + \frac{2}{A}\,\frac{d\chi_k}{dA} + \frac{(k/k_{re})^2}{A_{re}^2}\,\chi_k = 0, \tag{4.19}$$

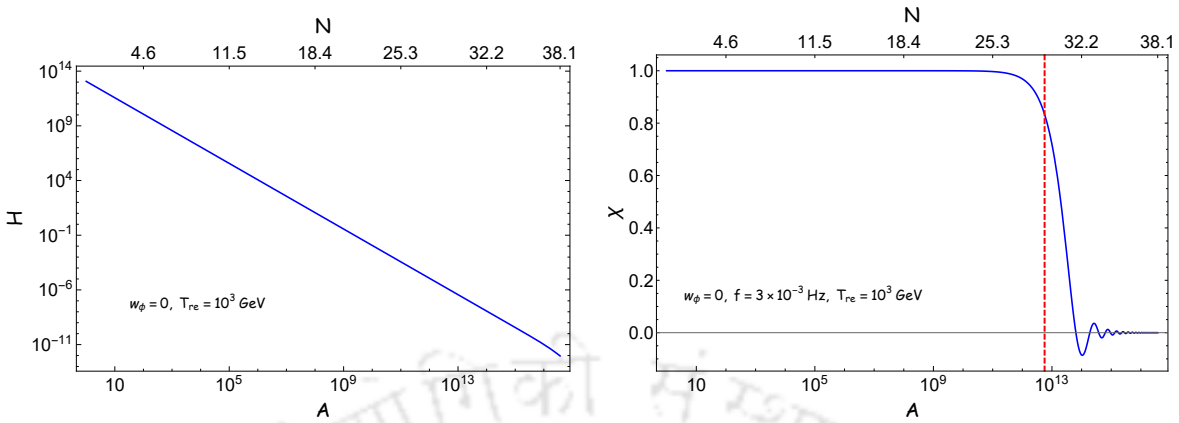

FIGURE 4.1: The evolution of the Hubble parameter H (in blue, on the left) and the amplitude of the tensor transfer function χ_k for a given wave number (in blue, on the right), obtained numerically in the case of the perturbative reheating scenarios, have been plotted as a function of $A = a/a_f$ over the domain $1 \leq A \leq A_{re}$, which corresponds to the period of reheating. We have also indicated the lapse in time in terms of e-folds (counted from the end of inflation) on the top of the two figures. We have assumed that $w_\phi = 0$ and have set $T_{re} = 10^3\,\mathrm{GeV}$ in plotting the quantities. We have chosen the wave number to be $k \simeq 2 \times 10^{12}\,\mathrm{Mpc}^{-1}$, which corresponds to the frequency of $f \simeq 3 \times 10^{-3}\,\mathrm{Hz}$ [cf. Eq. (4.1)]. The wave number has been chosen so that it renters the Hubble radius during the epoch of reheating. The slope of the straight line describing $H(A)$ (on the left) is $-3/2$, which is consistent with $w_\phi = 0$. We find that the slope changes as A approaches A_{re} indicating the beginning of the transition to the radiation dominated epoch. The vertical line (in red, on the right) indicates the time when the mode reenters the Hubble radius. As expected, the transfer function proves to be constant on super-Hubble scales and it oscillates once the mode is inside the Hubble radius.

where $k_{re} = a_{\rm re}\, H_{re}$ is the mode which reenters the Hubble radius at the end of the reheating era. The above differential equation can be immediately solved to arrive at the following general solution:

$$\chi_k^{\rm RD}(A) = \frac{1}{A}\left\{E_k\, \mathrm{e}^{-i\,(k/k_{re})\,[(A/A_{re})-1]} + F_k\, \mathrm{e}^{i\,(k/k_{re})\,[(A/A_{re})-1]}\right\}. \tag{4.20}$$

The coefficients E_k and F_k need to be determined by matching this solution and its derivative with the solution (4.11) during the epoch of reheating and its derivative at $A = A_{re}$. Upon carrying out the matching at the junction between the eras of reheating and the radiation domination, we find that the coefficients E_k and F_k can be expressed as

$$E_k = \frac{A_{re}}{2}\left[\left(1 + \frac{i\,k_{re}}{k}\right)\chi_k^{\rm RH}(A_{re}) + \frac{i\,k_{re}}{k}\,A_{re}\,\frac{d\chi_k^{\rm RH}(A_{re})}{dA}\right] = i\,\frac{A_{re}}{2}\,\frac{k_{re}}{k}\,\mathcal{E}_k, \tag{4.21a}$$

$$F_k = \frac{A_{re}}{2}\left[\left(1 - \frac{i\,k_{re}}{k}\right)\chi_k^{\rm RH}(A_{re}) - \frac{i\,k_{re}}{k}\,A_{re}\,\frac{d\chi_k^{\rm RH}(A_{re})}{dA}\right] = -i\,\frac{A_{re}}{2}\,\frac{k_{re}}{k}\,\mathcal{F}_k, \tag{4.21b}$$

where we have also introduced the quantities $\mathcal{E}_k$ and $\mathcal{F}_k$ which we shall make use of later. At this stage, we should mention that the quantities $\chi_k^{\rm RH}(A_{re})$ and $d\chi_k^{\rm RH}(A_{re})/dA$ and hence the coefficients E_k and F_k will depend on the details of the reheating mechanism. In particular, they will be different for two the types of reheating mechanisms under consideration.

Since we have set $h_k = h_k^{\rm P}\,\chi_k$, where $h_k^{\rm P}$ denotes the primordial amplitude of the tensor perturbations [cf. Eq. (1.116)], the energy density of GWs $\rho_{GW}(k,\eta)$ is given by [cf. Eq. (4.5)]

$$\rho_{GW}(k,\eta) = \frac{M_p^2}{a^2}\,\frac{k^3}{2\,\pi^2}\,|h_k^{\rm P}|^2\,\left(\frac{1}{2}\,|\chi_k^{\rm RD\,\prime}(\eta)|^2 + \frac{k^2}{2}\,|\chi_k^{\rm RD}(\eta)|^2\right). \tag{4.22}$$

On using the definition (1.106) of the inflationary tensor power spectrum $\mathcal{P}_{\rm T}(k)$, this energy density of GWs can be expressed as

$$\rho_{GW}(k,\eta) = \frac{M_p^2}{4\,a^2}\,\mathcal{P}_{\rm T}(k)\,\left(\frac{1}{2}\,|\chi_k^{\rm RD\,\prime}(\eta)|^2 + \frac{k^2}{2}\,|\chi_k^{\rm RD}(\eta)|^2\right). \tag{4.23}$$

Upon substituting the solution (4.20) in the above expression, we obtain $\rho_{GW}(k,\eta)$ to be

$$\begin{aligned}\rho_{GW}(k,\eta) \;=\; & \frac{M_p^2\,k^2}{8\,a_f^2\,A^4}\,\mathcal{P}_{\rm T}(k)\,\left\{\left(|E_k|^2 + |F_k|^2\right)\,\left[2 + \left(\frac{k_{re}\,A_{re}}{k\,A}\right)^2\right]\right. \\ & + E_k\,F_k^*\,\left(\frac{k_{re}\,A_{re}}{k\,A}\right)^2\,\left(1 + \frac{2\,i\,k\,A}{k_{re}\,A_{re}}\right)\,{\rm e}^{-2\,i\,(k/k_{re})\,[(A/A_{re})-1]} \\ & \left. + E_k^*\,F_k\,\left(\frac{k_{re}\,A_{re}}{k\,A}\right)^2\,\left(1 - \frac{2\,i\,k\,A}{k_{re}\,A_{re}}\right)\,{\rm e}^{2\,i\,(k/k_{re})\,[(A/A_{re})-1]}\right\}. \end{aligned} \tag{4.24}$$

We had mentioned earlier that we shall be interested in the range of wave numbers which reenter the Hubble radius during the epochs of reheating and radiation domination. At late times during radiation domination such that $A/A_{re} \gg 1$, all the modes of our interest would be well inside the Hubble radius, i.e. $k\,A \gg 1$. In such a case, we find that, the above expression for $\rho_{GW}(k,\eta)$ simplifies to be

$$\rho_{GW}(k,\eta) = \frac{M_p^2\,k^2}{4\,a_f^2\,A^4}\,\mathcal{P}_{\rm T}(k)\,\left(|E_k|^2 + |F_k|^2\right). \tag{4.25}$$

Hence, the corresponding dimensionless parameter describing the energy density of GWs, viz. $\Omega_{GW}(k,\eta)$, is given by

$$\Omega_{GW}(k,\eta) = \frac{k^2}{12\,a_f^2\,H^2\,A^4}\,\mathcal{P}_{\rm T}(k)\,\left(|E_k|^2 + |F_k|^2\right) = \frac{k_{re}^2\,A_{re}^2}{48\,a_f^2\,H^2\,A^4}\,\mathcal{P}_{\rm T}(k)\,\left(|\mathcal{E}_k|^2 + |\mathcal{F}_k|^2\right), \tag{4.26}$$

where we have made use of the expressions (4.21) relating the coefficients E_k and F_k to the quantities $\mathcal{E}_k$ and $\mathcal{F}_k$. During radiation domination, $H^2\,A^4 = H_{re}^2\,A_{re}^4$. Also, recall that, $k_{re} = a_{re}\,H_{re}$. On using these relations, at late times during radiation domination, we obtain that

$$\Omega_{GW}(k,\eta) = \frac{\mathcal{P}_{\rm T}(k)}{48}\,\left(|\mathcal{E}_k|^2 + |\mathcal{F}_k|^2\right). \tag{4.27}$$

The task that remains is to explicitly determine the quantities $\mathcal{E}_k$ and $\mathcal{F}_k$. In the special case of instantaneous reheating, $A_{re} = 1$ and $k_{re} = k_f$. Therefore, on using the conditions (4.8) and (4.9), one can readily show that

$$\mathcal{E}_k = \frac{1 - 2\,i\,(k/k_f) - 2\,(k^2/k_f^2)}{1 - i\,(k/k_f)}, \quad \mathcal{F}_k = \frac{1}{1 - i\,(k/k_f)}. \tag{4.28}$$

For $k \ll k_f$, we find that, $\mathcal{E}_k \simeq F_k \simeq 1$, which lead to

$$\Omega_{GW}(k,\eta) = \frac{\mathcal{P}_{_{\rm T}}(k)}{24} = \frac{H_I^2}{12\,\pi^2\,M_p^2}, \tag{4.29}$$

where, in arriving at the final expression, we have made use of the scale invariant inflationary tensor power spectrum (4.3). In other words, the dimensionless density parameter $\Omega_{GW}(k,\eta)$ is strictly scale invariant over all wave numbers in the instantaneous reheating scenario. Evidently, such a behavior can be expected to be hold true even when we have an epoch of reheating with $w_\phi = 1/3$, a result we shall encounter in due course.

Note that the energy density of GWs behaves as a^{-4} [cf. Eq. (4.25)], exactly as the energy density of radiation does. Such behavior should not come as a surprise and it arises due to the fact that the modes of interest are well inside the Hubble radius at late times (say, close to the epoch of radiation-matter equality) during radiation domination. On utilizing this property, the dimensionless energy density parameter $\Omega_{GW}(k)$ *today* can be expressed in terms of $\Omega_{GW}(k,\eta)$ as follows:

$$\Omega_{GW}(k)\,h^2 = \left(\frac{g_{r,\rm eq}}{g_{r,0}}\right)\left(\frac{g_{s,0}}{g_{s,\rm eq}}\right)^{4/3}\Omega_{_{\rm R}}\,h^2\,\Omega_{GW}(k,\eta) \simeq \left(\frac{g_{r,0}}{g_{r,\rm eq}}\right)^{1/3}\Omega_{_{\rm R}}\,h^2\,\Omega_{GW}(k,\eta), \tag{4.30}$$

where $\Omega_{_{\rm R}}$ denotes the present day dimensionless energy density of radiation. We should mention that, while $g_{r,\rm eq}$ and $g_{r,0}$ represent the number of relativistic degrees of freedom at equality and today, respectively, $g_{s,\rm eq}$ and $g_{s,0}$ represent the number of such degrees of freedom that contribute to the entropy at these epochs. Further, the Hubble parameter today, as usual, has been expressed as $H_0 = 100\,h\,{\rm km\,sec^{-1}\,Mpc^{-1}}$.

The spectrum of primordial GWs in the reheating scenario with an averaged EoS parameter can be expected to be different when compared to the one arising in the perturbative reheating scenario, In the following two sections, we shall derive the spectrum of primordial GWs at the present epoch in the two cases.

4.4 Spectrum of GWs in reheating described by an averaged EoS parameter

Before we go on to discuss the results, we should mention that the spectrum of GWs arising in the scenario wherein the epoch of reheating is described by an averaged EoS parameter and the transition to radiation domination is assumed to occur instantaneously at a given time has been evaluated earlier in the literature (see, for instance, Refs. [249, 251, 257]; for a recent discussion, see Ref. [88]). However, we find that, in the earlier investigations, the initial conditions that determine the dynamics during reheating have not always been chosen to be consistent with the dynamics during inflation. In this chapter, we shall consider a specific model of inflation and we shall show that model dependent initial conditions play a primary role in determining the range of frequencies which reenter the Hubble radius during reheating. Therefore, in this section, we shall reanalyze the effect of the averaged EoS parameter during reheating (with appropriate initial conditions) on the spectrum of GWs. We shall briefly discuss the derivation of the spectrum of GWs and arrive at the shape of the spectrum in the domains $k < k_{re}$ and $k > k_{re}$. In the next section, we shall compare the results with those that arise in the case of perturbative reheating.

It should be clear from the expression (4.27) that we shall require the quantities $\mathcal{E}_k$ and $\mathcal{F}_k$ to arrive at the spectrum of GWs. Using Eqs. (4.21), we can express $\mathcal{E}_k$ and $\mathcal{F}_k$ as

$$\mathcal{E}_k = \left(1 - \frac{i\,k}{k_{re}}\right) \chi_k^{\rm RH}(A_{re}) + A_{re}\,\frac{d\chi_k^{\rm RH}(A_{re})}{dA}, \tag{4.31a}$$

$$\mathcal{F}_k = \left(1 + \frac{i\,k}{k_{re}}\right) \chi_k^{\rm RH}(A_{re}) + A_{re}\,\frac{d\chi_k^{\rm RH}(A_{re})}{dA}. \tag{4.31b}$$

Also, recall that the transfer function at the end of the epoch of reheating $\chi_k^{\rm RH}(A_{re})$ is given by Eq. (4.11), with the coefficients C_k and D_k being described by Eqs. (4.13). During radiation domination, we have $H^2\,A^4 = H_{re}^2\,A_{re}^4$. Since $k_f = a_f\,H_I$ and $k_{re} = a_{re}\,H_{re}$, we find that we can write $A_{re} = (k_f/k_{re})^{1/\gamma}$. As a result, the Bessel functions in the expression (4.11) for $\chi_k^{\rm RH}(A_{re})$ depend on the ratio (k/k_{re}). Note that, in contrast, the coefficients C_k and D_k depend only on the ratio k/k_f. As we mentioned earlier, we have been interested in arriving at the spectrum over wave numbers such that $k < 10^{-2}\,k_f$. For small z, the Bessel function $J_\alpha(z)$ behaves as (see, for instance, Ref. [288])

$$\lim_{z \ll 1} J_\alpha(z) \simeq \frac{1}{\Gamma(1+\alpha)}\,\left(\frac{z}{2}\right)^\alpha, \tag{4.32}$$

where $\Gamma(z)$ denotes the Gamma function. Clearly, in such a limit, the Bessel functions involving the largest negative value for the index α can be expected to dominate. Since $0 \leq w_\phi \leq 1$, the quantities ν and γ are always positive [cf. Eq. (4.12)]. Hence, in the limit $k \ll k_f$, we find that it is the term involving D_k in Eq. (4.11) that will dominate. For the above reasons, the quantity $\chi_k^{\rm RH}(A_{re})$ can be approximated as follows:

$$\chi_k^{\rm RH}(A_{re}) \simeq A_{re}^{-\nu}\,D_k\,J_{\nu/\gamma}\left(\frac{k}{\gamma\,k_{re}}\right), \tag{4.33}$$

with the coefficient D_k being given by

$$D_k \simeq -\frac{\pi}{\Gamma(-\nu/\gamma)}\,\csc\left(\frac{\pi\,\nu}{\gamma}\right)\,\left(\frac{k}{2\,\gamma\,k_f}\right)^{-\nu/\gamma}. \tag{4.34}$$

Let us first arrive at the shape of the spectrum in the domain $k \ll k_{re}$. In such a domain, we can use the form (4.32) for the Bessel function $J_{\nu/\gamma}[k/(\gamma\,k_{re})]$ that appears in the expression (4.33) above for $\chi_k^{\rm RH}(A_{re})$. On doing so and utilizing the identity $\Gamma(z)\,\Gamma(1-z) = \pi/\sin(\pi\,z)$ [288], we find that, in the domain $k \ll k_{re}$, the quantity $\chi_k^{\rm RH}(A_{re})$ reduces to unity. Under the same conditions, we find that the quantity $d\chi_k^{\rm RH}(A_{re})/dA$ vanishes. Therefore, it should be evident from the expressions (4.31) that, in the limit $k \ll k_{re}$, $\mathcal{E}_k \simeq \mathcal{F}_k \simeq 1$. In other words, the spectrum of GWs today is scale invariant over this domain and its present day amplitude is given by

$$\Omega_{GW}(k)\,h^2 \simeq \left(\frac{g_{r,0}}{g_{r,\rm eq}}\right)^{1/3}\,\Omega_{\rm R}\,h^2\,\frac{\mathcal{P}_{\rm T}(k)}{24} \simeq \Omega_{\rm R}\,h^2\,\frac{H_I^2}{12\,\pi^2 M_p^2}. \tag{4.35}$$

In arriving at the final expression, we have assumed that $g_{r,0} \simeq g_{r,\rm eq}$ and have made use of the tensor power spectrum (4.3) arising in de Sitter inflation. We should mention that this result is the same as in the case of instantaneous reheating. This result should come as a surprise since these large scale modes are on super-Hubble scales during the epoch of reheating and hence are not influenced by it.

Let us now turn to the domain $k \gg k_{re}$. Since the limit $k \ll k_f$ continues to be valid, the term involving D_k in Eq. (4.11) remains the dominant term. Therefore, $\chi_k^{\rm RH}(A_{re})$ is again described by Eq. (4.33), with D_k given by Eq. (4.34). However, the argument of the Bessel function in Eq. (4.33) is now large. For large z, the Bessel function $J_\alpha(z)$ behaves as (see, for instance, Ref. [288])

$$\lim_{z\gg 1} J_\alpha(z) \simeq \sqrt{\frac{2}{\pi\, z}}\, \cos\left[z - \pi\,\alpha - (\pi/4)\right]. \tag{4.36}$$

Therefore, in the domain $k \gg k_{re}$, we find that the quantity $\chi_k^{\rm RH}(A_{re})$ and its derivative $d\chi_k^{\rm RH}(A_{re})/dA$ behave as

$$\chi_k^{\rm RH}(A_{re}) \simeq -\frac{1}{\sqrt{\pi}}\,\Gamma\left(1+\frac{\nu}{\gamma}\right)\left(\frac{k}{2\,\gamma\,k_{re}}\right)^{-(\nu/\gamma)-(1/2)} \cos\left(\frac{k}{2\,\gamma\,k_{re}} - \frac{\pi\,\nu}{\gamma} - \frac{\pi}{4}\right), \tag{4.37}$$

$$A_{re}\,\frac{d\chi_k^{\rm RH}(A_{re})}{dA} \simeq -\frac{2\,\gamma}{\sqrt{\pi}}\,\Gamma\left(1+\frac{\nu}{\gamma}\right)\left(\frac{k}{2\,\gamma\,k_{re}}\right)^{-(\nu/\gamma)+(1/2)} \sin\left(\frac{k}{2\,\gamma\,k_{re}} - \frac{\pi\,\nu}{\gamma} - \frac{\pi}{4}\right), \tag{4.38}$$

with ν and γ being given by Eq. (4.12). On substituting these expressions in Eqs. (4.31), we obtain the corresponding $\mathcal{E}_k$ and $\mathcal{F}_k$ to be

$$\mathcal{E}_k \simeq \mathcal{F}_k^* \simeq -\frac{2\,i\,\gamma}{\sqrt{\pi}}\,\Gamma\left(1+\frac{\nu}{\gamma}\right)\left(\frac{k}{2\,\gamma\,k_{re}}\right)^{-(\nu/\gamma)+(1/2)} \exp i\left(\frac{k}{2\,\gamma\,k_{re}} - \frac{\pi\,\nu}{\gamma} - \frac{\pi}{4}\right) \tag{4.39}$$

so that

$$|\mathcal{E}_k|^2 = |\mathcal{F}_k|^2 = \frac{4\,\gamma^2}{\pi}\,\Gamma^2\left(1+\frac{\nu}{\gamma}\right)\left(\frac{k}{2\,\gamma\,k_{re}}\right)^{n_{GW}}, \tag{4.40}$$

where we have defined n_{GW} to be

$$n_{GW} = 1 - \frac{2\,\nu}{\gamma} = -\frac{2\,(1-3\,w_\phi)}{1+3\,w_\phi}. \tag{4.41}$$

If we substitute these results in the expression (4.30), we obtain the spectrum of GWs today in the domain $k \gg k_{re}$ to be

$$\Omega_{GW}(k)\,h^2 \simeq \left(\frac{g_{r,0}}{g_{r,\rm eq}}\right)^{1/3} \Omega_{\rm R}\,h^2\,\frac{\mathcal{P}_{\rm T}(k)}{24}\,|\mathcal{E}_k|^2 \simeq \Omega_{\rm R}\,h^2\,\frac{H_I^2}{12\,\pi^2 M_p^2}\,\frac{4\,\gamma^2}{\pi}\,\Gamma^2\left(1+\frac{\nu}{\gamma}\right)\left(\frac{k}{2\,\gamma\,k_{re}}\right)^{n_{GW}}. \tag{4.42}$$

In other words, for wave numbers such that $k \gg k_{re}$, the spectrum of GWs today has the index n_{GW}. Notably, the index vanishes when $w_\phi = 1/3$. Also, while the spectrum is blue for $w_\phi > 1/3$, it is red for $w_\phi < 1/3$. Moreover, in the extreme cases wherein w_ϕ vanishes or is unity, we have $n_{GW} = -2$ and $n_{GW} = 1$, respectively.

On utilizing the expression (4.11) for the transfer function during reheating and the expressions (4.21) to determine the quantities $\mathcal{E}_k$ and $\mathcal{F}_k$, we can arrive at the complete spectrum of GWs by substituting the expressions in Eq. (4.27). In Fig. 4.2, we have plotted the spectrum of GWs today that arise in the case of the α-attractor model (1.130) for a set of values of the EoS parameter w_ϕ. In plotting the spectra, we have chosen the other parameters in such a fashion that the reheating temperature is $T_{re} = 3\,\text{GeV}$ in all the cases. The figure clearly illustrates the qualitative features we discussed above: (i) the spectrum is strictly scale invariant for $k < k_{re}$, and (ii) the spectrum has the index n_{GW} for $k > k_{re}$. We have

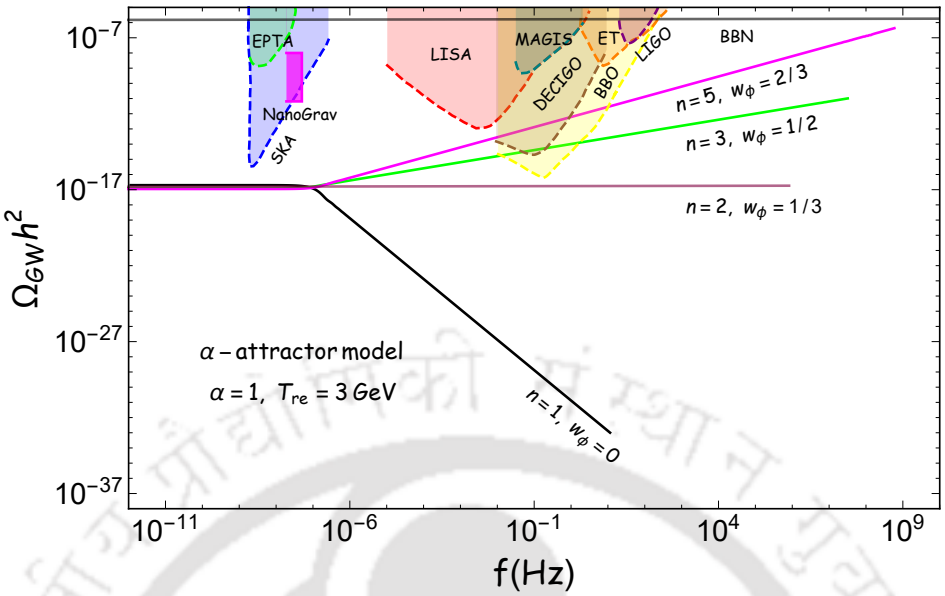

FIGURE 4.2: The behavior of the dimensionless energy density of primordial GWs observed today, viz. $\Omega_{GW}(f)$, has been plotted over a wide range of frequencies. The spectrum has been obtained analytically and it corresponds to the case wherein the post-inflationary phase is described by the EoS parameter w_ϕ and reheating is expected to occur instantaneously at a given time. We have considered the scenario wherein the inflationary potential is described by the α-attractor model (1.130). We have illustrated the spectra for the cases wherein $n = (1, 2, 3, 5)$ (in black, brown, green and magenta), which correspond to $w_\phi = (0, 1/3, 1/2, 2/3)$. We should mention that we have chosen the parameters such that $T_{re} = 3\,\mathrm{GeV}$ in all the cases. In the figure, we have also included the sensitivity curves of the different ongoing and forthcoming GW observatories (in varied colors, on top). Note that, as expected, the spectrum is strictly scaled invariant for frequencies such that $f < f_{\rm re} = k_{re}/(2\,\pi)$. However, for larger frequencies such that $f > f_{\rm re}$, while the spectrum has a red tilt for $w_\phi < 1/3$, it has a blue tilt for $w_\phi > 1/3$. Interestingly, we find that, for a suitably large value of w_ϕ, the spectrum of GWs already intersects the sensitivity curves of some of the observatories over a certain range of frequencies. Moreover, we find that, for a high value of w_ϕ, the spectra cross the BBN bound of $\Omega_{GW}\,h^2 < 10^{-6}$ at suitably large frequencies.

plotted the spectra for $w_\phi = (0, 1/3, 1/2, 2/3)$, which correspond to the values $n = (1, 2, 3, 5)$ for the index in the potential (1.130). We should mention that these cases lead to the indices $n_{GW} = (-2, 0, 2/5, 2/3)$, as expected. In the figure, we have also included the sensitivity curves of some of the current and forthcoming GW observatories (for a discussion on the sensitivity curves, see Ref. [289] and the associated web page). Interestingly, we find that, for a set of inflationary and reheating parameters, the spectra already intersect the sensitivity curves. Moreover, we find that the BBN bound, viz. $\Omega_{GW}(k_f)\,h^2 \leq 10^{-6}$ (in this context, see, for instance, Ref. [290] and the reviews [205, 206]), can be violated for $w_\phi > 1/3$, which leads to constraints on the EoS parameter w_ϕ for a given k_f and vice-versa. As we have emphasized, Fig. 4.2 depicts the interesting dependence of the value of k_f on the inflationary model parameter n due to different initial conditions at the beginning of reheating. This interdependence of k_f and the EoS parameter w_ϕ can be translated into the constraints on

the reheating temperature T_{re} and scalar spectral index n_s through the aforementioned BBN bound. For instance, in the figure, the spectrum corresponding to $w_\phi = 2/3$ clearly crosses the BBN bound at large frequencies. These clearly suggest that observations of the spectrum of GWs today can lead to interesting constraints on primordial physics.

4.5 Spectrum of GWs in the case of perturbative reheating

In the perturbative reheating scenario, the inflaton continuously transfers its energy to radiation after the end of the inflationary epoch. As a result, the effective EoS parameter during the reheating era, say, $w_{\rm eff}$, becomes time-dependent. It can be expressed as

$$w_{\rm eff} = \frac{3\, w_\phi\, \rho_\phi + \rho_R}{3\, (\rho_\phi + \rho_R)}, \tag{4.43}$$

where, recall that, the evolution of the energy densities of the inflaton and radiation, viz. ρ_ϕ and ρ_R, are governed by the Boltzmann equations (2.21) and (2.22), while w_ϕ is the EoS parameter describing the inflaton. Such a time dependence of the effective EoS parameter has been explicitly demonstrated earlier (see, for example, Refs. [91, 93]). It has been illustrated that, while immediately after the termination of inflation, $w_{\rm eff}$ is approximately equal to w_ϕ, after a certain time, the effective EoS parameter smoothly transits from w_ϕ to 1/3, which indicates the onset of the epoch of radiation domination. We should emphasize again here that such a reheating scenario is different from the case considered in the previous section where the inflaton energy density is assumed to be converted instantaneously into radiation after a certain period of time. Specifically, in the previous reheating scenario, $w_{\rm eff}$ remains equal to w_ϕ during the whole of reheating era and, at a particular time, $w_{\rm eff}$ sharply changes to 1/3. These differences in the dynamics of the reheating scenarios should be reflected in the spectrum of GWs today. The corresponding features in the GW spectrum can, in principle, help us probe the microscopic mechanisms operating during the era of reheating.

We shall now proceed to compute the spectrum of GWs at the present time, i.e. $\Omega_{GW}(k)$ or, equivalently, $\Omega_{GW}(f)$, in the case of the perturbative reheating scenario. As we had discussed, we shall analyze this case numerically. With the solution to the Hubble parameter $H(A)$ at hand, we proceed to solve for the transfer function $\chi_k(A)$ during the epoch of reheating, as we had outlined in section 4.2. The numerical solutions are determined using the initial conditions (4.8) and (4.9). With the solutions at hand, we arrive at the spectrum of GWs at the current epoch for different sets of reheating temperature and the EoS parameter w_ϕ describing the inflaton. The results we have obtained are illustrated in Figs. 4.3 and 4.4 for the cases of $w_\phi < 1/3$ and $w_\phi > 1/3$, respectively. Let us now highlight a few points concerning the results plotted in the two figures. Let us first broadly understand the spectra in Fig. 4.3 wherein we have plotted the results for $w_\phi = 0$. In the figure, we have illustrated the dimensionless energy density of GWs today as a function of the frequency f. We have considered the case wherein the inflationary potential is described by the α-attractor model (1.130), and have plotted the results for $n = 1$ (which corresponds to $w_\phi = 0$) and a set of values of T_{re}. We have also included behavior of the effective EoS parameter $w_{\rm eff}$, which we have plotted as a function of frequency using the relation $f = a\, H/(2\pi)$. The plot indicates the evolution of the parameter $w_{\rm eff}$ as the modes with different frequencies f reenter the Hubble radius (in this context, also see the earlier efforts [91, 93]). Note that larger wave numbers or, equivalently, larger frequencies reenter the Hubble radius earlier than the smaller ones. The plot clearly highlights

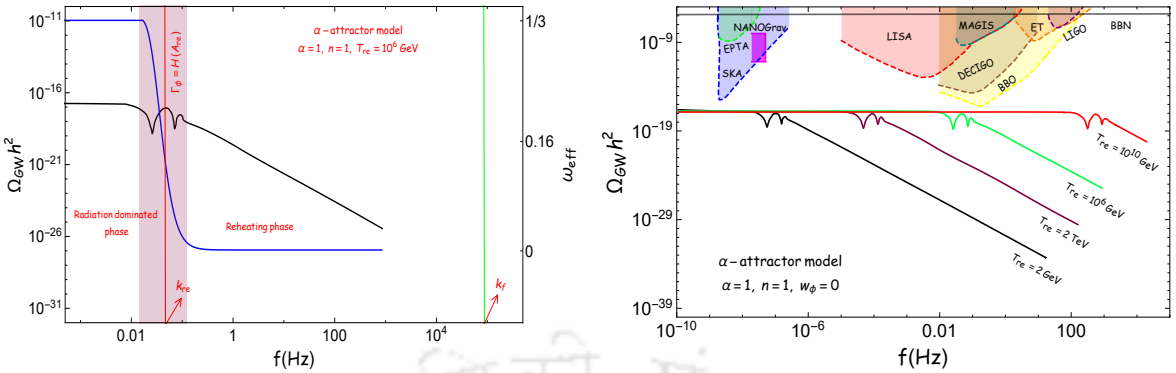

FIGURE 4.3: The behavior of the dimensionless energy density of primordial GWs today, viz. $\Omega_{GW}(f)$, has been plotted over a small (in black, on the left) as well as a wide range of frequencies (in red, green, brown and black, on the right). We have considered the scenario wherein the inflationary potential is described by the α-attractor model (1.130) with $n = 1$, which corresponds to $w_\phi = 0$. We have plotted the spectrum of GWs for the following values of the reheating temperature T_{re}: 10^{10} GeV (in red, on the right), 10^6 GeV (in black on the left and green on the right), 2 TeV and 2 GeV (in brown and black on the right). Note that, we have also illustrated the behavior of the effective EoS parameter $w_{\rm eff}$ (in blue, in the figure on the left) as a function of the frequency f, which has been determined using the relation $f = a\,H/(2\,\pi)$. In other words, $w_{\rm eff}(f)$ (marked on the y-axis on the right hand side of the figure on the left) represents the effective EoS parameter at the instant when the mode with the frequency f reenters the Hubble radius. We have also indicated the frequencies associated with the wave numbers k_{re} and k_f (as vertical red and green lines, on the left). Moreover, we have demarcated the regime (in pink) wherein the transition from $w_{\rm eff} = 0$ to $w_{\rm eff} = 1/3$ occurs. We should point out that the spectrum of GWs exhibits oscillations in the region of the transition. Further, we have included the sensitivity curves of different ongoing and forthcoming GW observatories (in the figure on the right).

the transition from the inflaton dominated universe to the epoch of radiation domination, achieved through the mechanism of perturbative reheating. The transition is clearly reflected in the behavior of the effective EoS parameter which changes smoothly from $w_{\rm eff} = 0$ at early times (i.e. at large frequencies) to $w_{\rm eff} = 1/3$ at late times (i.e. at small frequencies). In the figure, we have indicated the frequencies associated with the wave numbers k_f and k_{re} and have also marked the domain of the transition to highlight these points.

Let us now point out a few more aspects of the results presented in Fig. 4.3. In the figure, we have also plotted the spectrum of GWs for a few different values of the reheating temperature. Further, we have included the sensitivity curves of different current and forthcoming GW observatories. Note that the plots suggest that the spectra of GWs remain scale invariant over wave numbers $k < k_{re}$ which reenter the Hubble radius during the radiation dominated epoch. This result should not come as surprise. As we have pointed out earlier, these modes are on super-Hubble scales during the period of reheating and hence are unaffected by the process. Therefore, they carry the scale invariant nature of the spectrum of GWs generated during inflation. However, modes with wave numbers $k_{re} < k < k_f$ reenter the Hubble radius during the epoch of reheating and hence they carry the signatures of the mechanism of reheating. For the value of $w_\phi = 0$ we have worked with in Fig. 4.3, we find that the spectrum exhibits

a strong red tilt for $k > k_{re}$. In fact, we find that the red tilt occurs over this range of wave numbers whenever $w_\phi < 1/3$. Moreover, for lower values of the reheating temperature, the red tilt begins to occur at smaller wave numbers. Such a behavior can be attributed to the fact that when the reheating temperature is lower, the epoch of reheating lasts longer. Since reheating is delayed, the mode with wave number k_{re} reenters the Hubble radius at a later time or, equivalently, leaves the Hubble radius during inflation at an earlier time thereby suggesting that it will have a smaller wave number. We should mention here that these features in the spectrum of GWs are similar to the behavior in the simpler reheating scenario we discussed in the last section.

Interestingly, we find that the perturbative reheating scenario leaves telltale imprints on the spectrum of GWs which can possibly help us decipher finer details of the mechanism of reheating. We find that the spectrum exhibits a burst of oscillations near k_{re}. It should be clear from Fig. 4.3 that the oscillations occur over modes which leave the Hubble radius during the period of the transition when $w_{\rm eff}$ changes from its initial value of w_ϕ to the final value of 1/3. Recall that, in the perturbative reheating scenario, the reheating temperature is identified as the temperature associated with the energy density of radiation at the instance when $H(A_{re}) = \Gamma_\phi$. Consequently, it is at this point of time that the change in the effective EoS parameter with respect to the scale factor is the maximum. This aspect is reflected in the peak that arises in the spectrum of GWs exactly at the wave number k_{re} which re-enters the Hubble radius when $H(A_{re}) = \Gamma_\phi$. We should also mention that these features in the spectrum of GWs spectrum are not limited only to the case of $w_\phi = 0$ and $T_{re} = 10^6\,\mathrm{GeV}$, but also arise for all possible sets of values of $(w_\phi < 1/3, T_{re})$. In order to highlight this point, in Fig. 4.3, we have illustrated the spectrum $\Omega_{GW}(f)$ for different values of reheating temperature T_{re}. However, note that, the frequency around which the spectrum begins to exhibit a red tilt increases as the reheating temperature increases. This is expected for the reason we discussed above, viz. that the period of reheating is shorter for a higher reheating temperature as a result of which the wave number k_{re} of the mode which re-enters at the end of reheating turns out to be larger. Lastly, we should mention that, for $w_\phi < 1/3$, the spectrum of GWs is indeed compatible with the BBN constraints.

To illustrate the dependence of the spectrum of GWs on w_ϕ, in Fig. 4.4, we have plotted the spectrum for $w_\phi = 1/2$ [i.e. for $n = 3$ in the potential (1.130)] and a set of values of the reheating temperature, just as in Fig. 4.3. Clearly, the spectrum of GWs is scale-invariant over frequencies corresponding to $k < k_{re}$. But, in contrast to the $w_\phi = 0$ case, the spectrum has a strong blue tilt at higher frequencies. Also, as expected, the higher the reheating temperature, the larger is k_{re}, for reasons, we have discussed earlier. Moreover, we find that the spectrum exhibits a burst of oscillation around k_{re}, exactly as in the $w_\phi = 0$ case. Further, the maximum of the oscillation occurs at the instance when k_{re} reenters the Hubble radius and the width of the oscillation coincide with the period of transition from $w_{\rm eff} = w_\phi = 0.5$ to $w_{\rm eff} = 1/3$. Finally, we should mention that the spectra exhibit a blue tilt for $k > k_{re}$ whenever $w_\phi > 1/3$.

The above arguments clearly indicate that the details of epoch of reheating significantly affects the spectrum of GWs. Therefore, the characteristic features of $\Omega_{GW}(f)$ can considerably aid us in garnering an adequate amount of information regarding the reheating phase. Upon comparing Figs. 4.2 and 4.3 (or 4.4), it is clear that the perturbative reheating mechanism, wherein the transfer of energy from the inflaton to radiation occurs smoothly, leads to oscillations in the spectrum of GWs in contrast to the simpler model wherein the transition to radiation domination occurs instantaneously. We believe that such quantitative differences can provide us with stronger constraints on the mechanism of reheating. Specifically,

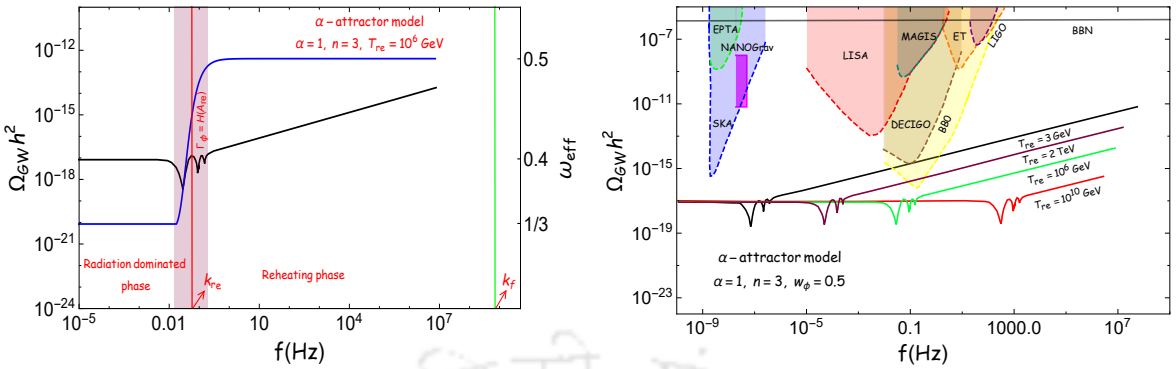

FIGURE 4.4: The spectrum of GWs today have been illustrated in the same manner as in the last figure. But, in contrast to the previous figure wherein we had considered the case $w_\phi = 0$ [or, equivalently, $n = 1$ in the potential (1.130)], we have set $w_\phi = 0.5$ (i.e. $n = 3$) in arriving at the plots above. Note that, as in the case of $w_\phi = 0$, the spectrum is scale invariant over frequencies corresponding to $k < k_{re}$. However, the spectrum has a strong blue tilt at higher frequencies. Importantly, for some values of the reheating temperature, the spectra intersect the sensitivity curves of the various GW observatories which immediately translate to constraints on the parameters w_ϕ and T_{re} that characterize the epoch of reheating. In the figure, we have also included the BBN constraint (as the horizontal black line, on the right), which corresponds to $\Omega_{GW}\, h^2 < 10^{-6}$.

- The presence of the oscillating feature in the spectrum of GWs, in particular, the width of the oscillation can provide us with information concerning the time scale over which $w_{\rm eff}$ makes the transition from w_ϕ to 1/3.
- As we have discussed above, the peak of the oscillation occurs at $k = k_{re}$. Thus, identifying the location of the peak of the oscillation in the spectrum can help us determine the Hubble scale at the end of reheating or, equivalently, the decay rate Γ_ϕ of the inflaton to radiation. In other words, the observation of the peak can indicate the strength of the coupling between the inflaton and radiation in given a decay channel.

4.6 Spectrum of GWs near the end of the inflation

Until now, while discussing the tensor power spectrum generated during inflation, for simplicity, we had assumed that inflation was of the de Sitter form. This had led to a scale invariant power spectrum for scales such that $k \ll k_f$ [cf. Eq. (4.3)], where k_f denotes the wave number that leaves the Hubble radius at the end of inflation. However, potentials such as the α-attractor model (1.130) of our interest actually leads to slow-roll inflation and, as we had mentioned earlier, in such cases, there will arise a small tensor spectral tilt. Moreover, even the slow roll approximation will cease to be valid towards the end of inflation. Therefore, to understand the nature of the inflationary tensor power spectrum close to the wave number k_f, the easiest method seems to evaluate the spectrum numerically.

There exists a standard procedure to evaluate the spectrum of perturbations generated during inflation (in this context, see, for instance, Ref. [291]). The modes are typically evolved from the Bunch-Davies initial conditions when they are well inside the Hubble radius and the spectra are evaluated in the super-Hubble domain when the amplitude of the perturbations

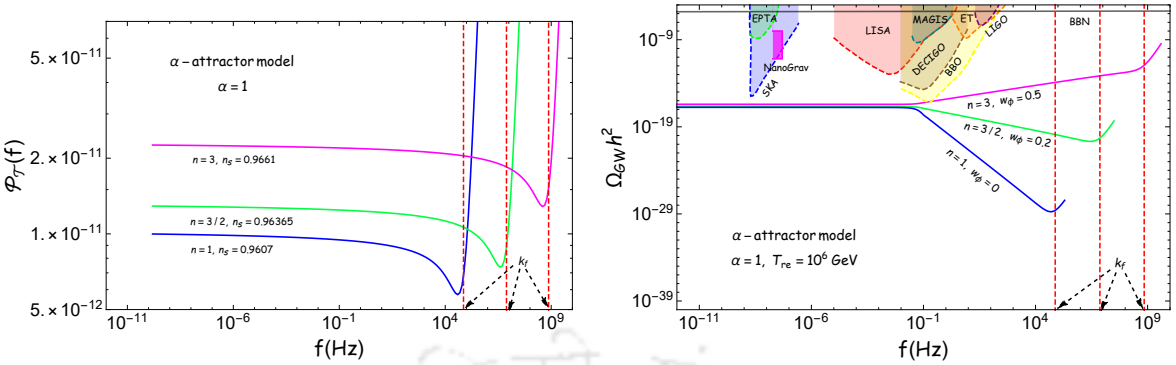

FIGURE 4.5: The inflationary tensor power spectrum arising in the α-attractor model of interest (on the left) as well as the corresponding spectrum of GWs today (on the right) have been plotted for frequencies close to the wave number k_f. The inflationary spectra have been computed numerically and we have made use of the analytical solutions for the tensor transfer function χ_k during the post-inflationary epochs to arrive at the spectrum of GWs today. We have plotted the spectrum of GWs today, viz. $\Omega_{GW}(f)$, for a few different values of the reheating EoS parameter w_ϕ and a specific reheating temperature. We find that, while the inflationary power spectrum begins to behave as k^2 near k_f, the corresponding spectra of GWs today behave as k^4.

have frozen. Such an approach works well for the large scale modes. But, since we are interested in the tensor power spectrum over small scales, in particular, with wave numbers close to k_f, these modes would not be able to spend adequate amount of time in the super-Hubble regime. Hence, in these situations, the best approach would be to evaluate the spectrum at the end of inflation. In Fig. 4.5, we have plotted the inflationary tensor power spectrum computed numerically in the α-attractor model of our interest. Actually, in the figure, we have also plotted the spectra of GWs today $\Omega_{GW}(f)$ for a few sets of values of the EoS parameter w_ϕ and a specific value of the reheating temperature. Having computed the inflationary spectra numerically, we have used the analytical forms for the tensor transfer function post-inflation to arrive at the $\Omega_{GW}(f)$. Note that the inflationary spectral shape begins to change for wave numbers close to k_f. In fact, we find that the inflationary tensor power spectrum $\mathcal{P}_{_{\rm T}}(k)$ behaves as k^2 for wave numbers close to and beyond k_f. This is not surprising and occurs due to the fact that these modes have either hardly left or remain inside the Hubble radius at the end of inflation. Therefore, the modes are essentially of the Minkowskian form leading to the k^2 behavior of the power spectrum. From the structure of energy density of GWs [cf. Eq. (1.116)], it is easy to establish that the corresponding $\Omega_{GW}(k)$ would behave as k^4 over this domain of wave numbers. It is easy to see from Fig. 4.5 that $\Omega_{GW}(f)$ indeed behaves as expected around and beyond k_f. Further, from the figure, we can see that k_f is crucially dependent on the structure of the inflationary potential. For reheating dynamics described by an effective EoS parameter w_ϕ, we can write k_f in terms of the potential parameter n, the reheating parameters $(T_{re}\, N_{re})$ and the inflationary parameter N_* as follows:

$$k_f = a_f\, H_{\rm f} = k_*\frac{H_{\rm f}}{H_I}\,{\rm e}^{N_*} = k_*\left(\frac{V_{\rm f}}{2\,H_I^2\,M_p^2}\right)^{1/2}{\rm e}^{N_*} = k_*\left(\frac{\pi^2 g_{re}}{90}\right)^{1/2}\frac{T_{re}^2}{H_I\,M_p}\,{\rm e}^{N_*+[3n/(n+1)]\,N_{re}}, \tag{4.44}$$

where we have been careful to distinguish between the value of $H_{k_*} \simeq H_I$ and $H_{\rm f}$, i.e. the

Hubble parameters evaluated at the moment when the pivot scale k_* crosses the Hubble radius and at the end of the inflation, respectively.

4.7 CMB, the spectrum of GWs, and the microscopic reheating parameters

As is well known, the observations of the anisotropies in the CMB by missions such as Planck can be explained in a simple and successful the manner by invoking an early phase of inflation [14, 16, 17, 21–27]). Nevertheless, the characterization of the inflaton is far from complete because of the lack of adequate observational constraints, particularly over scales smaller than the CMB scales. The spectrum of GWs is possibly the only probe that can provide us with direct access to the physics operating during the epochs of inflation and reheating. In this section, we shall discuss the manner in which we can extract the properties of the inflaton by combining the observations of the CMB and GWs.

As we have already mentioned, the spectrum of GWs carries signatures which reflect some details of the mechanism of reheating. Recall that, the primary aspect of the reheating phase is the time evolution of the EoS parameter from the initial value of w_ϕ associated with the inflaton to the final value of 1/3 corresponding to radiation. The phase can be generically divided into three stages based on the underlying physical processes that operate. In what follows, we shall discuss these stages and the corresponding imprints on $\Omega_{GW}(f)$.

To facilitate the discussion, let us introduce the spectral index $n_{GW} = d\ln\Omega_{GW}/d\ln k$ associated with the spectrum of GWs. Interestingly, we find that all the three stages leave distinct imprints on the spectral index n_{GW}, and we have illustrated the behavior of $n_{GW}(f)$ for the α-attractor model (1.130) in Fig. 4.6. Note that the first and longest stage is when $H \ll \Gamma_\phi$, i.e. when the inflaton is decaying very slowly and hence the background dynamics is dominated by the EoS parameter w_ϕ governing the inflaton. The spectral index n_{GW} is associated with modes that reenter the Hubble radius during the stage is given by $n_{GW} = 2\,(3\,w_\phi - 1)/(3\,w_\phi + 1)$. In Fig. 4.6, we have indicated the $n_{GW}(f)$ associated with $w_\phi = 0$ and 1/2. In the subsequent stage, as the Hubble parameter approaches Γ_ϕ, the decay of the inflaton becomes increasingly efficient, and the effective EoS parameter begins to change rapidly. The corresponding effects are reflected in the variation of n_{GW} over modes which reenter the Hubble radius during the transition, as highlighted in Fig. 4.6. However, this intermediate stage is the shortest among the three stages and it ends when $H_{re} = \Gamma_\phi$, i.e. when the rate of decay of the inflaton to radiation is at its maximum. The most important of the three stages is the final stage of thermalization which is characterized by the time scale $\Delta t_{\rm th}$. It is the time scale over which the decay products of the inflaton thermalize among themselves. In fact, it is this mechanism that determines the actual initial temperature of the radiation dominated phase contrary to the conventional definition of reheating temperature T_{re} defined when $H = \Gamma_\phi$. The thermalization process and the associated time scale $\Delta t_{\rm th}$ would crucially depend upon nature of all the decay products of the inflaton as well as the detailed dynamics of the decay process. These details will determine the manner in which the EoS parameter changes during this stage and its variation will be imprinted in the behavior of $n_{GW}(f)$ as we have illustrated in Fig. 4.6. Note that there arises a frequency range, say, $\Delta f_{\rm th}$, associated with the time scale $\Delta t_{\rm th}$, and the variation of the spectral index n_{GW} over this domain can provide us with clues to the physics operating during the stage.

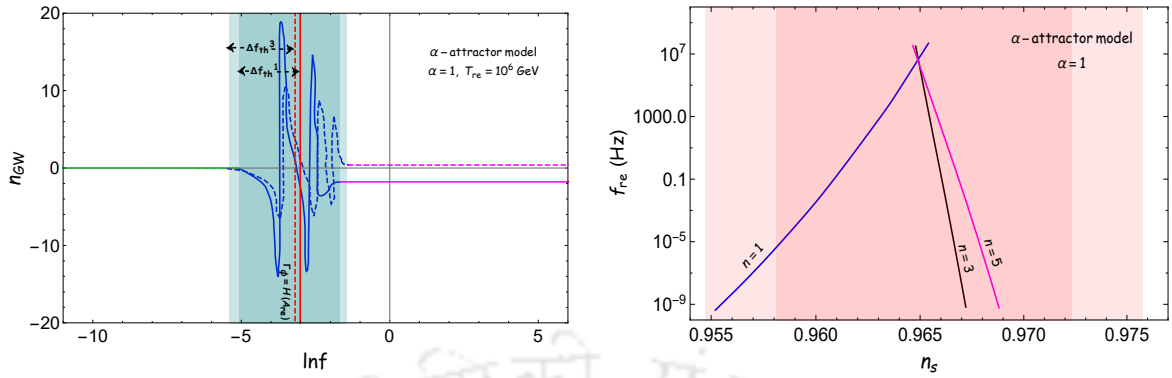

FIGURE 4.6: *Left:* The variation of the index n_{GW} associated the spectrum of primordial GWs observed today in the case of the perturbative reheating scenario has been plotted as a function of frequency f for two different values of the inflaton EoS parameter $w_\phi = (0, 1/2)$ (as solid and dashed lines) for the α-attractor potential (1.130). We have a fixed value of the reheating temperature to be $T_{re} = 10^6$ GeV in arriving at the plot. In the figure (on the left), we have also explicitly highlighted the behavior of n_{GW} for modes that re-enter the Hubble radius during the following regimes: (i) reheating phase dominated by the inflaton (as solid and dashed lines, in magenta), (ii) the period of rapid transition of the EoS parameter from w_ϕ to 1/3 (as solid and dashed lines in blue), and (iii) the radiation dominated epoch (in green). We have also demarcated the domain in frequency associated with the thermalization time scales in the figure (as shaded regions in dark and light blue). These quantities have been denoted as $\Delta f^1_{\rm th}$ and $\Delta f^3_{\rm th}$ for $w_\phi = 0$ and 1/2, respectively. *Right:* We have illustrated the variation of the frequency $f_{\rm re} = k_{re}/(2\,\pi)$ as a function of the scalar spectral index n_s for three different values of $n = (1, 3, 5)$ (in blue, black and pink) for the α-attractor model. We have also indicated the 1-σ and 2-σ confidence regions (as light and dark bands in red) associated with the constraint on scalar spectral index n_s from Planck [29]

Therefore, from the CMB observations and the spectrum of GWs, we can, in principle, extract the following essential information regarding the nature of the inflaton and the underlying physical process taking place during reheating.

(i) Effective inflaton EoS parameter w_ϕ: The nature of inflaton potential near its minimum or, equivalently, the effective EoS parameter w_ϕ associated with the decay of the inflaton can be determined from the spectral index of GWs through the relation

$$w_\phi = \frac{1}{3}\left(\frac{2 + n_{GW}}{2 - n_{GW}}\right). \tag{4.45}$$

(ii) Inflaton decay width Γ_ϕ: Once we have arrived at the EoS parameter describing the inflaton, the effective inflaton decay constant Γ_ϕ can be determined from the CMB and the spectrum of GWs in the following fashion. As we have already mentioned, for modes with wave numbers $k < k_{re}$, the amplitude of the tensor perturbations will remain approximately constant from the time the modes leave the Hubble radius during inflation till they renter the Hubble radius during the epoch of radiation domination. Due to this reason, over this range of modes, the spectrum of GWs at late times retains the same shape as the spectrum of tensor perturbations generated during inflation. Therefore, using Eq. (4.35), the scale-invariant amplitude of the spectrum of GWs can be utilized to estimate the approximate energy scale near the end of

inflation. In the limit of high reheating temperature, we have

$$\Omega_{GW}\, h^2 \simeq \Omega_{\rm R}\, h^2\, \frac{H_I^2}{6\,\pi^2\, M_p^2} \tag{4.46}$$

and, as a result,

$$H_I \simeq \left(\frac{6\,\pi^2\, M_p^2\, \Omega_{GW}\, h^2}{\Omega_{\rm R}\, h^2}\right)^{1/2} \tag{4.47}$$

which, in turn, allows us to express the energy density at the end of inflation as follows:

$$\rho_{\rm f} \simeq \frac{18\,\pi^2\, M_p^4\, \Omega_{GW}\, h^2}{\Omega_{\rm R}\, h^2}. \tag{4.48}$$

From the observed spectrum, we can, in principle, determine wave numbers k_{re} and k_f, which are the wave numbers that reenter at the end of the epoch of reheating and leaving the Hubble radius at the end of inflation, respectively. In Fig. 4.6, we have illustrated the dependence of k_{re} on the scalar spectral n_s for different values of the parameter n of the α-attractor model. In a manner similar to the existence of a maximum possible reheating temperature, we notice that there arises a maximum possible value for the frequency associated with the wave number k_{re}. We find that, generically, $f_{\rm re}^{\rm max} \simeq 10^7\,{\rm Hz}$, irrespective of the values of the other parameters involved. It would be interesting to study further implications of this point. Nonetheless, the aforementioned wave numbers satisfy the following relations

$$k_f = a_{\rm f}\, H_{\rm f} \simeq a_{\rm f}\, H_I, \quad k_{re} = a_{\rm re}\, H_{re} = A_{re}\, a_{\rm f}\, \Gamma_\phi. \tag{4.49}$$

Considering perturbative reheating, one can obtain an approximate analytical expression for the normalized scale factor A_{re} at the end of the reheating to be (in this context, see Ref. [93])

$$A_{re} = \left(\frac{4\,\rho_{\rm f}\,(1+w_\phi)^2}{\mathcal{G}^4\,\beta\,(5-3\,w_\phi)^2}\right)^{-1/(1-3\,w_\phi)}, \quad \beta = \frac{\pi^2\, g_{r,{\rm re}}}{30}, \quad \mathcal{G} = \left(\frac{43}{11\, g_{\rm re}}\right)^{1/3} \left(\frac{a_0\, H_I}{k_*}\right) T_0\, {\rm e}^{-N_*}. \tag{4.50}$$

The primary assumption in arriving at the above expressions is that the energy scale does not change significantly throughout the entire period of inflation. With all the above expressions at hand, we find that the inflaton decay constant Γ_ϕ can be written in terms of the observable quantities as

$$\Gamma_\phi = \frac{k_{re}\, H_I}{A_{re}\, k_f} = \frac{k_{re}}{k_f} \left(\frac{6\,\pi^2\, M_p^2\, \Omega_{GW}\, h^2}{\Omega_{\rm R}\, h^2}\right)^{1/2} \left(\frac{72\,\pi^2\, M_p^4\, \Omega_{GW}\, h^2\,(1+w_\phi)^2}{\Omega_{\rm R}\, h^2\, \mathcal{G}^4\, \beta\,(5-3\,w_\phi)^2}\right)^{1/(1-3\omega_\phi)}. \tag{4.51}$$

One can then immediately obtain the following analytic expression for the reheating temperature:

$$T_{re} = \frac{\mathcal{G}}{A_{re}} = \left(\frac{43}{11\, g_{\rm re}}\right)^{1/3} \frac{k_f\, H_I}{k_*\, H_0} \left(\frac{72\,\pi^2\, M_p^4\, \Omega_{GW}\, h^2\,(1+w_\phi)^2}{\Omega_{\rm R}\, h^2 \mathcal{G}^4\, \beta\,(5-3\,w_\phi)^2}\right)^{1/(1-3\,w_\phi)} T_0. \tag{4.52}$$

So far, we have expressed the inflation decay constant and the reheating temperature in terms of the observables associated with the CMB and the spectrum of GWs today. To understand the exact nature of the coupling, the subsequent thermalization processes right after reheating

(i.e. when $\Gamma_\phi = H_{re}$) becomes important. Therefore, let us now compute the thermalization time scale.

(iii) Thermalization time scale $\Delta t_{\rm th}$: Thermalization is an important non-equilibrium phenomenon that is ubiquitous in nature. At the end of the phase of reheating, when the rate at which the inflaton decays into radiation have attained a maximum, the subsequent thermalization phase leads to the epoch of radiation domination. In this process, thermalization time scale $\Delta t_{\rm th}$ is an important observable which crucially depends on the nature of the initial state as well as the interactions among the internal degrees of freedom. Also, it is the initial state which encodes the information about the coupling between the inflaton and the other fields to which the energy is being transferred. Hence, if we can arrive at $\Delta t_{\rm th}$ from the spectrum of GWs, valuable information regarding the fundamental nature of the coupling parameters between the inflation and other fields at very high energies can, in principle, be extracted. The thermalization time scale is defined as

$$\Delta t_{\rm th} = t_{\rm th} - t_{\rm re}, \tag{4.53}$$

where $t_{\rm re}$ is the time corresponding to the end of reheating and $t_{\rm th}$ denotes the time at the end of the thermalization process, which leads to the beginning of the actual radiation dominated epoch. In order to obtain an approximate analytic expression, during this regime, we shall assume that the scale factor behaves as $a \propto t^{2/3\,(1+w)}$. This can be justified since we can express the effective EoS parameter during the thermalization phase using the following perturbative expansion:

$$w = \frac{1}{t_{\rm th} - t_{\rm re}} \int_{t_{\rm re}}^{t_{\rm th}} dt \left[w_{\rm R} + (w_\phi - w_{\rm R})\, \frac{\rho_\phi}{\rho_{\rm R}} + \cdots \right] \simeq \frac{1}{3} + \left(w_\phi - \frac{1}{3} \right) x + \mathcal{O}(x^2), \tag{4.54}$$

where, $x = \frac{1}{t_{\rm th} - t_{\rm re}} \int_{t_{\rm re}}^{t_{\rm th}} dt\, \frac{\rho_\phi}{\rho_{\rm R}}$ and $w_{\rm R} = 1/3$ is the EoS parameter describing radiation. Note that, during the thermalization phase $\rho_\phi \ll \rho_{\rm R}$ and, hence, $x \ll 1$. This particular fact enables us to obtain the leading order expression for the thermalization time scale in terms of the observable quantities that we discussed. On utilizing the above form for the EoS parameter, we find that the leading order behavior of the scale factor at $\Gamma_\phi = H_{re}$ can be written as

$$a_{\rm re} \simeq \left(\frac{t_{\rm re}}{t_1} \right)^{2/[3\,(1+\omega_{\rm R})]} \left[1 - \frac{2\,x\,(w_\phi - w_{\rm R})}{3\,(1+w_{\rm R})^2} \ln \left(\frac{t_{\rm re}}{t_1} \right) + \cdots \right], \tag{4.55}$$

where t_1 is a constant we have introduced for purposes of normalization. Upon using the relations $k_{re} = a_{\rm re}\, H_{re}$, $k_{\rm th} = a_{\rm th}\, H_{\rm th}$ and $H_{re} = \Gamma_\phi$, we can express the reheating time $t_{\rm re}$ and the thermalization time $t_{\rm th}$ in terms of the wave numbers k_{re} and $k_{\rm th}$ as

$$t_{\rm re} = \left(\frac{k_{\rm th}}{p_{\rm R}} \right)^{1/(p_{\rm R}-1)} t_1^{p_{\rm R}/(p_{\rm R}-1)} + \mathcal{O}(x), \quad t_{\rm th} = \left(\frac{k_{\rm re}}{p_{\rm R}} \right)^{1/(p_{\rm R}-1)} t_1^{p_{\rm R}/(p_{\rm R}-1)} + \mathcal{O}(x). \tag{4.56}$$

We can also express Γ_ϕ in terms of normalized time t_1 as

$$\Gamma_\phi \sim \left(\frac{p_{\rm R}}{t_1} \right)^{p_{\rm R}/(p_{\rm R}-1)} k_{re}^{-1/(p_{\rm R}-1)} + \mathcal{O}(x), \tag{4.57}$$

where we have introduced the quantity $p_{\rm R} = 2/[3\,(1+\omega_{\rm R})]$. Utilizing all the above equations, we finally obtain the final expression for the thermalization time scale to the leading order in x

to be

$$\Delta t_{\rm th} \sim \begin{cases} k_{P_R}\, p_{\rm R}^{p_{\rm R}/(p_{\rm R}-1)} \left(\frac{k_{re}^{-1/(p_{\rm R}-1)}}{\Gamma_\phi}\right) + \mathcal{O}(x), & \text{in terms of } \Gamma_\phi, \\ k_{P_R}\, p_{\rm R}^{p_{\rm R}/(p_{\rm R}-1)} \left(\frac{G\, k_{re}^{-p_{\rm R}/(p_{\rm R}-1)}}{H_I\, T_{re}}\right) + \mathcal{O}(x), & \text{in terms of } T_{re}. \end{cases} \tag{4.58}$$

Here $k_{P_R} = \left(\frac{k_{th}}{p_{\rm R}}\right)^{1/(p_{\rm R}-1)} - \left(\frac{k_{re}}{p_{\rm R}}\right)^{1/(p_{\rm R}-1)}$. In the above expressions, an important point one should remember is that the value of the wave numbers k_{re} and $k_{\rm th}$ are, in general, dependent on the decay width of the inflaton. Therefore, the overall thermalization time scale is a non-trivial function of Γ_ϕ.

The thermalization time scale crucially depends on the initial number density of the decayed particles compared with the thermalized ones. The initial number density at the instant when $\Gamma_\phi = H_{re}$ can be approximately estimated to be $n_{\rm i} \simeq M_p^2\, H_{re}^2/m_\phi = M_p^2\, \Gamma_\phi^2/m_\phi$, and, in arriving at this expression, it has been assumed that the momentum of the decay products is as large as the mass m_ϕ of the inflaton [292, 293]. If we consider the particles to have thermalized at the reheating temperature T_{re}, then the number density can again be approximately determined to be $n_{\rm th} \simeq T_{re}^3 \simeq \Gamma_\phi^{3/2} M_p^{3/2}$. Hence, the ratio of the particle number densities $n_{\rm th}$ and $n_{\rm i}$ turns out to be

$$\frac{n_{\rm th}}{n_{\rm i}} \simeq \frac{m_\phi}{\sqrt{\Gamma_\phi\, M_p}} = \left(\frac{m_\phi^2\, A_{re}\, k_f}{M_p\, k_{re}\, H_I}\right)^{1/2}. \tag{4.59}$$

This is one of the crucial parameters in the context of the thermalizing plasma which dictates the kind of physical processes that occur during thermalization [292–296]. At this stage, we are unable to extract the inflaton mass m_ϕ from the observations in a model independent manner. However, given the mass of the inflaton, along with the CMB observations, Eq. (4.59) will have two generic possibilities, viz.

- $n_{\rm i} < n_{\rm th}$: The particle number density is smaller than the thermalized ones, which means that, at the end of reheating, the universe is under-occupied. For example, if one considers marginal inflaton-scalar (ξ) coupling such $\beta\, \phi\, \xi^3$, inflaton-Fermion (ψ) Yukawa coupling $\beta\, \phi\, \bar{\psi}\, \psi$, the inflaton decay width behaves as $\Gamma_\phi \sim \beta^2\, m_\phi$ which implies that $n_{\rm i}/n_{\rm th} \sim \sqrt{m_\phi/M_p} < 1$.

- $n_{\rm i} > n_{\rm th}$: The particle number density is larger than the thermalized ones, i.e. at the end of reheating, the universe is over occupied. For example, if one considers any Planck suppressed operator containing a coupling between the inflaton and the reheating field, the decay width behaves as $\Gamma_\phi \sim m_\phi^3/M_p^2$, which implies that $n_{\rm i}/n_{\rm th} \sim \sqrt{M_p}/m_\phi > 1$.

(iv) Determination of microscopic interactions: From our discussion above for the two cases, it is clear that if we can determine the value of $n_{\rm th}/n_{\rm i}$ from the combined observations of the CMB and GWs, the fundamental nature of the inflaton-reheating field coupling such as 'β' can be extracted. Furthermore, interestingly, it has been pointed out that, depending on the aforementioned two conditions for the initial, non-thermal states generated by the end of

reheating, the behavior of the thermalization time scale in terms of the microscopic variables will be very different, and will behave as (in this context, see Ref. [292])

$$\Delta t_{\rm th} \sim \begin{cases} \alpha^{-2}\, m_{\phi}^{1/2}\, T_{\rm th}^{-3/2}, & \text{for under-occupied initial states such that } n_{\rm i} < n_{\rm th}, \\ \alpha^{-2}\, T_{\rm th}^{-1}, & \text{for the over-occupied initial state scuh that } n_{\rm i} > n_{\rm th}, \end{cases} \tag{4.60}$$

where α denotes the gauge interaction strength among the decayed particles, and $T_{\rm th}$ is the final thermalization temperature. Hence, it is extremely important to recognize that, once we know the inflaton mass m_{ϕ} and the final thermalization temperature $T_{\rm th}$ [the latter can be computed once the reheating dynamics is fixed, by using Eqs. (4.59) and (4.60)], the gauge interaction strength can, in principle, be computed in terms of the observable quantities through the relations

$$\alpha \sim \begin{cases} T_{\rm th}^{-1/2}\, k_{P_R}^{-1/2}\, p_{\rm R}^{-p_{\rm R}/[2\,(p_{\rm R}-1)]} \left(\frac{k_{re}^{-1/(p_{\rm R}-1)}}{\Gamma_{\phi}}\right)^{-1/2}, & \text{for } H_I > \frac{m_{\phi}^2\, A_{re}\, k_f}{M_p\, k_{re}}, \\ \left(\frac{m_{\phi}}{T_{\rm th}^3}\right)^{1/2} k_{P_R}^{-1/2}\, p_{\rm R}^{p_{\rm R}/[-2\,(p_{\rm R}-1)]} \left(\frac{k_{re}^{-1/(p_{\rm R}-1)}}{\Gamma_{\phi}}\right)^{-1/2}, & \text{for } H_I < \frac{m_{\phi}^2\, A_{re}\, k_f}{M_p\, k_{re}}. \end{cases} \tag{4.61}$$

We expect to carry out a detailed study on these important issues in a future publication. Having examined the effects of the epoch of reheating on the spectrum of GWs today, let us now turn to discuss the effects that arise due to a secondary phase of reheating. As we shall see, such a phase can have an important implication for the recent observational results reported by NANOGrav [272, 273].

4.8 Spectrum of GWs with late time entropy production and implications for the recent NANOGrav observations

In Secs. 4.4 and 4.5, while arriving at the spectrum of GWs $\Omega_{GW}(f)$ today, we had assumed that the perturbations were generated during inflation and had evolved through the epochs of reheating and radiation domination. In such a scenario, the entropy of the universe is conserved from the end of reheating until today. In fact, we had earlier utilized the conservation of entropy to relate the temperature T_{re} at the end of reheating to the temperature T_0 today. Recall that, for simplicity, we had assumed that the spectrum of tensor perturbations generated during inflation was strictly scaled invariant [cf. Eq. (4.3)]. We also found that, for wave numbers $k < k_{re}$, the evolution of the tensor perturbations through the standard epochs of reheating and radiation domination does not alter the shape of the spectrum of GWs observed today, i.e. $\Omega_{GW}(f)$ remains scale invariant for $f < f_{re} = k_{re}/(2\,\pi)$.

Over the last decade or so, there has been an interest in examining scenarios wherein there arises a short, secondary phase of reheating sometime after the original phase of reheating which immediately follows the inflationary epoch (see, for example, Ref. [297]). It has been shown that such a modified scenario can also be consistent with the the various observations [257, 298, 299]. A secondary phase of entropy production can occur due to the decay of an additional scalar field (which we shall denote as σ) that can be present, such as the non-canonical scalar fields often considered in high energy physics or the moduli fields encountered in string theory*. In

*It is for this reason that the secondary phase is sometimes referred to as the moduli-dominated epoch. The scalar field could have emerged from an extra-dimensional modulus field or due to some higher curvature effects [300, 301]

this section, we shall discuss the effects of such a secondary phase of reheating (which occurs apart from the primary phase of reheating considered earlier) on the spectrum of GWs observed today. As we shall see, the secondary phase of entropy production leads to unique imprints on the spectrum of GWs which has interesting implications for the recent observations by NANOGrav [272, 273].

Let us first calculate the reheating temperature associated with the secondary phase of reheating. We can expect the entropy to be conserved during the radiation dominated epoch sandwiched between the two phases of reheating. On following the chronology of evolution mentioned above and, upon demanding the conservation of entropy, we can arrive at the relation between the temperature T_{re} at the end of the first phase of reheating and the temperature at the beginning of the second phase of reheating, say, $T_{\sigma R}$. We find that they can be related as follows:

$$g_{s,\mathrm{re}}\, a_{re}^3\, T_{re}^3 = g_{s,\sigma R}\, a_{\sigma R}^3\, T_{\sigma R}^3, \tag{4.62}$$

where $(g_{s,\mathrm{re}}, g_{s,\sigma R})$ and $(a_{re}, a_{\sigma R})$ denote the relativistic degrees of contributing to the entropy and the scale factor at the end of the primary reheating phase and at the start of the second phase of reheating (or, equivalently, at the end of the first epoch of radiation domination), respectively. Using the above relation, we can express the original reheating temperature T_{re} in terms of the temperature $T_{\sigma R}$ at the beginning of the secondary phase of reheating as

$$T_{re} = \left(\frac{g_{s,\sigma R}}{g_{s,\mathrm{re}}}\right)^{1/3} \mathrm{e}^{N_{\mathrm{RD}}^{(1)}}\, T_{\sigma R}, \tag{4.63}$$

where $N_{\mathrm{RD}}^{(1)} = \ln\left(a_{\sigma R}/a_{re}\right)$ denotes the duration of the first epoch of radiation domination in terms of the number of e-folds. Similarly, we can relate the temperature at the end of the secondary phase of reheating, say, T_σ, to the temperature T_0 today by demanding the conservation of entropy after the onset of the second epoch of radiation domination. On doing so, we obtain that

$$T_\sigma = \left(\frac{43}{11\, g_{s,\sigma}}\right)^{1/3} \left(\frac{a_0}{a_\sigma}\right) T_0, \tag{4.64}$$

where $g_{s,\sigma}$ and a_σ represent the degrees of freedom contributing to the entropy and the scale factor at the end of the the secondary phase of reheating. If a_{eq} denotes the scale factor at the epoch of matter-radiation equality, then the above expression for T_σ can be written as

$$T_\sigma = \left(\frac{43}{11\, g_{s,\sigma}}\right)^{1/3} \left(\frac{a_0}{a_{\mathrm{eq}}}\right) \mathrm{e}^{N_{\mathrm{RD}}^{(2)}}\, T_0. \tag{4.65}$$

The factor a_0/a_{eq} can be expressed in terms of the quantity a_0/a_k through the relation

$$\frac{a_0}{a_{\mathrm{eq}}} = \left(\frac{a_0}{a_k}\right) \mathrm{e}^{-\left[N_k + N_{re} + N_{\mathrm{RD}}^{(1)} + N_{\mathrm{sre}} + N_{\mathrm{RD}}^{(2)}\right]}, \tag{4.66}$$

where a_k denotes the scale factor when the mode with the wave number k crosses the Hubble radius during inflation, while N_k represents the number of e-folds from the time corresponding to a_k to the end of inflation. Moreover, recall that N_{re} denotes the duration of the first phase of reheating. It should be evident that the quantities N_{sre} and $N_{\mathrm{RD}}^{(2)}$ represents the duration (in terms of e-folds) of the secondary phase of (say, moduli dominated) reheating and the

second epoch of radiation domination, respectively. With k set to be the pivot scale k_*, on substituting the above expression for $a_0/a_{\rm eq}$ in Eq. (4.65), we obtain that

$$T_\sigma = \left(\frac{43}{11\, g_{s,\sigma}}\right)^{1/3} \left(\frac{a_0\, H_I}{k_*}\right) \mathrm{e}^{-\left[N_* + N_{re} + N^{(1)}_{\rm RD} + N_{\rm sre}\right]}\, T_0, \tag{4.67}$$

which is the temperature at the end of the secondary phase of reheating.

Note that the above expression for T_σ can be inverted to write $N^{(1)}_{\rm RD}$ as

$$\mathrm{e}^{N^{(1)}_{\rm RD}} = \left(\frac{43}{11\, g_{s,\sigma}}\right)^{1/3} \left(\frac{a_0\, H_I}{k_*}\right) \mathrm{e}^{-[N_* + N_{re} + N_{\rm sre}]} \left(\frac{T_0}{T_\sigma}\right). \tag{4.68}$$

This relation, along with Eq. (4.63), immediately leads to the following expression for the original reheating temperature T_{re} in terms of the parameters associated with the late time entropy production:

$$T_{re} = \left(\frac{43}{11\, g_{s,re}}\right)^{1/3} \left(\frac{a_0\, H_I}{k_*}\right) F^{-1/3}\, \mathrm{e}^{-(N_* + N_{re})}\, T_0. \tag{4.69}$$

In this relation, the factor F represents the ratio of the entropy at the end and at the beginning of the secondary phase of reheating, and it is given by

$$F = \frac{s(T_\sigma)\, a_\sigma^3}{s(T_{\sigma R})\; a_{\sigma R}^3}, \tag{4.70}$$

where $s(T)$ denotes the entropy at the temperature T. If we now assume that the secondary phase of reheating is described by the EoS parameter w_σ, then we can arrive at the following useful relations between the Hubble parameter and the temperature at the end and at the beginning of the secondary phase of reheating:

$$H_\sigma = \left(\frac{\gamma_1\, T_\sigma}{\gamma_2\, F^{1/3}\, T_{\sigma R}}\right)^{3\,(1+w_\sigma)/2} H_{\sigma R},\; T_\sigma = \left(\frac{\gamma_1}{\gamma_2\, F^{1/3}}\right)^{3\,(1+w_\sigma)/(1-3\,w_\sigma)} \left(\frac{g_{r,\sigma R}}{g_{r,\sigma}}\right)^{1/(1-3w_\sigma)} T_{\sigma R}, \tag{4.71}$$

where the quantities γ_1 and γ_2 are defined as

$$\gamma_1 = \left(\frac{g_{r,\rm re}}{g_{r,\sigma R}}\right)^{1/4}, \quad \gamma_2 = \left(\frac{g_{s,\rm re}}{g_{s,\sigma}}\right)^{1/3}. \tag{4.72}$$

Clearly, the factor F controls the extent of entropy produced at late times. And, in the absence of such entropy production, the factor F reduces to unity. Also, in such a case, the expression (4.69) for the reheating temperature T_{re} reduces to the earlier expression (4.17), as required.

Let us now turn to discuss the spectrum of GWs that arises in such a modified scenario. As we mentioned above, for simplicity, we shall assume that the secondary phase of reheating is described by the EoS parameter w_σ. In order to arrive at $\Omega_{GW}(k)$ in the new scenario, we shall follow the calculations described in sec. 4.4 wherein we have evaluated the spectrum analytically. To highlight all the relevant scales involved and also to aid our discussion below, in Fig. 4.7, we have illustrated the evolution of the comoving Hubble radius in the modified scenario. Specifically, in the figure, we have indicated the new scales $k_{\sigma R}$ and k_σ

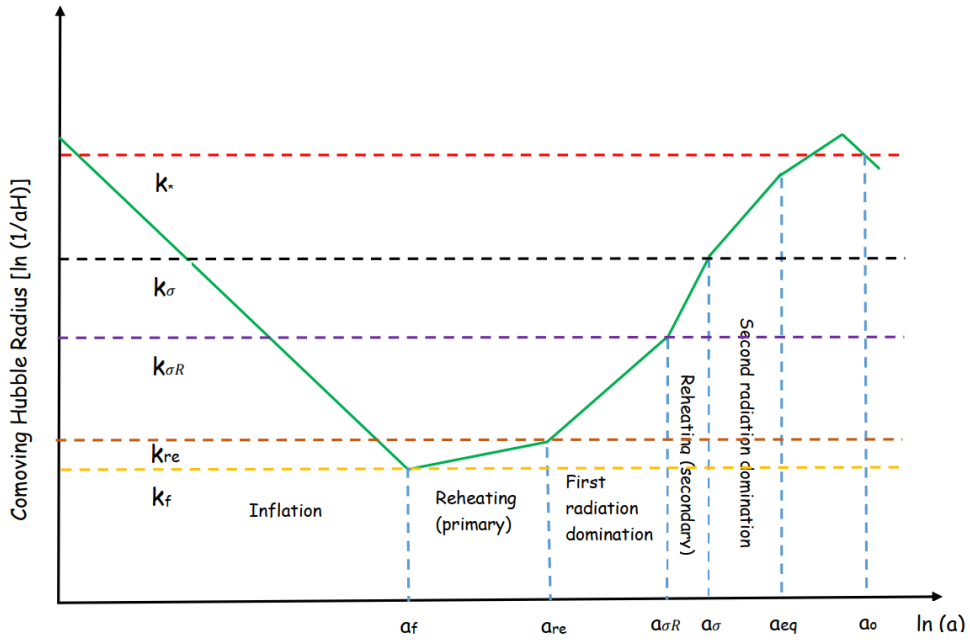

FIGURE 4.7: A schematic diagram illustrating the evolution of the comoving Hubble radius $(a\,H)^{-1}$ plotted (in green) against the number of e-folds $N = \ln a$. In the diagram, we have also delineated the various epochs that are relevant for our discussion. In the above plot, we have assumed that the EoS parameter w_ϕ describing the primary reheating phase is less than 1/3. However, we have assumed that the EoS parameter, say, w_σ, associated with a string modulus or a non-canonical scalar field driving the secondary phase of reheating is greater than 1/3. In the figure, apart from the wave numbers k_*, k_{re} and k_f we had encountered earlier (indicated as red, brown and yellow, dashed lines), we have indicated the scales $k_{\sigma R}$ and k_σ (as dashed lines in purple and black) which correspond to wave numbers that reenter the Hubble radius at the beginning and at the end of the second phase of reheating, respectively.

which are the wave numbers that reenter the Hubble radius at the start and at the end of the secondary phase of reheating.

Before we go on to illustrate the results, let us try to understand the the shape of $\Omega_{GW}(k)$ that we can expect in the modified scenario involving late time production of entropy.

- For wave numbers $k < k_\sigma$: As we mentioned above, k_σ represents the wave number of the mode that reenters the Hubble radius at the onset of the second epoch of radiation domination or, equivalently, at the end of the secondary phase of reheating. Therefore, the range of wave numbers $k < k_\sigma$ (but with wave numbers larger than those corresponding to the CMB scales) reenter the Hubble radius during the second epoch of radiation domination. Since they are on super-Hubble scales prior to their reentry, they are not influenced by the background dynamics during the earlier epochs. Hence, the spectrum of GWs for these range of modes can be expected to be scale invariant, which implies that the corresponding spectral index n_{GW} vanishes identically.

- For wave numbers $k_\sigma < k < k_{\sigma R}$: Recall that, $k_{\sigma R}$ denotes the wave number that reenters

the Hubble radius at the beginning of the secondary phase of reheating. As in the case of modes that reenter the primary phase of reheating, we can expect the spectrum of GWs over this range of wave numbers to exhibit a spectral tilt which depends on the EoS parameter w_σ. We find that, over this range of wave numbers, $\Omega_{GW}(k)$ behaves as

$$\Omega_{GW}(k) \sim k^{2\,(3\,w_\sigma - 1)/(3\,w_\sigma + 1)}. \tag{4.73}$$

Consequently, the spectral index of the primordial GWs over this range of wave numbers turns out to be $n_{GW} = 2\,(3\,w_\sigma - 1)/(3\,w_\sigma + 1)$. In others words, over the domain $k_\sigma < k < k_{\sigma R}$, the spectrum has a blue tilt for $w_\sigma > 1/3$ and a red tilt for $w_\sigma < 1/3$.

- For wave numbers $k_{\sigma R} < k < k_{re}$: These range of wave numbers reenter the Hubble radius during the first epoch of radiation domination. Hence, we can expect the spectrum of GWs to be scale invariant over this range. It is important to recognize that the amplitude of the spectrum $\Omega_{GW}(k)$ over this range will be greater or lesser than the amplitude over $k < k_\sigma$ (i.e. over wave numbers which reenter the Hubble radius during the second epoch of radiation domination) depending on whether the EoS parameter w_σ (characterizing the second phase of reheating) is greater than or less than 1/3.

- For wave numbers $k_{re} < k < k_f$: These correspond to wave numbers that reenter the Hubble radius during the first phase of reheating and, as we have discussed before, the spectrum of GWs over this range of wave numbers is expected to behave as

$$\Omega_{GW}(k) \sim k^{2\,(3\,w_\phi - 1)/(3\,w_\phi + 1)}. \tag{4.74}$$

In other words, the corresponding spectral index is given by $n_{GW} = 2\,(3\,w_\phi - 1)/(3\,w_\phi + 1)$, which has a blue or red tilt depending on whether w_ϕ is greater than or less than 1/3.

The behavior we have highlighted above can be clearly seen in Fig. 4.8 wherein we have plotted the quantity $\Omega_{GW}(f)$ in scenarios involving the second phase of reheating. In arriving at the plots in the figure, we have set the inflaton the EoS parameter to be $w_\phi = 0$ and have assumed that $T_{\sigma R} = 1\,\mathrm{GeV}$. Note that, for a given inflaton EoS parameter w_ϕ, we have two parameters, viz. n_s and F, which control the global shape of the spectrum of GWs. We have plotted the spectrum for different values of F with a fixed value of n_s as well as for different values of n_s with a fixed F. In order to highlight the effects due to the additional generation of entropy, we have plotted the results for the limiting values of zero and unity for the EoS parameter w_σ governing the second phase of reheating. We should point that if a canonical scalar field also dominates the secondary phase of reheating, then for $V(\sigma) \propto \sigma^{2\,n}$, we have $w_\sigma = (n-1)/(n+1)$ so that for the above mentioned limiting values can be achieved for $n = 1$ and $n \to \infty$, respectively. One can also consider a more exotic, non-canonical, scalar field with a Lagrangian density of the form $\mathcal{L} \sim (\partial\sigma)^\mu - \sigma^{2\,n}$, where μ is a rational number, to drive the second phase of reheating. In such a case, it can be shown that the EoS parameter is given by (in this context, see, for example, Ref. [302])

$$w_\sigma = \frac{n - \mu}{n\,(2\,\mu - 1) + \mu}, \tag{4.75}$$

with the expression reducing to the canonical result for $\mu = 1$, as required. Such a model can lead to the extreme values of $w_\sigma = 0$ (for $n = \mu$) and $w_\sigma \simeq 1$ for $[n \simeq \mu/(1-\mu)]$ that we have considered, without unnaturally large values for a dimensionless number, as it occurs in the

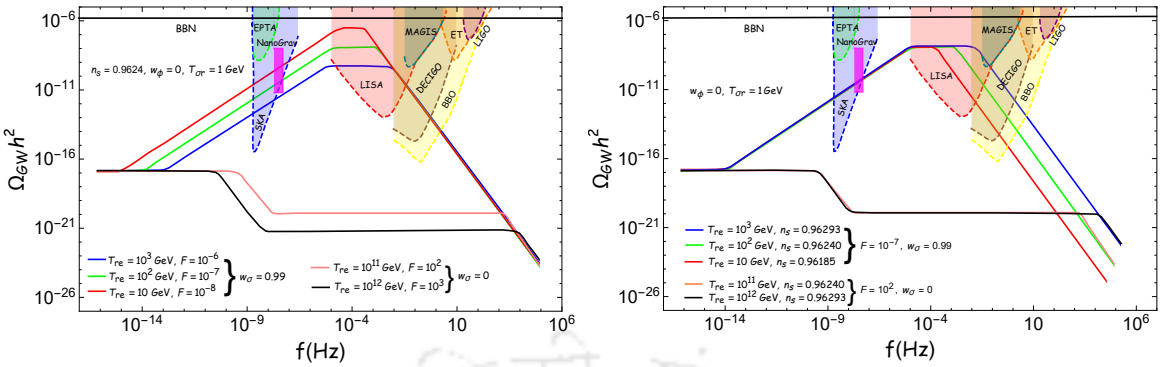

FIGURE 4.8: The spectrum of GWs observed today $\Omega_{GW}(f)$ has been plotted in the modified scenario with late time production of entropy. We have illustrated the results for the cases wherein n_s is fixed and the quantity F is varied (on the left) as well as for the cases wherein F is fixed and n_s is varied (on the right). We have set $w_\phi = 0$ and $T_{\sigma R} = 1\,\text{GeV}$ in arriving at the above plots. Also, we have considered the extreme values for w_σ to demonstrate the maximum levels of impact that the generation of entropy at late times can have on the spectrum of GWs. Interestingly, we find that for a set of values of the parameters associated the secondary phase of reheating, the spectrum Ω_{GW} can have amplitudes as suggested by the recent observations by NANOGrav [272, 273].

canonical case. It seems worthwhile to explore such models in some detail as they could have interesting phenomenological implications. We find that the effects on $\Omega_{GW}(f)$ over the range $f < f_{re}$ due to the late time creation of entropy has important implications for the recent observations by the NANOGrav mission. Recall that, recent observations by the NANOGrav mission suggest a stochastic GW background with an amplitude of $\Omega_{GW}\,h^2 \simeq 10^{-11}$ around the frequency of $10^{-8}\,\text{Hz}$ [272, 273]. Clearly, the frequency lies in the domain $f < f_{re}$. In the absence of a second phase of reheating, evidently, the amplitude of Ω_{GW} in the nano-Hertz range of frequencies is rather small, much below the sensitivity of the NANOGrav mission, as we had seen in Secs. 4.4 and 4.5. However, as we have discussed, the late time decay of an additional scalar field such as the moduli field leads to a spectrum with a blue tilt for $w_\sigma > 1/3$ over the frequency range $f_\sigma < f < f_{\sigma R}$, where f_σ and $f_{\sigma R}$ are the frequencies associated with the wave numbers k_σ and $k_{\sigma R}$. Therefore, in such a modified scenario, it is possible to construct situations that result in Ω_{GW} of the strength indicated by NANOGrav, albeit with rather large values for ω_σ and relatively low values of the reheating temperature of $10 < T_{re} < 10^3\,\text{GeV}$, as illustrated in Fig. 4.8. To motivate high values for the EoS parameter, as we mentioned, it seems interesting to consider a non-canonical model of a scalar field that leads to an EoS parameter as in Eq. (4.75). We should clarify that to avoid pathological behavior, in the model, we can consider parameters lying within the domains $n > 0$ and $\mu > 0$. In such a case, one can obtain that $w_\sigma \sim 1$ for μ in the range $0 < \mu < 1$. Moreover, note that, in the modified scenario with late time entropy production, to be compatible with the NANOGrav results, the reheating temperature T_{re} has to be less than $10^3\,\text{GeV}$, which implies a low decay width for the inflaton. Further, from Fig. 4.8, it can be easily seen that the modified scenario can be strongly constrained by many of the forthcoming GW observatories such as SKA, BBO, LISA and DECIGO.

In the pulsar-timing data considered by NANOGrav, the spectrum of the characteristic

strain $h_c(f)$ induced by the GWs is assumed to be a power law of the form [272, 273]

$$h_c(f) = A_{CP} \left(\frac{f}{f_{yr}}\right)^{(3-\gamma_{CP})/2}, \tag{4.76}$$

where A_{CP} refers to the amplitude at the reference frequency $f_{yr} = 1\,\mathrm{yr}^{-1} = 3.17 \times 10^{-8}\,\mathrm{Hz}$, and γ_{CP} is the timing-residual cross-power spectral density. The dimensionless energy density of GWs today $\Omega_{GW}(f)$ is related to characteristic strain $h_c(f)$ induced by the GWs through the relation (in this context, see the recent review [303])

$$\Omega_{GW}(f) = \frac{2\,\pi^2\,f^2}{3\,H_0^2}\,h_c^2(f). \tag{4.77}$$

Upon utilizing the form (4.76) for the characteristic strain, the energy density of GWs today can be expressed in terms of the amplitude A_{CP} and the index γ_{CP} as follows:

$$\Omega_{GW}(f) = \frac{2\,\pi^2\,f_{yr}^2}{3\,H_0^2}\,A_{CP}^2\left(\frac{f}{f_{yr}}\right)^{5-\gamma_{CP}}. \tag{4.78}$$

As we have discussed above, in the scenario with late time entropy production, it is the power associated with the modes that reenter the Hubble radius during the secondary phase of reheating that are consistent with the NANOGrav results [cf. Fig. 4.8]. Over this domain of wave numbers, since the index of the spectrum of GWs is given by $n_{GW} = 2\,(3\,w_\sigma - 1)/(3\,w_\sigma + 1)$, where w_σ is the EoS parameter describing the secondary phase of reheating, clearly, we can set $\gamma_{CP} = 5 - n_{GW}$. We can utilize the constraints from the NANOGRav results on the parameters A_{CP} and γ_{CP} to arrive at the corresponding constraints on, say, the EoS parameter w_σ and the reheating temperature T_{re} associated with the primary phase. We have illustrated these constraints in Fig. 4.9. We have illustrated the constraints for the two possibilities, viz. with the reheating temperature T_{re} associated with the primary phase fixed and the EoS parameter w_σ describing the secondary phase of reheating varied as well as with w_σ fixed and T_{re} varied. These constraints suggest that only low reheating temperatures (say, $T_{re} < 10\,\mathrm{GeV}$) and very high values of the EoS parameter w_σ (with $w_\sigma \simeq 1$) are compatible with the NANOGrav data.

4.9 Conclusions

In this chapter, we have attempted to understand the effects of reheating on the spectrum of primordial GWs observed today. As a specific example, we had considered the so-called α-attractor model of inflation and had evolved the tensor perturbations from the end of inflation through the epochs of reheating and radiation domination to eventually arrive at the spectrum of GWs today. Moreover, we had considered two different scenarios to achieve reheating. In the first scenario, the epoch is described by a constant EoS parameter w_ϕ and the transition to radiation domination is expected to occur instantaneously [45]. Such simpler modeling of the reheating mechanism allowed us to study the evolution of the GWs analytically. In the second and more realistic scenario of perturbative reheating wherein the evolution of the energy densities are governed by the Boltzmann equations, the inflaton decays gradually and the transition to the epoch of radiation domination occurs smoothly. The effective EoS parameter in such a scenario changes continuously from its initial value of $w_{\mathrm{eff}} = w_\phi$ to the final value

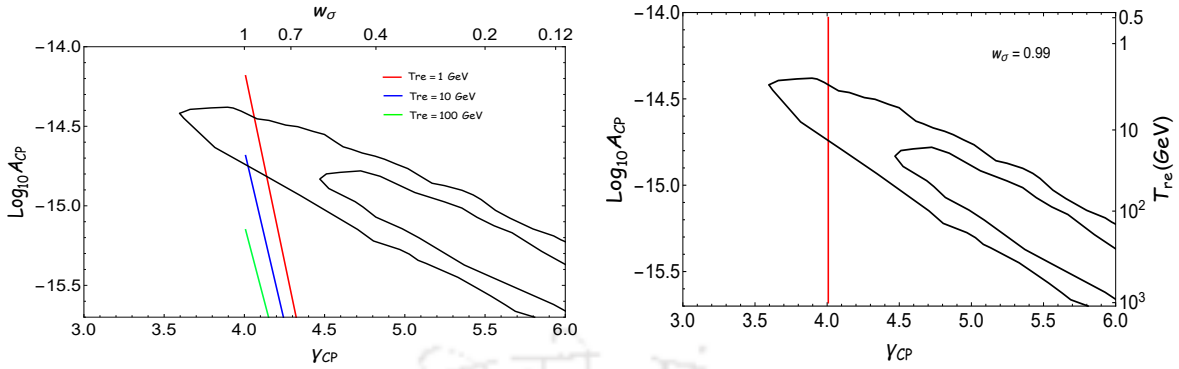

FIGURE 4.9: The constraints from NANOGrav on the parameters $A_{\rm CP}$ and $\gamma_{\rm CP}$ have been utilized to illustrate the corresponding constraints on the EoS parameter w_σ describing the secondary phase of reheating and the reheating temperature T_{re} associated with the primary phase. In the figures, we have included the 1-σ and 2-σ contours (in black) arrived at by the NANOGrav analysis based on the five-frequency power-law fit [272]. We have projected the results into the $\gamma_{\rm CP}$-$A_{\rm CP}$ plane for the following two possibilities: (i) a scenario wherein T_{re} is fixed and the parameter w_σ is varied (on the left), and (ii) a scenario wherein w_σ is fixed and T_{re} is varied (on the right). Note that we have assumed that $w_\phi = 0$ and $T_{\sigma R} = 0.1\,\mathrm{GeV}$ in arriving at the above plots.

of $w_{\rm eff} = 1/3$. As it proves to be difficult to obtain analytical solutions in the perturbative reheating scenario, we examined the problems at hand numerically.

Note that we are interested in the spectrum of GWs today over scales that are considerably smaller than the CMB scales. These scales reenter the Hubble radius either during the phase of reheating or during the epoch of radiation domination. In both the models of reheating we have considered, the spectrum of GWs today $\Omega_{GW}(f)$ is scale-invariant over wave numbers that reenter the Hubble radius during the epoch of radiation domination (i.e. for $k < k_{re}$). The scale invariant amplitude over this domain can help us extract the inflationary energy scale in terms of the present radiation abundance since $H_I^2/M_p^2 \sim 6\,\pi^2\,\Omega_{GW}/\Omega_{\rm R}$ [cf. Eq. (4.46)]. The spectrum of GWs today has a tilt over wave numbers $k_{re} < k < k_f$ which reenter the Hubble radius during the phase of reheating. The spectral tilt $n_{GW} = 2\,(3\,w_\phi - 1)/(3\,w_\phi + 1)$ is red or blue depending on whether $w_\phi < 1/3$ or $w_\phi > 1/3$. Clearly, the observation of the tilt will allow us to determine the reheating parameters such as the EoS parameter w_ϕ and the reheating temperature T_{re}. These will allow us to determine the behavior of the inflaton near the minimum of the potential. Moreover, the constraint on the reheating parameters, in turn, can help us constrain the inflationary parameters such as the scalar spectral index n_s. Further, in the realistic perturbative reheating scenario, there arises an important feature in the spectrum of GWs around wave numbers that reenter the Hubble radius towards the end of the phase of reheating. The spectrum exhibits distinct oscillations near the frequency f_{re} and we find that the width of the oscillation reflects the time scale over which the EoS parameter changes from the inflaton dominated value of w_ϕ to that of 1/3 in the radiation dominated epoch (cf. Figs. 4.3 and 4.4). In fact, the peak of the oscillation occurs at f_{re}, which can be associated with the end of perturbative reheating (i.e. when $H = \Gamma_\phi$). We find that, at this instant, the rate of change of the effective EoS parameter exhibits a maximum. This can help us further in determining the inflaton decay rate Γ_ϕ in terms of the observed

quantities, as expressed in Eq. (4.51). The end of reheating is to be followed by the most important stage of thermalization. From the width of the oscillation in the spectrum, one can extract information about thermalization time scale $\Delta t_{\rm th}$ [cf. Eq. (4.58)] as well as the nature of the thermalization process depending upon over-occupied or under occupied initial state set by the end of reheating [cf. Eq. (4.60)]. It turns out that the ratio of the thermalized particle density to the initial decaying particle density (i.e. $n_{\rm th}/n_{\rm i}$) depends on the inflaton mass, inflationary energy scale and the wave numbers k_{re} and k_f. Therefore, given the inflaton mass, the spectrum of primordial GWs at the present epoch can be utilized to determine the ratio $n_{\rm th}/n_{\rm i}$, which is one of the important parameters describing the thermalizing plasma. Once the value of $n_{\rm th}/n_{\rm i}$ is extracted, the strength of the gauge interaction, say, α, among the reheating decay products can be obtained [cf. Eq. (4.61)]. We should mention that the oscillatory feature in the spectrum of GWs is encountered for all possible values of w_ϕ and T_{re}. We find that the range of frequencies around which the oscillations arise shifts towards higher frequencies as the reheating temperature increases. This can be attributed to the fact that, for a higher value of T_{re}, the duration of reheating proves to be shorter and, as a result, the wave number k_{re} which reenters at the end of reheating becomes larger.

Apart from the effects due to the standard phase of reheating, we had also considered the signatures on the spectrum of GWs due to a secondary phase of reheating. Such a secondary phase can arise due to the decay of additional scalar fields such as the moduli fields, which can lead to the production of entropy at late times. The moduli-dominated phase, which can be described by a constant EoS parameter w_σ (as the primary phase of reheating), leads to a tilt in the spectrum over the range of wave numbers that reenter the Hubble radius during the epoch. Remarkably, we have shown that for $w_\sigma > 1/3$ and certain values of the reheating temperature, the production of entropy at late times can lead to $\Omega_{GW}(k)$ that correspond to the strengths of the stochastic GW background suggested by the recent NANOGrav observations [272, 273]. We should clarify that such a possibility cannot arise in the conventional reheating scenario wherein the entropy remains conserved from the end of reheating until the present epoch. In fact, the assumption of the secondary phase of reheating and the NANOGrav observations indicate a low reheating temperature of $T_{re} \lesssim 10^3$ GeV. We are currently examining different models to understand the wider implications of such interesting possibilities.

Gravitational production during reheating phase: the possibility of purely Gravitational reheating 5

> *"You sometimes speak of gravity as essential and inherent to matter. Pray do not ascribe that notion to me, for the cause of gravity is what I do not pretend to know, and therefore would take more time to consider of it."*
>
> *Isaac Newton*

In this chapter, we systematically develop a new reheating scenario where minimal gravitational interaction plays an important role which was ignored in the literature due to its supposedly weak strength. So far, our discussions were mainly focused on the reheating scenarios where direct couplings among inflaton and daughter fields are free parameter and hence naturally lacks robust cosmological predictions. In this section, we take a systematic approach toward building a reheating scenario that can provide model-independent observable predictions. We shall start our discussion in the dark matter (DM) sector first, where it is assumed to be produced from both inflaton and radiation bath through minimal gravitational interaction only. Since the gravitational production process is always present, we can't ignore this. However, to achieve the radiation-dominated universe, we introduce arbitrary coupling between inflaton and standard model particles. Subsequently, we remove this arbitrariness and switch off all possible unknown parameters, which implies the inflaton sector is coupled with the observable sector only through gravitational interaction. Interestingly, only gravitational interaction turned out to be enough to reheat our universe successfully.

Cosmological observation over more than half a century made us believe that the observable universe is made of visible and invisible components [24, 29, 42, 67–69, 247, 248]. Regarding the visible components, we have acquired and inculcated a great deal of knowledge about its very existence and fundamental properties. However, apart from the existential evidences through multiple observations such as galaxy rotation curve, large scale structure, CMB [29, 304–308], invisible components are far from our present understanding. Dark matter is one of the invisible components which attracts lot of attention due to its seemingly unavoidable entente with the visible components in quantum field theoretic framework [107, 108, 110–112, 114–117, 309–321]. Even though very few effective field theory parameters such as mass and cross-section are

sufficient to explain the very existence of dark matter (DM), ignorance/non-detection[322–326] of its fundamental characters may seem indicative to suffering of going beyond the present framework of experimental and theoretical approaches [327–330]. List of conventional particle physics approaches towards DM production being nearly exhaustive, ideas of gravitational mechanism of dark matter [331–342] seems to suggest that simplest possibilities going beyond the convention, still have a lot of unexplored provisions. Gravity so far plays an extremely passive role in understanding the physical properties of standard model particles. However, difficulties in incorporating gravity in the quantum field theory framework are due to fundamental reason. Nevertheless, based on our present understanding, the physical laws depend on the energy scale of interest. At low energy ($\lesssim 1$ TeV), the SM particles may have effectively isolated themselves from gravity as long as their fundamental properties are concerned. At high energy, however, this must not be true; rather, particles and gravity may not have independent identities on their own. String theory is an elegant example that subscribes to such an idea. The gravitational production of dark matter may fall along this line of thought. At the classical level, Einstein's equivalence principle suggests that gravity universally couples with particles irrespective of their intrinsic properties except for mass. However, suppose we tend to apply this at the quantum level, where two different particle sectors are coupled through gravitons. In that case, the production cross-section does depend on intrinsic properties such as spin and charge, hence violating the equivalence principle. In this section, we start our discussion one of such scenarios where DM is produced through inflaton annihilating into fermion/bosonic through s-channel graviton exchange. Given an inflationary model, our focus will be on the reheating phase of the universe. Reheating phase with matter domination has already been studied [334, 335]. We generalize such a study for an arbitrary reheating equation of state. We also include the effect of production from the radiation bath for completeness. Hence, the produced dark matter will have thermal and non-thermal components that are generically non-cold in nature. These different production mechanisms of non-cold DM lead us to further study in detail their phase-space distribution depending upon the reheating equation of state. We will see how depending upon the type of dark matter, the distribution function contains distinct features and its dependence on the reheating equation of state. Those properties play a significant role in the clustering of matter on galactic and sub-galactic scales. Observing those small scale matter power spectrum by mapping the Lyman-α [343–350] forest of absorption lines of light from low redshift ($z = 2 - 4$) quasars can differentiate different non-cold DM production mechanism and its intrinsic properties. [351–353].

After successfully generating the present dark matter abundance through gravitational production during the reheating phase, a natural question we can ask: *is it possible to reheat our universe purely gravitationally?*. Surprisingly, such a scenario has turned out to be possible because the energy scale of any physical processes during reheating could be as large as $\sim 10^{15}$ GeV, and that leads gravity mediated decay process to become strong enough to reheat the universe. This is the possibility we will also explore in this chapter. We will name it gravitational reheating (GRe). In this phase, DM mass is the only free parameter except, of course, the inflationary parameters. We will see how such less freedom naturally makes GRe a unique mechanism as compared to reheating scenarios discussed so far in the literature [4, 10, 45]. All the massless decay products from inflaton will be collectively called radiation, and massive ones are DM. Given the present state of the universe, we showed that the GRe scenario was consistent with a very limited class of inflation models and a narrow range of DM masses. However, if DM couples with the radiation bath, gravitational production sets the maximum limit on the DM mass [354]. It is the s-channel graviton exchange process through

which inflaton converts its energy to radiation and DM during reheating. Gravitaton exchange processes between radiation bath and DM will be ignored due to its sub-dominant contribution (see detailed study in [340, 354, 355]).

5.1 Gravitational dark matter production

After the period of exponential expansion, the inflaton field begins to oscillate around its minima with decaying amplitude. In the framework of quantum field theory, the time-dependent inflaton field can naturally decay into various daughter fields such as radiation, dark matter particles, etc. However, the decay process non-trivially depends on the inflaton coupling with those daughter fields. In order to have successful reheating, the inflaton is generically assumed to have direct coupling with the radiation field, which will be the dominating component after the end of reheating. However, we discuss the situation when all the interactions are purely gravitational in section 5.2.

In this section, we first describe the framework of such a scenario. For completeness, dark matter is assumed to be produced both from the radiation bath with a thermal-averaged cross-section $\langle\sigma v\rangle$ as a free parameter and from the gravitational decay of the inflaton field. The gravitational production of dark matter has been proved to be dominated by the annihilation of inflaton zero modes through the s-channel graviton exchange process; namely, $\phi\phi \to SS/ff/XX$, where ϕ is the inflaton and S, f, and X indicate scalar, fermionic and vector dark matter, respectively [337–339]. The interaction Lagrangian for s-channel gravitational production of dark matter can be universally described by the coupling of the dark matter energy-momentum tensor $T^{\mu\nu}$ with the tensor metric perturbation $h_{\mu\nu}$ as [331–333]

$$\mathcal{L} = \frac{1}{2M_p}\left(h_{\mu\nu}T^{\mu\nu}_{\phi} + h_{\mu\nu}T^{\mu\nu}_{S/f/X}\right) \quad . \tag{5.1}$$

Associated with this action, the corresponding decay widths can be calculated as [334, 336]

$$\Gamma_{\phi\phi\to SS} = \frac{\rho_\phi\, m_\phi}{1024\,\pi\, M_p^4}\left(1+\frac{m_s^2}{2\,m_\phi^2}\right)^2\sqrt{1-\frac{m_s^2}{m_\phi^2}} \quad , \tag{5.2}$$

$$\Gamma_{\phi\phi\to ff} = \frac{\rho_\phi\, m_f^2}{4096\,\pi\, M_p^4\, m_\phi}\left(1-\frac{m_f^2}{m_\phi^2}\right)^{\frac{3}{2}} \quad , \tag{5.3}$$

$$\Gamma_{\phi\phi\to XX} = \frac{\rho_\phi\, m_\phi}{32768\,\pi\, M_p^4}\sqrt{1-\frac{m_X^2}{m_\phi^2}}\left(4+4\,\frac{m_X^2}{m_\phi^2}+19\,\frac{m_X^4}{m_\phi^4}\right) \quad . \tag{5.4}$$

Where $m_{s/f/X}$ is the mass of the scalar, fermionic, and vector dark matter, respectively, and the effective mass of the inflaton is symbolized as m_ϕ. At this point, we would like to point out that gravitational production of dark matter from radiation is also possible, and the production rate per unit time per unit volume is followed by Eq.(5.18). Such production is strongly suppressed compared to the production from inflaton, which we have shown in sec-5.1.5 . However, for high reheating temperature $10^{15} \gtrsim T_{re} \gtrapprox 10^{13}$ GeV, fermion type dark matter gravitationally produced from the radiation bath has been observed to satisfy correct abundance in a certain range of fermion mass. We have numerically checked the result, which is shown in Fig.5.7. We will not include this possibility in detail in our subsequent mathematical discussions. However, we will describe the numerical results of such a scenario as we go along.

5.1.1 Boltzmann Framework

Let us discuss the setup for the gravitational production of dark matter in the context of conventional reheating dynamics where the inflaton decays into radiation with a constant decay width Γ_ϕ to reheat our universe. In this regard the Boltzmann equations for three density components for inflaton ρ_ϕ, radiation ρ_R, and the total dark matter number density $n_Y = \left(n_Y^r + n_Y^\phi\right)$ can be written as [4, 91, 270]

$$\dot{\rho}_\phi + 3\,H\,(1+\omega_\phi)\,\rho_\phi + (\,\Gamma_\phi + \Gamma_{\phi\phi\to YY}\,)\,\rho_\phi\,(1+\omega_\phi) = 0 \quad , \tag{5.5}$$

$$\dot{\rho}_R + 4\,H\,\rho_R - \Gamma_\phi\,\rho_\phi\,(\,1+\omega_\phi\,) - 2\,\langle\sigma v\rangle\,\langle E_Y\,\rangle^r\left[\,(n_Y^r)^2 - \left(n_Y^{eq}\right)^2\,\right] = 0 \quad , \tag{5.6}$$

$$\dot{n}_Y^r + 3\,H\,n_Y^r + \langle\sigma v\rangle\,\left[\,(n_Y^r)^2 - \left(n_Y^{eq}\right)^2\,\right] = 0 \quad , \tag{5.7}$$

$$\dot{n}_Y^\phi + 3\,H\,n_Y^\phi - \frac{\rho_\phi\,(\,1+\omega_\phi\,)}{\langle E_Y\,\rangle^\phi}\,\Gamma_{\phi\phi\to YY} = 0 \quad , \tag{5.8}$$

where n_Y^r and n_Y^ϕ are the DM number density gravitationally produced from the thermal bath and the decay of the inflaton field, respectively. $\langle\,E_Y\,\rangle^r = \sqrt{m_Y^2 + (3\,T_{rad})^2}$ and $\langle\,E_Y\,\rangle^\phi = \sqrt{m_Y^2 + m_\phi^2}$ are the average energy per dark matter particle produced from the thermal bath [4] and inflaton decay respectively. The equilibrium number density of the dark matter particles can be expressed by the modified Bessel function of the second kind as,

$$n_Y^{eq} = \frac{\tilde{g_Y}\,T_{rad}^3}{2\,\pi^2}\left(\frac{m_Y}{T_{rad}}\right)K_2\left(\frac{m_Y}{T_{rad}}\right) \quad , \tag{5.9}$$

Additionally, the energy associated with each gravitationally produced dark matter particle can be calculated from the energy and momentum conservation of the annihilation-like $\phi\phi \to SS/ff/XX$ process as

$$0 = p_1 + p_2 \;\;;\;\; 2\,m_\phi = \sqrt{p_1^2 + m_Y^2} + \sqrt{p_2^2 + m_Y^2} = 2\,\sqrt{p_1^2 + m_Y^2} \quad . \tag{5.10}$$

Here p_1 and p_2 are the momenta of two gravitationally produced dark matter particles. The above equations assume the fact that the homogeneous background inflaton is at rest, and hence the energy stored in each gravitationally produced dark matter particle will be of the order of m_ϕ. In order to solve the above set of Boltzmann equation we define the following dimensionless variables corresponding to different energy components,

$$\Phi = \frac{\rho_\phi\,A^{3\,(\,1+\omega_\phi\,)}}{(\,m_\phi^{end}\,)^4} \;,\; R = \frac{\rho_R\,A^4}{(\,m_\phi^{end}\,)^4} \;,\; Y^r = \frac{n_Y^r\,A^3}{(\,m_\phi^{end}\,)^3} \;,\; Y^\phi = \frac{n_Y^\phi\,A^3}{(\,m_\phi^{end}\,)^3} \quad . \tag{5.11}$$

Where, $A = a/a_{end}$ and m_ϕ^{end} are the normalized scalar factor and the effective mass of the inflaton field at the end of the inflation respectively.
We will focus our analysis on considering a class of inflationary model called the α-attractor model [32, 33], which unifies the large class of inflationary models parameterized by α and n. The details of this model are given in sec-1.4.3. One of the important parameters, the inflaton mass m_ϕ can be calculated from the second derivative of the inflaton potential. Since reheating happens near the minimum of the potential we first expand the inflaton potential Eqn.(1.130) in the limit of $\phi << M_p$ as

$$V(\phi) \simeq \lambda\,\phi^{2n}\,, \tag{5.12}$$

where $\lambda = \Lambda^4 \left(\sqrt{\frac{2}{3\,\alpha}}\,\frac{1}{M_p}\right)^{2n}$. Therefore,

$$m_\phi^2 = V''(\phi_0(t)) \simeq 2n\,(\,2n-1\,)\,\lambda^{\frac{1}{n}}\,\rho_\phi^{\frac{n-1}{n}} \tag{5.13}$$

In order to derive the above expression, we assume that the instantaneous value of the $\phi_0(t)$ fulfills the following relation

$$\rho_\phi(t) = V(\phi_0(t)) \tag{5.14}$$

The methodology concerning the standard perturbative scenarios is discussed in section-2.1.2.1. Furthermore, cosmological observation on the dark matter abundance $\Omega_Y h^2$ provides aconstraint relation as [2, 102]

$$\Omega_Y h^2 = m_Y\,\frac{\left(Y^r(A_F) + Y^\phi(A_F)\right)}{R\,(A_F)}\,\frac{T_F\,A_F}{T_{now}\,m_\phi^{end}}\,\Omega_r h^2 \;= 0.12 \quad , \tag{5.15}$$

where the present day radiation abundance $\Omega_R h^2 = 4.3 \times 10^{-5}$ and T_F is the radiation temperature determined at a very late time A_F, when both comoving radiation and dark matter energy density became constant. Solving Boltzmann equations and utilizing the conditions mentioned in Eqs.(2.6), (5.15), we can constrain the dark matter parameters $(\langle\,\sigma v\,\rangle,\, m_Y)$ in terms of (T_{re}, n_s). The dark matter particles produced from radiation bath populated the early universe with two possible mechanisms: 1) The produced dark matter particles reach thermal equilibrium, and as the temperature falls below the dark matter mass, the number density of dark matter freezes out. This mechanism is referred to as the freeze-out mechanism [132, 137, 356–361]. 2) The interaction of the dark matter particles with radiation bath could be too weak to attain thermal equilibrium before it freezes out. This mechanism is referred to as the freeze-in [362] mechanism, and the produced dark matter particles are generally known as feebly interacting dark matter (FIMP) [107, 108, 110–112, 114–117, 312]. For the gravitationally produced dark matter freeze-in mechanism will be effective, and dark matter produced from the radiation bath will have both possibilities of freeze-in and freeze-out production. However, we will consider the freeze-in mechanism for dark matter in both cases.

5.1.2 Constraining the dark sector

As already emphasized in the beginning, the production of gravitational dark matter is an interesting, physically motivated scenario that needs detailed exploration. Following the references on gravitational dark matter [331–334, 336], in this chapter we explore the observationally viable dark matter scenarios in terms of different inflationary models. Important reheating parameters such as the equation of state ω_ϕ associated with the inflaton potential and reheating temperature T_{re} will play an important role in constraining the parameters such as the maximum possible mass of the dark matter. Moreover, since we consider the dark matter production from the radiation bath, we also place constraints on the average cross-section times velocity $\langle\,\sigma\,v\,\rangle$. The dark sector may have different possibilities in terms of the nature of the dark matter and the number of components.

5.1.3 Single component dark matter

In our present framework, we have two different underlying production mechanisms. To understand the construction from each, one examines the evolution of different density components

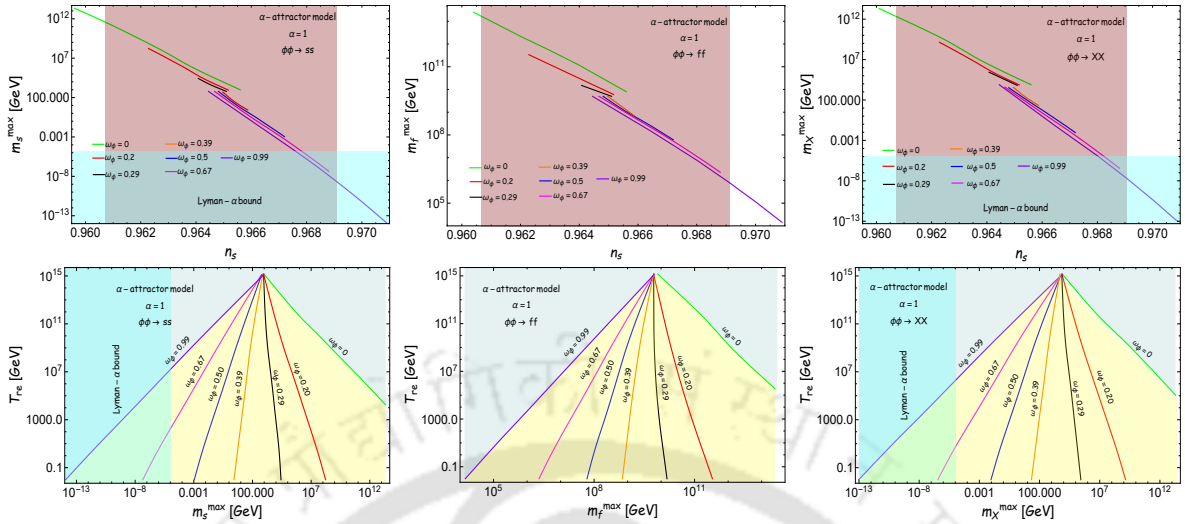

FIGURE 5.1: Upper panel: The variation of the maximum allowed values of the dark matter mass (m_Y^{max}) as a function of the scalar spectral index (n_s) corresponding to the fixed value of the dark matter abundance $\Omega_Y h^2 \simeq 0.12$ for the cases wherein $\omega_\phi = (0, 0.2, 0.29, 0.39, 0.5, 0.67, 0.99)$ (in green, red, black, orange, blue, magenta, and purple). We have considered the scenario where the $\alpha-$ attractor model describes the inflationary dynamics. We have indicated the $1-\sigma$ range of spectral index n_s (as the violet band) associated with the constraints from the Planck [29]. Further, the sky blue band corresponds to the dark matter masses lighter than 10 KeV, indicating the Lyman-α bound [350, 363]. Lower panel: We have illustrated the variation of the reheating temperature as a function of the maximum allowed dark matter mass for seven different values of ω_ϕ covering the entire possible range of ω_ϕ (0, 1). Further, the yellow region shows the allowed parameters space, whereas the light green indicates the forbidden region.

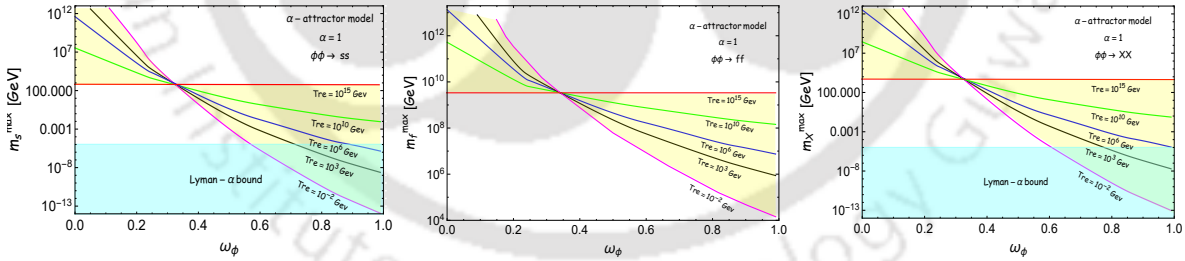

FIGURE 5.2: The variation of the maximum allowed dark matter mass m_Y^{max} over a range of inflaton equation of state $\omega_\phi = (0, 1)$ for five different values of the reheating temperature $T_{re} = (10^{-2}, 10^3, 10^6, 10^{10}, 10^{15})$ GeV (showed in magenta, black, blue, green, and red). The sky blue band indicates restriction from Lyman-α observations, and the yellow shaded region indicates the allowed parameters in $m_Y^{max} - \omega_\phi$ plane.

during reheating, as shown in Fig.5.3. The production of dark matter components due to gravity mediation will naturally occur at the very beginning of the reheating phase when the inflation energy density is maximum, and this is depicted by the green curve. On the other hand, the dark matter production from the radiation bath will follow the evolution of radiation itself which is depicted by a solid red curve. Therefore, maximum production will naturally

Table 5.1: Different inflaton equation of state, associated bound on scalar spectral index (n_s), reheating temperature T_{re} (measured in units of GeV) and dark matter mass m_Y (measured in units of GeV), considering purely gravitational production of dark matter.

Parameters	$\omega_\phi = 0$		$\omega_\phi = 0.5$		$\omega_\phi = 0.99$	
	$\phi\phi \to SS$	$\phi\phi \to ff$	$\phi\phi \to SS$	$\phi\phi \to ff$	$\phi\phi \to SS$	$\phi\phi \to ff$
n_s^{min}	0.9596	0.9604	0.9648	0.9648	0.9645	0.9645
n_s^{max}	0.9656	0.9656	0.9672	0.9672	0.9676	0.9700
T_{re}^{min}	1.8×10^4	3.5×10^5	10^{-2}	10^{-2}	1.4×10^7	10^{-2}
T_{re}^{max}	10^{15}	10^{15}	10^{15}	10^{15}	10^{15}	10^{15}
m_Y^{max}(min)	960	8.0×10^9	1.1×10^{-3}	6.1×10^7	10^{-5}	1.4×10^4
m_Y^{max}(max)	m_ϕ^{end}	m_ϕ^{end}	600	5.0×10^9	640	6.0×10^9

Table 5.2: Different reheating temperatures, associated bound on inflaton equation state ω_ϕ, and dark matter mass m_Y (measured in units of GeV), considering only gravitationally produced dark matter.

Parameters	$T_{re} = 10^{-2}$ GeV		$T_{re} = 10^3$ GeV		$T_{re} = 10^{10}$ GeV	
	$\phi\phi \to SS$	$\phi\phi \to ff$	$\phi\phi \to SS$	$\phi\phi \to ff$	$\phi\phi \to SS$	$\phi\phi \to ff$
ω_ϕ^{min}	0.11	0.15	0.05	0.09	0.0	0.0
ω_ϕ^{max}	0.56	1.0	0.71	1.0	1.0	1.0
m_Y^{max} (min)	10^{-5}	1.4×10^4	10^{-5}	8.7×10^5	9.2×10^{-3}	1.4×10^8
m_Y^{max} (max)	m_ϕ^{end}	m_ϕ^{end}	m_ϕ^{end}	m_ϕ^{end}	3.5×10^7	5.2×10^{11}

occur near the end of reheating, as depicted by the solid black line. Finally, combining both the gravitational production and production from radiation bath will contribute to the current dark matter abundance. An interesting aspect of such products of the same type of dark matter from two different mechanisms is that it will lead to a mixture of components with different velocity distribution, whose density perturbation may grow differently and provide distinct signatures in the small-scale structure, which will be studied in our future publication.

Anyway, for the case of a purely gravity-mediated scenario, the mass of the dark matter is the only parameter. Therefore, in this scenario reheating dynamics is controlled by two parameters (Γ_ϕ, m_Y) and two constraints relations Eq.(2.6), (5.15). Hence, the dynamics

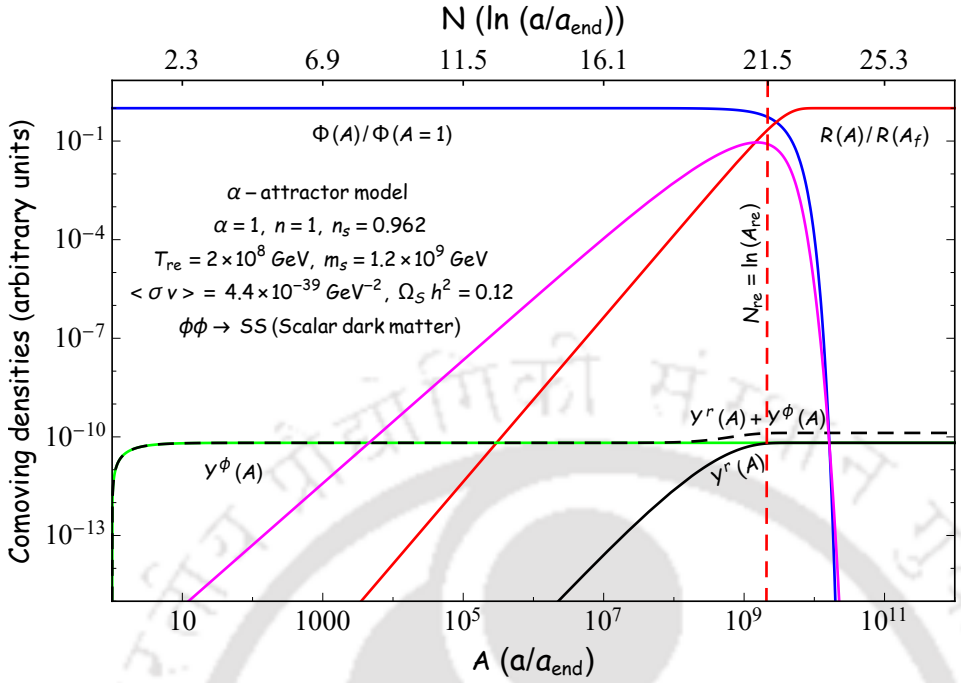

FIGURE 5.3: We have plotted the evolution of the different energy components (inflaton, radiation) and the number density of dark matter as a function of the normalized scale factor (alternatively, the e-folding number is counting after the inflation) for $\alpha-$ attractor model with $\alpha = 1$. The blue and red curve indicates the variation of the comoving densities of inflaton and radiation, respectively. Further, the black and green curve shows the evolution of the comoving number densities (Y^r, Y^ϕ) in arbitrary units produced from the radiation bath and the inflaton (mediated by gravity), accordingly. Moreover, the dotted black curve shows the evolution of the total comoving dark matter number density ($Y^r + Y^\phi$), where we are taking into account both possibilities of the dark matter production.

are determined completely by the inflation model under consideration instead of the non-gravitational dark matter production scenario, which contains annihilation cross-section as an additional parameter. A large class of inflationary models such as α-attractor endows with a degenerate prediction of large-scale observables, namely, scalar spectral index (n_s) and tensor to scalar ratio (r) but with distinguishing properties in terms of their effective inflaton equation of state ω_ϕ during reheating. Such degeneracy can be lifted during reheating, considering various other observables. For example, primordial gravitational waves encode distinct signatures depending on the reheating equation of state [88, 89]. In our present analysis also for a given equation of state ω_ϕ, solely gravitationally produced dark matter will assume distinct value of its mass m_Y^{max} in compatible with dark matter abundance as can be seen in the Fig.5.1, 5.2 and the shaded yellow regions are the only allowed parameter plane which are either bounded by the value of $\omega_\phi \sim (0, 1)$ or by the minimum $T_{re}^{min} \simeq 10^{-2}$GeV set by the BBN and maximum $T_{re}^{max} \simeq 10^{15}$ GeV set by the instantaneous reheating. Therefore, simple dark matter mass produced gravitationally during reheating can give valuable information about inflaton potential. An important point we should remember is that the condition $H = \Gamma_\phi$ leads to unique reheating temperature T_{re} for a given n_s and this is precisely the reason the present dark matter abundance is satisfied for a fixed dark matter mass. However, the suffix "max" in

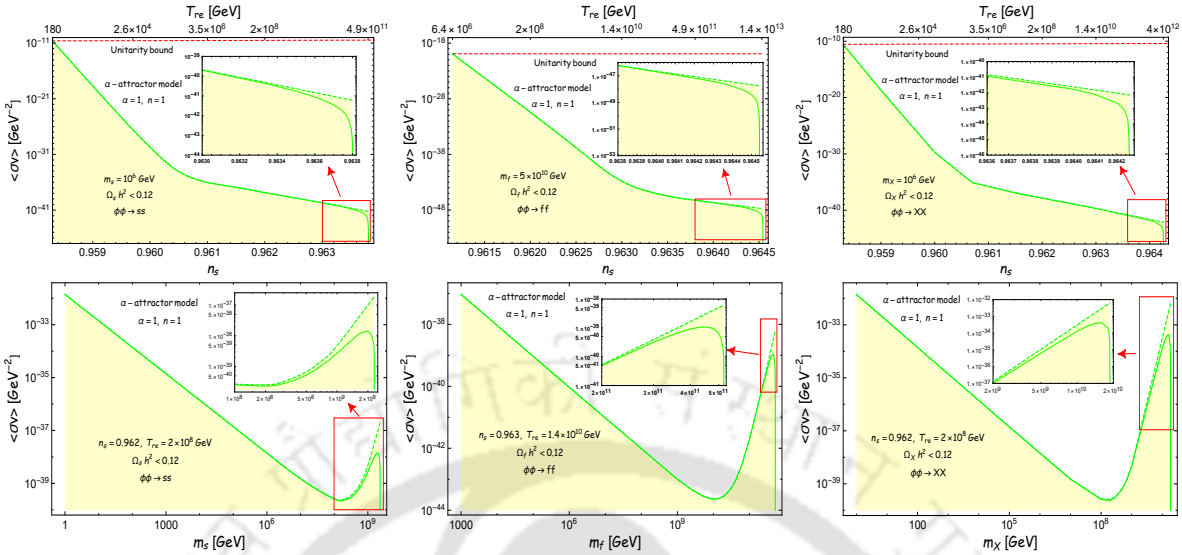

FIGURE 5.4: Upper panel : $\langle \sigma\, v \rangle$ vs. n_s plotted for three different gravitationally produced dark matter scenarios: $\phi\phi \to SS$ (scalar dark matter), $\phi\phi \to ff$ (fermionic dark matter) and $\phi\phi \to XX$ (vector dark matter) considering $\alpha-$attractor model with $\alpha = 1$, $n = 1$ (Higgs-Starobinsky model). The yellow-shaded region corresponds to the dark matter abundance $\Omega_Y h^2 \leq 0.12$. The dashed green line implied the results when we took into account one possibility: dark matter production from the radiation bath and the solid green line correspond to both possibilities: dark matter can be produced from the decay of inflaton as well as from the radiation bath. The lower limit on the spectral index is given by the perturbative unitarity limit of cross-section $\langle \sigma v \rangle_{max} = \frac{8\pi}{m_Y^2}$ (shown by the red dashed line). Whereas the upper limit is associated with that particular value of the spectral index or reheating temperature when only gravitational production of the dark matter is sufficient to produce the correct relic of the dark matter. So any value of n_s above this is excluded because this leads to an overabundance. Lower panel : Variation of $\langle \sigma\, v \rangle$ as function of dark matter mass m_Y. The upper limit on dark matter mass is associated with that particular value of the dark matter mass m_Y^{max} when only gravitational production of the dark matter is sufficient to produce the correct relic.

m_Y^{max} is due to the reason that this is the maximum possible dark matter mass in ($\langle \sigma v \rangle$ Vs m_Y) plane satisfies the abundance $\Omega_Y h^2 = 0.12$, when finite dark matter coupling with the radiation bath is included in the process; and it is in the limit $\langle \sigma v \rangle \to 0$, when $m_Y \to m_Y^{max}$ as shown in Figs. 5.4, 5.5. The generic expression of m_Y^{max} is assumed as,

$$m_Y^{max} = \frac{\mathcal{G}\,\beta\, T_{now}}{n_Y^{re}\, A_{re}^3} \left(\frac{\Omega_Y\, h^2}{\Omega_r\, h^2}\right)_{now}, \text{ where } A_{re} = \left(\frac{12\, M_p^2\, H_{end}^2\, (1+\omega_\phi)^2}{\mathcal{G}^4\, \beta\, (5-3\,\omega_\phi)^2}\right)^{\frac{-1}{(1-3\,\omega_\phi)}}. \quad (5.16)$$

The number density n_Y^{re} is calculated at the end of reheating with normalized scale factor A_{re} and associated expressions for each component are

$$n_X^{re} \approx \frac{3}{4096\,\pi} \frac{(1+\omega_\phi)}{(1+3\,\omega_\phi)} \left(\frac{H_{end}}{A_{re}}\right)^3, \quad (5.17)$$

$$n_s^{re} \approx \frac{3}{512\,\pi} \frac{(1+\omega_\phi)}{(1+3\,\omega_\phi)} \left(\frac{H_{end}}{A_{re}}\right)^3,$$

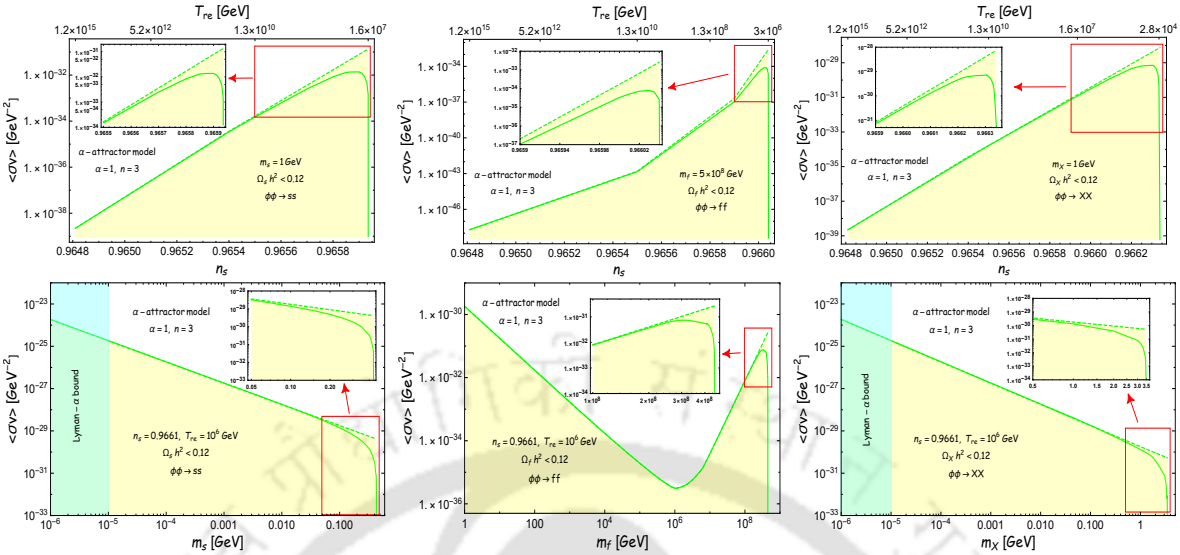

FIGURE 5.5: Upper panel : $\langle \sigma v \rangle$ vs. n_s, the description of this figure is the same as previous Fig.5.4; the main difference is that here we have plotted for $\alpha-$attractor model with $\alpha = 1$ and $n = 3$. In addition to that, the lower limit on the spectral index corresponds to instantaneous reheating ($N_{re} \to 0$). Lower panel : $\langle \sigma v \rangle$ vs. m_Y, the description of this figure is the same as previous Fig.5.4. The sky blue band indicates restriction from Lyman-α observations.

$$n_f^{re} \approx \frac{m_f^2 \, \lambda^{\frac{\omega_\phi - 1}{\omega_\phi + 1}} \, \nu(\omega_\phi)}{4096\,\pi\,(1+3\,\omega_\phi)\left(H_{end}^2 M_p^2\right)^{\frac{2\omega_\phi}{1+\omega_\phi}}} \left(\frac{H_{end}}{A_{re}}\right)^3 = \frac{3}{2048\,\pi}\,\frac{1+\omega_\phi}{1-\omega_\phi}\left(\frac{m_f}{m_\phi^{end}}\right)^2 \left(\frac{H_{end}}{A_{re}}\right)^3 .$$

We should emphasize at this point that the above expression for the dark matter mass is sensitive to (H_{end}, ω_ϕ). Detailed derivation and the associated symbols of the above expressions are given in the appendix 6.2. Any value of the dark matter mass above m_Y^{max} is excluded because of overabundance. In Fig.5.1, we have shown the allowed dark matter masses m_Y^{max} as a function of the spectral index and reheating temperature for different inflaton equations of state $\omega_\phi = (\,0,\, 0.2,\, 0.29,\, 0.39,\, 0.50,\, 0.67,\, 0.99\,)$ and assumed different single component dark matter species namely, scalar, fermion and vector. Therefore, we cover the whole possible range of inflaton equation of state $\omega_\phi = (\,0, 1\,)$ and the allowed parameter space is shown by the shaded yellow region in the $(T_{re} - m_Y^{max})$ plane. It suggests that for the entire range of inflaton equation of state between $(0, 1)$, the allowed mass of the scalar and vector dark matter must lie between $(10^{-13}, 10^{13})$ GeV. And for the fermionic dark matter, the possible range turns out to be $(10^4,\, 10^{13})$ GeV. Here, one should notice the distinct mass range allowed for the dark matter for boson and fermion. Bosonic dark matter mass can be as low as in the eV range, which can be identified as an axion-like particle . It would be interesting to study in detail in this direction. Anyway, as has already been pointed out, there is a one-to-one correspondence between the dark matter mass and the reheating temperature, we provide possible constraints on the value of $(\,n_s,\, T_{re},\, m_Y^{max}\,)$ in terms of different inflaton equations of states in Table-5.1. To determine the possible bound on the minimum value of the dark matter mass, we use the additional constraints arising from the Lyman-α forest data set, which in turn impose further restrictions on the inflationary and reheating parameters $(n_s,\, T_{re})$. Additionally, in Fig.5.2, we have shown the allowed dark matter mass as a function of the inflaton equation of state for

different sets of reheating temperature. Interestingly, depending upon the inflaton equation of state, the allowed DM mass range changes, and it shrinks to a point as ω_ϕ approaches towards 1/3. The analytic expression of that specific mass (cf. Eq.5.16 and 5.17) turned out to be dependent on the two factors, inflation energy scale H_{end} and inflaton equation of state ω_ϕ. Moreover, the possible bound on the inflaton equation of state and the mass of the dark matter for different sample values of reheating temperatures are shown in Table-5.2.

When dark matter production from radiation bath is included in the reheating process, Figs.5.4, 5.5 depict the region of allowed cross-section $\langle\sigma v\rangle$ in terms of n_s for two distinct values of the inflaton equation of state $\omega_\phi = (\,0,\, 0.5\,)$ respectively. It is clear from the figures that for finite cross-sections with $m_Y < m_Y^{max}$, the production from radiation bath is always dominating compared to that of gravitational production. However, as one approach toward m_Y^{max}, gravity-mediated dark matter production is increasingly dominated considering the fixed value of $\Omega_Y\, h^2 \simeq 0.12$. This fact entails the value of $\langle\sigma v\rangle$ approaching towards zero for not to overproduce the dark matter. Another important point is to note that for $m_Y > T_{re}$, there always exists a maximum cross-section for a given temperature once we fixed ω_ϕ. In the in-set of all the figures, we show how the cross-section is approaching zero, and gravitational dark matter contributes to the abundance. Last three plots of fig.5.4 and 5.5 also show the similar behavior in ($\langle\sigma v\rangle$ Vs m_Y) plane near the maximum possible dark matter mass.

Due to entropy conservation constraints, we generally observed that reheating temperature is sensitive to the inflationary scalar spectral index n_s. The spectral index n_s is observationally bounded with a central value [29, 364]. Because of this bounded region, one naturally obtains a limit on the reheating temperature. Furthermore, we get different bounds on this reheating temperature for different dark matter masses as all are intertwined through the reheating dynamics and inflationary dynamics. For example from fig.5.4, for $\omega_\phi = 0$ ($\omega_\phi < \omega_r$), the upper bound on the reheating temperature turns out as $T_{re}^{max} \simeq (\,4.9\times10^{11},\, 4.0\times10^{12}\,)$ GeV for scalar and vector dark matter respectively with $m_{s/X} = 10^6$ GeV, and $T_{re}^{max} \simeq 1.4\times10^{13}$ GeV for fermionic dark matter with $m_f = 5\times10^{10}$ GeV. However, for $\omega_\phi = 0.5 > 1/3$, one obtains $T_{re}^{min} \simeq (\,1.6\times10^{7},\, 2.8\times10^{4}\,)$ GeV for scalar and vector dark matter with $m_{s/X} = 1$ GeV and $T_{re}^{min} \simeq 3\times10^6$ GeV for fermionic dark matter with $m_f = 5\times10^8$ GeV. In addition to that, the lower limit on the scalar spectral index is set by the BBN temperature for those models where $\omega_\phi < 1/3$ and instantaneous reheating for $\omega_\phi > 1/3$. In the allowed range of n_s, the cross-section can not be arbitrarily large due to unitarity limit on the cross-section $\langle\,\sigma\,v\,\rangle_{max} = 8\pi/m_Y^2$. This will further constraint n_s and T_{re}. For $n = 1$ model, the lower limit on the scalar spectral index is modified due to the perturbative unitarity limit on the cross-section. Moreover, the modification on the lower limit of n_s changes the minimum allowed value of the reheating temperature. Such as for $\omega_\phi = 0$, $T_{re}^{min} \simeq (\,180,\, 6.4\times10^6\,)$ GeV for scalar/vector ($m_{s/X} = 10^6$ GeV) and fermionic dark matter ($m_f = 5\times10^{10}$) respectively.

5.1.4 Two-component dark matter

For the sake of completeness, in this section, we will briefly discuss the two-component dark matter scenario and the constraints on the parameter space. We explore possible allowed mass ranges when it is produced gravitationally. Since the behavior of scalar and vector dark matter is qualitative same, we assume the present-day abundance of total dark matter is composed of scalar and fermionic type particles. The dynamical equation will be the same as previously discussed in Eqs.(5.5)-(5.8), with no production from the radiation bath. From Fig.5.6, it is clear that not all the range of mass is allowed, and as expected, it is explicitly dependent upon

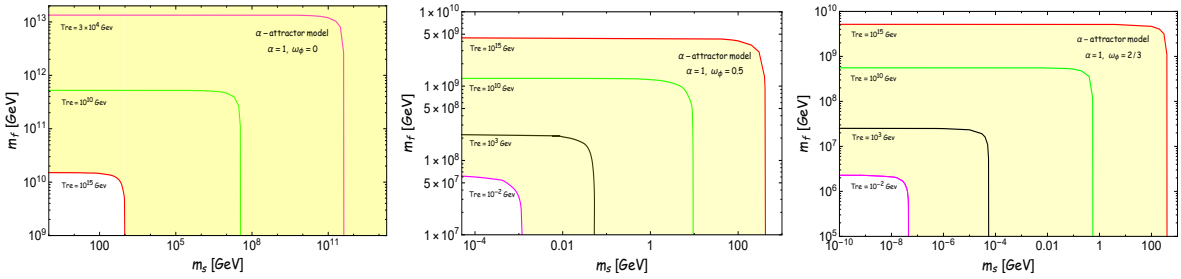

FIGURE 5.6: Two-component dark matter scenario: m_f vs. m_s were plotted for three different values of inflaton equation of state $\omega_\phi = (0,\ 0.5,\ 2/3)$ considering different reheating temperatures (shown by different colored line). Those lines corresponds to the fixed value of the present dark matter abundance $\Omega_{X(s+f)}\, h^2 \simeq 0.12$. For all the cases, we consider purely gravitationally produced dark matter. The dark matter sector consists of two sectors, one for scalar and another one for fermionic dark matter. Here the $\alpha-$ attractor model with $\alpha = 1$ describes the inflationary dynamics, and the yellow shaded region shows the allowed dark matter masses.

the reheating equation of state or rather types of the inflaton potential near its minimum. For each plot, the yellow shaded region is the allowed parameter space if we include all possibilities of reheating temperature. The region is either bounded by the maximum reheating temperature $\sim 10^{15}$ GeV, and the BBN Bound 10^{-2} GeV, or by m_Y^{max} discussed in the previous section.

An interesting observation of this analysis is that there exists a one-to-one correspondence between scalar and fermionic dark matter masses. For a fixed combination of (T_{re}, ω_ϕ), we can uniquely determine the mass of one component once another component is fixed. The maximum allowed mass for any one component is associated with the single component dark matter scenario, which we already discussed earlier. However, the minimum value of the mass approaches zero as the system starts dominated by only one component, either scalar or fermionic dark matter.

5.1.5 Comparison on gravitational DM production from inflaton and radiation bath

In our discussions so far, we considered gravitational dark matter production purely from the inflaton annihilation. However, in principle, gravitational production from the radiation bath will contribute, which we mentioned before, to be sub-leading compared to the production from inflaton. This section will show through an explicit calculation that this is indeed the case. For the case of s-channel DM production from inflaton we have decay rates in Eqs.(5.2)-(5.4). For the production of gravitational dark matter from the radiation bath during reheating has already been studied [117, 340–342], and the decay rate per unit physical volume is expressed as

$$R(T) = \gamma \frac{T^8}{M_p^4}\,, \tag{5.18}$$

where $\gamma = 1.9 \times 10^{-4}$ for scalar dark matter, $\gamma = 1.1 \times 10^{-3}$ for fermionic dark matter or $\gamma = 2.3 \times 10^{-3}$ for vector dark matter. In addition to usual inflaton and the DM component from inflation we have modified radiation dynamics and an additional dark matter production

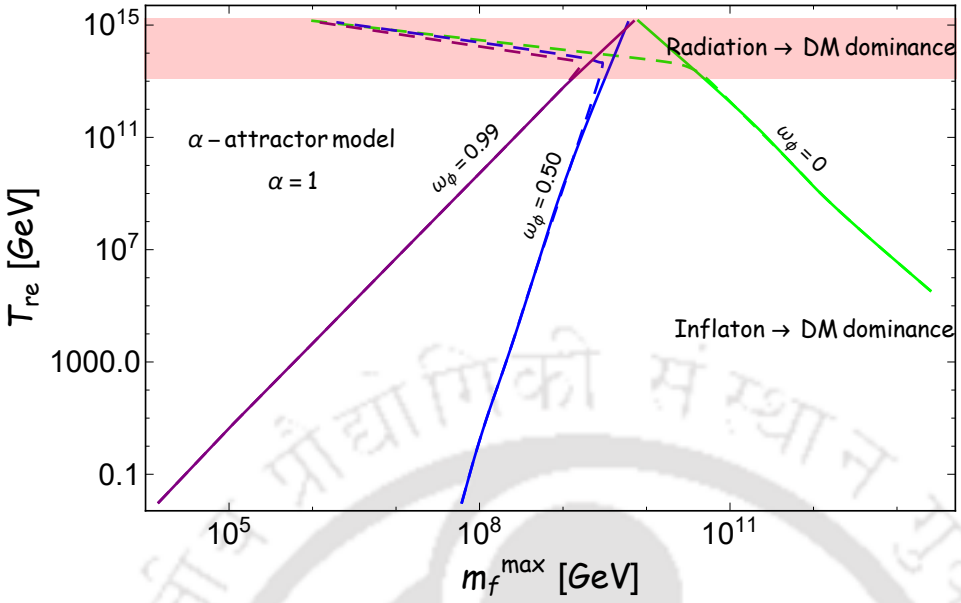

FIGURE 5.7: Variation of reheating temperature as a function of dark matter mass for two different gravitationally produced dark matter scenarios: 1) dark matter generated only from inflaton scattering (shown in solid line) 2) We took the contribution from inflaton as well as SM scattering (shown in dashed line). These results are for fermionic dark matter with three different inflaton equations of state $\omega_\phi = (0, 0.5, 0.99)$. Furthermore, the light red band indicates the dominating contribution in the dark matter relic from thermal bath over inflaton scattering.

channel from radiation bath as follows:

$$\dot{\rho}_r + 4\,H\,\rho_r - \Gamma_\phi\,\rho_\phi\,(1+\omega_\phi) + R(T)\,\langle E_Y\rangle^r = 0 \quad , \tag{5.19}$$

$$\dot{n}_{Y(R)} + 3\,H\,n_{Y(R)} - R(T) = 0 \quad , \tag{5.20}$$

where $n_{Y(R)}$ is the DM number density produced from the radiation bath due to gravitational interaction.

Now let us compare the results for dark matter production from radiation bath mediated by gravity with the production from inflaton. The associated expressions for comoving dark matter number density in terms of reheating temperature calculated at the end of reheating for different types of dark matter, produced from either inflaton or radiation bath are (see appendix 6.2)

$$\begin{aligned}
n_s^{re}\,A_{re}^3 \approx 8\,n_X^{re}\,A_{re}^3 &\approx \frac{3}{512\,\pi}\,\frac{(1+\omega_\phi)}{(1+3\,\omega_\phi)}\,\frac{\beta^2\,T_{re}^8\,e^{6\,N_{re}\,(1+\omega_\phi)}}{9\,M_p^4\,H_{end}}, \\
n_f^{re}\,A_{re}^3 &\approx \frac{3}{2048\,\pi}\,\frac{1+\omega_\phi}{1-\omega_\phi}\left(\frac{m_f}{m_\phi^{end}}\right)^2\,\frac{\beta^2\,T_{re}^8\,e^{6\,N_{re}\,(1+\omega_\phi)}}{9\,M_p^4\,H_{end}}\,, \\
n_{Y(R)}^{re}\,A_{re}^3 &\approx \frac{2\gamma}{3\,(1-\omega_\phi)}\,\frac{e^{\frac{3}{2}\,N_{re}\,(3+\omega_\phi)}\,T_{re}^8}{M_p^4\,H_{end}}\,.
\end{aligned} \tag{5.21}$$

To derive above equation, we use the following approximate relation, $H_{re}^2 = \rho_R^{re}/3\,M_p^2 = \beta\,T_{re}^8/(3\,M_p^2) = H_{end}^2\,A_{re}^{-3\,(1+\omega_\phi)}$, which indicates that at the end of reheating the universe is dominated by radiation. The dark matter production from the radiation bath is maximum when radiation temperature is maximum which is approximately equivalent to taking $N_{re} = 0$. Therefore, it would be sufficient to compare the above comoving densities for different production channels at the point of instantaneous reheating;

$$n_R^s = \frac{n_s^{re}\,A_{re}^3}{n_{Y(R)}^{re}\,A_{re}^3} = \left(\frac{3}{512\,\pi}\,\frac{(1+\omega_\phi)}{(1+3\,\omega_\phi)}\,\frac{\beta^2}{9}\right) \times \left(\frac{3\,(1-\omega_\phi)}{2\,\gamma}\right) \tag{5.22}$$

$$n_R^f = \frac{n_f^{re}\,A_{re}^3}{n_{Y(R)}^{re}\,A_{re}^3} = \left(\frac{3}{2048\,\pi}\,\frac{(1+\omega_\phi)}{(1-\omega_\phi)}\,\frac{\beta^2}{9}\left(\frac{m_f}{m_\phi^{end}}\right)^2\right) \times \left(\frac{3\,(1-\omega_\phi)}{2\,\gamma}\right) \tag{5.23}$$

From the above two equations it can be checked that for any ω_ϕ, $n_R^s >> 1$ (cf. Eq.5.21). Hence, comoving dark matter number density for scalar/vector produced from inflaton always dominates over the production from the radiation bath. However, for fermionic dark matter dominating production channel is crucially dependent on (m_f/m_ϕ^{end}). For example, if the reheating is instantaneous and the value of the fermionic dark matter mass produced from inflaton assumes $m_f \simeq 10^{-3}\,m_\phi^{end}$, then $n_R^f << 1$ which makes n_f^{re} sub-dominant compared to $n_{Y(R)}^{re}$. If we convert this into reheating temperatures, it can be easily shown that above $T_{re} \gtrapprox 10^{13}\,\text{GeV}$, the production of fermionic dark matter from radiation bath will always dominate over the production from inflaton field and it is less sensitive to the inflaton equation of state (see Fig.(5.7)). In Fig.5.7, solid lines correspond to gravitational dark matter production from inflaton scattering, and dotted lines correspond to dark matter production from both inflaton as well as radiation bath. The light red shaded region within $10^{15} \gtrsim T_{re} \gtrsim 10^{13}$ GeV clearly shows that the production from the inflaton field is sub-leading compared to that from the radiation bath. Depending upon the reheating equation of state, the mass range of the fermionic dark matte is observed to be slightly different.

So far, we have discussed dark matter production from both inflaton and radiation and its intimate connection with the inflationary and reheating parameters. In the following sections, we will focus on a minimal production mechanism called Gravitational reheating, where both radiation and dark matter are produced from inflaton through gravitational interaction only.

5.2 Gravitational reheating

Reheating is a natural physical phenomenon after inflation when DM and all SM fields can be produced. The simplest scenario would be the gravitational production of both DM and SM from inflaton through an s-channel graviton exchange, which is free from any choice of coupling. This production mechanism has a precise observational prediction and further restricts the evolution of the early universe. We will see that as we go along.
The dynamical equations in the context of Gravitational reheating (GRe) are [4]

$$\begin{aligned}
&\dot\rho_\phi + 3H(1+\omega_\phi)\rho_\phi + \Gamma_\phi^T\rho_\phi(1+\omega_\phi) = 0\,,\\
&\dot\rho_R + 4H\rho_R - \Gamma_{\phi\phi\to RR}^{Rad}\,\rho_\phi(1+\omega_\phi) = 0\,,\\
&\dot n_Y + 3Hn_Y - \frac{\Gamma_{\phi\phi\to YY}^{DM}}{m_\phi}\,\rho_\phi(1+\omega_\phi) = 0
\end{aligned} \tag{5.24}$$

where, (ρ_ϕ, ρ_R, n_Y) are inflaton energy density, radiation energy density and dark matter number density respectively. The total inflation decay width is $\Gamma^T_\phi = \Gamma^{Rad}_{\phi\phi\to RR} + \Gamma^{DM}_{\phi\phi\to YY}$. The gravitational decay width of inflaton to fundamental fields are given in Eqns.(5.2), (5.3) and (5.4) [331–334, 336]. The symbols (R, Y) represent scalar (S), fermion (f), and vector particles (X). Pauli spin blocking renders inflaton to fermion decay width proportional to the fermion mass m_f. This immediately indicates $\Gamma^{Rad}_{\phi\phi\to ff} \ll \Gamma^{Rad}_{\phi\phi\to SS}, \Gamma^{Rad}_{\phi\phi\to XX}$, as the mass of the radiation, constituents are small and hence, we ignore the fermionic contribution in radiation bath throughout. Consequently, $\Gamma^{Rad}_{\phi\phi\to RR} = \Gamma^{Rad}_{\phi\phi\to SS} + \Gamma^{Rad}_{\phi\phi\to XX} = (1+\gamma)\Gamma^{Rad}_{\phi\phi\to SS}$, with $\gamma = 1/8$. For DM, we analyze individual species. Massless graviton can also be part of the radiation bath through s-channel production, whose decay width will be suppressed due to its tensorial structure like the electromagnetic field. We ignore it in our analysis throughout.

5.2.1 Computing reheating parameters:

In order to calculate quantities during reheating namely, reheating e-folding number (N_{re}), reheating temperature (T_{re}), and maximum radiation temperature (T_{max}), we can evaluate following equation from Eq.(5.24),

$$d\left(\rho_R\, A^4\right) = \Gamma^{Rad}_{\phi\phi\to RR}\, \rho_\phi\, (1+\omega_\phi)\, \frac{A^3\, dA}{H} \tag{5.25}$$

where, $A = a/a_{end}$ is normalized scale factor. Suffix "*end*" corresponds to the end of inflation. The production of radiation will depend on the inflaton energy density only, and hence, maximum production occurs at the beginning of reheating. During this early stage, inflaton is naturally the dominating component. Neglecting decay term, therefore, ρ_ϕ approximately evolves as $\rho_\phi = \rho^{end}_\phi\, A^{-3\,(1+\omega_\phi)}$, where, $\rho^{end}_\phi = 3\, M_p^2\, H^2_{end}$ denotes the inflaton energy density at the end of inflation. Consequently, the Hubble parameter becomes,

$$H = \frac{\Lambda^2}{\sqrt{2}M_p}\left(\frac{2n}{2n+\sqrt{3\alpha}}\right)^n A^{-\frac{3}{2}(1+\omega_\phi)} = H_{end} A^{-\frac{3}{2}(1+\omega_\phi)}\,. \tag{5.26}$$

Upon substitution of Eqn.(5.26) in the expression of the comoving radiation energy density Eqn.(5.25), one can find

$$d\left(\rho_R\, A^4\right) = 3\,(1+\gamma)\, M_p^2\, H_{end}\, \Gamma^{Rad}_{\phi\phi\to SS}\, (1+\omega_\phi)\, A^{\frac{3}{2}\,(1+\omega_\phi)}\, dA \tag{5.27}$$

For gravitationally produced scalar radiation, corresponding decay width

$$\Gamma^{Rad}_{\phi\phi\to SS} \simeq \frac{\rho_\phi\, m_\phi}{1024\,\pi\, M_p^4}\,. \tag{5.28}$$

Where m_ϕ represents the effective mass of the inflaton that can be defined as

$$m_\phi = \sqrt{V''(\phi_0(t))} = \sqrt{\frac{2(1+\omega_\phi)\,(1+3\omega_\phi)}{(1-\omega_\phi)^2}}\, \lambda^{\frac{1-\omega_\phi}{2\,(1+\omega_\phi)}}\, \rho_\phi^{\frac{\omega_\phi}{1+\omega_\phi}} = m^{end}_\phi \left(\frac{\rho_\phi}{3\, M_p^2\, H_{end^2}}\right)^{\frac{\omega_\phi}{1+\omega_\phi}} \tag{5.29}$$

where, m^{end}_ϕ is the mass of the inflaton calculated at the end of the inflation. To derive above equation, we consider $\alpha-$ attractor model Eq.(1.130) as the inflationary model. With this we now calculate $(N_{re}, T_{re}, T_{max})$. Substitution of the decay term for scalar radiation Eq.(5.28)

into the comoving radiation energy density, Eqn.(5.27) and performing the integration, one can find

$$\rho_R = \frac{9\,(1+\gamma)\,H_{end}^3\,m_\phi^{end}\,(\,1+\omega_\phi\,)}{512\,\pi\,(1+15\omega_\phi)\,A^4}\left(1-A^{-\frac{1+15\,\omega_\phi}{2}}\right) \tag{5.30}$$

The above equation suggests that radiation production quickly happens at the beginning of reheating for large inflaton energy density and then comoving energy density freezes out. The behavior of this radiation plasma is that initially, it grows up to a maximum value, where we defined maximum temperature T_{max}; after that, it simply redshifts due to expansion. In order to calculate the maximum radiation temperature, we must first determine the scale factor A_{max} for which the radiation energy density maximized, $\frac{d\rho_R}{dA}|_{A=A_{max}} = 0$. This condition leads to

$$A_{max} = \left(\frac{3\;(3+5\,\omega_\phi)}{8}\right)^{\frac{2}{1+15\,\omega_\phi}}, \tag{5.31}$$

which implies that

$$(T_{max})^4 = \frac{9(1+\gamma)H_{end}^3 m_\phi^{end}(1+\omega_\phi)}{512\beta\pi(1+15\omega_\phi)A_{max}^4}\left(1-A_{max}^{-\frac{1+15\omega_\phi}{2}}\right) \tag{5.32}$$

Here, $\beta = \pi^2 g_{re}/30$ and g_{re} denotes the effective number of degrees of freedom associated with the radiation bath at the point of reheating.
End of reheating is defined at the point where $\rho_\phi = \rho_R$ as long as it satisfies BBN temperature bound. It turns out that when $\omega_\phi < 1/3$, the above condition is equivalent to $H \simeq \Gamma^{Rad}_{\phi\phi\to RR}$, which may not necessarily be true for $\omega_\phi > 1/3$. The reason behind this is that the inflaton dilutes itself much faster than its decay for higher EoS. Therefore, Eq.5.30 with the condition of reheating end one obtains the reheating e-folding number N_{re} as,

$$N_{re} = \frac{1}{3\omega_\phi - 1}\ln\left(\frac{512\,\pi\;M_p^2\,(1+15\,\omega_\phi)}{3\,(1+\gamma)H_{end}\,m_\phi^{end}\,(1+\omega_\phi)}\right), \tag{5.33}$$

By using the above equation (Eq.5.33) one immediately computes the reheating temperature as,

$$T_{re} = \left(\frac{9\,(1+\gamma)\,H_{end}^3\,m_\phi^{end}\,(\,1+\omega_\phi\,)}{512\,\beta\,\pi\,(1+15\omega_\phi)}\,e^{-4\,N_{re}}\right)^{1/4} \tag{5.34}$$

Furthermore, entropy conservation from the reheating end to present gives an additional important relation between (T_{re}, N_k) as [45]

$$T_{re} = \left(\frac{43}{11\,g_*^{re}}\right)^{1/3}\left(\frac{a_0\,H_{end}}{k}\right)e^{-(N_k+N_{re})}\,T_0\,, \tag{5.35}$$

Where, the use has been made of the relation $a_k H_k = a_0 H_0$ for k being CMB pivot scale, $k/a_0 = 0.05$ Mpc^{-1}. $T_0 = 2.725^0$ K is the present CMB temperature.
Model independent constraints: The Eq.5.34 along with Eq.5.35 is one of our most important results, which indicates that the reheating temperature is determined completely by the inflationary parameters, $(\omega_\phi, H_{end}, m_\phi^{end})$. Here, we first discuss the generic bounds on de-Sitter type inflation without specifying any particular model. Using the following

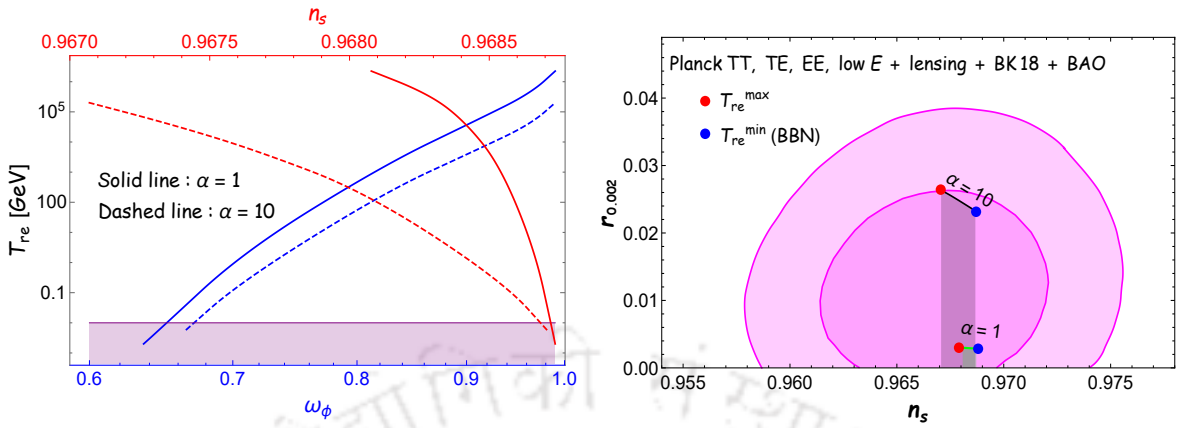

FIGURE 5.8: **Left panel:** Variation of T_{re} as a function ω_ϕ (blue line) and n_s (red line). The purple region below 10^{-2} GeV is forbidden from BBN bound. **Right panel:** Compare our result with the observational 68% and 95% CL constraints from BICEP/Keck data, in the (n_s, r) plane.

approximate relation $m_\phi^{end} \simeq \sqrt{(1+\omega_\phi)(4+12\omega_\phi)/(1-\omega_\phi)^2}\, H_{end}$ (under the assumption $\phi_{end} \sim M_p$), one immediately gets ω_ϕ within (0.60, 0.99) and H_{end} within $(1\times10^9, 5\times10^{13})$ GeV. This narrow and closed bound are derived form the minimum reheating temperature $T_{re}^{min} = T_{BBN} = 10^{-2}$ GeV and maximum possible value of the de-sitter Hubble scale at the end of inflation, $H_{end}^{max} \simeq \pi M_p \sqrt{r A_s/2}$ calculated at upper limit on $r = 0.036$ [364] (see Fig.5.8). Using these bounds GRe predicts reheating temperature to be $T_{re} \lesssim 10^8$ GeV. Furthermore, using Eq.5.35 we found that inflationary e-folding number N_k has to be within a very narrow range $(62, 63)$. *Therefore, to have successful GRe, viable de-Sitter inflation models will be those, which give* $N_k \sim (62, 63)$*, reheating EoS closer towards kination and predict reasonably low values of* T_{re}. This is indeed the case as we will discuss for α-attractor model.

Model dependent constraints: In order to see how GRe can constrain the α-attractor model, we numerically solve all the equations and the bounds on the model parameters are found to be, $\{(200 \geq n \geq 4.75), (200 \geq n \geq 5.15)\}$ and $\{(0.9681 \leq n_s \leq 0.9687), (0.9671 \leq n_s \leq 0.9687)\}$ for $\alpha = (1, 10)$ and can be decoded from Fig.5.8. The bounds are well within the $1\,\sigma$ range of $n_s = 0.9649 \pm 0.0042$ (68 % CL, Planck TT,TE,EE+lowE+lensing) from Planck [29]. CMB normalization $A_S \sim 10^{-9}$ is the only observed quantity that has been used in the above computation. The reheating temperature turned out to be bounded within $10^{-2}\text{GeV} \leq T_{re} \leq 2\times10^6\text{GeV}$ for $\alpha = 1$ and $10^{-2}\text{GeV} \leq T_{re} \leq 2\times10^5\text{GeV}$ for $\alpha = 10$, where the lower limit is set by BBN (see Fig.5.8). Maximum T_{re} predicted by the inflation model turns out to be consistent with the model-independent bound $T_{re} < 10^8$ GeV. Finally, model predicts N_k within $\{(62.5, 63.3), (64.6, 64.9)\}$ for $\alpha = (1, 10)$ accordingly. In our following discussions, we will consider all the above bounds to derive the DM mass.

5.2.2 DM phenomenology

In particle physics, DM is still an ill-understood subject. Experimental direct detection proves to be challenging due to its unknown but tiny interaction with the nucleons. However, if the interaction is only gravitational, which is explicitly known, we may need to go beyond the conventional methods of detecting it. Planckian interacting dark matter has recently gained

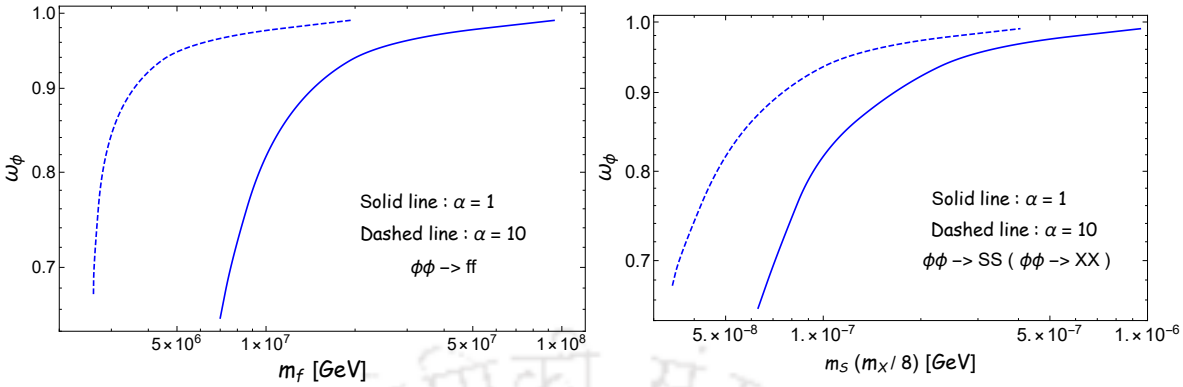

FIGURE 5.9: Variation of ω_ϕ with respect to DM mass.

interest in the literature [334, 336]. In our GRe scenario, similar to radiation, dark matter is also coupled with inflaton suppressed by Planck mass. Therefore, DM mass m_Y is the only free parameter. Interestingly such scenarios naturally fix the DM mass through its abundance and inflaton model under consideration. Dynamics of DM is governed by [cf.Eq.(5.24)]

$$d(n_Y\, A^3) = \frac{\Gamma_{\phi\phi\to YY}}{m_\phi}\,\frac{\rho_\phi\,(1+\omega_\phi)}{H}\,A^2\,dA. \tag{5.36}$$

One should note that $\Gamma^{DM}_{\phi\phi\to ff} \propto \rho_\phi/m_\phi$, which makes fermion production slower compared to bosonic one during reheating. However, production of both DMs and radiation are expected to be completed well before the end of reheating. As a result, the comoving (n_Y, ρ_R) become constant at reheating end. Therefore, present DM abundance can be safely calculated at the reheating end and is expressed as

$$\Omega_Y\, h^2 = \frac{m_Y\, n_Y(A_{re}) A^3_{re}}{\rho_R(A_{re}) A^4_{re}}\,\frac{A_{re} T_{re}}{T_0}\,\Omega_R\, h^2 \;= 0.12, \tag{5.37}$$

$\Omega_R h^2 = 4.16\times10^{-5}$ is the present radiation abundance.

After straightforwardly integrating the Eq.5.36, one finds the comoving DM number density, $n_Y^{com} = n_Y A^3_{re}$, at the end of reheating for *fermion* and scalar/vector(see Appendices 6.2 for details calculation),

$$\begin{aligned} n_f^{com} &\simeq \frac{3H^3_{end}}{2048\pi}\frac{1+\omega_\phi}{1-\omega_\phi}\left(\frac{m_f}{m_\phi^{end}}\right)^2\left(1-e^{-\frac{3N_{re}}{2}(1-\omega_\phi)}\right), \\ n_S^{com} &= 8 n_X^{com} = \frac{3H^3_{end}\,(1+\omega_\phi)}{512(\pi+3\pi\omega_\phi)}, \end{aligned} \tag{5.38}$$

respectively. Now, using this comoving number density and the abundance Eq.5.37 we constrain the DM mass.

Model independent constraints on m_Y: We have already obtained the model independent constraint on (H_{end}, ω_ϕ) on which $\Omega_Y\, h^2$ depends explicitly through Eqs.5.38. Therefore, successful GRe along with the correct DM relic abundance immediately put tight constraints on the allowed mass range for fermionic DM as, 2×10^5 GeV $\leq m_f \leq 3\times10^8$ GeV, and for scalar/vector DM as 50 eV $\leq m_S, \gamma m_X \leq 1000$ GeV. Origin of higher m_f can be understood

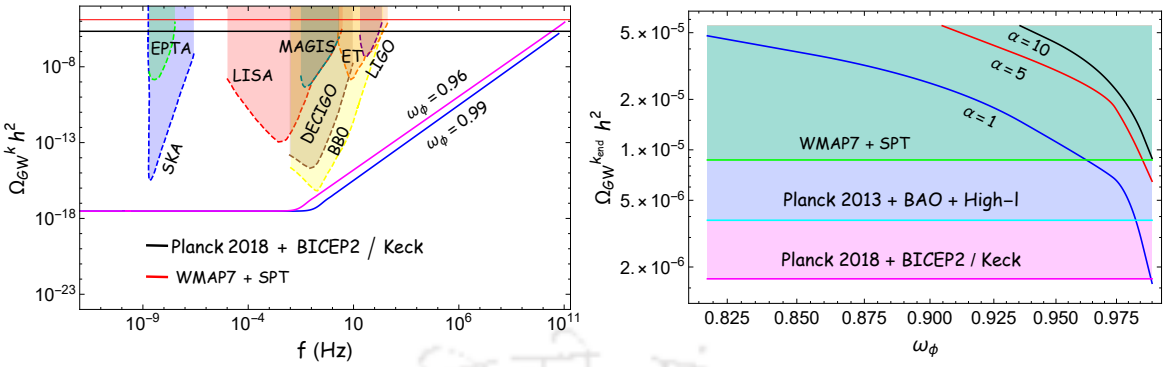

FIGURE 5.10: **Left panel :** Behavior of Ω^k_{GW} over a wide a range of frequency $f = k/2\pi$ for $\alpha = 1$ with two different ω_ϕ. **Right panel :** $\Omega^{k_{end}}_{GW}$ Vs ω_ϕ for three different values of α and the shaded regions are forbidden from three different BBN bounds.

from the additional mass suppression $(m_Y/m_\phi)^2$ in the $\phi\phi \to ff$ decay width, which suppresses the fermionic DM number density. This requires an enhanced value of m_f to satisfy the abundance.

Model dependent constraints on m_Y: Considering $\alpha = (1, 10)$ in the Fig.5.9 we plotted (m_Y Vs ω_ϕ) within the allowed range of ω_ϕ obtained previously. An important point to realize from the figure is that for a specific value of ω_ϕ DM mass is unique. The allowed fermionic masses turned out to be within $\{(7\times10^6, 9\times10^7), (3\times10^6, 2\times10^7)\}$ GeV for $\alpha = (1, 10)$. For bosonic DM, it is within $\{(60, 1000), (30, 400)\}$ eV for $\alpha = (1, 10)$. *Therefore, in addition to selecting a limited class of inflation models successful GRe predicts DM mass m_Y within a very narrow range of values.*

5.2.3 Primordial gravitationl waves (PGWs) and constraints:

PGWs, (see Refs.[203–206]) is one of the profound predictions of inflation. It plays as a unique probe of the early universe. Particularly, the evolution of GWs and their amplitude are sensitive to the inflationary energy scale and the post-inflationary EoS of the universe. Extremely weak coupling with matter fields helps PGWs to carry precise information about its origin and subsequent evolution over a large cosmological time scale. Even though, we have not observed PGWs yet [220, 222, 225, 232, 365, 366], simple cosmological upper bound on its strength during BBN will be shown to further tighten the bounds on the parameters discussed above. We focus on the behavior of PGWs spectrum for modes within $k_{re} < k < k_{end}$ which re-enter the horizon during GRe after inflation. (k_{re}, k_{end}) re-enter the horizon at the end of inflation and at the end of GRe respectively. Assuming GRe phase is dominated by ω_ϕ, the PGWs spectrum today is calculated as (see sec.4.4 in chapter-4 for detailed derivation)

$$\Omega^k_{GW}h^2 \simeq \Omega_R h^2 P_T(k)\frac{4\mu^2}{\pi}\Gamma^2\left(\frac{5+3\omega_\phi}{2+6\omega_\phi}\right)\left(\frac{k}{2\mu k_{re}}\right)^{n_{GW}} \tag{5.39}$$

Where, $\mu = \frac{1}{2}(1+3\omega_\phi)$ and the index of the spectrum, $n_{GW} = -(2-6\,\omega_\phi)/(1+3\omega_\phi)$. The tensor power spectrum is, $P_T(k) = H^2_{end}/12\pi^2M_p^2$. To this end we would like to state that for $k < k_{re}$, PGWs spectrum today is $\Omega^k_{GW}(k)h^2 \sim \Omega_R h^2\, H^2_{end}/12\,\pi^2 M_p^2$, which is scale-invariant for de-Sitter inflation. Eq.5.39 indicates that Ω^k_{GW} increases with increasing k for $\omega_\phi > 1/3$

(see Fig.5.10). The effective number of relativistic degrees of freedom during BBN place an upper limit on Ω^{k}_{GW} (see Fig.5.10) [290]. We will analyze how this upper limit will give even tighter constraints on the parameters.

Model independent constraints: The maximum possible $k = k_{end}$ and the relation $k_{end}/k_{re} = Exp[N_{re}(-1+3\omega_\phi)/2]$ indicate $\Omega^{k_{end}}_{GW}h^2$ being dependent only on (ω_ϕ, H_{end}), and hence provide further constraints in (ω_ϕ, H_{end}). Considering constraints on $\Omega^{k_{end}}_{GW}h^2$ within $(1.7\times10^{-6}, 8.4\times10^{-6})$ from different data set (see Fig.5.10), allowed range of EoS becomes $0.97 < \omega_\phi \leq 0.99$. This is much tighter compared to the constraints from GRe only and increasingly hints towards the GRe phase being kination domination. This stringent constraint on ω_ϕ turned out to be consistent only with the inflationary e-folding number around $N_k \simeq 62$. Constrain on (H_{re}, T_{re}, m_f) remains nearly same as before, but scalar DM mass range further tightens into $(400, 1000)$ eV.

Model dependent constraints: First panel of the Fig.5.10 suggests, if one considers most conservative bound on $\Omega^{k_{end}}_{GW}\,h^2 \leq 1.7\times10^{-6}$ obtained from data set Planck-2018 + BICEP2/Keck array [367], $\alpha = 1$ with $\omega_\phi \simeq 0.99$ appears to be the only allowed model which satisfies all the constraints. However, once relaxing the bound within $(1.7\times10^{-6} \leq \Omega^{k_{end}}_{GW} \leq 8.4\times10^{-6})$ taking into account WMAP7[1] and SPT[368], allowed range of ω_ϕ get narrowed down within $\{(0.96, 0.99), (0.986, 0.990)\}$ for $\alpha = (1, 5)$ accordingly. Whereas, any $\alpha > 10$ are completely excluded. Within the allowed value of $\alpha = (1, 10)$), maximum allowed range of scalar spectral index n_s becomes $(0.9671, 0.9683)$, reheating temperature T_{re} becomes $(2\times10^5, 2\times10^6)$ GeV, fermionic DM mass becomes $(10^7, 10^8)$ GeV, and scalar/vector DM mass becomes $(400, 1000)$ eV. However, all these ranges actually shrink towards their lower value as one goes from $\alpha = 1 \to 10$.

5.3 conclusions

In this chapter, our focus is on the background dynamics of reheating and DM phenomenology. In the first half, we studied the production of DM matter from the decay of inflaton mediated by gravitational interaction. For completeness, we also include the production from the radiation bath. This is the reason in the ($\langle\sigma v\rangle$ Vs m_Y) parameter space the gravitationally produced dark matter appeared to have unique mass value m_Y^{max} (see Figs.5.5, 5.4) for which the present dark matter abundance is satisfied. The value of m_Y^{max} is uniquely determined by the inflationary energy scale H_{end}, and inflaton effective equation of state during reheating ω_ϕ (see Fig.5.1, 5.2), which are expressed in Eq.5.17. We studied the constraint on the DM mass considering vector, scalar, and fermion type dark matter considering both the CMB power spectrum and the dark matter abundance. For bosonic dark matter, the observationally viable mass range turned out to be within $(10^{13} - 10^{-13})$ GeV. Therefore, gravitationally produced dark matter of mass in the eV range can be identified as an axion field. However, to obtain such a low bosonic dark matter mass through gravitational production, we found that the reheating equation of state needs to be closed to unity, which is equivalent to kination domination. We will study this fact in detail in the future. For fermionic dark matter mass range turned out to be $m_f^{max} = (10^{13} - 10^4)$ GeV. Importantly, it is observed that the allowed DM mass range shrinks to a point as ω_ϕ approaches $1/3$, which is clearly observed in Fig.5.2. We discussed single and two-component dark matter scenarios and the constraints on the dark matter parameters consistent with both CMB and dark matter abundance.

In the second half of the chapter, we moved our discussion to the GRe scenario, which

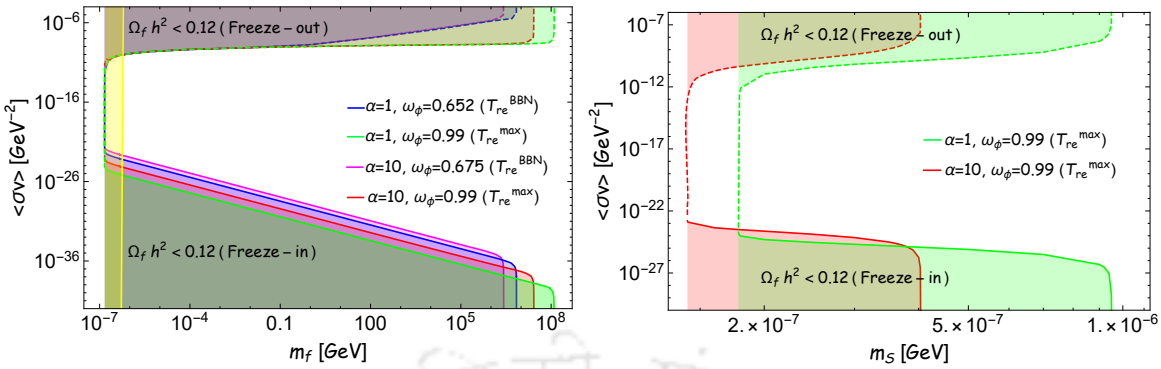

FIGURE 5.11: Plot of $\langle\sigma v\rangle$ Vs m_Y of fermionic (left panel) and scalar (right panel) DM. The Yellow band corresponds to minimum DM mass bound taken from [369].

successfully obtained our present state of the universe through only gravitational interaction after inflation. Being DM mass as the only free parameter, successful GRe puts stringent constraints on possible DM mass and may pave the way towards constructing DM models. The scenario further discards a large class of inflation models that are otherwise consistent with the PLANCK. Considering available bounds on PGWs spectrum and DM abundance, GRe selects those inflation models which gives around unique $N_k \sim 62$, and inflaton EoS within $0.97 < \omega_\phi \leq 0.99$ during reheating. Consequently reheating temperature must be $T_{re} < 10^8$ GeV, fermionic DM mass should lie within 2×10^5 GeV $< m_f < 3\times10^8$ GeV, and scalar/vector DM mass within 400 eV $< m_S, \gamma m_X <$ 1000 eV. The abovementioned results are obtained without specifying any model except the generic de-Sitter type inflation. However, considering a specific model such as α-attractor, narrower bounds are obtained due to its small prediction of r. α turned out to be strictly bounded within $(1, 10)$. Furthermore, n_s strictly lies within $(0.9671, 0.9683)$, T_{re} lies within $(2\times10^5, 2\times10^6)$ GeV, fermionic DM mass lies within $(10^7, 10^8)$ GeV, and scalar/vector DM mass lies within $(400, 1000)$ eV.

To this end, let us point out that if we take into account the modified decay widths properly accounting for the oscillating inflaton zero-mode [355], all our predictions remain quantitatively the same except the fermionic DM mass range shifted towards the lower value by one order. So far, if DM sector couples directly with the radiation bath with thermally averaged cross-section times velocity $\langle\sigma v\rangle$, then the DM masses obtained previously transformed into maximum one m_Y^{max} in $(\langle\sigma v\rangle, m_Y)$ space [354] (see Fig.5.11). Upon decreasing DM mass, to our surprise, the existence of nearly model-independent minimum DM mass m_Y^{min} is observed where freeze-in and freeze-out mechanisms meet together. Such observation was also never reported before in the literature. This phenomenon is expected as decreasing m_Y requires increasing $\langle\sigma v\rangle$ during freeze-in, and at its threshold value m_Y^{min} the DM thermalizes with radiation bath where freeze-out begins. The value of m_Y^{min} turned out as ~ 150 eV for fermion DM irrespective model parameters. However, for fermionic DM, the most compact DM-dominated object called dwarf spheroidal galaxies are known to provide the lowest bound (Tremaine-Gunn (TG) bound) on its mass $m_f \geq 590$ eV at 68% CL [369] shown in yellow shaded region. Finally, we want to point again that m_Y^{max} is set to be the maximum possible DM mass for both freeze-in ($\langle\sigma v\rangle \to 0$) and freeze-out ($\langle\sigma v\rangle \to \infty$) scenarios if one satisfies the present DM abundance. Therefore, if DM with $m_Y > m_Y^{max}$ is detected, it will rule out the possibility of purely gravitational reheating after inflation.

"We're always, by the way, in fundamental physics, always trying to investigate those things in which we don't understand the conclusions. After we've checked them enough, we're okay."

Richard P. Feynman

In this thesis, we have mainly focused our analysis on constraining the dynamics of reheating after inflation. Reheating phase influences the relationship between the physical scales of the CMB mode today and that at the time of Horizon exit during the beginning of the inflation. Consequently, one can expect some indirect bound on the dynamics of reheating from CMB through a particular inflation model. In this thesis keeping the CMB constraints, we further extend our analysis to connect reheating dynamics with various disconnected cosmological parameters, which help us to investigate the new possibility of understanding this era.
We have focused on two main directions: 1) Investigate the background dynamics of reheating to explain the present state of our Universe more reasonably. 2) Understanding the imprints of reheating on different cosmological observables. Below we discuss the main findings of the thesis.

6.1 Summary of chapters

Chapter 1:

In this chapter, we prepare the introduction and the motivation leading to the thesis work. This chapter begins with a brief introduction to the standard cosmological scenario. We first shed light on FLRW cosmology, discuss both Horizon and the flatness problem and show how the period of inflation successfully solves the Horizon as well as the flatness problem. Then we give a brief summary of the inflationary paradigm, such as homogeneous dynamics of inflation, slow roll conditions, end of slow-roll inflation, and introduce conventional perturbative reheating dynamics. Finally, we discuss Cosmological perturbations from inflation, the spectrum of the gravitational wave during inflation, and conclude this chapter with this thesis's motivation.

Some of the brief outlines of different chapters can be found in this chapter, which are some initial ideas regarding the work done in other chapters.

Chapter 2:

In Conventional perturbative reheating, inflaton energy density gradually decays into the energy density of the daughter particles assuming a specific interaction between inflaton and daughter fields. However, there must be an initial stage of reheating involving highly nonperturbative processes, known as preheating, when the occupation number of field quanta for both the inflaton and daughter field(s) grows exponentially due to parametric resonance. A systematic study of reheating constraints incorporating the nonperturbative phase for various interactions and inflationary modes is missing in the literature. Therefore, in this chapter, after discussing the possible models of single-phase reheating and how this model can be constraints through CMB considering a particular inflation model, we moved our discussion towards a proposed model of reheating, named Two-phase reheating, where the initial nonperturbative preheating phase is described by an effective equation of state followed by the usual perturbative reheating. Some of the important universal results of lattice simulation during preheating, which is irrespective of the inflationary model, have been considered crucial inputs in our Two-phase dynamics. In this framework, detailed phenomenological constraints have been obtained on the inflaton couplings with reheating fields and dark matter parameters in terms of the cosmic microwave background (CMB) through the constrained inflationary scalar spectral index. It is observed that the conventional reheating scenario generically predicts the maximum reheating temperature $T_{re}^{max} \sim 10^{15}$ GeV, corresponding to an almost instantaneous transition from the end of inflation to radiation domination. This fact will naturally lead to the problem of nonperturbative inflaton decay, which is in direct conflict with the perturbative reheating itself. Taking into account this effective nonperturbative dynamics as the initial phase, our model of Two-phase reheating scenarios also predicts a model-independent maximum reheating temperature, which does not correspond to the instantaneous process. Furthermore, T_{re}^{max} is predicted to lie within $\left(10^{13}, 10^{10}\right)$ GeV if CMB constraints on inflaton couplings with a different reheating field are taken into account. We have further studied in detail the dark matter phenomenology in a model-independent manner and show how dark matter parameter space can be constrained through CMB parameters via the inflationary spectral index. Considering dark matter production during reheating via the freeze-in mechanism, its parameter space has been observed to be highly constrained by our Two-phase reheating than the constraints predicted by the conventional reheating scenarios, which are believed to be theoretically incomplete.

Chapter 3:

Till now, there are no direct observational probes of the reheating period, and as a result, our understanding is severely limited. The primordial magnetic field, together with CMB, can provide a probe of the early reheating phase. In this chapter, we will specifically focus on how the present-day Large-scale magnetic field (LSMF) combined with the CMB anisotropy can probe the reheating phase of the universe, followed by the standard inflationary phase. For LSMF we consider simple model of primordial magnetogeneis. This chapter shows that the reheating phase can play a crucial role in alleviating strong coupling and back-reaction problems in the inflationary magnetogenesis model along with the cosmic microwave background. The

electrical conductivity is assumed to be negligible during the entire period of reheating, and the Faraday electromagnetic induction changes the magnetic field's dynamics drastically. Our detailed analysis reveals that this physical phenomenon not only converts a large class of magnetogenesis model observationally viable without any theoretical problem but also can uniquely fix the perturbative average inflaton equation of state, $\omega_\phi = p - 2/p + 2$ during reheating given a specific value of the large scale magnetic field. This observation hints at the inflaton to assume the potential of the form $V(\phi) \sim \phi^p$ near its minimum with $p \geq 3.5$ if one considers the limitations of the present-day strength of the large-scale magnetic field to be $B_0 \geq 10^{-18}$ G. Our analysis opens up a new avenue toward constraining the inflationary and magnetogenesis model together via reheating.

Chapter 4:

Primordial gravitational waves (GWs) carry the imprints of the dynamics of the universe during its earliest stages. With a variety of GW detectors being proposed to operate over a wide range of frequencies, there is great expectation that observations of primordial GWs can provide us with an unprecedented window into the physics operating during inflation and reheating. In this chapter, we closely examine the effects of the regime of reheating on the spectrum of primordial GWs observed today. We consider a scenario wherein the phase of reheating is described by an averaged equation of state (EoS) parameter with an abrupt transition to radiation domination as well as a scenario wherein there is a gradual change in the effective EoS parameter to that of radiation due to the perturbative decay of the inflaton. We show that the perturbative decay of the inflaton leads to oscillations in the spectrum of GWs, which, if observed, can possibly help us decipher finer aspects of the reheating mechanism. We also examine the effects of a secondary phase of reheating arising due to a brief epoch driven possibly by an exotic, non-canonical, scalar field. Interestingly, we find that, for suitable values of the EoS parameter governing the secondary phase of reheating, the GWs can be of strength as suggested by the recent NANOGrav observations. We conclude with a discussion of the wider implications of our analysis.

Chapter 5:

In this chapter, we have started our discussion with a minimal production mechanism of DM during reheating, where DM is assumed to be produced from inflaton and radiation baths through only the gravitational interaction. The gravitational process is always present; we can't ignore this process. Ignoring other internal parameters except for the DM mass and spin, a particular inflation model such as α-attractor, with a specific scalar spectral index n_s has been shown to fix the dark matter mass of the present Universe uniquely. For fermion type dark matter we found the mass m_f should be within $(10^4 - 10^{13})$ GeV, and for boson (vector) type DM, the mass $m_{s/X}$ turned out to be within $(10^{-13} - 10^{13})$ GeV. Interestingly, if the inflaton equation of state $\omega_\phi \to 1/3$, the DM mass also approaches towards unique value, $m_f \sim 10^{10}$ GeV and $m_{s/X} \sim 10^3\,(\,8 \times 10^3\,)$ GeV . However, here we assume that inflaton decays into radiation with a constant decay width to achieve a radiation-dominated universe at the end of reheating. Such an approach generally lacks potential cosmological predictions and is difficult to verify through observation. Accordingly, we moved our discussion to take a systematic approach toward such a goal to shed light on the model-independent observable predictions. Without introducing any arbitrary interactions among the fields, we propose a

reheating scenario where the inflaton is coupled with all the daughter fields only gravitationally. This scenario not only successfully reheats the Universe but also discards many possible models of dark matter and inflation that are otherwise consistent with PLANCK.

6.2 Future plan

Several perspectives have been found during the thesis work that needs further study. Some of them are listed below, subject to my future research direction.

- **Primordial black hole formation during reheating:** Primordial black holes (PBHs) formation in the early universe can be described as a result of huge contraction during the Big Bang. The PBHs are one of the intriguing dark matter candidates as they behave as stable, cold, non-interacting massive objects. Moreover, the gravitational wave (GW) from PBHs received interest in terms of detection after the discovery by LIGO (GW detection event GW150914) of gravitational radiation from merging BHs. In the context of the impact of reheating on PBH production, very few studies are available in the literature. Moreover, a systematic study of PBH formation incorporating reheating phase is also missing. Accordingly, our primary goal is to analyze the effects of reheating on PBH formation in a systematic manner for different scenarios.

- **Growth of the density perturbations during reheating phase** Reheating phase is very difficult to probe; till now, this phase has been ill-understood. Small-scale density perturbations can provide a probe of the early Universe. The density perturbation of dark matter (DM) may grow during this phase due to gravitational instability. The early DM microholes can be formed from that enhanced perturbation if the free-steaming length is smaller than the horizon, which can open up new possibilities to learn about the reheating phase using gamma-ray observation. Then it becomes fascinating to understand the evolution of the density perturbations in both radiation and DM for various background dynamics of reheating.

- **Dark matter production from inflaton freeze-out:** After the inflation, the inflaton field generically oscillates around the minimum of its potential. Reheating fields coupled with the oscillating inflaton are in general prone to nonperturbative particle production. This study can be done by using the publicly available numerical package LATTICEEASY and its parallelized version CLUSTEREASY. Extensive works on nonperturbative reheating analysis yield an important fact that roughly the 50% of the total comoving inflaton energy density is getting transferred into the daughter field. Additionally, the inflaton equation of state tends to achieve a steady-state value depending upon the power-law form of the inflaton potential near its minimum. If the inflaton equation of state $\omega_\phi < 1/3$, then the inflaton field reaches thermal equilibrium with radiation bath, and comoving inflaton energy density freezes before reaching the radiation equation of state. Therefore, to get radiation dominated universe, we need to decay this inflaton field perturbatively, which can be the sole source of non-thermal dark matter. Finally, we must find the suitable dark matter parameter space to get the correct present-day dark matter relic.

- **Observing various characteristics of inflation and reheating through the imprints on the gravitational waves:** Primordial gravitational waves (GWs) carry

the imprints of the dynamics of the universe during its earliest stages. With a variety of GW detectors being proposed to operate over a wide range of frequencies, there is great expectation that observations of primordial GWs can provide us with an unprecedented window to the physics operating during inflation and reheating. GWs spectrum can decode various aspects of reheating. For example, during the initial stage of reheating, the inflaton field oscillates, which can be coupled with some reheating field. The numerical package LATTICEEASY can obtain the dynamical evolution of those fields, and can be imprinted through the gravitational wave spectrum. In addition to that, The end of reheating is to be followed by the most important stage of thermalization. Some important information about this thermalization process, like thermalization time scale and the nature of the thermalization process depending upon the over-occupied or under-occupied initial state set by the end of reheating, can be extracted from GWs spectrum.

Appendices

Two-phase reheating: Analytic study

Analytic expression of T_{max}

After the end of the effective non-perturbative dynamics, the usual perturbative analysis follows and the governing Boltzmann equations are

$$\dot{\rho_\phi} + 3H(1+\omega_\phi^1)\rho_\phi = -\Gamma_\phi \rho_\phi (1+\omega_\phi^1) \tag{1}$$

$$\dot{\rho_R} + 4H\rho_R = \Gamma_\phi \rho_\phi (1+\omega_\phi^1) + 2\langle E_X\rangle\langle\sigma v\rangle \left(n_X^2 - n_{X,eq}^2\right) \tag{2}$$

$$\dot{n_X} + 3Hn_X = -\langle\sigma v\rangle \left(n_X^2 - n_{X,eq}^2\right) \tag{3}$$

In order to solve analytically, we assume the inflaton energy density to follow the equation,

$$\rho_\phi = \rho_\phi^{in}\left(\frac{a}{a_{in}}\right)^{-3(1+\omega_\phi^1)} e^{-\Gamma_\phi(1+\omega_\phi^1)(t-t_i)} \simeq \rho_\phi^{in}\left(\frac{a}{a_{in}}\right)^{-3(1+\omega_\phi^1)} . \tag{4}$$

Here Γ_ϕ is the time-independent inflaton decay constant. Notice that the effect of the decay constant is being ignored assuming the fact that at the initial stage of perturbative reheating inflaton energy is the dominant one. ρ_ϕ^i and t_i are initial density and initial time during the perturbative era respectively. Using the above equation the radiation energy can be solved as follows,

$$\begin{aligned} d\left(\rho_R a^4\right) &= \left(\Gamma_\phi\rho_\phi(1+\omega_\phi^1)a^4 + 2\langle E_X\rangle\langle\sigma v\rangle\left(n_X^2 - n_{X,eq}^2\right)a^4\right)dt \\ &= \left(\Gamma_\phi\rho_\phi^{in} e^{-\Gamma_\phi(t-t_i)} a_{in}^{3(1+\omega_\phi^1)} a^{1-3\omega_\phi^1}(1+\omega_\phi^1) + 2\langle E_X\rangle\langle\sigma v\rangle\left(n_X^2 - n_{X,eq}^2\right)a^4\right)dt \\ &\simeq \Gamma_\phi\rho_\phi^{in} a_{in}^{3(1+\omega_\phi^1)} a^{-3\omega_\phi^1}\frac{da}{H} + 2\langle E_X\rangle\langle\sigma v\rangle\left(n_X^2 - n_{X,eq}^2\right)a^3\frac{da}{H} . \end{aligned} \tag{5}$$

Using the following expression for the Hubble parameter,

$$H = \frac{\sqrt{\rho_\phi^{in}\left(\frac{a}{a_{in}}\right)^{-3(1+\omega_\phi^1)} + \rho_R^{in}\left(\frac{a}{a_{in}}\right)^{-4}}}{\sqrt{3}M_p} , \tag{6}$$

where ρ_R^{in} is the initial radiation density at the beginning of perturbative phase. For the reheating temperature computation, we ignore the effect of dark matter whose contribution has

been verified to be negligible in our full numerical computation. By solving Eq.5 we obtain,

$$\begin{aligned}
\rho_R a^4 &= \rho_R a_{in}^4 + \Gamma_\phi \rho_\phi^{in} a_{in}^3 \int_{a_{in}}^{a} \frac{(a/a_{in})^{-3\omega_\phi^1}(1+\omega_\phi^1)da}{(\sqrt{3}M_P)^{-1}\sqrt{\rho_\phi^{in}\left(\frac{a}{a_{in}}\right)^{-3(1+\omega_\phi^1)} + \rho_R^{in}\left(\frac{a}{a_{in}}\right)^{-4}}} \\
\rho_R x^4 &= \rho_R^{in} + \Gamma_\phi \rho_\phi^{in}(1+\omega_\phi^1)\int_1^x \frac{x^{2-3\omega_\phi^1}dx}{(\sqrt{3}M_P)^{-1}\sqrt{\rho_\phi^{in}x^{1-3\omega_\phi^1} + \rho_R^{in}}} \qquad (7) \\
&= \rho_R^{in} + \frac{\Gamma_\phi \rho_\phi^{in}(1+\omega_\phi^1)}{H_{in}}\int_1^x \frac{x^{\frac{3-c}{2}}dx}{\sqrt{1+\frac{\rho_R^{in}}{\rho_\phi^{in}}x^{c-1}}} \simeq \rho_R^{in} + \frac{\Gamma_\phi \rho_\phi^{in}(1+\omega_\phi^1)}{H_{in}}\int_1^x x^{\frac{3-c}{2}}\left(1-\frac{\rho_R^{in}}{2\rho_\phi^{in}}x^{c-1}\right)dx
\end{aligned}$$

In the above expression, we neglected higher-order terms of $\rho_R^{in}/\rho_\phi^{in}$. Additionally in terms of radiation temperature $T_{rad} = \left(\frac{30}{\pi^2 g_*}\rho_R\right)^{1/4}$ the above equation transforms into following expression,

$$\frac{\beta T^4 x^4}{\rho_\phi^{in}} = \frac{\Gamma_\phi(1+\omega_\phi^1)}{H_{in}}\left[\frac{2}{5-c}\left(x^{\frac{5-c}{2}}-1\right) + \frac{\rho_R^{in}}{\rho_\phi^{in}}\left(\frac{1-x^{\frac{c+3}{2}}}{c+3} + \frac{H_{in}}{\Gamma_\phi(1+\omega_\phi^1)}\right)\right] . \qquad (8)$$

Here x, β, c and H_{in} defined as

$$x = \frac{a}{a_{in}} \ , \ \beta = \frac{\pi^2 g_*(T)}{30} \ , \ c = 3\omega_\phi^1 \ , \ H_{in} = \frac{\sqrt{\rho_\phi^{in}}}{\sqrt{3}M_P} \ . \qquad (9)$$

The maximum radiation temperature can be found by taking derivative of the above equation (8) with respect to x and set it to zero

$$\frac{4\beta T^3}{\rho_\phi^{in}}\frac{dT}{dx} = \frac{-4\Gamma_\phi(1+\omega_\phi^1)}{H_{in}x^5}\left[\frac{\frac{3+c}{4}x^{\frac{5-c}{2}}-2}{5-c} + \frac{\rho_R^{in}}{\rho_\phi^{in}}\left(\frac{\frac{c-5}{8}x^{\frac{c+3}{2}}+1}{c+3} + \frac{H_{in}}{\Gamma_\phi(1+\omega_\phi^1)}\right)\right] = 0 \ . \qquad (10)$$

In the limit of $\rho_\phi/\rho_R \ll 1$ (perturbative approximation), the values of x at the point of maximum radiation temperature appear as

$$x_{max,p} = \left(\frac{8}{3+c}\right)^{\frac{2}{5-c}} . \qquad (11)$$

In our present analysis, the expression of x associated with maximum radiation temperature leads to the following relation

$$x_{max} \simeq \left(\frac{8}{3+c}\right)^{\frac{2}{5-c}}\left[1-\frac{\rho_R^{in}}{\rho_\phi^{in}}\left(\frac{c-5}{8(c+3)}x_{max,p}^{\frac{c+3}{2}} + \frac{1}{c+3} + \frac{H_{in}}{\Gamma_\phi(1+\omega_\phi^1)}\right)\right] = x_{max,p}\left[1-z\right] \quad ,(12)$$

where $z = \frac{\rho_R^{in}}{\rho_\phi^{in}}\left(\frac{c-5}{8(c+3)}x_{max,p}^{\frac{c+3}{2}} + \frac{1}{c+3} + \frac{H_{in}}{\Gamma_\phi(1+\omega_\phi^1)}\right)$. Now after replacing the expression of x_{max} into the above Eq.8, the maximum radiation temperature turns out as

$$T_{max} \simeq \left(\frac{\Gamma_\phi(1+\omega_\phi^1)\rho_\phi^{in}}{\beta H_{in}x_{max,p}^4}\frac{2}{3+c}\right)^{1/4}\left[1+\frac{3+c}{2}\frac{\rho_R^{in}}{\rho_\phi^{in}}\left(\frac{1-x_{max,p}^{\frac{c+3}{2}}}{c+3} + \frac{H_{in}}{\Gamma_\phi(1+\omega_\phi^1)}\right)\right]^{1/4} \qquad (13)$$

$$\simeq \left(\frac{\Gamma_\phi(1+\omega_\phi^1)\rho_\phi^{in}}{\beta H_{in} x_{max,p}^4}\frac{2}{3+c}\right)^{1/4}\left[1+\frac{3+c}{8}\frac{\rho_R^{in}}{\rho_\phi^{in}}\left(\frac{1-x_{max,p}^{\frac{c+3}{2}}}{c+3}+\frac{H_{in}}{\Gamma_\phi(1+\omega_\phi^1)}\right)\right] \quad . \tag{14}$$

In the above expression we have neglected higher order terms of $\rho_R^{in}/\rho_\phi^{in}$. Next, we will try to express all initial densities in terms of the inflaton energy density at the end of the inflation ρ_ϕ^{end}. The effective non-perturbative phase-I dynamics solves the radiation and inflaton energy density in terms of ρ_ϕ^{end}. Therefore, during phase I the dimensionless radiation energy density $R^I(A)$ can be correlate with inflaton energy density $\Phi^I(A)$ (using (2.36), (2.37) and (2.41)) as

$$R^I(A) = \frac{3\omega_{eff}}{(1-3\omega_{eff})}\Phi^I(A)\ A \quad . \tag{15}$$

The initial densities during phase II (perturbative era) in terms of dimensionless comoving energy densities are identified as

$$\rho_\phi^{in} = \Phi(A_{npre})A_{npre}^{-3(1+\omega_\phi^1)}m_\phi^4\ ,\ \rho_R^{in} = R(A_{npre})A_{npre}^{-4}m_\phi^4 \quad . \tag{16}$$

Furthermore, we can relate the $\Phi(A_{npre})$ in terms of $\Phi(A=1)$ as,

$$\Phi(A_{npre}) = (1-3\omega_{eff})\,\Phi(A=1)A_{npre}^{-3\omega_{eff}} \quad , \tag{17}$$

where, A_{npre} is the normalized scale factor at the end of the effective dynamics. A_{npre} is defined when the dimensionless comoving radiation energy density becomes 50% of the total comoving energy density, $\frac{R(A_{npre})}{\Phi(A_{npre})+R(A_{npre})} \simeq \frac{1}{2} \implies \Phi(A_{npre}) \simeq R(A_{npre})$. Using Eq.15 one can find A_{npre} and corresponding e-folding number N_{npre} as

$$A_{npre} = \frac{1-3\omega_{eff}}{3\omega_{eff}}\ ,\ N_{npre} = \ln\left(A_{npre}\right) \quad . \tag{18}$$

From our analytic expression above, we obtain $N_{npre} \sim (5.8, 12.7)$ for two values of $\omega_{eff} = (10^{-3}, 10^{-6})$ accordingly. These values of the e-folding number during phase I almost exactly match our numerical result.
The final expression for the maximum radiation temperature in terms of comoving energy densities is given by

$$T_{max} \simeq D^{1/4}\left[1+\frac{(3+c)R(A_{npre})}{8\Phi(A_{npre})A_{npre}^{1-c}}\left(\frac{1-x_{max,p}^{\frac{c+3}{2}}}{c+3}+\frac{\sqrt{\Phi(A_{npre})A_{npre}^{-3(1+\omega_\phi^1)}m_\phi^4}}{\sqrt{3}M_p\Gamma_\phi(1+\omega_\phi^1)}\right)\right] \quad , \tag{19}$$

where

$$D = \left(\frac{2\Gamma_\phi(1+\omega_\phi^1)\sqrt{3M_p^2\Phi(A_{npre})A_{npre}^{-3(1+\omega_\phi^1)}m_\phi^4}}{(3+c)\beta x_{max,p}^4}\right)^{1/4} \quad . \tag{20}$$

Combining equations from (15) to (20), we obtain maximum radiation temperature as a function of $\Phi(A=1)$ (dimensionless comoving inflaton energy density at the end of the inflation).

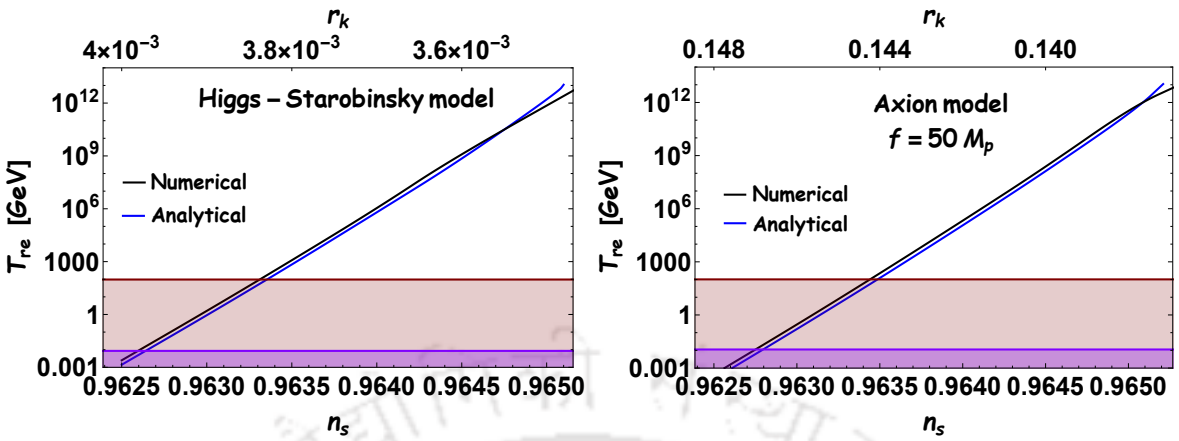

Figure 1: Variation of reheating temperature (T_{re}) as a function of n_s for Higgs-Starobinsky and axion inflation model with $\omega_{eff} = 10^{-3}$ in the framework of two-phase analysis. The solid blue line indicates the result from approximate analytical expression (equation 21) whereas the solid black line shows results from numerical analysis. The light brown region is below the electroweak scale $T_{ew} \backsim 100\ GeV$, and the violet region below $10^{-2}\ GeV$ would ruin the predictions of big bang nucleosynthesis (BBN).

.

Analytic expression of inflaton decay width Γ_ϕ and T_{re}

Assuming the end point of reheating as $x_{re} = a_{re}/a_{npre}$, and considering equation (8), reheating temperature can be obtained as

$$T_{re}^4 = \frac{\Gamma_\phi \rho_\phi^{in}(1+\omega_\phi^1)x_{re}^{-4}}{\beta H_{in}}\left[\frac{2}{5-c}\left(x_{re}^{\frac{5-c}{2}}-1\right)+\frac{\rho_R^{in}}{\rho_\phi^{in}}\left(\frac{1-x_{re}^{\frac{c+3}{2}}}{c+3}+\frac{H_{in}}{\Gamma_\phi(1+\omega_\phi^1)}\right)\right]. \tag{21}$$

Using Eq.2.49 (entropy conservation of thermal radiation), one arrives at the following relation

$$T_{re}^4 = \left(\frac{43}{11g_{re}}\right)^{4/3}\left(\frac{a_0T_0}{k}\right)^4 H_k^4 e^{-4N_k}e^{-4N_{npre}}e^{-4N_{pre}} = G^4\left(\frac{a_{re}}{a_{npre}}\right)^{-4} = G^4 x_{re}^{-4}\ , \tag{22}$$

where

$$G = \left(\frac{43}{11g_{re}}\right)^{1/3}\left(\frac{a_0T_0}{k}\right)H_k e^{-N_k}e^{-N_{npre}}\ . \tag{23}$$

Comparing equation (21) and (22), we obtain Γ_ϕ in terms of x_{re}

$$\begin{aligned}\Gamma_\phi &= \left(\frac{G^4\beta}{\rho_\phi^{in}}-\frac{\rho_R^{in}}{\rho_\phi^{in}}\right)\frac{H_{in}}{(1+\omega_\phi^1)}\left[\frac{2}{5-c}\left(x_{re}^{\frac{5-c}{2}}-1\right)+\frac{\rho_R^{in}}{\rho_\phi^{in}}\left(\frac{1-x_{re}^{\frac{c+3}{2}}}{c+3}\right)\right]^{-1}, \\ &\simeq \left(\frac{G^4\beta}{\rho_\phi^{in}}-\frac{\rho_R^{in}}{\rho_\phi^{in}}\right)\frac{H_{in}}{(1+\omega_\phi^1)}\frac{5-c}{2}x_{re}^{\frac{c-5}{2}}\left[1+\frac{5-c}{2\,(c+3)}\frac{\rho_R^{in}}{\rho_\phi^{in}}x_{re}^{c-1}\right].\end{aligned} \tag{24}$$

Reheating temperature is defined when the inflaton field comes in thermal equilibrium with the radiation bath at the point,

$$H(x_{re})^2 = \frac{\rho_\phi(x_{re})+\rho_R(x_{re})}{3M_p^2} \simeq \frac{\rho_R(x_{re})}{3M_p^2} = \Gamma_\phi^2\ . \tag{25}$$

In the above equation, we ignore the contribution of inflaton energy density to be negligible. Using the expression for the radiation energy density we can obtain the decay width as follows,

$$\Gamma_\phi^2 \simeq \left(\frac{G^4\beta}{\rho_\phi^{in}} - \frac{\rho_R^{in}}{\rho_\phi^{in}}\right)^2 \frac{H_{in}^2}{(1+\omega_\phi^1)^2}\left(\frac{5-c}{2}\right)^2 x_{re}^{c-5}\left[1+\frac{5-c}{c+3}\,\frac{\rho_R^{in}}{\rho_\phi^{in}}\,x_{re}^{c-1}\right] \quad . \tag{26}$$

In the earlier expression, we can ignore the second term in the third bracket since $x_{re} \gg 1$ for most of the values of the spectral index. As a result, the Γ_ϕ^2 can now be written as

$$\Gamma_\phi^2 \simeq \left(\frac{G^4\beta}{\rho_\phi^{in}} - \frac{\rho_R^{in}}{\rho_\phi^{in}}\right)^2 \frac{H_{in}^2}{(1+\omega_\phi^1)^2}\left(\frac{5-c}{2}\right)^2 x_{re}^{c-5} \quad . \tag{27}$$

Furthermore, the radiation energy density at the ending point of reheating era $\rho_R(x_{re})$ can be expressed as

$$\rho_R(x_{re}) \simeq x_{re}^{-4}\rho_\phi^{in}\left[\frac{2}{5-c}\frac{\Gamma_\phi\left(1+\omega_\phi^1\right)}{H_{in}}x_{re}^{\frac{5-c}{2}} + \frac{\rho_R^{in}}{\rho_\phi^{in}}\left(1-\frac{\Gamma_\phi\left(1+\omega_\phi^1\right)}{H_{in}}\frac{x_{re}^{\frac{c+3}{2}}}{c+3}\right)\right] \tag{28}$$

Combining equations (24) and (28) one can find

$$\rho_R(x_{re}) = \beta T_{re}^4 \simeq x_{re}^{-4}\rho_\phi^{in}\left[\frac{G^4\beta}{\rho_\phi^{in}} + \frac{5-c}{2\,(c+3)}\frac{\rho_R^{in}}{\rho_\phi^{in}}\left(\frac{G^4\beta}{\rho_\phi^{in}} - \frac{\rho_R^{in}}{\rho_\phi^{in}}\right)x_{re}^{c-1}\right] \quad . \tag{29}$$

Now equating this above equation with Γ_ϕ^2 (eqn 27), one arrives at the following expression

$$x_{re} = \left(\frac{\alpha}{\eta}\right)^{\frac{1}{c-1}} \quad , \tag{30}$$

Here

$$\alpha = \frac{G^4\beta}{\rho_\phi^{in}} \;,\; \eta = \frac{5-c}{2}\left(\frac{G^4\beta}{\rho_\phi^{in}} - \frac{\rho_R^{in}}{\rho_\phi^{in}}\right)\left[\frac{\rho_R^{in}}{(c+3)\,\rho_\phi^{in}} + \frac{5-c}{2}\frac{3M_p^2H_{in}^2}{\rho_\phi^{in}\left(1+\omega_\phi^1\right)^2}\left(\frac{G^4\beta}{\rho_\phi^{in}} - \frac{\rho_R^{in}}{\rho_\phi^{in}}\right)\right] . \tag{31}$$

By utilizing the above equation, we can easily fix decay width (Eqn 24) and reheating temperature (Eqn 29) as they are the function of x_{re}. Besides, the maximum reheating temperature and associated maximum possible value of the spectral index (n_s^{max}) can also be defined at the point $x_{re} \to 1$ ($N_{pre} \to 0$). To check whether our analytical calculations predict the correct result, we plot reheating temperature as a function of the spectral index (Fig.1) and compare it with our numerical result.

Analytical expression of dark matter abundance and origin of maximum dark matter mass M_X^{max}

The relevant Boltzmann equation for the evolution of dark matter during perturbative reheating phase is expressed as

$$d(\,n_X\,a^3\,) = -a^3\,\langle\,\sigma\,v\,\rangle\,\left[\,n_X^2 - (\,n_X^{eq}\,)^2\,\right]\,dt = -a^2\,\langle\,\sigma\,v\,\rangle\,\left[\,n_X^2 - (\,n_X^{eq}\,)^2\,\right]\,\frac{dt}{H} \quad . \tag{32}$$

Let us assume that the dark matter particles are relativistic ($M_X << T$) and never reach chemical equilibrium ($n_X << n_X^{eq}$) during reheating. Therefore Eqn.32 can be approximated as

$$d(\, n_X\, a^3\,) = \frac{a^3\,\langle\,\sigma\,v\,\rangle\,(\,n_X^{eq}\,)^2}{a\,H}\,da \simeq \frac{g^2}{\pi^4}\,\frac{a^2\,\langle\sigma\,v\,\rangle\,T^6}{H}\,da \quad , \tag{33}$$

where we use the equilibrium distribution of the dark matter in the relativistic limit

$$n_X^{eq} = \frac{g\,T^3}{\pi^2} \quad . \tag{34}$$

Here g counts the number of degrees of freedom associated with the dark matter particles. The Hubble parameter during perturbative reheating can be expressed as

$$H = H_{in} x^{-3\,(1+\omega_\phi^1)}\,;\; x = a/a_{in}\,. \tag{35}$$

In terms of new variable x, the expression (33) can be rewritten as

$$d(\, n_X\, x^3\,) = \frac{g^2}{\pi^4}\,\frac{x^2\,\langle\sigma\,v\,\rangle\,T^6}{H}\,dx \quad , \tag{36}$$

Upon substitution of the Eqns (8) and (35) in Eqn.(36), one can find

$$d(\, n_X\, x^3\,) \simeq \gamma_1\,\langle\sigma v\rangle\left(x^{\frac{11+c}{4}} - \frac{3\,(5-c)}{4\gamma}\,\frac{\rho_R^{in}}{\rho_\phi^{in}}\,x^{\frac{1}{4}(7+5\,c)}\right)\,dx \tag{37}$$

where,

$$\gamma = \frac{\Gamma_\phi\left(1+\omega_\phi^1\right)}{H_{in}}\,;\; \gamma_1 = \frac{g^2\,\rho_\phi^{in}}{\pi^4}\left(\frac{2\gamma}{\beta(5-c)}\right)^{3/2}\sqrt{3}\,M_p \tag{38}$$

Straightforward integration of the above Eqn.(37), the comoving number density is found to be

$$n_X^f x_f^3 \simeq n_X^{in} + \langle\sigma v\rangle f(x_f) \quad , \tag{39}$$

where $f(x_f)$ can be expressed as

$$f(x_f) = \gamma_1\left[\frac{4}{15+c}\left(x_f^{\frac{15+c}{4}} - 1\right) - \frac{3\,(5-c)}{(11+5\,c)\;\gamma}\,\frac{\rho_R^{in}}{\rho_\phi^{in}}\left(x_f^{\frac{11+5c}{4}} - 1\right)\right] \tag{40}$$

Here, the rescaled factor at the point of freeze-in is defined as x_f, when both comoving dark matter and radiation components become constant. The dark matter relic can be obtained in terms of radiation abundance Ω_R ($\Omega_R h^2 = 4.3\times10^{-5}$) as

$$\Omega_X h^2 = \frac{\rho_X(x_f)}{\rho_R(x_f)}\frac{T(x_f)}{T_{now}}\Omega_R h^2 = \frac{\langle E_X\rangle_f x_f^{-3} n_X^f(x_f) x_f^3}{\rho_R(x_f)}\frac{T(x_f)}{T_{now}}\Omega_R h^2 = 0.12 \quad . \tag{41}$$

Inserting the expression of $n_X^f x_f^3$ (equation (39)) into the above equation, one can arrive at the following equation for the dark matter abundance,

$$\Omega_X h^2 \simeq \frac{\langle E_X\rangle_f x_f^{-3}}{\rho_R(x_f)}\frac{T(x_f)}{T_{now}}\left(n_X^{in} + \langle\sigma v\rangle f(x_f)\right)\Omega_R h^2 \quad , \tag{42}$$

The average energy of the single component dark matter at the point of freeze-in can be expressed as

$$\langle E_X \rangle_f \simeq \sqrt{M_X^2 + 9T(x_f)^2} \simeq 3T(x_f)\left(1 + \frac{M_X^2}{18T(x_f)^2}\right) \quad \text{(relativistic approximation)} \quad (43)$$

Therefore, by Connecting the above two equations (42) and (43), one arrives at the following expression

$$\Omega_X h^2 \simeq \frac{3x_f^{-3}\rho_R(x_f)^{-1/2}(1 + \frac{M_X^2\beta^{1/2}\rho_R(x_f)^{-1/2}}{18})}{\beta^{1/2}T_{now}} \left(n_X^{in} + \langle\sigma v\rangle f(x_f)\right)\Omega_R h^2 \quad . \quad (44)$$

Maximum possible dark matter mass (M_X^{max})

The approximate analytical expression of dark matter abundance (equation (44)) indicates that the dark matter abundance increases with increasing dark matter mass. Moreover, at a particular value of the dark matter mass, the dark matter component's initial number density (n_X^{in}) is sufficient to produce the present observed value of the dark matter abundance $\Omega_X h^2 = 0.12$. We define this particular value of the dark matter mass as M_X^{max}. We can clearly see from equation (44), if the mass of the dark matter $M_X > M_X^{max}$, the abundance $\Omega_X h^2$ always ≥ 0.12. Therefore the condition for the maximum possible dark matter mass can be written as

$$\Omega_X h^2 \simeq \frac{\sqrt{M_X^2 + 9T(x_f)^2}x_f^{-3}}{\rho_R(x_f)} \frac{T(x_f)n_X^{in}}{T_{now}} \Omega_R h^2 = 0.12 \quad . \quad (45)$$

The outcome of this equation is the maximum possible mass, M_X^{max}, which is determined to be

$$M_X^{max} = T(x_f)\sqrt{\left(0.12\frac{\beta}{n_X^{in}}\frac{T_{now}T(x_f)^2}{\Omega_R h^2 x_f^{-3}}\right)^2 - 9} \quad . \quad (46)$$

Gravitational dark matter production: Analytic study

Analytic expression of maximum dark matter mass m_Y^{max}

The expression for the relic abundance Eq.5.15 indicates that the dark matter abundance increases with increasing the dark matter mass. Consequently, there should exist a maximum allowed dark matter mass m_Y^{max} associated with each viable value of the spectral index or reheating temperature. The evolution of the gravitationally produce dark matter number density follows from the equation

$$d\,(\,n_Y\,a^3\,) = \frac{\Gamma_{\phi\phi\to YY}}{m_\phi}\,\frac{\rho_\phi\,(\,1+\omega_\phi\,)}{H}\,a^2\,da \quad . \tag{47}$$

Comoving number density of scalar dark matter: The comoving number density at the end of the reheating era is followed by the equations (5.2), (47) and found to be

$$n_s^{re}\,A_{re}^3 = \int_1^{A_{re}} \frac{\rho_\phi^2\,(\,1+\omega_\phi\,)}{1024\,\pi\,M_p^4}\left(1+\frac{m_s^2}{2\,m_\phi^2}\right)\sqrt{1-\frac{m_s^2}{m_\phi^2}}\,\frac{A^2\,dA}{H} \approx \int_1^{A_{re}} \frac{\rho_\phi^2\,(\,1+\omega_\phi\,)}{1024\,\pi\,M_p^4}\,\frac{A^2\,dA}{H} \quad . \tag{48}$$

Ignoring the sub-dominated effect of the dark matter production in the evolution of the inflaton energy density, the inflaton energy density shall follow the following equation

$$\rho_\phi = \rho_\phi^{end}\,A^{-3\,(\,1+\omega_\phi\,)}\,e^{-\Gamma_\phi\,(\,1+\omega_\phi\,)\,(t-t_{end}\,)} \approx \rho_\phi^{end}\,A^{-3\,(\,1+\omega_\phi\,)} \quad , \tag{49}$$

where ρ_ϕ^{end} is the inflaton energy density at the end of the inflation. As the initial stage of the perturbative reheating is dominated by the inflaton energy density, the main contribution in the gravitationally produced dark matter sector is coming at the initial stage. Therefore, we can ignore the effect of the decay constant Γ_ϕ in determining the gravitationally produced dark matter number density. The Hubble parameter during perturbative reheating can be approximated as

$$H = H_{end}\,A^{-\frac{3}{2}\,(\,1+\omega_\phi\,)} \quad , \tag{50}$$

where $H_{end} = \sqrt{\rho_\phi^{end}/3\,M_p^2}$ is the Hubble parameter at the end of the inflation. Upon substituting the equations (49) and (50) in the expression of the comoving gravitationally produced dark matter number density (Eqns.48), we obtain

$$n_s^{re}\,A_{re}^3 \approx \frac{(\,\rho_\phi^{end}\,)^2\,(\,1+\omega_\phi\,)}{1024\,\pi\,M_p^4\,H_{end}}\int_1^{Are} A^{-\frac{1}{2}\,(\,5+3\,\omega_\phi\,)}\,dA = \frac{3}{512\,\pi}\,\frac{(\,1+\omega_\phi\,)}{(\,1+3\,\omega_\phi\,)}\,H_{end}^3\left[1-A_{re}^{-\frac{3}{2}\,(\,1+3\,\omega_\phi\,)}\right]. \tag{51}$$

Comoving number density of fermionic dark matter: The relic abundance of the dark matter is obtained from the comoving dark matter number density, calculated at the end of the reheating. Inserting the expression for the decay width Eq.5.3) into the Eq.47, the corresponding number density of the dark matter for this present scenario turns out to be

$$n_f^{re}\,A_{re}^3 = \int_1^{A_{re}} \frac{\rho_\phi^2\,m_f^2\,(1+\omega_\phi)}{4096\,\pi\,M_p^4\,m_\phi^2}\left(1-\frac{m_f^2}{m_\phi^2}\right)\frac{A^2\,dA}{H} \approx \int_1^{A_{re}} \frac{\rho_\phi^2\,m_f^2\,(1+\omega_\phi)}{4096\,\pi\,M_p^4\,m_\phi^2}\,\frac{A^2\,dA}{H}\quad . \tag{52}$$

The inflaton mass m_ϕ^2 can be calculated from the second derivative of the inflaton potential. Since reheating happens near the minimum of the potential we first expand the inflaton potential in the limit of $\phi << M_p$ as

$$V(\phi) \simeq \lambda\,\phi^{2n}\,, \tag{53}$$

where $\lambda = \Lambda^4\left(\sqrt{\frac{2}{3\,\alpha}}\,\frac{1}{M_p}\right)^{2n}$. Therefore,

$$m_\phi^2 = V''(\phi_0(t)) \simeq 2n\,(2n-1)\,\lambda^{\frac{1}{n}}\,\rho_\phi^{\frac{n-1}{n}} \tag{54}$$

Upon substituting the equations (54), (50) and (49) into the expression (52), one can find the gravitationally produced comoving fermionic dark matter number density at the end of reheating as

$$n_f^{re}A_{re}^3 = \frac{H_{end}^3\,m_f^2\,\lambda^{\frac{\omega_\phi-1}{\omega_\phi+1}}\,\nu(\omega_\phi)}{4096\,\pi\,(1+3\,\omega_\phi)\left(H_{end}^2M_p^2\right)^{\frac{2\,\omega_\phi}{1+\omega_\phi}}}\left[1-A_{re}^{-\frac{3}{2}(1-\omega_\phi)}\right] \simeq \frac{3}{2048\,\pi}\,\frac{1+\omega_\phi}{1-\omega_\phi}\,H_{end}^3\left(\frac{m_f}{m_\phi^{end}}\right)^2\,, \tag{55}$$

where $\nu(\omega_\phi) = 3^{\frac{1-\omega_\phi}{1+\omega_\phi}}\,(1-\omega_\phi)$ and m_ϕ^{end} indicates effective mass calculated at the end of the inflation. We use the relation $\omega_\phi = (n-1)/(n+1)$, to find the above relation of comoving dark matter number density in terms of ω_ϕ.

Comoving number density of vector dark matter: For vector dark matter, the comoving number density can be written as (Combining Eqns.5.4 and 47)

$$n_X^{re}\,A_{re}^3 = \int_1^{A_{re}} \frac{\rho_\phi^2\,(1+\omega_\phi)}{32768\,\pi\,M_p^4}\sqrt{1-\frac{m_X^2}{m_\phi^2}}\left(4+4\,\frac{m_X^2}{m_\phi^2}+19\,\frac{m_X^4}{m_\phi^4}\right)\frac{A^2\,dA}{H} \approx \int_1^{A_{re}} \frac{\rho_\phi^2\,(1+\omega_\phi)}{8192\,\pi\,M_p^4}\,\frac{A^2\,dA}{H}\quad . \tag{56}$$

We can see that in the limit of $m_X << m_\phi$, the above expression can be related with the comoving number density for the scalar dark matter (Eqn.48) through a 1/8 factor. Therefore,

$$n_X^{re}\,A_{re}^3 = \frac{1}{8}\,n_s^{re}\,A_{re}^3 = -\frac{3}{4096\,\pi}\,\frac{(1+\omega_\phi)}{(1+3\,\omega_\phi)}\,H_{end}^3\left[A_{re}^{-\frac{3}{2}(1+3\,\omega_\phi)}-1\right]\quad . \tag{57}$$

Expression for m_Y^{max}: As we mentioned earlier, the dark matter relic $\Omega_Y h^2$ could be expressed in terms of present radiation abundance $\Omega_R\,h^2$ as

$$\Omega_Y\,h^2 = \frac{\rho_Y\,(A_{re})}{\rho_R\,(A_{re})}\,\frac{T_{re}}{T_{now}}\,\Omega_r\,h^2 = \frac{m_Y\,A_{re}^{-3}\,(n_Y^{re}\,A_{re}^3)}{\beta\,T_{re}^3\,T_{now}}\,\Omega_r\,h^2\quad , \tag{58}$$

where $\beta = \pi^2 g_{re}/30$. In the context of the perturbative reheating dynamics, one can obtain the approximate analytical expression for the reheating temperature T_{re} and the normalized scale factor A_{re} at the end of the reheating to be (in this context, see Ref. [93])

$$T_{re} = \mathcal{G}\, Are^{-1},\ \mathcal{G} = \left(\frac{43}{11\, g_{s,re}}\right)^{\frac{1}{3}} \left(\frac{a_0\, T_0}{k}\right) H_k\, e^{-N_k},\ A_{re} = \left(\frac{12\, M_p^2\, H_{end}^2\, (\,1+\,\omega_\phi\,)^2}{\mathcal{G}^4\, \beta\, (\,5-\,3\,\omega_\phi\,)^2}\right)^{\frac{-1}{(1-3\,\omega_\phi)}}. \tag{59}$$

Inserting expression of the reheating temperature into the expression of the present-day dark matter relic (admitting only gravitationally produced dark matter), the maximum allowed dark matter mass can be written as

$$m_Y^{max} = \frac{\mathcal{G}\,\beta\, T_{now}}{n_Y^{re}\, A_{re}^3}\, \frac{\Omega_Y\, h^2}{\Omega_r\, h^2}\,. \tag{60}$$

By utilizing the above equations with the expression of the comoving number density for gravitationally produced dark matter (Eqns. 51, 55 and 57), we can easily fix m_Y^{max}.

Comoving number density of the gravitationally produced dark matter from SM scattering:

The evolution of the gravitational produced dark matter number density from radiation bath is followed by the Eqn.5.20 as

$$d(n_{Y(R)}\, A^3) = \gamma\, \frac{T^8}{M_p^4}\, \frac{A^2\, dA}{H}\,. \tag{61}$$

In the perturbative reheating scenario, the analytical expression for the radiation temperature during reheating can be obtained as

$$T = \gamma_3^{1/4}\, A^{-\frac{3}{8}\,(1+\omega_\phi)},\ \gamma_3 = \frac{6}{5-3\,\omega_\phi}\, \frac{M_p^2\, H_{end}}{\beta}\, \Gamma_\phi\, (\,1+\omega_\phi\,)\quad . \tag{62}$$

Upon substitution of the Eqn.62 along with Eqn.50 in equation 61, the comoving number density turns out to be

$$n_{Y(R)}^{re}\, A_{re}^3 = \frac{\gamma\, \gamma_3^2}{M_p^4\, H_{end}} \int_1^{A_{re}} A^{\frac{1}{2}\,(1-3\omega_\phi\,)}\, dA = \frac{2}{3\,(1-\omega_\phi)}\, \frac{\gamma\, \gamma_3^2}{M_p^4\, H_{end}} \left[A_{re}^{\frac{3}{2}\,(1-\omega_\phi)} - 1\right] \tag{63}$$

As the normalized scale factor at the end of the reheating $A_{re} >> 1$ (except for the temperature associated with the instantaneous reheating), the above equation is simplified as

$$n_{Y(R)}^{re}\, A_{re}^3 = \frac{2}{3\,(1-\omega_\phi)}\, \frac{\gamma\, \gamma_3^2}{M_p^4\, H_{end}}\, A_{re}^{\frac{3}{2}\,(1-\omega_\phi)} \simeq \frac{2\gamma}{3\,(\,1-\omega_\phi\,)}\, \frac{e^{\frac{3}{2}\,N_{re}\,(\,3+\,\omega_\phi\,)}\, T_{re}^8}{M_p^4\, H_{end}}\,. \tag{64}$$

To find the above-simplified form, we use the approximate analytic expression for reheating temperature $T_{re} = \gamma_3^{1/4}\, A_{re}^{-\frac{3}{8}\,(1+\omega_\phi)}$ [92, 93].

Bibliography

[1] WMAP collaboration, *Seven-Year Wilkinson Microwave Anisotropy Probe (WMAP) Observations: Cosmological Interpretation*, *Astrophys. J. Suppl.* **192** (2011) 18 [1001.4538].

[2] Planck collaboration, *Planck 2018 results. VI. Cosmological parameters*, *Astron. Astrophys.* **641** (2020) A6 [1807.06209].

[3] A.D. Linde, *Chaotic Inflation*, *Phys. Lett. B* **129** (1983) 177.

[4] G.F. Giudice, E.W. Kolb and A. Riotto, *Largest temperature of the radiation era and its cosmological implications*, *Phys. Rev. D* **64** (2001) 023508 [hep-ph/0005123].

[5] A. Albrecht, P.J. Steinhardt, M.S. Turner and F. Wilczek, *Reheating an Inflationary Universe*, *Phys. Rev. Lett.* **48** (1982) 1437.

[6] L.F. Abbott, E. Farhi and M.B. Wise, *Particle Production in the New Inflationary Cosmology*, *Phys. Lett. B* **117** (1982) 29.

[7] A.D. Dolgov and D.P. Kirilova, *ON PARTICLE CREATION BY A TIME DEPENDENT SCALAR FIELD*, *Sov. J. Nucl. Phys.* **51** (1990) 172.

[8] J.H. Traschen and R.H. Brandenberger, *Particle Production During Out-of-equilibrium Phase Transitions*, *Phys. Rev. D* **42** (1990) 2491.

[9] M.E. Peskin and D.V. Schroeder, *An Introduction to quantum field theory*, Addison-Wesley, Reading, USA (1995).

[10] M. Drewes, J.U. Kang and U.R. Mun, *CMB constraints on the inflaton couplings and reheating temperature in α-attractor inflation*, *JHEP* **11** (2017) 072 [1708.01197].

[11] Particle Data Group collaboration, *Review of Particle Physics*, *Chin. Phys. C* **40** (2016) 100001.

[12] P.B. Greene and L. Kofman, *Preheating of fermions*, *Phys. Lett. B* **448** (1999) 6 [hep-ph/9807339].

[13] H. Kodama and M. Sasaki, *Cosmological Perturbation Theory*, *Prog. Theor. Phys. Suppl.* **78** (1984) 1.

[14] V.F. Mukhanov, H.A. Feldman and R.H. Brandenberger, *Theory of cosmological perturbations. Part 1. Classical perturbations. Part 2. Quantum theory of perturbations. Part 3. Extensions*, *Phys. Rept.* **215** (1992) 203.

[15] A. Riotto, *Inflation and the theory of cosmological perturbations*, *ICTP Lect. Notes Ser.* **14** (2003) 317 [hep-ph/0210162].

[16] D. Baumann, *Inflation*, in *Theoretical Advanced Study Institute in Elementary Particle Physics: Physics of the Large and the Small*, 7, 2009, DOI [0907.5424].

[17] L. Sriramkumar, *An introduction to inflation and cosmological perturbation theory*, 0904.4584.

[18] J. Yokoyama, *Inflation: 1980–201X*, *PTEP* **2014** (2014) 06B103.

[19] J.M. Bardeen, *Gauge Invariant Cosmological Perturbations*, *Phys. Rev. D* **22** (1980) 1882.

[20] M. Maggiore, *Gravitational wave experiments and early universe cosmology*, *Phys. Rept.* **331** (2000) 283 [gr-qc/9909001].

[21] J. Martin, *Inflation and precision cosmology*, *Braz. J. Phys.* **34** (2004) 1307 [astro-ph/0312492].

[22] J. Martin, *Inflationary cosmological perturbations of quantum-mechanical origin*, *Lect. Notes Phys.* **669** (2005) 199 [hep-th/0406011].

[23] B.A. Bassett, S. Tsujikawa and D. Wands, *Inflation dynamics and reheating*, *Rev. Mod. Phys.* **78** (2006) 537.

[24] D. Baumann and H.V. Peiris, *Cosmological Inflation: Theory and Observations*, *Adv. Sci. Lett.* **2** (2009) 105 [0810.3022].

[25] L. Sriramkumar, *On the generation and evolution of perturbations during inflation and reheating*, in *Vignettes in Gravitation and Cosmology*, L. Sriramkumar and T.R. Seshadri, eds. (2012), DOI.

[26] A. Linde, *Inflationary Cosmology after Planck 2013*, in *100e Ecole d'Ete de Physique: Post-Planck Cosmology*, 2, 2014, DOI [1402.0526].

[27] J. Martin, *The Observational Status of Cosmic Inflation after Planck*, *Astrophys. Space Sci. Proc.* **45** (2016) 41 [1502.05733].

[28] L.A. Boyle and P.J. Steinhardt, *Probing the early universe with inflationary gravitational waves*, *Phys. Rev. D* **77** (2008) 063504 [astro-ph/0512014].

[29] Planck collaboration, *Planck 2018 results. X. Constraints on inflation*, *Astron. Astrophys.* **641** (2020) A10 [1807.06211].

[30] K. Freese, J.A. Frieman and A.V. Olinto, *Natural inflation with pseudo - Nambu-Goldstone bosons*, *Phys. Rev. Lett.* **65** (1990) 3233.

[31] K. Freese and W.H. Kinney, *Natural Inflation: Consistency with Cosmic Microwave Background Observations of Planck and BICEP2*, *JCAP* **03** (2015) 044 [1403.5277].

[32] R. Kallosh and A. Linde, *Universality Class in Conformal Inflation*, *JCAP* **07** (2013) 002 [1306.5220].

[33] R. Kallosh, A. Linde and D. Roest, *Superconformal Inflationary α-Attractors*, *JHEP* **11** (2013) 198 [1311.0472].

[34] A.A. Starobinsky, *A New Type of Isotropic Cosmological Models Without Singularity*, *Phys. Lett. B* **91** (1980) 99.

[35] F.L. Bezrukov and M. Shaposhnikov, *The Standard Model Higgs boson as the inflaton*, *Phys. Lett. B* **659** (2008) 703 [0710.3755].

[36] D. Maity and P. Saha, *Minimal plateau inflationary cosmologies and constraints from reheating*, *Class. Quant. Grav.* **36** (2019) 045010 [1902.01895].

[37] A.H. Guth, *The Inflationary Universe: A Possible Solution to the Horizon and Flatness Problems*, *Phys. Rev. D* **23** (1981) 347.

[38] A.D. Linde, *A New Inflationary Universe Scenario: A Possible Solution of the Horizon, Flatness, Homogeneity, Isotropy and Primordial Monopole Problems*, *Phys. Lett. B* **108** (1982) 389.

[39] A. Albrecht and P.J. Steinhardt, *Cosmology for Grand Unified Theories with Radiatively Induced Symmetry Breaking*, *Phys. Rev. Lett.* **48** (1982) 1220.

[40] V.F. Mukhanov and G.V. Chibisov, *Quantum Fluctuations and a Nonsingular Universe*, *JETP Lett.* **33** (1981) 532.

[41] L. Senatore, *Lectures on Inflation*, in *Theoretical Advanced Study Institute in Elementary Particle Physics: New Frontiers in Fields and Strings*, pp. 447–543, 2017, DOI [1609.00716].

[42] G. Steigman, *Primordial Nucleosynthesis in the Precision Cosmology Era*, *Ann. Rev. Nucl. Part. Sci.* **57** (2007) 463 [0712.1100].

[43] P. Adshead, R. Easther, J. Pritchard and A. Loeb, *Inflation and the Scale Dependent Spectral Index: Prospects and Strategies*, *JCAP* **02** (2011) 021 [1007.3748].

[44] S. Dodelson, *How much can we learn about the physics of inflation?*, *Phys. Rev. Lett.* **112** (2014) 191301 [1403.6310].

[45] L. Dai, M. Kamionkowski and J. Wang, *Reheating constraints to inflationary models*, *Phys. Rev. Lett.* **113** (2014) 041302 [1404.6704].

[46] P. Creminelli, D. López Nacir, M. Simonović, G. Trevisan and M. Zaldarriaga, ϕ^2 *Inflation at its Endpoint*, *Phys. Rev. D* **90** (2014) 083513 [1405.6264].

[47] J.L. Cook, E. Dimastrogiovanni, D.A. Easson and L.M. Krauss, *Reheating predictions in single field inflation*, *JCAP* **04** (2015) 047 [1502.04673].

[48] A.D. Dolgov and A.D. Linde, *Baryon Asymmetry in Inflationary Universe*, *Phys. Lett. B* **116** (1982) 329.

[49] L. Kofman, A.D. Linde and A.A. Starobinsky, *Reheating after inflation*, *Phys. Rev. Lett.* **73** (1994) 3195 [hep-th/9405187].

[50] Y. Shtanov, J.H. Traschen and R.H. Brandenberger, *Universe reheating after inflation*, *Phys. Rev. D* **51** (1995) 5438 [hep-ph/9407247].

[51] D. Boyanovsky, M. D'Attanasio, H.J. de Vega, R. Holman, D.S. Lee and A. Singh, *Reheating the postinflationary universe*, hep-ph/9505220.

[52] M. Yoshimura, *Catastrophic particle production under periodic perturbation*, *Prog. Theor. Phys.* **94** (1995) 873 [hep-th/9506176].

[53] D.I. Kaiser, *Post inflation reheating in an expanding universe*, *Phys. Rev. D* **53** (1996) 1776 [astro-ph/9507108].

[54] L. Kofman, A.D. Linde and A.A. Starobinsky, *Towards the theory of reheating after inflation*, *Phys. Rev. D* **56** (1997) 3258 [hep-ph/9704452].

[55] J.-F. Dufaux, D.G. Figueroa and J. Garcia-Bellido, *Gravitational Waves from Abelian Gauge Fields and Cosmic Strings at Preheating*, *Phys. Rev. D* **82** (2010) 083518 [1006.0217].

[56] D.G. Figueroa, J. García-Bellido and F. Torrentí, *Gravitational wave production from the decay of the standard model Higgs field after inflation*, *Phys. Rev. D* **93** (2016) 103521 [1602.03085].

[57] J.T. Giblin and E. Thrane, *Estimates of maximum energy density of cosmological gravitational-wave backgrounds*, *Phys. Rev. D* **90** (2014) 107502 [1410.4779].

[58] J.R. Bond, A.V. Frolov, Z. Huang and L. Kofman, *Non-Gaussian Spikes from Chaotic Billiards in Inflation Preheating*, *Phys. Rev. Lett.* **103** (2009) 071301 [0903.3407].

[59] S. Antusch, F. Cefala and S. Orani, *Gravitational waves from oscillons after inflation*, *Phys. Rev. Lett.* **118** (2017) 011303 [1607.01314].

[60] K.D. Lozanov and M.A. Amin, *Equation of State and Duration to Radiation Domination after Inflation*, *Phys. Rev. Lett.* **119** (2017) 061301 [1608.01213].

[61] J.B. Munoz and M. Kamionkowski, *Equation-of-State Parameter for Reheating*, *Phys. Rev. D* **91** (2015) 043521 [1412.0656].

[62] J. Martin, C. Ringeval and V. Vennin, *Observing Inflationary Reheating*, *Phys. Rev. Lett.* **114** (2015) 081303 [1410.7958].

[63] J. Martin, C. Ringeval and V. Vennin, *Information Gain on Reheating: the One Bit Milestone*, *Phys. Rev. D* **93** (2016) 103532 [1603.02606].

[64] R.J. Hardwick, V. Vennin, K. Koyama and D. Wands, *Constraining Curvatonic Reheating*, *JCAP* **08** (2016) 042 [1606.01223].

[65] J. Martin, C. Ringeval and V. Vennin, *Encyclopædia Inflationaris*, *Phys. Dark Univ.* **5-6** (2014) 75 [1303.3787].

[66] A.R. Liddle and S.M. Leach, *How long before the end of inflation were observable perturbations produced?*, *Phys. Rev. D* **68** (2003) 103503 [astro-ph/0305263].

[67] M. Kawasaki, K. Kohri and N. Sugiyama, *Cosmological constraints on late time entropy production*, *Phys. Rev. Lett.* **82** (1999) 4168 [astro-ph/9811437].

[68] M. Kawasaki, K. Kohri and N. Sugiyama, *MeV scale reheating temperature and thermalization of neutrino background*, *Phys. Rev. D* **62** (2000) 023506 [astro-ph/0002127].

[69] B.D. Fields, P. Molaro and S. Sarkar, *Big-Bang Nucleosynthesis*, *Chin. Phys. C* **38** (2014) 339 [1412.1408].

[70] O.E. Núñez, J. Socorro and R. Hernández-Jiménez, *Hamilton's approach in cosmological inflation with an exponential potential and its observational constraints*, *Astrophys. Space Sci.* **364** (2019) 69 [1806.01190].

[71] E.W. Kolb, A.D. Linde and A. Riotto, *GUT baryogenesis after preheating*, *Phys. Rev. Lett.* **77** (1996) 4290 [hep-ph/9606260].

[72] A. Dolgov, K. Freese, R. Rangarajan and M. Srednicki, *Baryogenesis during reheating in natural inflation and comments on spontaneous baryogenesis*, *Phys. Rev. D* **56** (1997) 6155 [hep-ph/9610405].

[73] A. Riotto and M. Trodden, *Recent progress in baryogenesis*, *Ann. Rev. Nucl. Part. Sci.* **49** (1999) 35 [hep-ph/9901362].

[74] J. Garcia-Bellido, D.Y. Grigoriev, A. Kusenko and M.E. Shaposhnikov, *Nonequilibrium electroweak baryogenesis from preheating after inflation*, *Phys. Rev. D* **60** (1999) 123504 [hep-ph/9902449].

[75] R. Allahverdi, B.A. Campbell and J.R. Ellis, *Reheating and supersymmetric flat direction baryogenesis*, *Nucl. Phys. B* **579** (2000) 355 [hep-ph/0001122].

[76] S. Davidson, M. Losada and A. Riotto, *A New perspective on baryogenesis*, *Phys. Rev. Lett.* **84** (2000) 4284 [hep-ph/0001301].

[77] A. Megevand, *Effect of reheating on electroweak baryogenesis*, *Phys. Rev. D* **64** (2001) 027303 [hep-ph/0011019].

[78] NEWSdm collaboration, *New Experiment NEWSdm for Direct Searches for Heavy Dark Matter Particles*, *Phys. Atom. Nucl.* **83** (2020) 83.

[79] M.S. Turner and F. Wilczek, *Relic gravitational waves and extended inflation*, *Phys. Rev. Lett.* **65** (1990) 3080.

[80] A. Kosowsky, M.S. Turner and R. Watkins, *Gravitational waves from first order cosmological phase transitions*, *Phys. Rev. Lett.* **69** (1992) 2026.

[81] F. Finelli and R.H. Brandenberger, *Parametric amplification of gravitational fluctuations during reheating*, *Phys. Rev. Lett.* **82** (1999) 1362 [hep-ph/9809490].

[82] R. Easther, J.T. Giblin, Jr. and E.A. Lim, *Gravitational Wave Production At The End Of Inflation*, *Phys. Rev. Lett.* **99** (2007) 221301 [astro-ph/0612294].

[83] J. Garcia-Bellido and D.G. Figueroa, *A stochastic background of gravitational waves from hybrid preheating*, *Phys. Rev. Lett.* **98** (2007) 061302 [astro-ph/0701014].

[84] J. Garcia-Bellido, D.G. Figueroa and A. Sastre, *A Gravitational Wave Background from Reheating after Hybrid Inflation*, *Phys. Rev. D* **77** (2008) 043517 [0707.0839].

[85] J.F. Dufaux, A. Bergman, G.N. Felder, L. Kofman and J.-P. Uzan, *Theory and Numerics of Gravitational Waves from Preheating after Inflation*, *Phys. Rev. D* **76** (2007) 123517 [0707.0875].

[86] N. Bernal and F. Hajkarim, *Primordial Gravitational Waves in Nonstandard Cosmologies*, *Phys. Rev. D* **100** (2019) 063502 [1905.10410].

[87] K.D. Lozanov and M.A. Amin, *Gravitational perturbations from oscillons and transients after inflation*, *Phys. Rev. D* **99** (2019) 123504 [1902.06736].

[88] S.S. Mishra, V. Sahni and A.A. Starobinsky, *Curing inflationary degeneracies using reheating predictions and relic gravitational waves*, *JCAP* **05** (2021) 075 [2101.00271].

[89] M.R. Haque, D. Maity, T. Paul and L. Sriramkumar, *Decoding the phases of early and late time reheating through imprints on primordial gravitational waves*, *Phys. Rev. D* **104** (2021) 063513 [2105.09242].

[90] J. Martin and C. Ringeval, *First CMB Constraints on the Inflationary Reheating Temperature*, *Phys. Rev. D* **82** (2010) 023511 [1004.5525].

[91] D. Maity and P. Saha, *Connecting CMB anisotropy and cold dark matter phenomenology via reheating*, *Phys. Rev. D* **98** (2018) 103525 [1801.03059].

[92] D. Maity and P. Saha, *CMB constraints on dark matter phenomenology via reheating in Minimal plateau inflation*, *Phys. Dark Univ.* **25** (2019) 100317 [1804.10115].

[93] M.R. Haque, D. Maity and P. Saha, *Two-phase reheating: CMB constraints on inflation and dark matter phenomenology*, *Phys. Rev. D* **102** (2020) 083534 [2009.02794].

[94] D.G. Figueroa and F. Torrenti, *Parametric resonance in the early Universe—a fitting analysis*, *JCAP* **02** (2017) 001 [1609.05197].

[95] D. Maity and P. Saha, *(P)reheating after minimal Plateau Inflation and constraints from CMB*, *JCAP* **07** (2019) 018 [1811.11173].

[96] S. Antusch, D.G. Figueroa, K. Marschall and F. Torrenti, *Energy distribution and equation of state of the early Universe: matching the end of inflation and the onset of radiation domination*, *Phys. Lett. B* **811** (2020) 135888 [2005.07563].

[97] K.D. Lozanov and M.A. Amin, *Self-resonance after inflation: oscillons, transients and radiation domination*, *Phys. Rev. D* **97** (2018) 023533 [1710.06851].

[98] D.I. Podolsky, G.N. Felder, L. Kofman and M. Peloso, *Equation of state and beginning of thermalization after preheating*, *Phys. Rev. D* **73** (2006) 023501 [hep-ph/0507096].

[99] V. Mukhanov, *Physical Foundations of Cosmology*, Cambridge University Press, Oxford (2005), 10.1017/CBO9780511790553.

[100] Planck collaboration, *Planck 2015 results. XX. Constraints on inflation*, *Astron. Astrophys.* **594** (2016) A20 [1502.02114].

[101] BICEP2, Keck Array collaboration, *Improved Constraints on Cosmology and Foregrounds from BICEP2 and Keck Array Cosmic Microwave Background Data with Inclusion of 95 GHz Band*, *Phys. Rev. Lett.* **116** (2016) 031302 [1510.09217].

[102] WMAP collaboration, *Seven-Year Wilkinson Microwave Anisotropy Probe (WMAP) Observations: Sky Maps, Systematic Errors, and Basic Results*, *Astrophys. J. Suppl.* **192** (2011) 14 [1001.4744].

[103] R. Allahverdi, R. Brandenberger, F.-Y. Cyr-Racine and A. Mazumdar, *Reheating in Inflationary Cosmology: Theory and Applications*, *Ann. Rev. Nucl. Part. Sci.* **60** (2010) 27 [1001.2600].

[104] M.A. Amin, M.P. Hertzberg, D.I. Kaiser and J. Karouby, *Nonperturbative Dynamics Of Reheating After Inflation: A Review*, *Int. J. Mod. Phys. D* **24** (2014) 1530003 [1410.3808].

[105] G.N. Felder and I. Tkachev, *LATTICEEASY: A Program for lattice simulations of scalar fields in an expanding universe*, *Comput. Phys. Commun.* **178** (2008) 929 [hep-ph/0011159].

[106] G.N. Felder, *CLUSTEREASY: A program for lattice simulations of scalar fields in an expanding universe on parallel computing clusters*, *Comput. Phys. Commun.* **179** (2008) 604 [0712.0813].

[107] T. Tenkanen, *Feebly Interacting Dark Matter Particle as the Inflaton*, *JHEP* **09** (2016) 049 [1607.01379].

[108] M. Heikinheimo, T. Tenkanen, K. Tuominen and V. Vaskonen, *Observational Properties of Feebly Coupled Dark Matter*, *PoS* **ICHEP2016** (2016) 825 [1611.04951].

[109] N. Bernal, M. Heikinheimo, T. Tenkanen, K. Tuominen and V. Vaskonen, *The Dawn of FIMP Dark Matter: A Review of Models and Constraints*, *Int. J. Mod. Phys. A* **32** (2017) 1730023 [1706.07442].

[110] L.J. Hall, K. Jedamzik, J. March-Russell and S.M. West, *Freeze-In Production of FIMP Dark Matter*, *JHEP* **03** (2010) 080 [0911.1120].

[111] X. Chu, Y. Mambrini, J. Quevillon and B. Zaldivar, *Thermal and non-thermal production of dark matter via Z'-portal(s)*, *JCAP* **01** (2014) 034 [1306.4677].

[112] M. Blennow, E. Fernandez-Martinez and B. Zaldivar, *Freeze-in through portals*, *JCAP* **01** (2014) 003 [1309.7348].

[113] A. Ibarra, A.S. Lamperstorfer, S. López-Gehler, M. Pato and G. Bertone, *On the sensitivity of CTA to gamma-ray boxes from multi-TeV dark matter*, *JCAP* **09** (2015) 048 [1503.06797].

[114] Y. Mambrini, N. Nagata, K.A. Olive, J. Quevillon and J. Zheng, *Dark matter and gauge coupling unification in nonsupersymmetric SO(10) grand unified models*, *Phys. Rev. D* **91** (2015) 095010 [1502.06929].

[115] N. Nagata, K.A. Olive and J. Zheng, *Weakly-Interacting Massive Particles in Non-supersymmetric SO(10) Grand Unified Models*, *JHEP* **10** (2015) 193 [1509.00809].

[116] S.-L. Chen and Z. Kang, *On UltraViolet Freeze-in Dark Matter during Reheating*, *JCAP* **05** (2018) 036 [1711.02556].

[117] N. Bernal, M. Dutra, Y. Mambrini, K. Olive, M. Peloso and M. Pierre, *Spin-2 Portal Dark Matter*, *Phys. Rev. D* **97** (2018) 115020 [1803.01866].

[118] Y. Mambrini, K.A. Olive, J. Quevillon and B. Zaldivar, *Gauge Coupling Unification and Nonequilibrium Thermal Dark Matter*, *Phys. Rev. Lett.* **110** (2013) 241306 [1302.4438].

[119] M.A.G. Garcia and M.A. Amin, *Prethermalization production of dark matter*, *Phys. Rev. D* **98** (2018) 103504 [1806.01865].

[120] M. Dutra, M. Lindner, S. Profumo, F.S. Queiroz, W. Rodejohann and C. Siqueira, *MeV Dark Matter Complementarity and the Dark Photon Portal*, *JCAP* **03** (2018) 037 [1801.05447].

[121] R. Allahverdi, K. Dutta and A. Maharana, *Constraining Non-thermal Dark Matter by CMB*, *JCAP* **10** (2018) 038 [1808.02659].

[122] P. Arias, N. Bernal, A. Herrera and C. Maldonado, *Reconstructing Non-standard Cosmologies with Dark Matter*, *JCAP* **10** (2019) 047 [1906.04183].

[123] N. Bernal, X. Chu, S. Kulkarni and J. Pradler, *Self-interacting dark matter without prejudice*, *Phys. Rev. D* **101** (2020) 055044 [1912.06681].

[124] N. Bernal, F. Elahi, C. Maldonado and J. Unwin, *Ultraviolet Freeze-in and Non-Standard Cosmologies*, *JCAP* **11** (2019) 026 [1909.07992].

[125] L. Heurtier and F. Huang, *Inflaton portal to a highly decoupled EeV dark matter particle*, *Phys. Rev. D* **100** (2019) 043507 [1905.05191].

[126] C. Miller, A.L. Erickcek and R. Murgia, *Constraining nonthermal dark matter's impact on the matter power spectrum*, *Phys. Rev. D* **100** (2019) 123520 [1908.10369].

[127] A. Ahmed, B. Grzadkowski and A. Socha, *Gravitational production of vector dark matter*, *JHEP* **08** (2020) 059 [2005.01766].

[128] K. Griest and M. Kamionkowski, *Unitarity Limits on the Mass and Radius of Dark Matter Particles*, *Phys. Rev. Lett.* **64** (1990) 615.

[129] N. Fornengo, A. Riotto and S. Scopel, *Supersymmetric dark matter and the reheating temperature of the universe*, *Phys. Rev. D* **67** (2003) 023514 [hep-ph/0208072].

[130] W.T. Emond, P. Millington and P.M. Saffin, *Boltzmann equations for preheating*, *JCAP* **09** (2018) 041 [1807.11726].

[131] E.W. Kolb and M.S. Turner, *The Early Universe*, vol. 69 (1990), 10.1201/9780429492860.

[132] P. Gondolo and G. Gelmini, *Cosmic abundances of stable particles: Improved analysis*, *Nucl. Phys. B* **360** (1991) 145.

[133] M. Hindmarsh and O. Philipsen, *WIMP dark matter and the QCD equation of state*, *Phys. Rev. D* **71** (2005) 087302 [hep-ph/0501232].

[134] M. Laine and Y. Schroder, *Quark mass thresholds in QCD thermodynamics*, *Phys. Rev. D* **73** (2006) 085009 [hep-ph/0603048].

[135] M. Drees, F. Hajkarim and E.R. Schmitz, *The Effects of QCD Equation of State on the Relic Density of WIMP Dark Matter*, *JCAP* **06** (2015) 025 [1503.03513].

[136] M. Drees and F. Hajkarim, *Dark Matter Production in an Early Matter Dominated Era*, *JCAP* **02** (2018) 057 [1711.05007].

[137] M. Srednicki, R. Watkins and K.A. Olive, *Calculations of Relic Densities in the Early Universe*, *Nucl. Phys. B* **310** (1988) 693.

[138] B. Ratra, *Cosmological 'seed' magnetic field from inflation*, *Astrophys. J. Lett.* **391** (1992) L1.

[139] J. Martin and J. Yokoyama, *Generation of Large-Scale Magnetic Fields in Single-Field Inflation*, *JCAP* **01** (2008) 025 [0711.4307].

[140] R.J.Z. Ferreira, R.K. Jain and M.S. Sloth, *Inflationary magnetogenesis without the strong coupling problem*, *JCAP* **10** (2013) 004 [1305.7151].

[141] T. Kobayashi and M.S. Sloth, *Early Cosmological Evolution of Primordial Electromagnetic Fields*, *Phys. Rev. D* **100** (2019) 023524 [1903.02561].

[142] K. Subramanian, *The Origin of large scale galactic magnetic fields*, in *7th Asian-Pacific Regional Meeting of the International Astronomical Union (IAU)*, 8, 1996 [astro-ph/9609123].

[143] T. Kobayashi and N. Afshordi, *Schwinger Effect in 4D de Sitter Space and Constraints on Magnetogenesis in the Early Universe*, *JHEP* **10** (2014) 166 [1408.4141].

[144] T. Fujita and R. Namba, *Pre-reheating Magnetogenesis in the Kinetic Coupling Model*, *Phys. Rev. D* **94** (2016) 043523 [1602.05673].

[145] Y. Shtanov, *Viable inflationary magnetogenesis with helical coupling*, *JCAP* **10** (2019) 008 [1902.05894].

[146] P. Qian and Z.-K. Guo, *Model of inflationary magnetogenesis*, *Phys. Rev. D* **93** (2016) 043541 [1512.05050].

[147] M.S. Turner and L.M. Widrow, *Inflation Produced, Large Scale Magnetic Fields*, *Phys. Rev. D* **37** (1988) 2743.

[148] K. Bamba, *Generation of large-scale magnetic fields, non-Gaussianity, and primordial gravitational waves in inflationary cosmology*, *Phys. Rev. D* **91** (2015) 043509 [1411.4335].

[149] V. Demozzi, V. Mukhanov and H. Rubinstein, *Magnetic fields from inflation?*, *JCAP* **08** (2009) 025 [0907.1030].

[150] R. Sharma, S. Jagannathan, T.R. Seshadri and K. Subramanian, *Challenges in Inflationary Magnetogenesis: Constraints from Strong Coupling, Backreaction and the Schwinger Effect*, *Phys. Rev. D* **96** (2017) 083511 [1708.08119].

[151] D. Grasso and H.R. Rubinstein, *Magnetic fields in the early universe*, *Phys. Rept.* **348** (2001) 163 [astro-ph/0009061].

[152] P.P. Kronberg, *Extragalactic magnetic fields*, *Rept. Prog. Phys.* **57** (1994) 325.

[153] L.M. Widrow, *Origin of galactic and extragalactic magnetic fields*, *Rev. Mod. Phys.* **74** (2002) 775 [astro-ph/0207240].

[154] Z.-R. Wang, S.-Q. Xi, R.-Y. Liu, R. Xue and X.-Y. Wang, *Constraints on the intergalactic magnetic field from γ-ray observations of GRB 190114C*, *Phys. Rev. D* **101** (2020) 083004 [2001.01186].

[155] K. Takahashi, M. Mori, K. Ichiki and S. Inoue, *Lower Bounds on Intergalactic Magnetic Fields from Simultaneously Observed GeV-TeV Light Curves of the Blazar Mrk 501*, *Astrophys. J. Lett.* **744** (2012) L7 [1103.3835].

[156] K. Takahashi, M. Mori, K. Ichiki, S. Inoue and H. Takami, *Lower Bounds on Magnetic Fields in Intergalactic Voids from Long-term GeV-TeV Light Curves of the Blazar Mrk 421*, *Astrophys. J. Lett.* **771** (2013) L42 [1303.3069].

[157] J. Asplund, G. Jóhannesson and A. Brandenburg, *On the measurement of handedness in Fermi Large Area Telescope data*, *Astrophys. J.* **898** (2020) 124 [2005.13065].

[158] M. Kachelriess and B.C. Martinez, *Searching for primordial helical magnetic fields*, *Phys. Rev. D* **102** (2020) 083001 [2008.06279].

[159] A. Neronov and I. Vovk, *Evidence for strong extragalactic magnetic fields from Fermi observations of TeV blazars*, *Science* **328** (2010) 73 [1006.3504].

[160] W. Essey, S. Ando and A. Kusenko, *Determination of intergalactic magnetic fields from gamma ray data*, *Astropart. Phys.* **35** (2011) 135 [1012.5313].

[161] J.D. Finke, L.C. Reyes, M. Georganopoulos, K. Reynolds, M. Ajello, S.J. Fegan et al., *Constraints on the Intergalactic Magnetic Field with Gamma-Ray Observations of Blazars*, *Astrophys. J.* **814** (2015) 20 [1510.02485].

[162] S. Saga, H. Tashiro and S. Yokoyama, *Limits on primordial magnetic fields from direct detection experiments of gravitational wave background*, *Phys. Rev. D* **98** (2018) 083518 [1807.00561].

[163] T.A. Dzhatdoev, E.I. Podlesnyi and I.A. Vaiman, *Can we constrain the extragalactic magnetic field from very high energy observations of GRB 190114C?*, *Phys. Rev. D* **102** (2020) 123017 [2002.06918].

[164] K. Jedamzik and A. Saveliev, *Stringent Limit on Primordial Magnetic Fields from the Cosmic Microwave Background Radiation*, *Phys. Rev. Lett.* **123** (2019) 021301 [1804.06115].

[165] A. Boyarsky, J. Frohlich and O. Ruchayskiy, *Self-consistent evolution of magnetic fields and chiral asymmetry in the early Universe*, *Phys. Rev. Lett.* **108** (2012) 031301 [1109.3350].

[166] J.H. Matthews, A.R. Bell, K.M. Blundell and A.T. Araudo, *Amplification of perpendicular and parallel magnetic fields by cosmic ray currents*, *Mon. Not. Roy. Astron. Soc.* **469** (2017) 1849 [1704.02985].

[167] A.Z. Dolginov and M.E. Katz, *Interaction of cosmic rays with magnetohydrodynamical turbulence in cosmic media*, *Phys. Rept.* **239** (1994) 285.

[168] H. Sol, G. Pelletier and E. Asseo, *Two flows model for extragalactic radio JETS*, .

[169] A. Brandenburg, K. Enqvist and P. Olesen, *Large scale magnetic fields from hydromagnetic turbulence in the very early universe*, *Phys. Rev. D* **54** (1996) 1291 [astro-ph/9602031].

[170] S. Sur, A. Shukurov and K. Subramanian, *Galactic dynamos supported by magnetic helicity fluxes*, *Mon. Not. Roy. Astron. Soc.* **377** (2007) 874 [astro-ph/0612756].

[171] D. Boyanovsky, H.J. de Vega and M. Simionato, *Large scale magnetogenesis from a nonequilibrium phase transition in the radiation dominated era*, *Phys. Rev. D* **67** (2003) 123505 [hep-ph/0211022].

[172] J.M. Wagstaff and R. Banerjee, *Extragalactic magnetic fields unlikely generated at the electroweak phase transition*, *JCAP* **01** (2016) 002 [1409.4223].

[173] T. Vachaspati, *Magnetic fields from cosmological phase transitions*, *Phys. Lett. B* **265** (1991) 258.

[174] Y. Zhang, T. Vachaspati and F. Ferrer, *Magnetic field production at a first-order electroweak phase transition*, *Phys. Rev. D* **100** (2019) 083006 [1902.02751].

[175] T. Patel, H. Tashiro and Y. Urakawa, *Resonant magnetogenesis from axions*, *JCAP* **01** (2020) 043 [1909.00288].

[176] V. Domcke and K. Mukaida, *Gauge Field and Fermion Production during Axion Inflation*, *JCAP* **11** (2018) 020 [1806.08769].

[177] P. Adshead, J.T. Giblin, T.R. Scully and E.I. Sfakianakis, *Magnetogenesis from axion inflation*, *JCAP* **10** (2016) 039 [1606.08474].

[178] K. Atmjeet, I. Pahwa, T.R. Seshadri and K. Subramanian, *Cosmological Magnetogenesis From Extra-dimensional Gauss Bonnet Gravity*, *Phys. Rev. D* **89** (2014) 063002 [1312.5815].

[179] J.D. Barrow, C.G. Tsagas and K. Yamamoto, *Origin of cosmic magnetic fields: Superadiabatically amplified modes in open Friedmann universes*, *Phys. Rev. D* **86** (2012) 023533 [1205.6662].

[180] A. Neronov, A.M. Taylor, C. Tchernin and I. Vovk, *Measuring the correlation length of intergalactic magnetic fields from observations of gamma-ray induced cascades*, *Astron. Astrophys.* **554** (2013) A31 [1307.2753].

[181] T. Vachaspati, *Fundamental Implications of Intergalactic Magnetic Field Observations*, *Phys. Rev. D* **95** (2017) 063505 [1606.06186].

[182] T. Fujita and S. Mukohyama, *Universal upper limit on inflation energy scale from cosmic magnetic field*, *JCAP* **10** (2012) 034 [1205.5031].

[183] R.J.Z. Ferreira, R.K. Jain and M.S. Sloth, *Inflationary Magnetogenesis without the Strong Coupling Problem II: Constraints from CMB anisotropies and B-modes*, *JCAP* **06** (2014) 053 [1403.5516].

[184] D. Green and T. Kobayashi, *Constraints on Primordial Magnetic Fields from Inflation*, *JCAP* **03** (2016) 010 [1511.08793].

[185] R.Z. Ferreira, J. Ganc, J. Noreña and M.S. Sloth, *On the validity of the perturbative description of axions during inflation*, *JCAP* **04** (2016) 039 [1512.06116].

[186] M. Gasperini, M. Giovannini and G. Veneziano, *Primordial magnetic fields from string cosmology*, *Phys. Rev. Lett.* **75** (1995) 3796 [hep-th/9504083].

[187] K. Bamba and J. Yokoyama, *Large scale magnetic fields from inflation in dilaton electromagnetism*, *Phys. Rev. D* **69** (2004) 043507 [astro-ph/0310824].

[188] S. Kanno, J. Soda and M.-a. Watanabe, *Cosmological Magnetic Fields from Inflation and Backreaction*, *JCAP* **12** (2009) 009 [0908.3509].

[189] N. Barnaby, R. Namba and M. Peloso, *Observable non-gaussianity from gauge field production in slow roll inflation, and a challenging connection with magnetogenesis*, *Phys. Rev. D* **85** (2012) 123523 [1202.1469].

[190] T. Suyama and J. Yokoyama, *Metric perturbation from inflationary magnetic field and generic bound on inflation models*, *Phys. Rev. D* **86** (2012) 023512 [1204.3976].

[191] R.K. Jain and M.S. Sloth, *Consistency relation for cosmic magnetic fields*, *Phys. Rev. D* **86** (2012) 123528 [1207.4187].

[192] R.K. Jain and M.S. Sloth, *On the non-Gaussian correlation of the primordial curvature perturbation with vector fields*, *JCAP* **02** (2013) 003 [1210.3461].

[193] S. Nurmi and M.S. Sloth, *Constraints on Gauge Field Production during Inflation*, *JCAP* **07** (2014) 012 [1312.4946].

[194] T. Fujita and S. Yokoyama, *Critical constraint on inflationary magnetogenesis*, *JCAP* **03** (2014) 013 [1402.0596].

[195] J. Ganc and M.S. Sloth, *Probing correlations of early magnetic fields using mu-distortion*, *JCAP* **08** (2014) 018 [1404.5957].

[196] D. Maity, S. Pal and T. Paul, *Effective Theory of Inflationary Magnetogenesis and Constraints on Reheating*, *JCAP* **05** (2021) 045 [2103.02411].

[197] K. Bamba, E. Elizalde, S.D. Odintsov and T. Paul, *Inflationary magnetogenesis with reheating phase from higher curvature coupling*, *JCAP* **04** (2021) 009 [2012.12742].

[198] R. Sharma, *Constraining models of inflationary magnetogenesis with NANOGrav data*, *Phys. Rev. D* **105** (2022) L041302 [2102.09358].

[199] S. Hawking, *The Development of Irregularities in a Single Bubble Inflationary Universe*, *Phys. Lett. B* **115** (1982) 295.

[200] A.H. Guth and S. Pi, *Fluctuations in the New Inflationary Universe*, *Phys. Rev. Lett.* **49** (1982) 1110.

[201] A.A. Starobinsky, *Dynamics of Phase Transition in the New Inflationary Universe Scenario and Generation of Perturbations*, *Phys. Lett. B* **117** (1982) 175.

[202] J.M. Bardeen, P.J. Steinhardt and M.S. Turner, *Spontaneous Creation of Almost Scale - Free Density Perturbations in an Inflationary Universe*, *Phys. Rev. D* **28** (1983) 679.

[203] L.P. Grishchuk, *Amplification of gravitational waves in an istropic universe*, *Zh. Eksp. Teor. Fiz.* **67** (1974) 825.

[204] A.A. Starobinsky, *Spectrum of relict gravitational radiation and the early state of the universe*, *JETP Lett.* **30** (1979) 682.

[205] M.C. Guzzetti, N. Bartolo, M. Liguori and S. Matarrese, *Gravitational waves from inflation*, *Riv. Nuovo Cim.* **39** (2016) 399 [1605.01615].

[206] C. Caprini and D.G. Figueroa, *Cosmological Backgrounds of Gravitational Waves*, *Class. Quant. Grav.* **35** (2018) 163001 [1801.04268].

[207] LIGO Scientific, Virgo collaboration, *GW150914: The Advanced LIGO Detectors in the Era of First Discoveries*, *Phys. Rev. Lett.* **116** (2016) 131103 [1602.03838].

[208] LIGO Scientific, Virgo collaboration, *GW150914: First results from the search for binary black hole coalescence with Advanced LIGO*, *Phys. Rev. D* **93** (2016) 122003 [1602.03839].

[209] LIGO Scientific, Virgo collaboration, *Properties of the Binary Black Hole Merger GW150914*, *Phys. Rev. Lett.* **116** (2016) 241102 [1602.03840].

[210] LIGO Scientific, Virgo collaboration, *Observation of Gravitational Waves from a Binary Black Hole Merger*, *Phys. Rev. Lett.* **116** (2016) 061102 [1602.03837].

[211] LIGO Scientific, Virgo collaboration, *GW151226: Observation of Gravitational Waves from a 22-Solar-Mass Binary Black Hole Coalescence*, *Phys. Rev. Lett.* **116** (2016) 241103 [1606.04855].

[212] LIGO Scientific, VIRGO collaboration, *GW170104: Observation of a 50-Solar-Mass Binary Black Hole Coalescence at Redshift 0.2*, *Phys. Rev. Lett.* **118** (2017) 221101 [1706.01812].

[213] LIGO Scientific, Virgo collaboration, *GW170608: Observation of a 19-solar-mass Binary Black Hole Coalescence*, *Astrophys. J. Lett.* **851** (2017) L35 [1711.05578].

[214] LIGO Scientific, Virgo collaboration, *GW170814: A Three-Detector Observation of Gravitational Waves from a Binary Black Hole Coalescence*, *Phys. Rev. Lett.* **119** (2017) 141101 [1709.09660].

[215] LIGO Scientific, Virgo collaboration, *GW170817: Observation of Gravitational Waves from a Binary Neutron Star Inspiral*, *Phys. Rev. Lett.* **119** (2017) 161101 [1710.05832].

[216] LIGO Scientific, Virgo collaboration, *GW190412: Observation of a Binary-Black-Hole Coalescence with Asymmetric Masses*, *Phys. Rev. D* **102** (2020) 043015 [2004.08342].

[217] LIGO Scientific, Virgo collaboration, *GW190425: Observation of a Compact Binary Coalescence with Total Mass* $\sim 3.4 M_\odot$, *Astrophys. J. Lett.* **892** (2020) L3 [2001.01761].

[218] LIGO Scientific, Virgo collaboration, *GW190814: Gravitational Waves from the Coalescence of a 23 Solar Mass Black Hole with a 2.6 Solar Mass Compact Object*, *Astrophys. J.* **896** (2020) L44 [2006.12611].

[219] LIGO Scientific, Virgo collaboration, *Upper Limits on the Stochastic Gravitational-Wave Background from Advanced LIGO's First Observing Run*, *Phys. Rev. Lett.* **118** (2017) 121101 [1612.02029].

[220] M. Punturo et al., *The Einstein Telescope: A third-generation gravitational wave observatory*, *Class. Quant. Grav.* **27** (2010) 194002.

[221] B. Sathyaprakash et al., *Scientific Objectives of Einstein Telescope*, *Class. Quant. Grav.* **29** (2012) 124013 [1206.0331].

[222] J. Crowder and N.J. Cornish, *Beyond LISA: Exploring future gravitational wave missions*, *Phys. Rev.* **D72** (2005) 083005 [gr-qc/0506015].

[223] V. Corbin and N.J. Cornish, *Detecting the cosmic gravitational wave background with the big bang observer*, *Class. Quant. Grav.* **23** (2006) 2435 [gr-qc/0512039].

[224] J. Baker et al., *Space Based Gravitational Wave Astronomy Beyond LISA*, 1907.11305.

[225] N. Seto, S. Kawamura and T. Nakamura, *Possibility of direct measurement of the acceleration of the universe using 0.1-Hz band laser interferometer gravitational wave antenna in space*, *Phys. Rev. Lett.* **87** (2001) 221103 [astro-ph/0108011].

[226] S. Kawamura et al., *The Japanese space gravitational wave antenna: DECIGO*, *Class. Quant. Grav.* **28** (2011) 094011.

[227] S. Sato et al., *The status of DECIGO*, *J. Phys. Conf. Ser.* **840** (2017) 012010.

[228] DECIGO WORKING GROUP collaboration, *Primordial gravitational wave and DECIGO*, *PoS* **KMI2019** (2019) 019.

[229] P. Amaro-Seoane et al., *eLISA/NGO: Astrophysics and cosmology in the gravitational-wave millihertz regime*, *GW Notes* **6** (2013) 4 [1201.3621].

[230] LISA collaboration, *Laser Interferometer Space Antenna*, 1702.00786.

[231] E. Barausse et al., *Prospects for Fundamental Physics with LISA*, *Gen. Rel. Grav.* **52** (2020) 81 [2001.09793].

[232] G. Janssen et al., *Gravitational wave astronomy with the SKA*, *PoS* **AASKA14** (2015) 037 [1501.00127].

[233] R. Easther and E.A. Lim, *Stochastic gravitational wave production after inflation*, *JCAP* **04** (2006) 010 [astro-ph/0601617].

[234] K.N. Ananda, C. Clarkson and D. Wands, *The Cosmological gravitational wave background from primordial density perturbations*, *Phys. Rev.* **D75** (2007) 123518 [gr-qc/0612013].

[235] D. Baumann, P.J. Steinhardt, K. Takahashi and K. Ichiki, *Gravitational Wave Spectrum Induced by Primordial Scalar Perturbations*, *Phys. Rev.* **D76** (2007) 084019 [hep-th/0703290].

[236] R. Saito and J. Yokoyama, *Gravitational wave background as a probe of the primordial black hole abundance*, *Phys. Rev. Lett.* **102** (2009) 161101 [0812.4339].

[237] R. Saito and J. Yokoyama, *Gravitational-Wave Constraints on the Abundance of Primordial Black Holes*, *Prog. Theor. Phys.* **123** (2010) 867 [0912.5317].

[238] S. Kuroyanagi, T. Chiba and T. Takahashi, *Probing the Universe through the Stochastic Gravitational Wave Background*, *JCAP* **11** (2018) 038 [1807.00786].

[239] J.R. Espinosa, D. Racco and A. Riotto, *A Cosmological Signature of the SM Higgs Instability: Gravitational Waves*, *JCAP* **09** (2018) 012 [1804.07732].

[240] K. Kohri and T. Terada, *Semianalytic calculation of gravitational wave spectrum nonlinearly induced from primordial curvature perturbations*, *Phys. Rev. D* **97** (2018) 123532 [1804.08577].

[241] K. Inomata, K. Kohri, T. Nakama and T. Terada, *Gravitational Waves Induced by Scalar Perturbations during a Gradual Transition from an Early Matter Era to the Radiation Era*, *JCAP* **10** (2019) 071 [1904.12878].

[242] K. Inomata, K. Kohri, T. Nakama and T. Terada, *Enhancement of Gravitational Waves Induced by Scalar Perturbations due to a Sudden Transition from an Early Matter Era to the Radiation Era*, *Phys. Rev. D* **100** (2019) 043532 [1904.12879].

[243] M. Braglia, D.K. Hazra, F. Finelli, G.F. Smoot, L. Sriramkumar and A.A. Starobinsky, *Generating PBHs and small-scale GWs in two-field models of inflation*, *JCAP* **08** (2020) 001 [2005.02895].

[244] H.V. Ragavendra, P. Saha, L. Sriramkumar and J. Silk, *Primordial black holes and secondary gravitational waves from ultraslow roll and punctuated inflation*, *Phys. Rev. D* **103** (2021) 083510 [2008.12202].

[245] H.V. Ragavendra, L. Sriramkumar and J. Silk, *Could PBHs and secondary GWs have originated from squeezed initial states?*, *JCAP* **05** (2021) 010 [2011.09938].

[246] S. Bhattacharya, S. Mohanty and P. Parashari, *Implications of the NANOGrav result on primordial gravitational waves in nonstandard cosmologies*, 2010.05071.

[247] E. Aubourg et al., *Cosmological implications of baryon acoustic oscillation measurements*, *Phys. Rev. D* **92** (2015) 123516 [1411.1074].

[248] J.A. Vázquez, L.E. Padilla and T. Matos, *Inflationary Cosmology: From Theory to Observations*, 1810.09934.

[249] M.S. Turner, M.J. White and J.E. Lidsey, *Tensor perturbations in inflationary models as a probe of cosmology*, *Phys. Rev. D* **48** (1993) 4613 [astro-ph/9306029].

[250] P.M. Sa and A.B. Henriques, *Parametric Resonance and Cosmological Gravitational Waves*, *Phys. Rev. D* **77** (2008) 064002 [0712.2697].

[251] K. Nakayama, S. Saito, Y. Suwa and J. Yokoyama, *Probing reheating temperature of the universe with gravitational wave background*, *JCAP* **06** (2008) 020 [0804.1827].

[252] K. Nakayama, S. Saito, Y. Suwa and J. Yokoyama, *Space laser interferometers can determine the thermal history of the early Universe*, *Phys. Rev. D* **77** (2008) 124001 [0802.2452].

[253] P.M. Sa and A.B. Henriques, *Gravitational wave generation in hybrid quintessential inflationary models*, *Phys. Rev. D* **81** (2010) 124043 [1003.4112].

[254] S. Kuroyanagi, K. Nakayama and S. Saito, *Prospects for determination of thermal history after inflation with future gravitational wave detectors*, *Phys. Rev. D* **84** (2011) 123513 [1110.4169].

[255] S. Kuroyanagi, T. Takahashi and S. Yokoyama, *Blue-tilted Tensor Spectrum and Thermal History of the Universe*, *JCAP* **02** (2015) 003 [1407.4785].

[256] H. Assadullahi and D. Wands, *Gravitational waves from an early matter era*, *Phys. Rev. D* **79** (2009) 083511 [0901.0989].

[257] K. Nakayama and J. Yokoyama, *Gravitational Wave Background and Non-Gaussianity as a Probe of the Curvaton Scenario*, *JCAP* **01** (2010) 010 [0910.0715].

[258] R. Durrer and J. Hasenkamp, *Testing Superstring Theories with Gravitational Waves*, *Phys. Rev. D* **84** (2011) 064027 [1105.5283].

[259] L. Alabidi, K. Kohri, M. Sasaki and Y. Sendouda, *Observable induced gravitational waves from an early matter phase*, *JCAP* **05** (2013) 033 [1303.4519].

[260] F. D'Eramo and K. Schmitz, *Imprint of a scalar era on the primordial spectrum of gravitational waves*, *Phys. Rev. Research.* **1** (2019) 013010 [1904.07870].

[261] A. Ricciardone and G. Tasinato, *Primordial gravitational waves in supersolid inflation*, *Phys. Rev. D* **96** (2017) 023508 [1611.04516].

[262] S. Koh, B.-H. Lee and G. Tumurtushaa, *Constraints on the reheating parameters after Gauss-Bonnet inflation from primordial gravitational waves*, *Phys. Rev. D* **98** (2018) 103511 [1807.04424].

[263] T. Fujita, S. Kuroyanagi, S. Mizuno and S. Mukohyama, *Blue-tilted Primordial Gravitational Waves from Massive Gravity*, *Phys. Lett. B* **789** (2019) 215 [1808.02381].

[264] N. Bernal, A. Ghoshal, F. Hajkarim and G. Lambiase, *Primordial Gravitational Wave Signals in Modified Cosmologies*, *JCAP* **11** (2020) 051 [2008.04959].

[265] S. Weinberg, *Damping of tensor modes in cosmology*, *Phys. Rev. D* **69** (2004) 023503 [astro-ph/0306304].

[266] A. Mangilli, N. Bartolo, S. Matarrese and A. Riotto, *The impact of cosmic neutrinos on the gravitational-wave background*, *Phys. Rev. D* **78** (2008) 083517 [0805.3234].

[267] Y. Watanabe and E. Komatsu, *Improved Calculation of the Primordial Gravitational Wave Spectrum in the Standard Model*, *Phys. Rev. D* **73** (2006) 123515 [astro-ph/0604176].

[268] S. Kuroyanagi, T. Chiba and N. Sugiyama, *Precision calculations of the gravitational wave background spectrum from inflation*, *Phys. Rev. D* **79** (2009) 103501 [0804.3249].

[269] R.R. Caldwell, T.L. Smith and D.G.E. Walker, *Using a Primordial Gravitational Wave Background to Illuminate New Physics*, *Phys. Rev. D* **100** (2019) 043513 [1812.07577].

[270] D.J.H. Chung, E.W. Kolb and A. Riotto, *Production of massive particles during reheating*, *Phys. Rev. D* **60** (1999) 063504 [hep-ph/9809453].

[271] M.R. Haque and D. Maity, *Reheating constraints on the inflaton and dark matter: Swampland conjecture*, *Phys. Rev. D* **99** (2019) 103534 [1902.09491].

[272] NANOGrav collaboration, *The NANOGrav 12.5 yr Data Set: Search for an Isotropic Stochastic Gravitational-wave Background*, *Astrophys. J. Lett.* **905** (2020) L34 [2009.04496].

[273] NANOGrav collaboration, *Astrophysics Milestones For Pulsar Timing Array Gravitational Wave Detection*, 2010.11950.

[274] S. Kuroyanagi, T. Takahashi and S. Yokoyama, *Blue-tilted inflationary tensor spectrum and reheating in the light of NANOGrav results*, *JCAP* **01** (2021) 071 [2011.03323].

[275] K. Inomata, M. Kawasaki, K. Mukaida and T.T. Yanagida, *NANOGrav results and LIGO-Virgo primordial black holes in axion-like curvaton model*, 2011.01270.

[276] H.W.H. Tahara and T. Kobayashi, *Nanohertz gravitational waves from a null-energy-condition violation in the early universe*, *Phys. Rev. D* **102** (2020) 123533 [2011.01605].

[277] N. Kitajima, J. Soda and Y. Urakawa, *Nano-Hz gravitational wave signature from axion dark matter*, 2010.10990.

[278] G. Domènech and S. Pi, *NANOGrav Hints on Planet-Mass Primordial Black Holes*, 2010.03976.

[279] H.-H. Li, G. Ye and Y.-S. Piao, *Is the NANOGrav signal a hint of dS decay during inflation?*, *Phys. Lett. B* **816** (2021) 136211 [2009.14663].

[280] L. Bian, R.-G. Cai, J. Liu, X.-Y. Yang and R. Zhou, *Evidence for different gravitational-wave sources in the NANOGrav dataset*, *Phys. Rev. D* **103** (2021) L081301 [2009.13893].

[281] S. Blasi, V. Brdar and K. Schmitz, *Has NANOGrav found first evidence for cosmic strings?*, *Phys. Rev. Lett.* **126** (2021) 041305 [2009.06607].

[282] V. De Luca, G. Franciolini and A. Riotto, *NANOGrav Data Hints at Primordial Black Holes as Dark Matter*, *Phys. Rev. Lett.* **126** (2021) 041303 [2009.08268].

[283] V. Vaskonen and H. Veermäe, *Did NANOGrav see a signal from primordial black hole formation?*, *Phys. Rev. Lett.* **126** (2021) 051303 [2009.07832].

[284] J. Ellis and M. Lewicki, *Cosmic String Interpretation of NANOGrav Pulsar Timing Data*, *Phys. Rev. Lett.* **126** (2021) 041304 [2009.06555].

[285] W. Buchmuller, V. Domcke and K. Schmitz, *From NANOGrav to LIGO with metastable cosmic strings*, *Phys. Lett. B* **811** (2020) 135914 [2009.10649].

[286] K. Kohri and T. Terada, *Solar-Mass Primordial Black Holes Explain NANOGrav Hint of Gravitational Waves*, *Phys. Lett. B* **813** (2021) 136040 [2009.11853].

[287] S. Vagnozzi, *Implications of the NANOGrav results for inflation*, *Mon. Not. Roy. Astron. Soc.* **502** (2021) L11 [2009.13432].

[288] I.S. Gradshteyn and I.M. Ryzhik, *Table of integrals, series, and products*, Elsevier/Academic Press, Amsterdam, seventh ed. (2007).

[289] C. Moore, R. Cole and C. Berry, *Gravitational-wave sensitivity curves*, *Class. Quant. Grav.* **32** (2015) 015014 [1408.0740].

[290] L. Pagano, L. Salvati and A. Melchiorri, *New constraints on primordial gravitational waves from Planck 2015*, *Phys. Lett. B* **760** (2016) 823 [1508.02393].

[291] D.K. Hazra, L. Sriramkumar and J. Martin, *BINGO: A code for the efficient computation of the scalar bi-spectrum*, *JCAP* **05** (2013) 026 [1201.0926].

[292] A. Kurkela and G.D. Moore, *Thermalization in Weakly Coupled Nonabelian Plasmas*, *JHEP* **12** (2011) 044 [1107.5050].

[293] K. Harigaya and K. Mukaida, *Thermalization after/during Reheating*, *JHEP* **05** (2014) 006 [1312.3097].

[294] J.R. Ellis, K. Enqvist, D.V. Nanopoulos and K.A. Olive, *Inflationary Fluctuations, Entropy Generation and Baryogenesis*, *Phys. Lett. B* **191** (1987) 343.

[295] J. McDonald, *Reheating temperature and inflaton mass bounds from thermalization after inflation*, *Phys. Rev. D* **61** (2000) 083513 [hep-ph/9909467].

[296] R. Allahverdi, *Thermalization after inflation and reheating temperature*, *Phys. Rev. D* **62** (2000) 063509 [hep-ph/0004035].

[297] M. Kawasaki and F. Takahashi, *Late-time entropy production due to the decay of domain walls*, *Phys. Lett. B* **618** (2005) 1 [hep-ph/0410158].

[298] S. Kuroyanagi, C. Ringeval and T. Takahashi, *Early universe tomography with CMB and gravitational waves*, *Phys. Rev. D* **87** (2013) 083502 [1301.1778].

[299] H. Hattori, T. Kobayashi, N. Omoto and O. Seto, *Entropy production by domain wall decay in the NMSSM*, *Phys. Rev. D* **92** (2015) 103518 [1510.03595].

[300] N. Banerjee and T. Paul, *Inflationary scenario from higher curvature warped spacetime*, *Eur. Phys. J. C* **77** (2017) 672 [1706.05964].

[301] E. Elizalde, S.D. Odintsov, T. Paul and D. Sáez-Chillón Gómez, *Inflationary universe in $F(R)$ gravity with antisymmetric tensor fields and their suppression during its evolution*, *Phys. Rev. D* **99** (2019) 063506 [1811.02960].

[302] S. Unnikrishnan, V. Sahni and A. Toporensky, *Refining inflation using non-canonical scalars*, *JCAP* **08** (2012) 018 [1205.0786].

[303] J. Yokoyama, *Implication of Pulsar Timing Array Experiments on Cosmological Gravitational Wave Detection*, 2105.07629.

[304] CMB-S4 collaboration, *CMB-S4 Science Book, First Edition*, 1610.02743.

[305] Y. Sofue and V. Rubin, *Rotation curves of spiral galaxies*, *Ann. Rev. Astron. Astrophys.* **39** (2001) 137 [astro-ph/0010594].

[306] V. Sahni, *Dark matter and dark energy*, *Lect. Notes Phys.* **653** (2004) 141 [astro-ph/0403324].

[307] R. Catena and P. Ullio, *A novel determination of the local dark matter density*, *JCAP* **08** (2010) 004 [0907.0018].

[308] Q. Guo, S. White, C. Li and M. Boylan-Kolchin, *How do galaxies populate Dark Matter halos?*, *Mon. Not. Roy. Astron. Soc.* **404** (2010) 1111 [0909.4305].

[309] N. Arkani-Hamed, D.P. Finkbeiner, T.R. Slatyer and N. Weiner, *A Theory of Dark Matter*, *Phys. Rev. D* **79** (2009) 015014 [0810.0713].

[310] J.L. Feng, *Dark Matter Candidates from Particle Physics and Methods of Detection*, *Ann. Rev. Astron. Astrophys.* **48** (2010) 495 [1003.0904].

[311] M. Pospelov, A. Ritz and M.B. Voloshin, *Secluded WIMP Dark Matter*, *Phys. Lett. B* **662** (2008) 53 [0711.4866].

[312] F. Elahi, C. Kolda and J. Unwin, *UltraViolet Freeze-in*, *JHEP* **03** (2015) 048 [1410.6157].

[313] N. Bernal, C. Cosme and T. Tenkanen, *Phenomenology of Self-Interacting Dark Matter in a Matter-Dominated Universe*, *Eur. Phys. J. C* **79** (2019) 99 [1803.08064].

[314] M.A.G. Garcia, K. Kaneta, Y. Mambrini and K.A. Olive, *Reheating and Post-inflationary Production of Dark Matter*, *Phys. Rev. D* **101** (2020) 123507 [2004.08404].

[315] M.A.G. Garcia, Y. Mambrini, K.A. Olive and S. Verner, *On the Realization of WIMPflation*, *JCAP* **10** (2021) 061 [2107.07472].

[316] Y. Hochberg, E. Kuflik, T. Volansky and J.G. Wacker, *Mechanism for Thermal Relic Dark Matter of Strongly Interacting Massive Particles*, *Phys. Rev. Lett.* **113** (2014) 171301 [1402.5143].

[317] Y. Hochberg, E. Kuflik, H. Murayama, T. Volansky and J.G. Wacker, *Model for Thermal Relic Dark Matter of Strongly Interacting Massive Particles*, *Phys. Rev. Lett.* **115** (2015) 021301 [1411.3727].

[318] Y. Hochberg, E. Kuflik and H. Murayama, *SIMP Spectroscopy*, *JHEP* **05** (2016) 090 [1512.07917].

[319] N. Bernal and X. Chu, $\mathbb{Z}_2$ *SIMP Dark Matter*, *JCAP* **01** (2016) 006 [1510.08527].

[320] A. Falkowski, J.T. Ruderman and T. Volansky, *Asymmetric Dark Matter from Leptogenesis*, *JHEP* **05** (2011) 106 [1101.4936].

[321] L. Lopez Honorez and C.E. Yaguna, *The inert doublet model of dark matter revisited*, *JHEP* **09** (2010) 046 [1003.3125].

[322] XENON100 collaboration, *Dark Matter Results from 225 Live Days of XENON100 Data*, *Phys. Rev. Lett.* **109** (2012) 181301 [1207.5988].

[323] XENON collaboration, *Dark Matter Search Results from a One Ton-Year Exposure of XENON1T*, *Phys. Rev. Lett.* **121** (2018) 111302 [1805.12562].

[324] PandaX-II collaboration, *Dark Matter Results from First 98.7 Days of Data from the PandaX-II Experiment*, *Phys. Rev. Lett.* **117** (2016) 121303 [1607.07400].

[325] LUX collaboration, *Results from a search for dark matter in the complete LUX exposure*, *Phys. Rev. Lett.* **118** (2017) 021303 [1608.07648].

[326] BOSS collaboration, *The clustering of galaxies in the SDSS-III Baryon Oscillation Spectroscopic Survey: baryon acoustic oscillations in the Data Releases 10 and 11 Galaxy samples*, *Mon. Not. Roy. Astron. Soc.* **441** (2014) 24 [1312.4877].

[327] S. Capozziello, S. Nojiri, S.D. Odintsov and A. Troisi, *Cosmological viability of f(R)-gravity as an ideal fluid and its compatibility with a matter dominated phase*, *Phys. Lett. B* **639** (2006) 135 [astro-ph/0604431].

[328] S. Capozziello and M. De Laurentis, *Extended Theories of Gravity*, *Phys. Rept.* **509** (2011) 167 [1108.6266].

[329] C.G. Boehmer, T. Harko and F.S.N. Lobo, *Dark matter as a geometric effect in f(R) gravity*, *Astropart. Phys.* **29** (2008) 386 [0709.0046].

[330] S. Nojiri, S.D. Odintsov and V.K. Oikonomou, *Modified Gravity Theories on a Nutshell: Inflation, Bounce and Late-time Evolution*, *Phys. Rept.* **692** (2017) 1 [1705.11098].

[331] J.F. Donoghue, *General relativity as an effective field theory: The leading quantum corrections*, *Phys. Rev. D* **50** (1994) 3874 [gr-qc/9405057].

[332] S.Y. Choi, J.S. Shim and H.S. Song, *Factorization and polarization in linearized gravity*, *Phys. Rev. D* **51** (1995) 2751 [hep-th/9411092].

[333] B.R. Holstein, *Graviton Physics*, *Am. J. Phys.* **74** (2006) 1002 [gr-qc/0607045].

[334] Y. Mambrini and K.A. Olive, *Gravitational Production of Dark Matter during Reheating*, *Phys. Rev. D* **103** (2021) 115009 [2102.06214].

[335] N. Bernal and C.S. Fong, *Dark matter and leptogenesis from gravitational production*, *JCAP* **06** (2021) 028 [2103.06896].

[336] B. Barman and N. Bernal, *Gravitational SIMPs*, *JCAP* **06** (2021) 011 [2104.10699].

[337] Y. Ema, R. Jinno, K. Mukaida and K. Nakayama, *Gravitational Effects on Inflaton Decay*, *JCAP* **05** (2015) 038 [1502.02475].

[338] Y. Ema, R. Jinno, K. Mukaida and K. Nakayama, *Gravitational particle production in oscillating backgrounds and its cosmological implications*, *Phys. Rev. D* **94** (2016) 063517 [1604.08898].

[339] Y. Ema, K. Nakayama and Y. Tang, *Production of Purely Gravitational Dark Matter*, *JHEP* **09** (2018) 135 [1804.07471].

[340] M. Garny, M. Sandora and M.S. Sloth, *Planckian Interacting Massive Particles as Dark Matter*, *Phys. Rev. Lett.* **116** (2016) 101302 [1511.03278].

[341] M. Garny, A. Palessandro, M. Sandora and M.S. Sloth, *Theory and Phenomenology of Planckian Interacting Massive Particles as Dark Matter*, *JCAP* **02** (2018) 027 [1709.09688].

[342] Y. Tang and Y.-L. Wu, *On Thermal Gravitational Contribution to Particle Production and Dark Matter*, *Phys. Lett. B* **774** (2017) 676 [1708.05138].

[343] M. Viel, G.D. Becker, J.S. Bolton and M.G. Haehnelt, *Warm dark matter as a solution to the small scale crisis: New constraints from high redshift Lyman-α forest data*, *Phys. Rev. D* **88** (2013) 043502 [1306.2314].

[344] V.K. Narayanan, D.N. Spergel, R. Dave and C.-P. Ma, *Constraints on the mass of warm dark matter particles and the shape of the linear power spectrum from the Lyα forest*, *Astrophys. J. Lett.* **543** (2000) L103 [astro-ph/0005095].

[345] M. Viel, J. Lesgourgues, M.G. Haehnelt, S. Matarrese and A. Riotto, *Constraining warm dark matter candidates including sterile neutrinos and light gravitinos with WMAP and the Lyman-alpha forest*, *Phys. Rev. D* **71** (2005) 063534 [astro-ph/0501562].

[346] J. Baur, N. Palanque-Delabrouille, C. Yèche, C. Magneville and M. Viel, *Lyman-alpha Forests cool Warm Dark Matter*, *JCAP* **08** (2016) 012 [1512.01981].

[347] V. Iršič et al., *New Constraints on the free-streaming of warm dark matter from intermediate and small scale Lyman-α forest data*, *Phys. Rev. D* **96** (2017) 023522 [1702.01764].

[348] N. Palanque-Delabrouille, C. Yèche, N. Schöneberg, J. Lesgourgues, M. Walther, S. Chabanier et al., *Hints, neutrino bounds and WDM constraints from SDSS DR14 Lyman-α and Planck full-survey data*, *JCAP* **04** (2020) 038 [1911.09073].

[349] A. Garzilli, A. Magalich, O. Ruchayskiy and A. Boyarsky, *How to constrain warm dark matter with the Lyman α forest*, 1912.09397.

[350] G. Ballesteros, M.A.G. Garcia and M. Pierre, *How warm are non-thermal relics? Lyman-α bounds on out-of-equilibrium dark matter*, *JCAP* **03** (2021) 101 [2011.13458].

[351] A. Lazar, J.S. Bullock, M. Boylan-Kolchin, R. Feldmann, O. Çatmabacak and L. Moustakas, *Out of sight, out of mind? The impact of correlated clustering in substructure lensing*, *Mon. Not. Roy. Astron. Soc.* **502** (2021) 6064 [2012.03958].

[352] BOSS collaboration, *The clustering of galaxies in the completed SDSS-III Baryon Oscillation Spectroscopic Survey: cosmological analysis of the DR12 galaxy sample*, *Mon. Not. Roy. Astron. Soc.* **470** (2017) 2617 [1607.03155].

[353] P. Bode, J.P. Ostriker and N. Turok, *Halo formation in warm dark matter models*, *Astrophys. J.* **556** (2001) 93 [astro-ph/0010389].

[354] M.R. Haque and D. Maity, *Gravitational dark matter: free streaming and phase space distribution*, 2112.14668.

[355] S. Clery, Y. Mambrini, K.A. Olive and S. Verner, *Gravitational portals in the early Universe*, *Phys. Rev. D* **105** (2022) 075005 [2112.15214].

[356] P. Hut, *Limits on Masses and Number of Neutral Weakly Interacting Particles*, *Phys. Lett. B* **69** (1977) 85.

[357] B.W. Lee and S. Weinberg, *Cosmological Lower Bound on Heavy Neutrino Masses*, *Phys. Rev. Lett.* **39** (1977) 165.

[358] M.I. Vysotsky, A.D. Dolgov and Y.B. Zeldovich, *Cosmological Restriction on Neutral Lepton Masses*, *JETP Lett.* **26** (1977) 188.

[359] K. Griest and D. Seckel, *Three exceptions in the calculation of relic abundances*, *Phys. Rev. D* **43** (1991) 3191.

[360] G. Arcadi, M. Dutra, P. Ghosh, M. Lindner, Y. Mambrini, M. Pierre et al., *The waning of the WIMP? A review of models, searches, and constraints*, *Eur. Phys. J. C* **78** (2018) 203 [1703.07364].

[361] Y. Hochberg, E. Kuflik, R. Mcgehee, H. Murayama and K. Schutz, *Strongly interacting massive particles through the axion portal*, *Phys. Rev. D* **98** (2018) 115031 [1806.10139].

[362] N. Bernal, J. Rubio and H. Veermäe, *UV Freeze-in in Starobinsky Inflation*, *JCAP* **10** (2020) 021 [2006.02442].

[363] F. D'Eramo and A. Lenoci, *Lower mass bounds on FIMP dark matter produced via freeze-in*, *JCAP* **10** (2021) 045 [2012.01446].

[364] BICEP, Keck collaboration, *Improved Constraints on Primordial Gravitational Waves using Planck, WMAP, and BICEP/Keck Observations through the 2018 Observing Season*, *Phys. Rev. Lett.* **127** (2021) 151301 [2110.00483].

[365] LIGO Scientific, Virgo collaboration, *Upper Limits on the Stochastic Gravitational-Wave Background from Advanced LIGO's First Observing Run*, *Phys. Rev. Lett.* **118** (2017) 121101 [1612.02029].

[366] LISA collaboration, *Laser Interferometer Space Antenna*, 1702.00786.

[367] T.J. Clarke, E.J. Copeland and A. Moss, *Constraints on primordial gravitational waves from the Cosmic Microwave Background*, *JCAP* **10** (2020) 002 [2004.11396].

[368] R. Keisler et al., *A Measurement of the Damping Tail of the Cosmic Microwave Background Power Spectrum with the South Pole Telescope*, *Astrophys. J.* **743** (2011) 28 [1105.3182].

[369] J. Alvey, N. Sabti, V. Tiki, D. Blas, K. Bondarenko, A. Boyarsky et al., *New constraints on the mass of fermionic dark matter from dwarf spheroidal galaxies*, *Mon. Not. Roy. Astron. Soc.* **501** (2021) 1188 [2010.03572].